

Design of a Meandering Ramp

Dissertation

vorgelegt von

Mag. Dipl.-Ing. Christine Sindelar

verfasst am

Institut für Wasserbau und Wasserwirtschaft

eingereicht an der

Fakultät für Bauingenieurwissenschaften, Technische Universität Graz

zur Erlangung des akademischen Grades

Doktorin der technischen Wissenschaften (Dr. techn.)

Begutachtung:

Univ.-Prof. Dipl.-Ing. Dr. Gerald Zenz (Technische Universität Graz)

Prof. Ing. Stefano Pagliara (Università di Pisa)

Graz, März 2011

Design of a Meandering Ramp

Dissertation

by
Mag. Dipl.-Ing. Christine Sindelar

created at the
Institute of Hydraulic Engineering and Water Resources Management

submitted to the
Faculty of Civil Engineering, University of Technology Graz

In partial fulfillment of the requirements for the academic degree
Doktorin der technischen Wissenschaften (Dr. techn.)

Experts:
Univ.-Prof. Dipl.-Ing. Dr. Gerald Zenz (University of Technology Graz)
Prof. Ing. Stefano Pagliara (Università di Pisa)

Graz, March 2011

Table of Contents

Abstract	v
TOC Appendix (on CD only)	vii
List of Figures.....	viii
List of Tables.....	xv
List of Symbols.....	xvii
Danksagung	xxiv
1 Introduction.....	1
2 Scope of the Thesis.....	3
2.1 Scope	3
2.2 Limitations	3
2.3 Basics	3
2.3.1 Particle Size Distribution	3
2.3.2 Filter Criterion	5
3 Literature Review.....	6
3.1 Lateral Drop Structures	6
3.1.1 Components of a Lateral Drop Structure	6
3.1.2 Historical development	7
3.1.3 The Straight Drop Spillway Basin after Donnelly and Blaisdell	8
3.1.4 The U.S.B.R. Short Stilling Basin III after Peterka	11
3.1.5 The U.S.B.R. Baffled Apron Basin IX after Peterka	13
3.2 Ramps – historical development.....	15
3.2.1 Block ramp after Schauburger.....	15
3.2.2 Further developments.....	18
3.3 Block ramps	21
3.3.1 Supercritical Flow Over a Rough Bed After Scheuerlein and Hartung	21
3.3.2 Design rules for block ramps after Knauss	22
3.3.3 Design rules for block ramps after Whittaker / Jäggi.....	23
3.3.4 Design Rules for Trough-Shaped Block Ramps After Platzer.....	28
3.3.5 Investigations on Block Ramps by Pagliara et al.	34
3.4 Step-pool ramps	40
3.4.1 Introduction.....	40
3.4.2 Natural step-pool systems.....	42
3.4.3 Investigations on step-pool-ramps by Volkart	46

3.4.4	Sediment Transport in Step-pool Streams by Whittaker	51
3.4.5	Practical examples of step-pool-ramps by Gebler	52
3.4.6	Investigations on step-pool-ramps by Vogel.....	54
3.4.7	Investigations on step-pool-ramps by Korecky	56
3.4.8	Investigations on step-pool-systems by Rosport and Aberle.....	57
3.4.9	The Meandering Ramp by O. Grober	58
3.4.10	Advantages of a Meandering Ramp over Conventional Step-Pool Ramps	60
3.5	Key Features of Ramps	60
3.5.1	Hydraulic Efficiency of Drop Structures and Ramps.....	60
3.5.2	Failure Mechanisms.....	64
3.6	Artificial Roughness Elements	65
3.6.1	Classification of Flow Regimes Over Roughness Elements by Peterson & Mohanty ...	65
3.6.2	Design Rules for Channels With Artificial Roughness Elements after Morris	67
3.7	Concluding Remarks	71
4	Physical Model Test for a Meandering Ramp for the “Große Tulln” River	73
4.1	Project Area.....	73
4.2	Initial Design of the Meandering Ramp.....	76
4.3	Sediment Samples Of the Große Tulln and Model Sediments.....	77
4.4	Bed Load Transport – Calculations.....	80
4.5	Measurement Variables and Equipment.....	80
4.5.1	Water Levels	80
4.5.2	Discharge	80
4.5.3	3D Velocity Measurements with ADV-probe	80
4.5.4	1D-Velocity Measurements with a Hydrometric Impeller	82
4.5.5	Digital Elevation Model by Means of Digital Photogrammetry.....	82
4.6	Experimental Setup	86
4.6.1	Model Laws.....	86
4.6.2	Model plan.....	86
4.7	PHASE 1 – Model Calibration	88
4.8	PHASE 2 – mobile bed experiments	90
4.8.1	Development of the ramp design.....	90
4.8.2	Experiments PHASE 2	91
4.8.3	Upstream Scours	92
4.8.4	Results PHASE 2.....	94
4.9	PHASE 3 – Mobile Bed Experiments – Final Design.....	103

4.9.1	Results PHASE 3	103
4.9.2	Final Design	112
4.9.3	Construction Costs of the Meandering Ramp Große Tulln in Neulengbach	116
4.10	Recommendations.....	119
4.11	Conclusions.....	120
5	Basic Flume Test for Step-Pool Ramps	121
5.1	Introduction.....	121
5.1.1	Purpose and Scope of Investigation	121
5.2	Experimental Setup	122
5.2.1	Flume and Ramp Construction	122
5.2.2	Measuring Equipment and Methods.....	129
5.2.3	Automatic Positioning and Data Acquisition.....	133
5.2.4	Post Processing.....	136
5.2.5	Documentation.....	139
5.3	Test Procedure	139
5.3.1	Preliminary Tests	139
5.3.2	Test Procedure	140
5.3.3	Test Program	141
5.4	Results and Discussion	143
5.4.1	Water levels without step installations.....	143
5.4.2	Tumbling Flow Regime	144
5.4.3	Unstable Flow and Rapid Flow Regime	146
5.4.4	Velocity and Turbulence Profiles.....	149
5.4.5	Rough and Smooth Bed.....	151
5.4.6	Laterally Inclined Steps vs Horizontal Steps.....	153
5.4.7	Step Spacing	154
5.4.8	Flow Transition from Tumbling to Rapid Flow	158
5.4.9	Flow Transition from Rapid to Tumbling Flow – Hysteresis.....	159
5.4.10	Flow Transition and Slope – Narrow Flume Experiments	161
5.4.11	Flow Transition and Antidunes.....	163
5.4.12	Pressure Measurements.....	171
5.4.13	Stability of a Step.....	184
5.5	Conclusions.....	190
5.5.1	Objective 1 – find formula for transitional discharge	190
5.5.2	Objective 2 – Morris’ formula appropriate?	190

5.5.3	Objective 3 – Laterally inclined steps dissipate more energy?	191
5.5.4	Objective 4 – determine Pressure Distribution Around Roughness Element	191
6	Field Survey of the Prototype Ramp in the “Stübmingbach” Stream.....	192
7	Design Guidelines for Meandering Ramps	195
7.1	Morphological and Hydrological Preconditions	195
7.2	Dimensioning of the Ramp	196
7.2.1	Step Shape	198
7.2.2	Step Dimensions & Build	198
7.2.3	Channel Widening – Slow-Down Pool	199
7.2.4	Additional Armoring	199
7.2.5	Leveled Step	199
7.2.6	Head- and Tailwater Protection Required?	200
7.2.7	Bank Stability	201
7.3	Comments and Explanations	201
8	Conclusions and Prospects	203
9	Acknowledgements	205
	References.....	206

Abstract

Step-pool systems develop naturally in steep mountain streams and have been adopted for man-made step-pool ramps for streams and mildly sloped rivers alike. Step-pool ramps consist of a sequence of “steps” made of natural boulders that extend across the river width and “pools” in between. The “meandering ramp” is a special kind of step-pool ramp. The steps of a meandering ramp are alternately inclined to the left and the right bank. This lateral inclination induces a meandering flow on low discharges which leads to reduced velocities along the ramp. Unlike for other step-pool designs, no additional armoring is needed for the pools of the meandering ramp in general. This enables natural processes of scouring and deposition.

The meandering ramp takes advantage of the so-called “tumbling flow” regime, a cascading flow with critical depth above the steps and small hydraulic jumps in the pools. As long as the tumbling flow regime can be preserved, the energy dissipation along the ramp is optimal in the sense that the specific energy head above a step is as small as theoretically possible.

On higher discharges a flow transition from tumbling flow to the so-called “rapid flow” regime takes place. In the latter regime the flow skims over the tops of the steps at supercritical conditions. Apart from the reduced energy dissipation along the ramp for the rapid flow regime, it is the flow transitional process itself that marks **the** critical loading case for the stability of the steps of the ramp. This is one of the major findings of this thesis.

In the first stage of the study a physical model test for a specific meandering ramp located at a small river in Lower Austria was performed. The design of the ramp was optimized in mobile bed experiments. In the course of the experiments it turned out that on rising discharges the hydraulic jump in a pool shifts from the upper region of the pool to the lower region until it is finally washed over the pool. These conditions mark the flow transition from tumbling flow to rapid flow. Scour holes immediately upstream of the step may occur which endanger the stability of the step. This type of scour pattern can be reduced if not avoided if the longitudinal cut of a step has a triangular shape. This can either be achieved by a step that consists of a main boulder and two smaller boulders up- and downstream of the main boulder or by a single boulder that is placed such that its top face is adversely sloped. In the rapid flow regime, a recirculating vortex with an axis in horizontal lateral direction develops at the pool bottom.

The thesis does not provide a scour criterion as the tested ramp geometry was too complex to derive general results. It turned out, though, that the presence of a bed load transport helps to prevent the scour holes from reaching a depth that endangers the stability of the steps. Hence, it is a precondition for the construction of a meandering ramp without pool armoring that the natural bed-load transport is not interrupted by bed-load traps or hydropower plants upstream of the ramp. Moreover, the meandering ramp is only recommended for river sediments with characteristic diameters as least as large as for the tested ramp.

In the second stage of the study a basic flume test was performed to relate the flow transitional discharge from tumbling to rapid flow to the design parameters step spacing, step height and ramp slope. It turned out that an existing criterion to distinguish 2D from 3D antidunes based on linearized

potential flow theory (Kennedy, 1961) can be adopted to determine the flow transition from tumbling flow to rapid flow. This way a semi-empirical criterion to calculate the flow transitional discharge subject to the above-mentioned design parameters could be derived. There is a very good agreement between the experimental data of the basic flume test and the semi-empirical criterion.

In a third stage of the study pressure measurements around a single boulder of a step were carried out. From these measurements it was possible to calculate the drag force and the lift force acting on the single boulder. Force and moment equilibrium considerations of this boulder were made which prove that the flow transitional discharge is **the** crucial loading case for the stability of the boulder and hence the ramp. Higher discharges that are well in the rapid flow regime are less severe. This can partly be explained by the stunning fact that for the flow transitional discharge the lift force dominates the drag force exerted by the flow by a multiplicative factor up to 2.6.

As a result of the investigations design guidelines for meandering ramps are provided. The meandering ramp is suitable for small rivers with moderate design discharges.

TOC Appendix (on CD only)

- A.1. Water level measurements for model calibration (chapter 4)
- A.2. Morphology of the ramp for each test run (chapter 4)
- A.3. Velocity measurements before and after increase in bank roughness (chapter 4)
- A.4. Plan of the final ramp design (chapter 4)
- A.5. Compilation of water level measurements (chapter 5)
- A.6. Compilation of ADV-velocity measurements (chapter 5)
- A.7. Calculation sheet for the stability considerations (chapter 5)

List of Figures

Figure 2.1 Example of a particle size distribution of gravel, characteristic diameter d_{90} indicated by dashed line	4
Figure 3.1 Straightening of the river Aist in Schwertberg, Upper Austria: course of the river 1867 (left) and today including old course of the river in red (right); data from GIS Upper Austria.....	6
Figure 3.2 Hydraulic jump characteristics for drop structures (Figure a), b) in: Keutner 1937b, Figure c)-f) in: Keutner 1937a).....	7
Figure 3.3 Straight Drop Spillway (Rand 1955)	7
Figure 3.4 Vertical Drop with Stilling Basin (Morris, Johnson 1943).....	8
Figure 3.5 Straight Drop Spillway Basin (Donnelly, Blaisdell 1965)	9
Figure 3.6 Hydraulic Jump characteristic according to different values of the Froude number	11
Figure 3.7 Chute Spillway Basin, recommended proportions (Peterka 1964), labels modified by author	12
Figure 3.8 Baffle types for chute spillway basin, (Peterka 1964).....	13
Figure 3.9 The U.S.B.R. Baffled Apron Basin IX, recommended proportions, (Peterka 1964), labels modified by author.....	14
Figure 3.10 Vertical drop in the “Alm” river in 1951, km 5.9, (left) The first Schauburger block ramp in the “Alm” river, km 2.76, in Bad Wimsbach, Upper Austria (right) (see Schauburger 1973)	15
Figure 3.11 The first Schauburger block ramp in the “Alm” river, km 2.76, in Bad Wimsbach, Upper Austria: dimensions in m (left) and scouring pattern downstream of this ramp after a flood event on January 21 st 1954 (right, see Garbrecht 1957).....	16
Figure 3.12 Scouring pattern (plan view) for a vertical drop (left) and a doubly bent ramp (right)	16
Figure 3.13 Sketch of a Schauburger ramp in a bent river section (plan view)	17
Figure 3.14 scour patterns for different ramp submergences (Niel 1960): $q = 7.7 \text{ m}^3/\text{s}/\text{m}$ (left), $q = 22 \text{ m}^3/\text{s}/\text{m}$ (right).....	18
Figure 3.15 weir with wing walls (left), weir with connecting banks (right).....	19
Figure 3.16 scouring pattern for different end sill constructions: a. straight end sill with wing wall b. straight end sill with connecting banks c. doubly bent end sill with wing walls d. doubly bend end sill with connecting banks (Garbrecht 1957)	19
Figure 3.17 Smooth ramp after Höss (1968).....	20
Figure 3.18 “loose ramp (left) and “standing ramp” (right) after (Whittaker, Jäggi 1986)	23
Figure 3.19 variation of τ^* , c in dependence of the protrusion of the grain (Fenton, Abott 1977) (left), boundaries of overpassing and embedding conditions (Raudkivi, Ettema 1982) (right), figures slightly modified after (Whittaker, Jäggi 1986)	25
Figure 3.20 Definition sketch for the parameters used in the analysis of the effects at the interface (after (Whittaker, Jäggi 1986))	26
Figure 3.21 Scour protection measures (Whittaker, Jäggi 1986).....	28
Figure 3.22 sketch of a trough-shaped ramp (modified after Platzer 2000)	29
Figure 3.23 sketch of a creek (modified after Platzer, 2000).....	31
Figure 3.24 riprap protection downstream of the ramp (Platzer 2000, labels translated by author).....	34
Figure 3.25 sketch of the ramp for the investigation of energy dissipation on block ramps (modified after Pagliara, Chiavaccini 2006a)	34
Figure 3.26 sketch of a scour downstream of a block ramp (modified after Pagliara, 2007).....	38

Figure 3.27 Sketch of expanded stilling basin, plan view (modified after Pagliara & Palermo, 2008b) ..	39
Figure 3.28 Sketches of morphological patterns 1 – 4 (Schälchli 1991, labels modified by author)	40
Figure 3.29 Example of a step-pool ramp near Teisendorf, Bavaria (© Wasserwirtschaftsamt Traunstein)	41
Figure 3.30 ramps with pool cluster: Saalach river, km 4.6 at low flow conditions (left), physical model of the Salzach river ramp, km 51.9 (right).....	42
Figure 3.31 Various definitions morphological parameters step height K and step spacing in natural step-pool systems (Nickolotsky & Pavlowsky 2007, labels modified by author)	42
Figure 3.32 Correlation between slope and relative spacing in natural step-pool systems, R^2 is a measure for the goodness of the fitted power function ($R^2=1$ means that all data points lie on the power function)	45
Figure 3.33 Sketch of a step-pool sequence without armor layer (modified after Volkart 1972)	46
Figure 3.34 Sketch of a step-pool sequence with armor layer (modified after Volkart 1972)	46
Figure 3.35 Erosion of the downstream part of the pool (Volkart 1972)	47
Figure 3.36 Location of the maximum scour depth within one pool (Volkart 1972)	48
Figure 3.37 Critical discharge for the incipient motion of a step-pool sequence with armor layer (modified after Volkart, 1972).....	50
Figure 3.38 step-pool ramp with low-flow channel (sketches modified after Gebler 1991), picture bottom right from Gebler 2009)	53
Figure 3.39 Sketch of a step-pool ramp, $I = 1: 20$ (Vogel 2003)	54
Figure 3.40 Sketch of a meandering ramp, plan view (Mende, Gassmann 2009, labels translated by author).....	59
Figure 3.41 Sketch of a longitudinal section of a meandering ramp in river axis.....	59
Figure 3.42 Natural model for the meandering ramp (left), first prototype meandering ramp, Stübmingbach (right).....	60
Figure 3.43 direct erosion of blocks (Whittaker, Jäggi 1986)	64
Figure 3.44 Erosion of bed material (Whittaker, Jäggi 1986)	64
Figure 3.45 Blocks are swept away into the scour hole downstream of the ramp (Whittaker, Jäggi 1986)	65
Figure 3.46 Flow regimes over artificial roughness elements according to Peterson & Mohanty (1960)	65
Figure 3.47 Design parameters for large roughness elements.....	66
Figure 3.48 cross sectional shapes of roughness elements (Morris 1986).....	68
Figure 3.49 Flow patterns over roughness elements (Knight, Macdonald 1979).....	70
Figure 3.50 Graphical determination of Roughness parameter χ and flow resistance (Knight, Macdonald 1979).....	70
Figure 3.51 Comparison of different design rules, non-filled symbols: traditional block ramps, filled symbols: step-pool ramps for $d_{xx} = 1$ m, $\rho_S = 2650$ kg/m ³ , $\rho_W = 1000$ kg/m ³	72
Figure 4.1 Project area: Neulengbach – Große Tulln river	73
Figure 4.2 100-year flood hydrograph in the project area calculated from a rainfall runoff simulation model.....	74
Figure 4.3 Old weir, Neulengbach, Große Tulln river, km 23.5.....	75
Figure 4.4 facsimile of the river regulation project 1969, standard section.....	75
Figure 4.5 sketch of the initial ramp design by O. Grober, units in (m).....	76
Figure 4.6 Sediment samples of the Große Tulln river	78

Figure 4.7 Model sediments (transformed to full scale) and averaged field samples, shaded area marks the range of the field samples.....	79
Figure 4.8 Nortek-ADV-probe: measuring principle (left), side-looking probe (right)	81
Figure 4.9 Carriage for ADV-probe moving on rails	82
Figure 4.10 Determination of the mean velocity using 1 measuring point (ÖNORM B 2403)	82
Figure 4.11 Principle of the stereoscopic image evaluation	83
Figure 4.12 Images for digital photogrammetry taken from the crane bridge	84
Figure 4.13 3D surface (left) and orthorectified image (right) of the model resulting from digital photogrammetry	84
Figure 4.14 Longitudinal section (top) and plan view (bottom) of the initial model (dimensions in model scale).....	87
Figure 4.15 Construction of the model: view from the downstream end of the model (left), pavement of the bed with coarse gravel (right).....	87
Figure 4.16 Increase of roughness by means of mortar elements (variant 1, left) and pimple mat (variant 3, right).....	88
Figure 4.17 Model calibration, roughness variants: 1-year flood, HEC-RAS calculation vs. water level measurements (averaged in lateral direction).....	89
Figure 4.18 Water level measurement 1-year flood: lateral inclination of water level	89
Figure 4.19 Ramp design D2	91
Figure 4.20 Bed changes around submerged groins with a.) horizontal and b.) inclined crest, station and height in (cm)	93
Figure 4.21 Scour around a bridge pier (Bezzola, 2004).....	94
Figure 4.22 Upstream scours: a.) test run no. 3: 1-year flood, S1 b.) test run no. 11: 1-year flood, S4 c.) test run no. 12: 30-year flood, S4 d.) initial bed surface prior to each test run.....	95
Figure 4.23 Erection of design variant D8, viewing direction: upstream.....	96
Figure 4.24 Plan view ramp design D8.....	96
Figure 4.25 1-year flood for ramp design D8, direction of flow from right to left, pools of ramp 1 are labeled	97
Figure 4.26 Ramp design D8: initial bed surface, pools of ramp 1 and slow-down pool labeled.....	97
Figure 4.27 ramp design D8: bed changes after a 1-year flood.....	98
Figure 4.28 Ramp Design D8 - bed changes after a 30-year flood.....	99
Figure 4.29 100-year flood hydrograph, sediment addition and water depths - model scale!.....	99
Figure 4.30 Control section X=5 for water level regulation via flap	100
Figure 4.31 Ramp Design D8: 100-year flood wave, flow direction from right to left!	100
Figure 4.32 Ramp Design D8, bed changes after a 100-year flood wave	102
Figure 4.33 Bank roughness before (left) and after experiment no. 21, tailwater section with end sill.....	103
Figure 4.34 Plan view ramp design D9 - ramp area and tailwater section	105
Figure 4.35 Configuration of a step, ramp design D9	105
Figure 4.36 Ramp Design D9 - initial bed surface	106
Figure 4.37 Ramp Design D9 - bed levels after a 1-year flood, (test run 18).....	106
Figure 4.38 Ramp design D9 - bed levels after a 30-year flood, no flap (test run 19).....	107
Figure 4.39 Check of the model roughness, position of the water level measurements X=126.....	107
Figure 4.40 Check of the model roughness, velocities and water depths (test run 20).....	108
Figure 4.41 Ramp Design D9 - bed levels after a 100-year flood, flap-regulated (test run 20).....	108
Figure 4.42 No flap, overfall into the sand trap (left) wooden board at the downstream end of the sand trap (right)	110

Figure 4.43 Ramp Design D9, bed levels after a 30-year flood, no flap (test run 22).....	110
Figure 4.44 Pool armoring, longitudinal cut in the centerline (model scale, dimensions in cm)	111
Figure 4.45 Final design, 100-year flood hydrograph, sediment addition (model scale)	112
Figure 4.46 Final design, initial bed surface.....	113
Figure 4.47 Final design, bed levels after the 100-year flood wave (test run 23)	113
Figure 4.48 Final design, stability test series	114
Figure 4.49 Stability test series, bed changes, longitudinal cut Y=-4.....	115
Figure 4.50 Stability test series, bed changes, longitudinal cut Y=0.....	115
Figure 4.51 Stability test series, bed changes, longitudinal cut Y=+4.....	116
Figure 4.52 Prototype Ramp: Reinforced areas.....	118
Figure 5.1 Design parameter.....	121
Figure 5.2 Section (top) and plan view (bottom) of the flume, dimensions in (m)	122
Figure 5.3 Flow straightener: steel grates and perforated sheet (left), plastic honeycombs (right) ...	123
Figure 5.4 Ramp frame constructed from aluminum profiles	124
Figure 5.5 Elements comprising the ramp construction (side view): longitudinal profile, vertical column, roughness elements, panels with gravel, rubber seal.....	125
Figure 5.6 Roughness element: dimensions (mm)	125
Figure 5.7 Step cross section of the meandering ramp on a gravel panel, effective element height (top), step cross section of a horizontal step on a smooth panel (bottom), dimensions in (mm)	126
Figure 5.8 Roughness element for pressure measurements: sketch (left), original upside-down with mounted pressure transducers (right)	127
Figure 5.9 step panel without roughness elements (left), pool panel (middle) and smooth panel (right)	128
Figure 5.10 Overview of four ramp configurations resulting from three different pool panels	129
Figure 5.11 Ultrasonic probes on measurement carriage	131
Figure 5.12 Side-looking ADV-probe “Vectrino” on positioning system at the downstream end of the flume	132
Figure 5.13 Kulite-Pressure Transducer XTL-123C-190, dimensions in inch and mm (in parenthesis), respectively	133
Figure 5.14 positioning system (left), measurement cabinet with control unit (right)	134
Figure 5.15 Coordinate systems CSP for ultrasonic probe in the centerline and CSR, dimensions in (mm)	135
Figure 5.16 Carriage with ultrasonic probes aligned differently in vertical direction	135
Figure 5.17 Unfiltered output signal (left), elimination of outliers equaling the upper range bound (right).....	137
Figure 5.18 Example illustration, longitudinal cut of water levels.....	138
Figure 5.19 Example illustrations, water levels in cross section.....	138
Figure 5.20 Example illustration, ADV-measurement, streamwise velocities u (cm/s).....	138
Figure 5.21: Example photo documentation	139
Figure 5.22 Design parameters, step-pool unit numbering, step numbering and water surface properties	143
Figure 5.23 Example of tumbling flow patterns for slope $I = 2.5\%$: Variant I25_K8_L80, rough, meander	144
Figure 5.24 Detail of Figure 5.23: critical flow over steps (a., b., c.), rising water depth (cf. c. and d.)	145
Figure 5.25 Tumbling Flow Pattern, variant: I25_K8_L70, rough bed, $Q = 158$ l/s.....	145

Figure 5.26 Example of tumbling flow patterns for slope $I = 6.5\%$: Variant I65_K8_L80, rough.....	145
Figure 5.27 Detail of Figure 5.26: supercritical flow over steps, step-pool unit 4.....	146
Figure 5.28 Example water surface for instable flow, variant: I25_K6_L70, rough, $Q = 130$ l/s, rooster tails	147
Figure 5.29 water surface instable Flow, 3 rooster tails per cross section (Volkart 1972).....	147
Figure 5.30 Instable flow pattern, variant: I25_K8_L70, rough bed, $Q = 158$ l/s.....	147
Figure 5.31 Water surface for stable rapid flow, variant: I25_K6_L70, rough, $Q = 200$ l/s, horizontal water levels in cross section.....	147
Figure 5.32 Stable rapid flow pattern, variant: I25_K8_L70, rough bed, $Q = 200$ l/s	148
Figure 5.33 Flow regimes and transitional discharges TF2RF and RF2TF	148
Figure 5.34 Maximum Froude numbers above step for the rapid flow regimes.....	149
Figure 5.35 Typical cross sectional velocity distribution above step 1: variant I25_K8_L80, smooth bed, $Q=178$ l/s, Rapid Flow: streamwise velocities (left), secondary flow (right).....	149
Figure 5.36 Typical cross sectional velocity distribution tumbling flow: variant I25_K8_L80, rough bed, step 5, $Q=178$ l/s: streamwise velocities (left), secondary flow (right)	150
Figure 5.37 Typical cross sectional velocity distribution rapid flow: variant I25_K8_L93, rough bed, step 5, $Q=240$ l/s, rapid flow: streamwise velocities (left), secondary flow (right)	150
Figure 5.38 Typical TKE pattern with the smallest values in the high velocity region.....	150
Figure 5.39 Varying bed roughness: variant I25_K8_L80, smooth bed (left) and rough bed (right)	151
Figure 5.40 Comparison of mean water depths for smooth and rough bed: I25_K8_L80, tumbling flow	151
Figure 5.41 Comparison of mean water depths for smooth and rough bed: I25_K8_L80, rapid flow..	152
Figure 5.42 Comparison of streamwise velocities for smooth and rough bed: I25_K8_L80, step 1	152
Figure 5.43 Comparison of streamwise velocities for smooth and rough Bed: I25_K8_L80, step 5	152
Figure 5.44 Comparison of mean water depths for horizontal and laterally inclined steps: I25_K8_L80, tumbling flow	153
Figure 5.45 Comparison of mean water depths for horizontal and laterally Inclined Steps: I25_K8_L80, rapid flow	153
Figure 5.46 Comparison of streamwise velocities for horizontal and laterally inclined steps: I25_K8_L80, step 1	154
Figure 5.47 Comparison of streamwise velocities for horizontal and laterally inclined steps: I25_K8_L80, step 5	154
Figure 5.48 Pool water depths for variant I65-K8, rough bed: a.) $L = 622$ mm, b.) $L = 933$ mm, $Q = 100$ l/s, TF	155
Figure 5.49 Location of pool cross sections A-A, B-B, C-C, D-D	155
Figure 5.50 Velocity plots (cm/s) pool cross sections, narrow spacing: variant I65-K8-L62, rough bed, $Q = 170$ l/s, RF, cross sections A-A (above) and B-B (below) of step-pool unit 6	156
Figure 5.51 Velocity plots (cm/s) pool cross sections, wide spacing: variant I65-K8-L93, rough bed, $Q = 170$ l/s, RF, cross sections C-C (above) and D-D (below) of step-pool unit 4	157
Figure 5.52 Velocity direction in X-Z-plane: $I = 6.5\%$, $K = 80$ mm, rough bed; left: step-pool unit 6, narrow spacing; right: step-pool unit 4, wide spacing; tumbling flow (top); rapid flow (bottom)	157
Figure 5.53 Flow Transition from Tumbling Flow to Rapid Flow	158
Figure 5.54 Flow Transition for Rough and Smooth Bed	159
Figure 5.55 Flow Transition Underlies Hysteresis, Flow Transition TF2RF and RF2TF.....	160
Figure 5.56 Cut-out of the lower part of the narrow flume (dimensions in mm)	161

Figure 5.57 Flow Transition and Slope, Narrow Flume, $K = 75 \text{ mm}$, $L = 700 \text{ mm}$	162
Figure 5.58 Flow Pattern 2D-antidunes (Núñez-González, Martín-Vide 2010) (top) – Tumbling Flow for variant: I25-K6-L80, rough bed, $Q = 145 \text{ l/s}$ (bottom), flow from left to right for both pictures	163
Figure 5.59 Flow Pattern 3D-Antidunes (Núñez-González, Martín-Vide 2010) (left), Rapid Flow for variant: I25-K8-L80, rough bed, flow from background to foreground for both pictures	164
Figure 5.60 Defining parameter antidunes (left) and large roughness elements (right).....	165
Figure 5.61 Calculation of Mean Water Depth for Each Step Pool Unit from Experimental Results	165
Figure 5.62 Tumbling flow and rapid flow regime for each step pool unit	166
Figure 5.63 Detail of Figure 5.62, experimental flow regime incoherent with theoretical classification	166
Figure 5.64 Experimental flow regime incoherent with theoretical classification: roll waves in the lower part of the ramp	167
Figure 5.65 Surface wave amplitude and step height for variant I25-K8-L80, rough bed: $Q = 75 \text{ l/s}$ (left), $Q = 175 \text{ l/s}$ (right), flow transitional discharge: $Q = 182 \text{ l/s}$	167
Figure 5.66 Flow Pattern and Mean Water Depth at Flow Transition.....	168
Figure 5.67 Linear Approximation for the Dimensionless Control Depth y_1	169
Figure 5.68 Calculated vs Experimental Transitional Discharge (Equation 5-12)	170
Figure 5.69 Location of the roughness element with the pressure transducers in the flume	171
Figure 5.70 Location of the 14 pressure transducers on the roughness element.....	171
Figure 5.71 Pressure measurements: experimental setup, sixth pool labeled	172
Figure 5.72 Characteristic pressure time series: upstream face	174
Figure 5.73 Characteristic pressure time series: downstream face	174
Figure 5.74 Characteristic pressure time series: top face	175
Figure 5.75 Characteristic pressure time series: side faces	175
Figure 5.76 Mean total pressure head around roughness element, $qP = 3.1 \text{ m}^3/\text{sm}$, Tumbling Flow	177
Figure 5.77 Mean total pressure head around roughness element, $qP = 4.6 \text{ m}^3/\text{sm}$, Tumbling Flow	177
Figure 5.78 Mean total pressure head around roughness element, $qP = 4.6 \text{ m}^3/\text{sm}$, Rapid Flow	178
Figure 5.79 Mean total pressure head around roughness element, $qP = 6.2 \text{ m}^3/\text{sm}$	179
Figure 5.80 Mean total pressure distribution around roughness element, $qP = 3.1 \text{ m}^3/\text{sm}$	179
Figure 5.81 Mean total pressure head for all tested flow regimes	180
Figure 5.82 Mean dynamic pressure head for all tested flow regimes	181
Figure 5.83 Forces acting on roughness elements, measured parameters $p_1 - p_{14}$, y_{step} , pressure transducers 11 and 12 located at the side faces are not displayed.....	182
Figure 5.84 Weighted pressure integration.....	182
Figure 5.85 Shape of roughness elements: own experiment (left), Morris - square (middle), Morris - triangle top (right)	184
Figure 5.86 Forces acting on a single substitute boulder, longitudinal cut	185
Figure 5.87 Required boulder mass for low specific discharges, meandering ramp and step-pool ramp with a slope $I = 3 \%$ according to Korecky (2007),	189
Figure 6.1 Melt Water Discharge on March, 25 th 2010, 18:27, CET (left), Sediment Sorting in Step-Pool Unit 4 of the Meandering Ramp (right).....	192
Figure 6.2 Meandering ramp Stübmingbach, field survey results, December 2009: Plan view of the ramp (top), longitudinal cuts (bottom, vertical exaggeration: 2)	193

Figure 6.3 Meandering ramp Stübmingbach, field survey results, December 2009, plan view: Measuring points (top) and sediment sorting classification (bottom).....	194
Figure 7.1 Meandering ramp scheme, plan view (top), longitudinal cut in river axis (bottom), cross section see Figure 7.2.....	195
Figure 7.2 Ramp geometry: plan view and sections – relative elevation of the steps	197
Figure 7.3 Required boulder mass M (t/m) to ensure stability.....	199
Figure 7.4 Comparison of energy levels for head and tailwater of the ramp.....	200
Figure 7.5 Upstream Scour in the Physical Model of a Meandering for the “Große Tulln” River, longitudinal cut, steps without up- and downstream scour protection, rounded gravel, (Sindelar & Knoblauch 2010).....	201
Figure 7.6 Maximum scour depth - equivalent step height K	202

List of Tables

Table 3.1 Overpassing and embedding condition of a single exposed D_1 -grain, case 1	25
Table 3.2 Stability of a single particle thick armor layer, case 2	26
Table 3.3 Maximum discharge to prevent erosion of bed material.....	27
Table 3.4 Design rules after Platzer (2000)	34
Table 3.5 Relative submergence categories.....	35
Table 3.6 Coefficients for calculating the energy dissipation on block ramps with a free jump	36
Table 3.7 Coefficients for calculating the increased energy dissipation on block ramps due to protruding boulders	37
Table 3.8 Coefficients for calculating the energy dissipation on block ramps with a submerged jump.....	37
Table 3.9 Morphological patterns, classification according to Schälchli (1991)	40
Table 3.10 Examples of cluster ramps, parameters	41
Table 3.11 Morphological parameters in natural step-pool systems	44
Table 3.12 Filter and armor materials for a step-pool sequence with armor layer (mm)	50
Table 3.13 Coefficients to reduce or increase the calculated mass of stones from equation 3-73.....	56
Table 3.14 Existing meandering ramps	59
Table 3.15 Flow Regimes for vertical drop structures according to Franke (1970)	62
Table 3.16 Design rules used for Figure 3.51	72
Table 4.1 Morphology and hydrology	74
Table 4.2 parameters of the initial ramp design	77
Table 4.3 Sediment samples of the Große Tulln river.....	77
Table 4.4 Model sediments (converted to full scale).....	78
Table 4.5 Technical data of ADV-probe Vectrino ⁺	81
Table 4.6 Comparison of digital photogrammetry and leveling, standard deviation, measured control sections	85
Table 4.7 Model laws using Froude similitude.....	86
Table 4.8 Relation between model and prototype discharge.....	86
Table 4.9 Roughness variants in the model	88
Table 4.10 Gradual development of a final ramp design	90
Table 4.11 Complete list of test runs in PHASE 2 in chronological order.....	91
Table 4.12 Choice of parameters for MPM's formula for a 30-year flood.....	98
Table 4.13 Complete list of test runs in PHASE 3 in chronological order.....	104
Table 4.14 Water depths before and after the increase of roughness.....	109
Table 4.15 Measures of the step stone sample, model scale	117
Table 4.16 Lengths of the steps and stones masses	117
Table 4.17 Steps: lengths and volume, full scale.....	118
Table 4.18 Scour protection: number of boulders and volume, full scale	118
Table 4.19 Pool armorings: areas and volume, full scale.....	118
Table 4.20 Items of the description service "river engineering"	119
Table 5.1 Color, height and number of roughness elements.....	126
Table 5.2 Panel set, dimensions (mm)	128
Table 5.3 Ultrasonic probes.....	130
Table 5.4 Ultrasonic probes, accuracy test	130

Table 5.5 Kulite-Pressure Transducer XTL-123C-190, key features	133
Table 5.6 Offset of measurement devices with respect to the profiles of the positioning system	135
Table 5.7: Test program wide flume	142
Table 5.8: Test program narrow flume	142
Table 5.9: Froude numbers without step installations	143
Table 5.10: Comparison of present study with Peterson & Mohanty: flow depths (TF) above steps as multiples of the critical flow depth, y_1 denotes the flow depth above upstream crest of the step	146
Table 5.11 Flow transitional discharges of all wide flume experiments in tabular form.....	160
Table 5.12 Narrow Flume Experiments: Normalized Control Depth y_1/y_c , critical depth y_c , control depth y_1 above upstream face, depth y_2 above downstream face.....	162
Table 5.13 Tested flow regimes for pressure measurements.....	172
Table 5.14 Number of pressure measurements per test series and discharge (not listed: 0 l/s – measurements).....	173
Table 5.15 Lift and drag force and its ratio, drag coefficient calculated from the pressure measurements for 5 tested flow regimes.....	183
Table 5.16 Comparison of drag coefficients calculated from own experimental result and according to Morris' formulas 3-101 and 3-102	184
Table 5.17 Dimensions of the substitute boulder	187
Table 5.18 Maximum permissible drag force, approach velocity and specific discharge for each pair (cD , FL/FD) to guarantee stability, grey shaded area: cD and FL/FD values at flow transition	187
Table 5.19 Dimensions of main boulder and scour protection boulders (cf. Table 7.3).....	188
Table 7.1 Morphological and Hydrological Preconditions	196
Table 7.2 Ramp geometry	196
Table 7.3 Axes of the block-shaped boulders of a step: denotations	198
Table 7.4 Boulder Dimensions to ensure stability for a maximum design discharge of 10 m ³ /sm ..	198
Table 7.5 Relative Spacing L/K for $L_{step} = 1.5$ m and for different step spacings, corresponding flow transitional discharge according to equation 5-12	202

List of Symbols

Γ	boulder concentration (Pagliara)
Ψ	boulder coverage (–) (Vogel)
Ω	tolerance parameter (–) (Korecky)
β	ratio W/w of inlet to crest width (–) (Morris & Johnson)
ξ_s	location of maximum scour depth (–) (Volkart)
ξ_{max}	location of maximum water depth (–) (Volkart)
ξ_{min}	location of minimum water depth (–) (Volkart)
ρ	density (kg/m^3)
ρ_s	sediment density (kg/m^3)
ρ_w	density of water (kg/m^3)
τ_*	dimensionless shear stress
$\tau_{*,c}$	dimensionless critical shear stress, Shields parameter
φ	angle of repose (degree)
χ	shape parameter of roughness elements, (m) (Knight and Macdonald)
A_{\perp}	projected area of an obstacle perpendicular to the flow (m^2) (see drag force F_D)
a	wave amplitude (m) (Antidunes)
a_B	wave amplitude of the wavy bed (m) (Antidunes)
a_W	wave amplitude of the wavy surface (m) (Antidunes)
c	coefficient (multiple) of critical depth (–) (Peterson & Mohanty, chapter 5)
c_D	drag coefficient of drag force F_D (–)
c_L	lift coefficient of lift force F_L (–)
d_f	diameter of the filter layer (m)
$d_{f,min}$	minimum diameter of the filter layer (m) (Platzer)
d_s	equivalent spherical diameter (m)
d_m	mean particle diameter (m) (Meyer-Peter Müller)

d_{max}	maximum boulder diameter (m) (Schälchli)
d_{xx}	characteristic diameter where xx % of the particles are finer (m)
e	spacing of longitudinal sills (m) (Morris & Johnson)
E	extent of turbulence in step-pool systems (W/m^3) (Gebler)
f_b	bed friction factor (–) (Knight and Macdonald)
F_B	buoyancy force (N)
F_D	drag force (N)
F_L	lift force (N)
F_W	weight force (N)
F_R	resistance (friction) force (N)
Fr	Froude number (–)
Fr _c	critical Froude number to distinguish 2D from 3D antidunes (–) (Kennedy)
Fr _q	Froude number of the specific discharge (–) (Platzer)
Fr _{d_{xx}}	densimetric Froude number (–) (Pagliara)
g	gravitational acceleration (m/s^2)
g'	reduced gravitational acceleration (m/s^2), defined as $g' = (\frac{\rho_s}{\rho} - 1) \cdot g$ (Pagliara)
h_a	side wing height at the end of the stilling basin (m) (Morris & Johnson)
h	drop height of drop structure (m) (Rand, Morris & Johnson, Höss)
h	ramp height (m) (Platzer)
h	height of baffle pier for baffled apron (m) (Peterka)
h_1	height of chute block (m) (Peterka)
h_3	height of baffle pier for chute spillway basin (m) (Peterka)
h_{crest}	height of ramp crest (m) (Platzer)
h_e	end sill height in stilling basin (m) (Donnelly & Blaisdell, Peterka)
h_f	block height in stilling basin (m) (Donnelly & Blaisdell)
$h_{i,13}$	vertical distance between pressure transducers i and 13 (m) (chapter 5)
h_{scour}	maximum scour depth in pool (m) (chapter 7)
h_{scour}	scour depth downstream of ramp toe (m) (Platzer)

Δh	water level difference of two adjacent pools (m) (Gebler)
I_{TW}	slope of tailwater in per mill (Platzer)
k	ramp roughness, equals $l_a/3$ (m) (Platzer)
K	step/roughness height (m) (Knight and Macdonald, Morris, Volkart)
L	spacing of the steps/roughness elements (m) (Knight and Macdonald, Morris, Volkart)
L	length of the ramp (m) (Platzer)
L_1	horizontal distance between drop crest and location where the upper nappe strikes the stilling basin floor (m) (Rand)
L_2	length of the hydraulic jump (m) (Rand)
l_a	vertical axis of main boulder (m) (chapter 7)
$l_{a,rein}$	vertical axis of scour protection boulder (m) (chapter 7)
$l_{a,s}$	vertical axis of substitute boulder (m) (chapter 7)
l_b	lateral axis of main boulder (m) (chapter 7), middle axis of boulder (m) (Platzer)
L_B	length of stilling basin (m) (Morris & Johnson, Höss)
l_c	horizontal axis in flow direction of main boulder (m) (chapter 7)
$l_{c,rein}$	horizontal axis in flow direction of scour protection boulder (m) (chapter 7)
$l_{c,s}$	horizontal axis in flow direction of substitute boulder (m) (chapter 7)
L_C	chute length of smooth ramp (m) (Höss)
l_D	perpendicular distance of turning point T to action point of the drag force of the substitute boulder (m) (chapter 7)
L_H	horizontal ramp length (m) (Pagliara, chapter 7)
L_{HJ}	horizontal distance from location of the hydraulic jump to the ramp toe (m) (Pagliara)
L_R	length of smooth ramp (m) (Höss)
l_s	length of scour (m) (Platzer, Pagliara)
L_s	dimensionless length of scour (—) (Pagliara)
n	ramp slope 1: n (Platzer)
P	protrusion of a particle above the mean bed level
p_h	hydrostatic pressure (m)

Q	total flow discharge (m^3/s)
Q_M	total flow discharge in a scaled model (l/s)
q	flow discharge per unit width (m^3/sm)
q_{cr}	maximum permissible flow discharge for the stability of a step-pool formation (m^3/sm) (Aberle)
$q_{crit,flow\ transition}$	flow discharge per unit width for the transition from tumbling flow to rapid flow (m^3/sm)
$q_{crit,sed}$	flow discharge per unit width for the incipient motion of the sediments (m^3/sm)
q_P	prototype flow discharge per unit width (m^3/sm)
q_b	bed load discharge (kg/ms) (Volkart)
r	conical shape parameter of trough-shaped ramp (–) (Platzer)
s	height of longitudinal sill (m) (Morris & Johnson)
s	shape factor l_a/l_b (–) (Platzer)
s_1	spacing between chute blocks (m) (Peterka)
s_3	spacing between baffle piers for chute spillway basin (m) (Peterka)
s_e	height of end sill (m) (Morris & Johnson)
T	lateral spacing of 3-dimensional roughness elements (m) (Morris)
u, v, w	velocity component in streamwise, lateral and vertical direction, respectively (m/s)
\bar{u}	mean velocity in streamwise direction (m/s) (Aberle)
u_*, v_*	shear velocity (m/s) (Raudkivi, Whittaker & Jäggi)
U_{60}	non-uniformity coefficient (–), defined as: $U_{60} = d_{60}/d_{10}$
U_{84}	non-uniformity coefficient (–), defined as: $U_{84} = \sqrt{d_{84}/d_{16}}$
v_a	mean approach velocity (m/s) (chapter 7)
$v_{a,g}$	maximum permissible approach velocity to prevent gliding (m/s) (chapter 7)
$v_{a,t}$	maximum permissible approach velocity to prevent overturning (m/s) (chapter 7)
v_c	critical velocity corresponding to critical depth y_c (m/s)
v_{cr}	critical velocity for the stability of a ramp (m/s) (Hartung, Scheuerlein)
\bar{y}	mean water depth of a step-pool unit or antidunes (m) (chapter 5)

y_1, y_2	water depths above step (m) (chapter 5)
y_3, y_4	water depths in the pools (m) (chapter 5)
y_1	supercritical depth entering the hydraulic jump (m)
y_2	subcritical depth after the hydraulic jump (m)
y_c	critical depth (m)
y_{cr}	maximum permissible water depth to guarantee stability of a block ramp (m) (Hartung, Scheuerlein, Knauss, Aberle)
y_{HW}	headwater flow depth (m) (Höss)
y_{pool}	mean pool water depth (m) (chapter 5)
y_{step}	mean step water depth (m) (chapter 5 and 7)
y_{TW}	tailwater flow depth (m) (Donnelly & Blaisdell)
y_u	uniform flow depth (m) (Pagliara)
Y_{max}	maximum scour depth (m) (Volkart)
v_c	critical velocity corresponding to critical depth y_c
v_{cr}	maximum permissible velocity to guarantee stability of a block ramp (m/s) (Hartung, Scheuerlein, Knauss)
V_p	volume of a pool (m ³) (Gebler)
w	width of the ramp crest (m) (Morris & Johnson)
w	width of the ramp (m) (Platzer)
w_1	width of chute block (m) (Peterka)
w_3	width of baffle pier for chute spillway basin (m) (Peterka)
W	width of inlet section to the drop structure (m) (Morris & Johnson)
w_{creek}	width of the creek downstream of a ramp (m) (Platzer)
w_{crest}	width of the ramp crest (m) (Platzer)
w_{toe}	width of the ramp toe (m) (Platzer)
\bar{Z}	mean water depth (m) (Volkart)
$\Delta z_{w_{crest}}$	trough height (m) (Platzer)
z_m	mean scour depth (m) (Pagliara)
Z_m	dimensionless mean scour depth (m) (Pagliara)

z_{max}	maximum scour depth (m) (Pagliara)
Z_{max}	dimensionless maximum mean scour depth (–) (Pagliara), maximum water depth (m) (Volkart)
Z_{min}	minimum water depth (m) (Volkart)

Danksagung

Ich bedanke mich bei meinem Dissertations-Betreuer Prof. Gerald Zenz, dass er meinem selbstgewählten Forschungsthema "instream river training" mit Interesse begegnet ist. Gerald brachte vor allem bei den Stabilitätsbetrachtungen zur Pendelrampe wesentliche Ideen ein. Er hat viel Zeit in die Durchsicht meiner Arbeit investiert und konnte so wertvolle Kommentare und Verbesserungsvorschläge einbringen, die zur leichteren Lesbarkeit und zum besseren Verständnis der Arbeit beigetragen haben.

Meinen Zweitgutachter Prof. Stefano Pagliara von der Universität Pisa habe ich 2008 bei einer internationalen Tagung für JungwissenschaftlerInnen in Pisa kennen gelernt, von der ich sehr profitiert habe. Ich bedanke mich dafür, dass er die Zweitbegutachtung meiner Arbeit übernommen hat. Sein feedback zu meiner Arbeit war stets sehr motivierend.

Es ist der freundlichen und unkomplizierten Art von Ass.-Prof. Dr. Helmut Knoblauch zu verdanken, dass ich im Juni 2005 die Möglichkeit bekam, eine Stelle als Projektmitarbeiterin am Institut für Wasserbau und Wasserwirtschaft der TU Graz anzutreten. Ich bedanke mich bei Helmut für seine Offenheit mir gegenüber und bei Herrn Prof. Günther Heigerth dafür, dass er sich als damaliger Institutsleiter auf das Experiment mit einer Mathematikerin eingelassen hat. All meinen Kollegen und Kolleginnen rechne ich es hoch an, dass sie Geduld mit mir hatten, als ich die einfachsten hydraulischen Grundlagen erst lernen musste.

Die Durchführung der beiden Modellversuche wäre ohne die tatkräftige Unterstützung meiner Kollegen aus der Werkstatt und ohne unsere Techniker nicht möglich gewesen. Allen voran haben Ing. Christian Kraker, Ing. Wolfgang Rois und Dietmar Schäfauer wesentlich zum Gelingen des Glasgerinneversuchs beigetragen. Es war sehr tragisch, als Christian vor einem Jahr ganz plötzlich aus seinem Leben gerissen wurde. Ich durfte auch auf die engagierte Mitarbeit der Studenten Thomas Gomerski, Herbert Geiger und Shkelzen Kryeziu bauen.

Von Anfang an war es mein Ziel, die unkonventionellen Bauweisen von Otmar Grober wissenschaftlich zu untersuchen. Er hat mir mit der von ihm entwickelten "Pendelrampe" nicht nur zu einem ausgesprochen faszinierenden Thema verholfen, sondern er ist für mich auch ein großes Vorbild darin, für die eigenen Überzeugungen beherzt einzustehen.

Meine Eltern haben mich in meiner Ausbildung immer sehr unterstützt und mir auch meine Diplom-Studien finanziert. Von meinem Vater habe ich außerdem den Forschergeist geerbt. Mit ihm kann ich abenteuerliche Gedankenexperimente über die Grenzen der Wissenschaft vollführen. Von meiner Mutter habe ich die Zielstrebigkeit. Ihre hohen Wertvorstellungen haben mich geprägt und sind mit ein Grund, dass mir ökologische und gesellschaftspolitische Fragen ein großes Anliegen sind.

Das Projekt "Dissertation" ist sehr zeitintensiv. Mein Freund Johannes hat meine häufige Diss-bedingte Abwesenheit physischer oder auch nur geistiger Natur und meine gelegentlichen Frustphasen ohne Murren überstanden, wofür ich ihm sehr dankbar bin. Er ist mein künstlerischer Freigeist und mein Lehrmeister in Sachen Gelassenheit.

Meinen Eltern

Otmar

und Johannes

in Dankbarkeit gewidmet

1 Introduction

In rivers lateral structures that extend across the river section have long been an integral part. Two main reasons for the construction of lateral structures can be identified: One is to raise the water level upstream of the structure. The created energy head is used for energy production either as a run-off-river hydro power plant or a diversion hydro power plant. In earlier times lateral structures and diversions were often used to run a mill. The other main reason for lateral structures is a direct consequence of the straightening of the rivers. Cutting off a bent river section and connecting the up- and downstream end of this section through a straight line steepens the slope, increases velocities and shear stresses and leads to the erosion of the river bed. To avoid this, the original slope was eventually kept when straightening a river. The shorter straight section left a residual height that had to be overcome. This was achieved by constructing vertical drops. Lateral structures, whether they are used for energy production or overcoming a residual height due to the straightening of the rivers, interrupt the continuity of the rivers for aquatic animals. Using lateral structures to fix a cross sectional profile might have further reasons: to raise the surface water level as a means to raise the ground water level or to conduct discharge measurements. The object of the latter is to have a consumption curve so that one can relate the measured water depth directly to the discharge.

Up until the 1980ies ecological aspects were not a crucial point in the planning and construction of a hydro power plant (HPP). Neither was this the case in river engineering and flood protection measures. Slowly but scarcely ecological aspects began to matter in the western societies. The growing ecological consciousness eventually manifested in nature conservation laws on national and transnational levels. In Austria nature conservation laws are defined on a state level. There are nine different laws, one for each federal state. In Styria the first nature conservation law came into effect in 1976. Carinthia was the last to enact nature conservation laws in 2002. Nature conservation laws are also defined on a European level. Amongst other directives, the members of the European Union have to fulfill the Water Framework Directive (WFD, 2000). These directives have to be incorporated into national law. The objectives of the Water Framework Directive include the aim to achieve “good chemical and ecological status” for surface water bodies by 2015. The ecological status is defined by biological parameters such as the composition and abundance of benthic invertebrate and fish and by hydromorphological requirements, e.g. “the undisturbed migration of aquatic organisms and sediment transport” (WFD 2000).

Austria’s surface waters have a good chemical status but have shortcomings with respect to the ecological status mainly because of the lateral structures that interrupt the continuity of the rivers. According to the Austrian river basin management plan there are 28.000 lateral structures in Austria’s rivers that are not passable for fish and other aquatic animals. About 10 % of these lateral barriers are HPPs. While newly built HPPs nowadays must provide a fishway there are lots of older HPPs where this is not the case.

In order to ameliorate the fish passability, fishways have to be built to bypass HPPs. Other non fish-passable lateral structures (typically: vertical drops) have to be replaced by fish-passable ramps.

Traditional block ramps with slopes typically in the range of 1:10 and steeper often do not provide fish passability because the water velocities are very high on such ramps. Besides there is the danger that the ramp dries up at low discharges. Flat-sloped ramps with lower velocities along the ramp and

low-flow channels that prevent the ramp from drying up are therefore becoming more and more popular.

This thesis deals with a new ramp type, the so-called “meandering ramp”. The meandering ramp is a special kind of step-pool ramp. The steps of the ramp are alternately inclined to the left and right bank, thus inducing a meandering flow at low discharges. Due to the lateral inclination of the steps, the flow concentrates in a small part of the cross sectional profile at low discharges. It is the aim of this thesis to derive practical design guidelines for the construction of the ramp.

This thesis is inspired by the ideas of Viktor Schaubberger (1885 – 1958), an Austrian forest warden, who had gained a high reputation for his well functioning economic timber-floating systems, one of which is described in the *Review of World's Forestry* (Heske, Shepard 1937). His timber-floating systems took advantage of secondary flow by means of very small submerged vanes in the channel. He was an astute observer of nature rather than an academic theorist. “Comprehend and copy nature” - one of his basic principles - remained unheard in a time when people strived to control and dominate nature. Nowadays this principle is the motto of modern bionic. At Schaubberger's time though, many rivers were straightened and regulated. Schaubberger was a keen fighter against such an unnatural treatment and may well be regarded as one of the first ecowarriors. About 20 of his ideas were patented. The patents concerning river engineering prove that he had an understanding of spiral flow, a concept which, due to the complexity of its theory, has not long been an issue in engineering science.

2 Scope of the Thesis

2.1 Scope

It is the aim of this thesis to derive practical design guidelines for meandering ramps on the basis of theoretical considerations (chapter 3), a physical model test for a specific meandering ramp (chapter 4), a basic flume test on characteristic flow regimes on step-pool sequences (chapter 5) and field measurements at an existing meandering ramp (chapter 6). These design guidelines are provided in chapter 7.

As long as not stated otherwise SI units are used throughout the thesis. Where possible, the notation is standardized: the variable y (with or without subscripts) refers to water depths, the variable h (with or without subscripts) refers to heights of a structure, e.g. ramp height, height of end sill, etc.

2.2 Limitations

The influence of the tailwater level is not investigated. In the basic flume test the worst case, i.e. no influence of the tailwater, is assumed. This thesis does not provide a scour criterion, although mobile bed experiments were performed for a specific meandering ramp (chapter 4). These results, however, are only valid for a rather complex ramp geometry and an individual grain size distribution. A quantitative generalization of the results is not permissible.

While this thesis focuses on hydraulic and sedimentological processes, the ramp also has ecological implications. Indeed, effects on ecological quality can be expected from the substantial depth and flow variations induced by the meandering ramp. These variations are commonly regarded as indicators of ecological quality in rivers (WFD, 2000, Annex 5, p. 39) and are a known key control on the self-cleaning capacity of a running water ecosystem. An experimental approach using bedforms of different heights showed that regions of differing depth and velocity host different types of microbial communities. Thus, an increased variation of depth and flow supports an increased microbial biodiversity. Increased biodiversity translates into a higher capacity of microbes to deal with natural resources or pollutants, thereby increasing important ecosystem functions such as the self-cleaning capacity (Singer, Besemer et al. 2010).

2.3 Basics

This chapter provides some fundamentals that are often used throughout the thesis in a nutshell.

2.3.1 Particle Size Distribution

A key property of sediments in rivers is their particle size distribution. A very common method to determine (estimate) the particle size distribution is the so-called sieve-analysis: a sediment sample is poured into a column of sieves of different mesh sizes (coarsest mesh atop). In doing so the sediment sample is partitioned into grain size classes as defined by the mesh size of two adjacent sieves. The cumulative mass fraction (in percent) of each grain size class is displayed on a semi-log chart (Figure 2.1). According to the Austrian standard Ö B 4412 mesh sizes are: 0.063, 0.125, 0.25, 0.5, 1, 2, 4, 8, 16, 31.5, 63 mm, respectively.

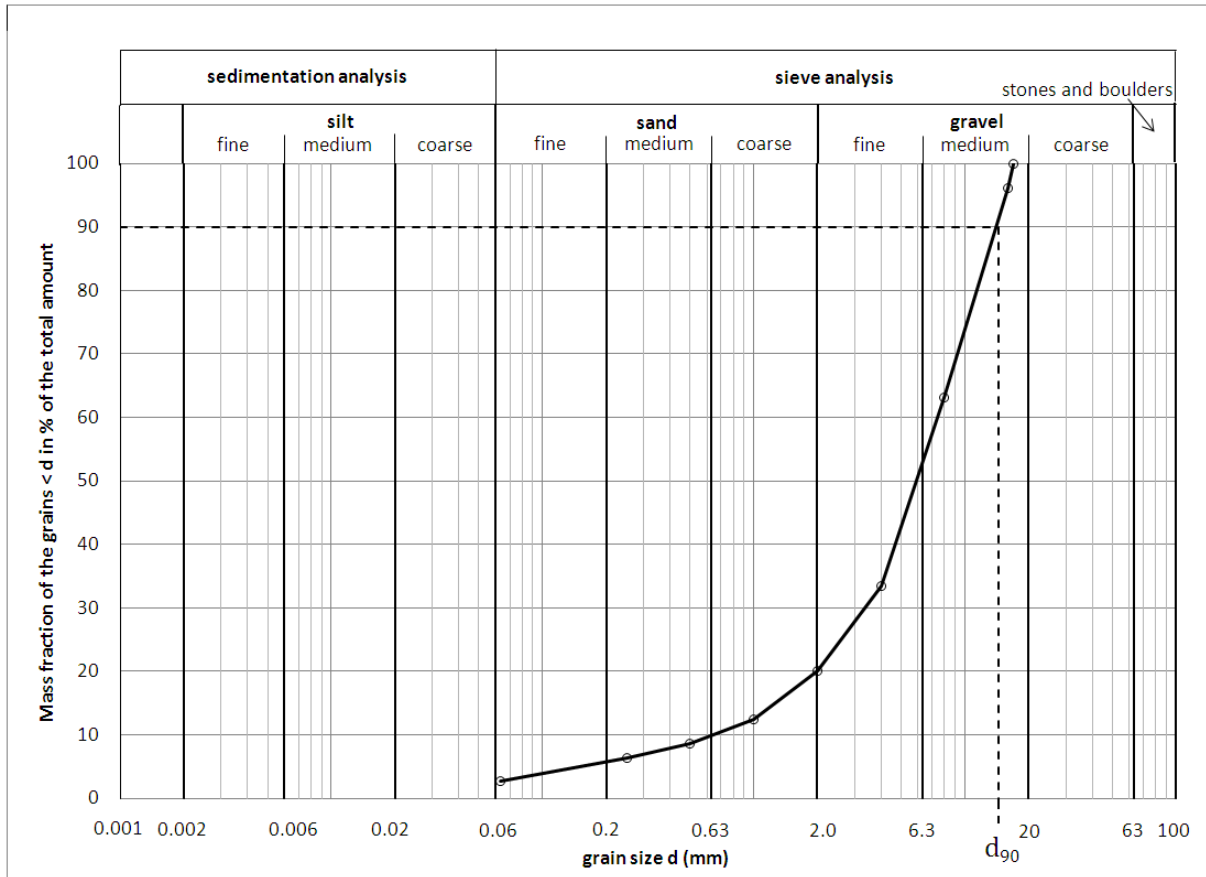


Figure 2.1 Example of a particle size distribution of gravel, characteristic diameter d_{90} indicated by dashed line

The particle size distribution allows for the determination of characteristic diameters d_{xx} and the mean diameter d_m of a sediment sample.

Characteristic diameter d_{xx}

Grain size diameter such that xx % of the sediment sample is finer

2-1

Mean diameter

$$d_m = \sum_{i=1}^{n-1} \Delta p_i \cdot \bar{d}_i$$

2-2

n , Δp_i and \bar{d}_i denote the number of grain size classes of the sieve analysis, the mass fraction of the grain size class i and the mean diameter of the grain size class i , respectively. Another property of a sediment sample is the non-uniformity parameter U . Two approaches are common to calculate the non-uniformity parameter.

Non-uniformity parameter (ÖNORM, DIN)

$$U_{60} = d_{60}/d_{10}$$

2-3

Non-uniformity parameter

$$U_{84} = \sqrt{d_{84}/d_{16}}$$

2-4

In German literature this non-uniformity parameter is typically denoted by U (for “Ungleichförmigkeits-zahl”). In English publications the Greek symbol σ is widely used instead.

2.3.2 Filter Criterion

The Austrian soil engineer Karl von Terzaghi (1883-1963) provides empirical rules for the design of a filter used to protect a hydraulic structure (concrete dam, weir, rock-fill dam, cofferdam) against erosion induced by seepage. Typically a filter layer coarser than the bed material is designed to protect the structure. The filter layer shall be designed such that it is impermeable for the finer base material. After years of practical design and laboratory experiments Terzaghi finally came up with an empirical formula to design the filter layer which was first published at the 2nd International Congress on Large Dams held at Washington in 1936 (Fannin 2008):

$$\text{Filter Criterion Terzaghi} \qquad 4 \cdot d_{85,b} > d_{15,f} > 4 \cdot d_{15,b} \qquad \text{2-5}$$

d_{xx} denotes the characteristic grain diameter, the subscripts b and f denote the base and the filter material, respectively.

3 Literature Review

3.1 Lateral Drop Structures

There are two main reasons for lateral drop structures in rivers. One is to raise the headwater level in order to use the increased energy head for energy production. The other reason is to overcome drops that are - if man-made – a direct consequence of river straightening. As the original slope was usually kept when straightening a river, the resulting shorter thalweg left over a residual height.



Figure 3.1 Straightening of the river Aist in Schwertberg, Upper Austria: course of the river 1867 (left) and today including old course of the river in red (right); data from GIS Upper Austria

Figure 3.1 illustrates the river Aist in Schwertberg, Upper Austria, in the year 1867 (slope about 0.5 %) and today. The river bend of 1867 has been straightened meanwhile. The bend from point A to B had a length of 550 m, the straightened section from A to B today has a length of 377 m. Assuming that the straightened section has the same slope as the curved section, then there remains a residual height of 0.87 m.

3.1.1 Components of a Lateral Drop Structure

A lateral structure for raising the head water level and a structure for overcoming a residual height have a lot in common. Each structure consists of three main parts:

1. Drop crest
2. Drop area
3. Stilling basin

The more the crest protrudes from the original bed level the higher the raise of the headwater. Depending on the design of the drop area, the flow might separate from the structure as a jet. The tailwater level determines whether the jet is submerged or aerated. Typically there are subcritical flow conditions upstream and downstream of the drop area. Unless the tailwater level is extremely high there are supercritical flow conditions along the drop area so there are two flow transitions from subcritical to supercritical to subcritical along the structure. A common definition of the effectiveness of a drop structure is the occurrence of the described flow transitions (see chapter 3.5.1, page 60).

Due to the steepness of the drop area the kinetic energy is very high. The excess energy height compared to the energy level of the tailwater section has to be dissipated in a stilling basin

downstream of the drop area. The stilling basin has to be designed such that the hydraulic jump takes place within this zone.

3.1.2 Historical development

Until the Second World War Germany had played *the* leading role in hydraulics. Already during the war the United States took over the leadership role. In the field of drop structures they developed standards that are still valid today or influence further development (Hager 1993).

Early works on drop structures are empirically based. The systematic investigation of different designs of drop structures was not yet an issue (Hager 1993). Keutner defines flow conditions on both sloping drops (Keutner 1937b) and vertical drops (Keutner 1937a). For sloping drops Keutner distinguishes between an undular jump, $1 < y_1/y_2 < 1.7$ (Figure 3.2a) and a hydraulic jump with an immersion jet ("Tauchstrahl") and a surface roller where $y_1/y_2 > 1.7$ (Figure 3.2b). For vertical drops Keutner lists four types of flow regimes: drop with supercritical tailwater (Figure 3.2c), drop with hydraulic jump where jet impinges the tailwater (Figure 3.2d), submerged drop with an undular jump (Figure 3.2f.), submerged drop with an immersion jet and a surface roller (Figure 3.2e). He suggests the design of a drop such that submerged conditions occur. If the drop height exceeds 50 cm he recommends a stilling basin made of concrete or flagstone to keep the costs of maintenance low. He concludes that general design criteria for drops are not possible.

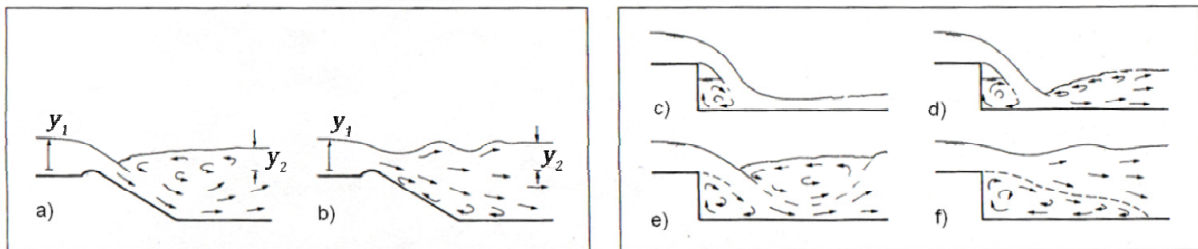


Figure 3.2 Hydraulic jump characteristics for drop structures (Figure a), b) in: Keutner 1937b, Figure c)-f) in: Keutner 1937a)

Feuerhake (1957) gives some practical examples of vertical drops but no design rules.

Rand (1955, 1956a, 1956b) investigates vertical drops with a subcritical headwater and an aerated jet. He distinguishes between a non-submerged and a submerged tailwater, respectively.

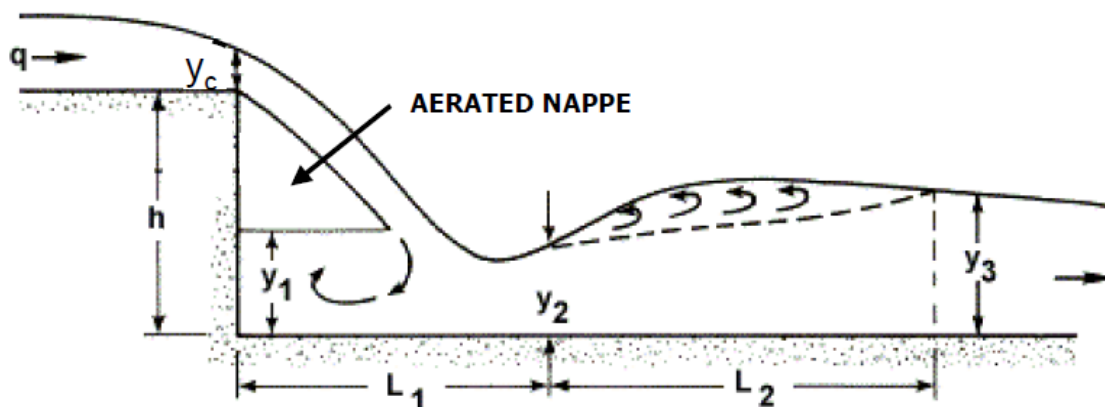


Figure 3.3 Straight Drop Spillway (Rand 1955)

He gives relations between independent variables such as drop height and discharge and dependent variables e.g. water depths or length from the drop wall to the location where the jet impinges the tailwater. He also gives the length of the hydraulic jump from momentum balance considerations.

In the USA Morris and Johnson (1943) were one of the first to give design rules for a vertical drop including a stilling basin.

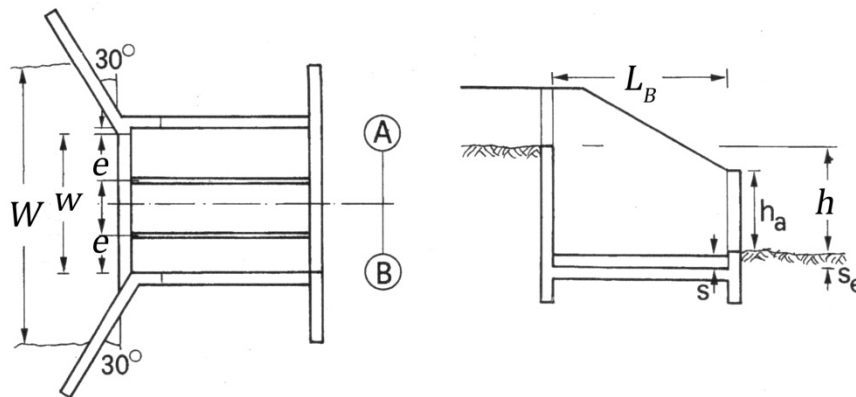


Figure 3.4 Vertical Drop with Stilling Basin (Morris, Johnson 1943)

The drop structure consists of a linearly narrowing inlet, the vertical drop section and a stilling basin with longitudinal sills and a transverse end sill. The linearly narrowing inlet is achieved by wing walls which form a 30 degree angle with the vertical drop section. The length of the basin L_B is the sum of two components: distance from the drop wall to the point where the surface of the upper nappe strikes the stilling basin floor and length of the hydraulic jump, i.e. $L_B = L_1 + L_2$ with L_1 and L_2 as in Figure 3.3. The design parameters for the drop structure are the critical depth y_c (referring to the crest width w) and the drop height h , respectively. The drop height h should be at least y_c . Then the length of the stilling basin L_B is given by equation 3-1. The height of the end sill s_e should be half of the critical depth y_c . If $\beta = W/w > 1$ (W being the inlet width), longitudinal sills of height $s = 3/4s_e$ and a spacing of $e = 0.29 \cdot (\tanh(\beta - 1))^{1/3} \cdot b$. The side wing height at the end of the stilling basin h_a has to be at least $2 \cdot y_c$.

Stilling basin length
Morris & Johnson

$$\frac{L_B}{(h \cdot y_c)^{1/2}} = 2.5 + 1.1 \cdot \frac{y_c}{h} + 0.7 \cdot \left(\frac{y_c}{h}\right)^3 \quad 3-1$$

Based on Morris and Johnson, Blaisdell and Donnelly developed the "Inlet Drop Spillway" (Blaisdell, Donnelly 1954, Blaisdell, Donnelly 1955) with a three-sided drop area and an expanding stilling basin to reduce its length. Like its predecessor the stilling basin consists of longitudinal sills. After years of experience in the field they gained the insight that the Inlet Drop Spillway does not always prevent scours downstream of the stilling basin.

3.1.3 The Straight Drop Spillway Basin after Donnelly and Blaisdell

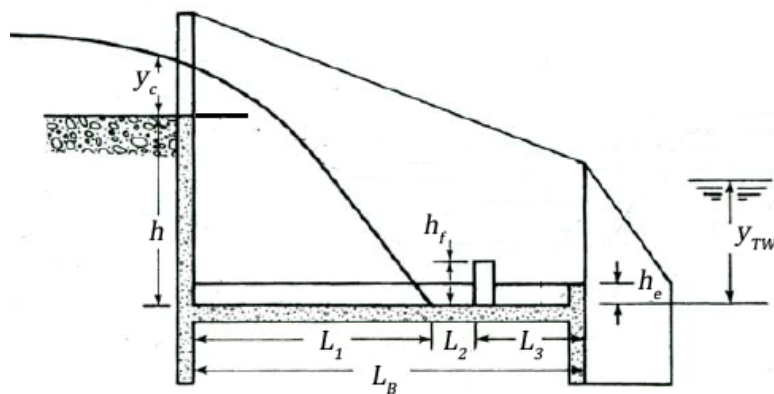
In 1965 Donnelly and Blaisdell present the "Straight Drop Spillway Basin" (Donnelly, Blaisdell 1965, Rand 1965, Donnelly, Blaisdell 1966) where the authors focus on the design of a stilling basin. The basin consists of floor blocks that are laterally aligned. The longitudinal sills are optional in this approach, they are not a hydraulic necessity like this was the case for the "Inlet Drop Spillway". They

might serve as a means to reinforce the structure. The following design criteria are valid under the following conditions:

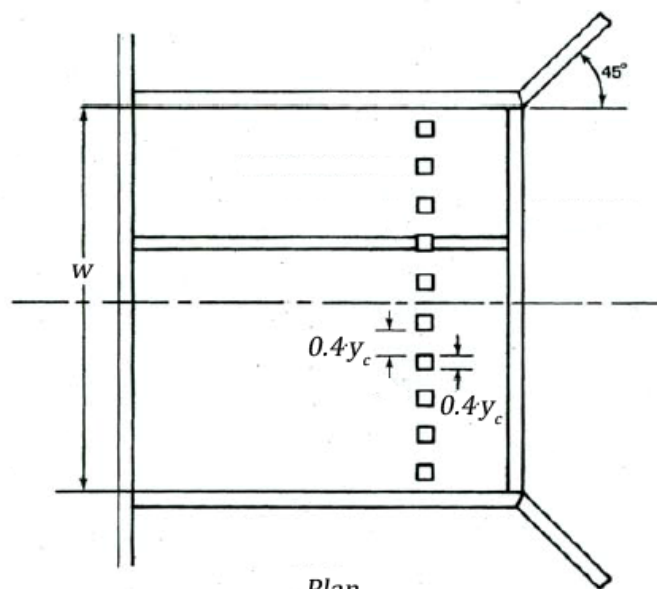
1. Drop height $h < 4.6$ m
2. Relative drop height $h/y_c = 1 \div 15$
3. Crest width $w > 1.5 \cdot y_c$

The length of the basin $L_B = L_1 + L_2 + L_3$ is the sum of three components (Figure 3.5):

- L1. distance from the drop wall to the point where the surface of the upper nappe strikes the stilling basin floor, L_1 the mean of L_f and L_s , where L_f is the horizontal distance from the crest to the point where the upper surface of the free-falling nappe strikes the stilling basin floor. L_s is the horizontal distance from the crest the point where the upper surface of the submerged nappe strikes the basin floor. The tangent at the point of submergence is supposed to be the submerged nappe trajectory.
- L2. length from the point where the surface of the upper nappe strikes the stilling basin floor to the upstream face of the floor blocks
- L3. length from the upstream face of the floor blocks to the end of the basin



Section at center line



Plan

Figure 3.5 Straight Drop Spillway Basin (Donnelly, Blaisdell 1965)

$$L_f/y_c = \left(-0.406 + \sqrt{3.195 - 4.386 \frac{h}{y_c}} \right)$$

$$L_s/y_c = \frac{\left(0.691 + 0.228 \left(\frac{L_t}{y_c} \right)^2 - \left(\frac{h}{y_c} \right) \right)}{0.185 + 0.456 \left(\frac{L_t}{y_c} \right)}$$

where L_t is the horizontal distance from the spillway crest to the point at which the surface of the upper nappe plunges into the tailwater and y_t is the vertical distance from the crest to the tailwater surface.

$$L_t/y_c = \left(-0.406 + \sqrt{3.195 - 4.386 \frac{y_t}{y_c}} \right)$$

L_2 is L_3 were determined by a series of physical model tests:

$$L_2/y_c = 0.8, \quad L_3/y_c \geq 1.75$$

One would guess that the most critical case for a stilling basin is the lowest tailwater level that may occur. Donnelly and Blaisdell report an interesting finding however: if the tailwater level is near the spillway crest then the nappe might land beyond the end of the stilling basin causing scour. Therefore a stilling basin that works well for low tailwater levels may fail (because it's too short) for high tailwater levels. Donnelly and Blaisdell observed this effect in their model tests as well as in the field and give the following explanation: Assuming a horizontal inflow from the headwater the trajectory of the free falling nappe is parabolic. This is due to the vertical velocity component accelerating under the effect of gravity. As soon as the nappe hits the tailwater the effect of gravity vanishes. The submerged nappe follows the tangent of the point of the parabola at which the nappe enters the tailwater. The lower the tailwater level, the higher the slope of the point where the free falling nappe hits the tailwater. When the tailwater level is about two thirds the critical depth above the crest, the nappe becomes a surface nappe, floating on or near the surface water. A surface nappe doesn't endanger the bed downstream of the stilling basin. In other words, two thirds the critical depth above the crest level is the maximum tailwater depth that affects the length of the stilling basin.

On the other hand it is certainly true that the tailwater level must be sufficiently high so that the water leaving the stilling basin doesn't plunge and scour the downstream bed. Donnelly and Blaisdell found the minimum tailwater level to be

$$y_{TW} \geq 2.15 \cdot y_c$$

The floor blocks height correlates with the bank erosion while the height of the end sill has a primary effect on the depth of the bed scour. Donnelly and Blaisdell give the following design criteria for the floor block height h_f and the end sill height h_e respectively.

$$h_f = 0.8 \cdot y_c, \quad h_e = 0.4 \cdot y_c$$

The width and spacing of the floor blocks should be $0.4 \cdot y_c$ with an admissible variation of $\pm 0.15 \cdot y_c$. The floor blocks should cover 50 to 60% of the basin width.

Although the concept of the Straight Drop Spillway Stilling Basin is more than 40 years old by now, the given design rules have not changed and this structure is still recommended today, for example in the guidelines “Hydraulic Design of Energy Dissipators for Culverts and Channels” of the U.S. National Highway Institute (Thompson, Kilgore 2006) or in the “Guidelines for Stabilizing Waterways” (<http://ldm.melbournewater.com.au/>).

3.1.4 The U.S.B.R. Short Stilling Basin III after Peterka

In his comprehensive investigation on nine different energy dissipating structures Peterka (1964) begins with defining four kinds of hydraulic jumps classified by values of the Froude number. y_1 and y_2 refer to the supercritical water depth before the jump and the conjugate subcritical depth after the jump, respectively. If the Froude number lies in the range of 1 to 1.7 there are only small surface ruffles that disturb the smoothness of the water surface. For Froude number between 1.7 and 2.5 surface rollers develop (Figure 3.6a.). Froude numbers ranging from 2.5 to 4.5 produce oscillating jets that appear at the bottom and at the surface at no fixed period (Figure 3.6b.). These oscillations may travel downstream for some kilometers causing serious damage to banks and armoring structures. Hydraulic jumps at Froude numbers between 4.5 and 9 are characterized by a highly energy dissipating stable jump that is not very sensitive to tailwater variations (Figure 3.6c.). Hydraulic jumps with Froude numbers above 9 dissipate extremely much energy (up to 85%), but the concurrence of surface rollers and the high-velocity jet creates a rough wavy surface that may proceed further downstream (Figure 3.6d.).

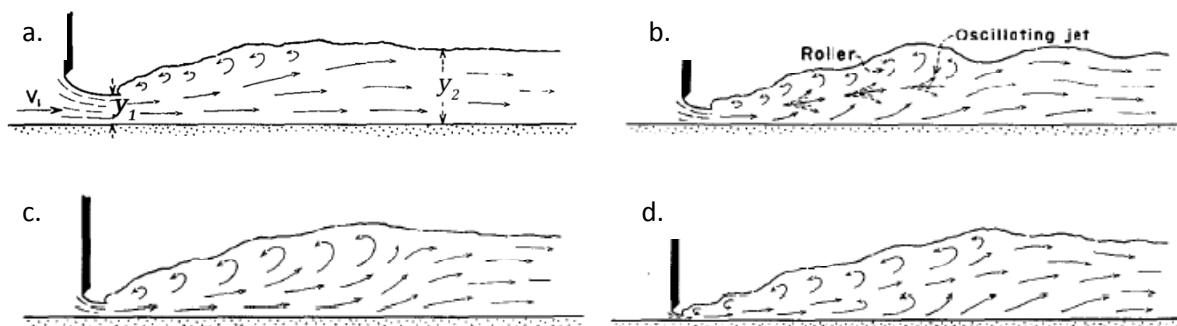


Figure 3.6 Hydraulic Jump characteristic according to different values of the Froude number

Peterka develops design rules for three different stilling basins that gain in complexity:

1. stilling basin with a horizontal apron
2. stilling basin with a horizontal apron with chute blocks and a dentated end sill
3. stilling basin with a horizontal apron, chute blocks, baffle blocks and a (non-dentated) end sill

First Peterka finds that the formula for conjugate depths for a horizontal hydraulic jump derived from momentum considerations also holds true for sloping entering depths (Peterka 1964, Peterka 1964):

$$\frac{y_2}{y_1} = \frac{1}{2} \left(\sqrt{1 + 8Fr_1^2} - 1 \right)$$

Fr_1 is the Froude number entering the jump.

By adding chute blocks and a dentated end sill to the horizontal apron the length of the hydraulic jump and thus the length of the stilling basin reduces about 33 %. By introducing baffle blocks and a solid end sill the length of the basin reduces about 60%. The latter structure will be described in more detail:

The Chute Spillway Stilling Basin III (Peterka 1964) consists of a chute with chute blocks at the toe of the chute, baffle piers in the middle of the basin which are responsible for the main energy dissipation and an end sill for scour control. Velocities at the toe of the chute must not exceed 15.2 – 18.3 m/s (50 – 60 ft/s) and the Froude number should be above 4.5.

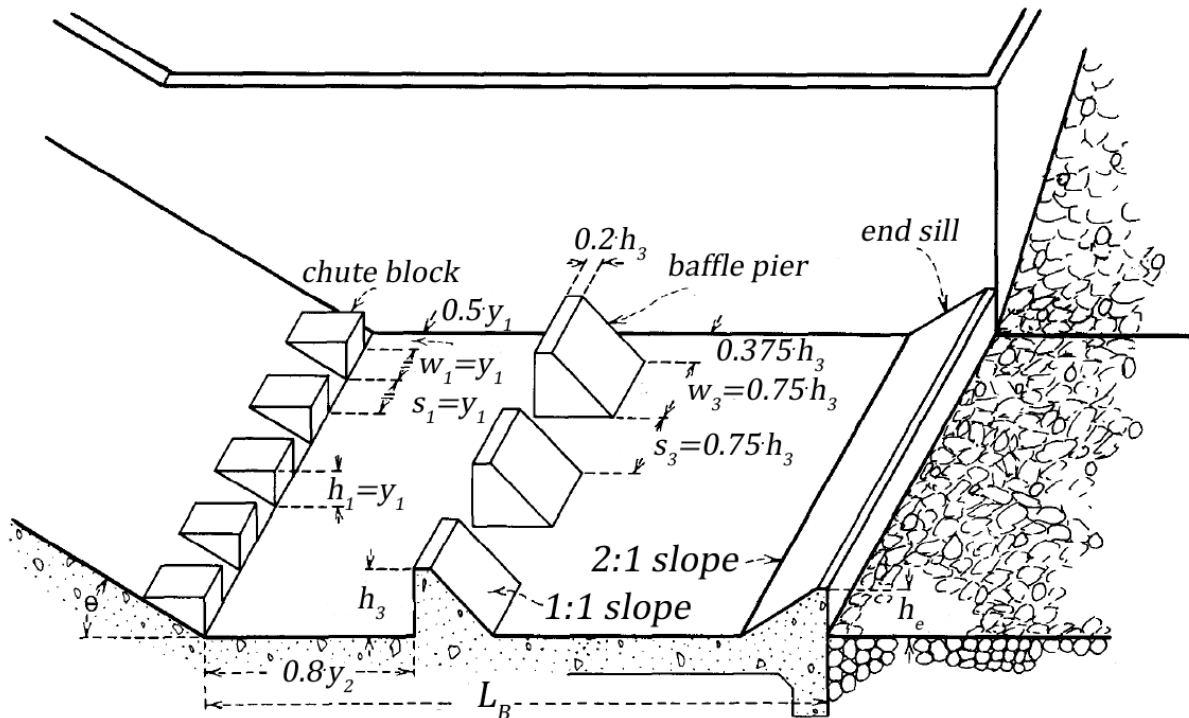


Figure 3.7 Chute Spillway Basin, recommended proportions (Peterka 1964), labels modified by author

Peterka reports that as for the shape of the baffle blocks the vertical upstream face is crucial to gain the desired results, i.e. an almost vertical hydraulic jump just upstream of the baffle blocks and a good energy dissipation. Block “e” and block “f” (Figure 3.8) are equally effective but from a construction point block “f” is preferable. With blocks “c” and “d” the flow tends to jump over the block at an angle of about 45° degrees causing a wavy flow downstream of the blocks. Sharp corners of the pier edges produce eddies that dissipate energy. Even a slight rounding of the baffles (block “g”) reduces the amount of energy dissipation and should therefore be avoided. Small chamfers on the pier edges to obtain a better forming of the concrete are acceptable though. A second row (design “h”) of any of the baffles has little effect. The total baffle width should equal the total spacings. This is in agreement with Donnelly and Blaisdell who state that the floor blocks should cover 50-60% of the basin width (Donnelly, Blaisdell 1965, Rand 1965, Donnelly, Blaisdell 1966).

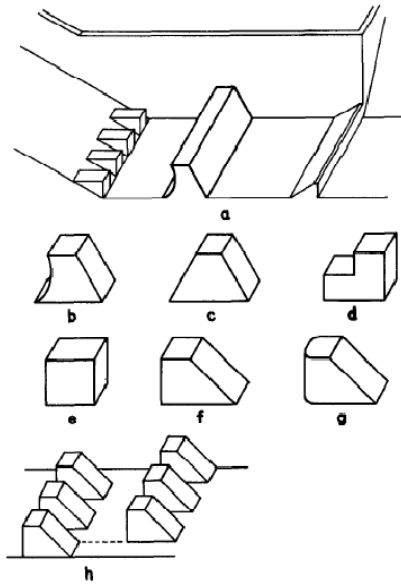


Figure 3.8 Baffle types for chute spillway basin (Peterka, 194)

The design rules (given in Figure 3.7) are given in terms of y_1 and y_2 referring to the water depth entering the jump and the conjugate subcritical depth after the jump, respectively. Baffle pier height h_3 , end sill height h_e and stilling basin length L_B also depend on the design parameters y_1 and y_2 . They are determined by charts which are not plotted here. The reader may refer to (Peterka 1964).

Donnelly and Blaisdell's drop structure consists of similar components as the well known Chute Spillway Stilling Basin III.

3.1.5 The U.S.B.R. Baffled Apron Basin IX after Peterka

The baffled apron is designed for overcoming drops. The sloping apron consists of baffle blocks that lead to a highly turbulent flow that dissipates much energy. The acceleration of the flow is thus prevented and there is no need of an additional stilling basin no matter what the drop height might be. The maximum discharge is $5.6 \text{ m}^3/\text{sm}$ (60 cfs/ft). The design rules apply for slopes between 1:2 and 1:4. The entering velocity should be well below the critical velocity. Ideally the inlet velocity is $v_c - 1.52 \text{ m/s}$ ($v_c - 5 \text{ ft/s}$) where v_c is the critical velocity. If this cannot be achieved a short energy dissipating pool is needed upstream of the chute. The baffled apron is not a device to reduce the velocity of the incoming flow; rather, it is intended only to prevent excessive acceleration of the flow passing down the chute. The lateral velocity distribution should be uniform. The transition from the horizontal inlet to the chute should be rounded to prevent vertical contraction. The radius should be small however. The first row of baffles should be 0.3 m (1 ft) below the crest at maximum. Alternate rows are staggered. The height of a baffle pier h should be $0.8 y_c$. The baffle width equals the spacing width and may range between one and one and a half times the baffle height. Other baffle pier dimensions are not critical. The spacing of two rows (upstream face to upstream face) is twice the baffle height if the slope of the chute is 1:2. For flatter slopes up to 1:4 the vertical distance between two rows should be the same as for the 1:2 slope. At least four rows are necessary to produce the desired turbulent flow (cf. Morris 1969, p31). The side walls should be three times the baffle height.

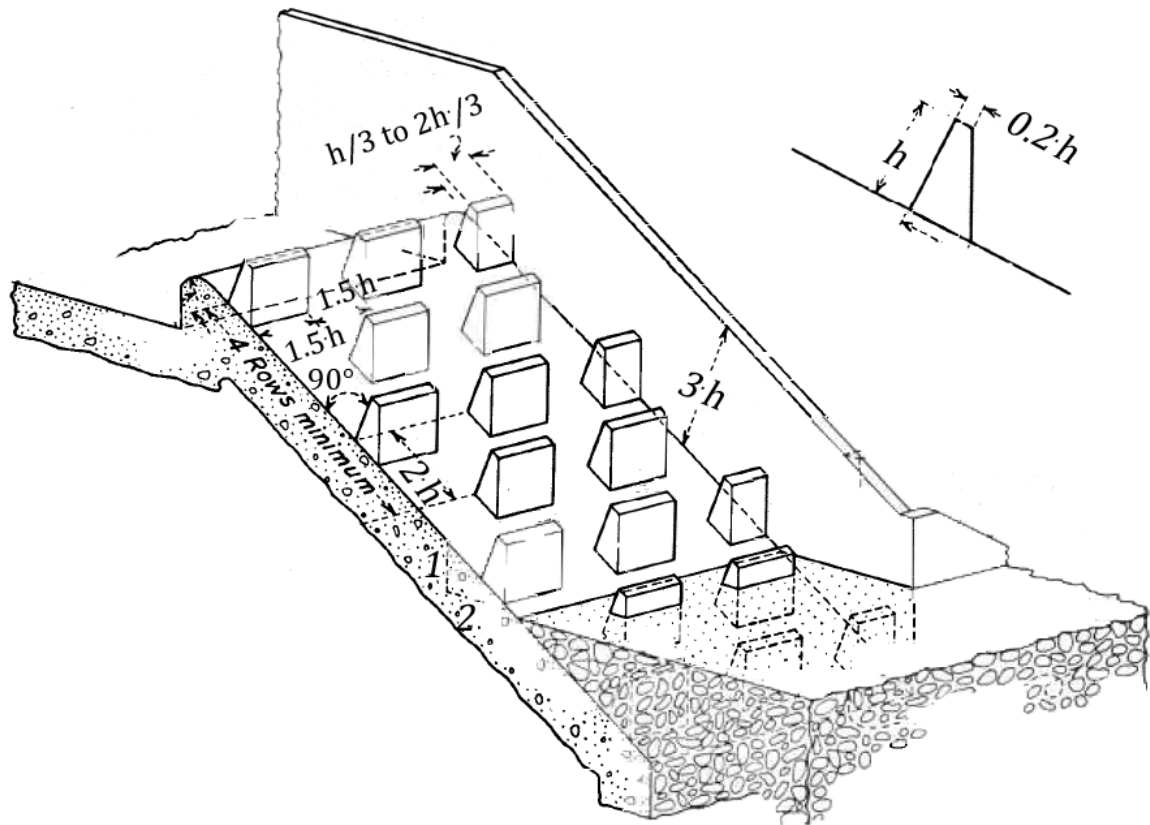


Figure 3.9 The U.S.B.R. Baffled Apron Basin IX, recommended proportions, (Peterka 1964), labels modified by author

In his investigations of the baffled apron basin Peterka measures the water surface levels which show a cascading characteristic. A classification of different flow regimes is not given. This can be found in Peterson & Mohanty (1960).

It is noteworthy that the engineers took advantage of three dimensional effects in the design of drop structures yet the design criteria were derived from one-dimensional considerations.

The U.S.B.R. chute spillway and the baffled apron represent a seamless transition from vertical drop structures (e.g. Keutner 1937b, Rand 1955, Donnelly, Blaisdell 1965) to rough ramps made of big boulders (see chapter 3.3) as the supercritical jet passes over a sloping chute. In fact in the German language concrete spillway chutes are also referred to as “smooth ramps”(Knauss 1976).

3.2 Ramps – historical development

3.2.1 Block ramp after Schauberger

While in the U.S.A. concrete river training structures (e.g. drop structures) were acceptable the engineers of the Alpine region began to develop more ecological structures: Walter Schauberger (a relative to Viktor Schauberger – see Introduction) reports that up until 1951 vertical drop structures were built in the “Alm” river (Figure 3.11, left) which had a high impact on landscape and biology. Fish passes, if built at all, were inefficient. The Austrian engineers W. Schauberger and Riedinger invented the doubly bent block ramp in the beginning of the 1950es (Knauss 1976, Schauberger 1957, Schauberger 1973). Having to redevelop the vertical drop structure in the “Alm” river in Upper Austria, Riedinger suggested to build a rough ramp instead - a new kind of structure made of natural boulders - that he happened to see in the “Isel” river in East Tyrol (Schauberger 1973). Schauberger proposed a doubly bent crest section: a concave arc crest in plan view and a flat parabolic cross sectional profile. The purpose of the double curvature is to prevent bank scour along and downstream of the ramp. He had observed that this kind of doubly bent crest sections at small vertical drops (e.g. in the stream “Gosaubach” in 1940) worked very well so he adopted this idea for the new ramp which later became known as the “Schauberger ramp”. The first Schauberger ramp was built in 1954 in the “Alm” river in Bad Wimsbach (Figure 3.11, right). In Figure 3.11a the dimensions of this ramp are given. Figure 3.11b illustrates the scouring pattern downstream of the ramp after a flood event in 1954 right after the completion of the construction works. The scour is drawn-out and located in the center of the river. There are sediment depositions near the bank areas.

In the Alpine region the “Schauberger ramp” has been well known since its development in the 1950es and is still constructed today.

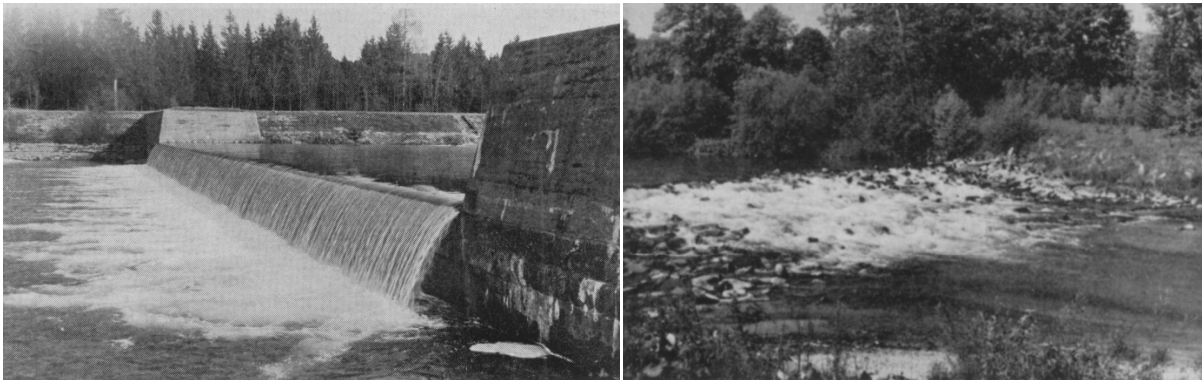


Figure 3.10 Vertical drop in the “Alm” river in 1951, km 5.9, (left) The first Schauberger block ramp in the “Alm” river, km 2.76, in Bad Wimsbach, Upper Austria (right) (see Schauberger 1973)

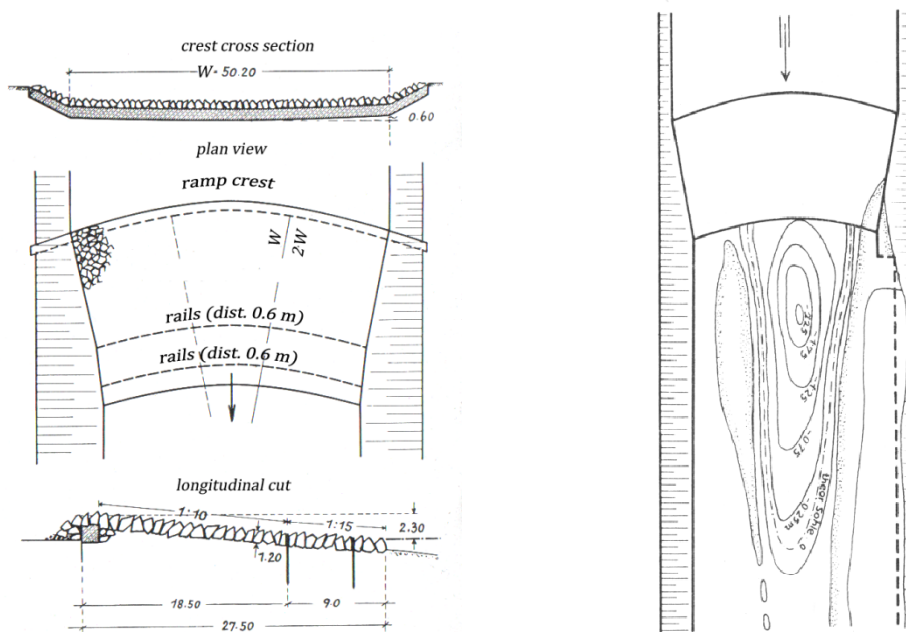


Figure 3.11 The first Schauberger block ramp in the “Alm” river, km 2.76, in Bad Wimsbach, Upper Austria: dimensions in m (left) and scouring pattern downstream of this ramp after a flood event on January 21st 1954 (right, see Garbrecht 1957)

Schauberger summarizes some scientific contributions on block ramps, (e.g. Niel 1960, Garbrecht 1957), and the experience he has gained since the construction of the first Schauberger ramp in Schauberger (Schauberger 1975). The following design rules and recommendations are given:

Design rules

The ramp crest is both bent in plan view and cross section (Figure 3.11, left) concentrating the flow in the centerline and reducing bank erosion (Figure 3.12).

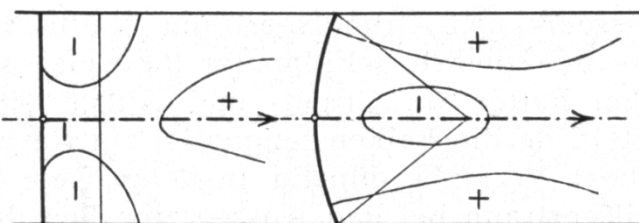


Figure 3.12 Scouring pattern (plan view) for a vertical drop (left) and a doubly bent ramp (right)

- ramp slope $\varphi = 1:10$ (up to $\varphi = 1:8$, if the length of ramp is smaller than the width downstream of the ramp and the width is small)
- ramp toe armed with rails
- scour protection approx. 3-5 m downstream of the ramp toe with boulders, where necessary armed with another rail row
- shape of crest (plan view): circular arc, radius $R = 5/4 W$
- shape of crest cross section: flat parabolic, $W = 16$ m, $h_{xs} = 0.3$ m, $W = 50$ m, $h_{xs} = 0.6$ m
- crest consists of a crest wall with boulders on top casted halfway in concrete
- boulders connect the crest to the upstream bed at a slope of 1:1
- bank slope 1: n along the ramp: 1: 1 to 1: 1.5
- required diameter of boulders $d_s \sim y_m \cdot 10 \cdot \tan \varphi$ (y_m mean flow depth)

- maximum specific discharge: $9 \text{ m}^3/\text{sm}$
- maximum flow depth on crest: 2.7 m

The ramp can also be built in a river bend. In this case the arc crest has to be rotated towards the inner bend.

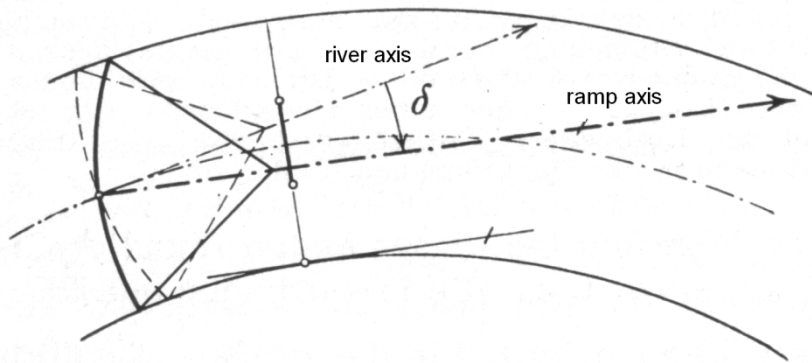


Figure 3.13 Sketch of a Schauberger ramp in a bent river section (plan view)

Recommendations

- Big boulders, preferably granite, densely placed, as rough as possible
- fill up remaining holes with gravel instead of concrete to prevent inhomogeneous settling
- whole ramp has the shape of a flat trough
- expansion of the crest width W to reduce specific discharge, $W = W_1 + 2 \cdot n \cdot h$, where h is the ramp height, W_1 is the tailwater width and $1:n$ is the bank slope.
- transition from the headwater width W_0 to the crest width W within a length of $\sim 2 - 3 \cdot W_1$
- the headwater flow has to be concentrated in the middle of the river, if necessary groins have to be installed to direct the flow towards the centerline (Prof. Simmler) [note of the author: no detailed reference is given by Schauberger as to where and when Prof. Simmler from the "Technische Hochschule Graz" (nowadays "Technische Universität Graz") recommends groins]

Schauberger ramp vs vertical drop structures

Schauberger lists advantages of a block ramp over vertical drop structures:

- integrates well into the landscape
- maintains the character of the water and its biological values
- biological self-cleaning, high air entrainment
- highest economic efficiency (a cost reduction up to 50% over a vertical drop structure)
- fish-passable at all discharges [debatable in the light of today, note of the author]
- if the river bed downstream degrades, the ramp can be extended further downstream easily
- insensitive to coarse sediments, easy maintenance
- deposition of sediments upstream of the ramp up until the crest, therefore protection of the upstream banks

Concluding remarks

One crucial element of the Schauberger ramp is the doubly bent crest cross section (Figure 3.11, left) which causes scouring only in the center line region of the river and not in the bank area (Figure

3.14). Schauberger explains this scouring pattern by “very slowly rotating, sediment depositing eddies” (trans. “sehr langsam drehende, geschiebeablagernde Randwalzen”, (Schauberger 1975))

Niel (1960) reports however, that for very high discharges the scours downstream of the ramp change their location from the river centerline to the banks. The scour patterns look like in Figure 3.16a. Niel, following (knowingly?) Garbrecht’s argument (3.2.2, 1st paragraph), explains that for high water depths the flow separation from the banks downstream of the ramp is not pronounced enough as to produce a bank-protecting dead-water zone. He further concludes that rivers having a small width are not able to produce bank-protecting dead-water zones even for low discharges. In these cases a reinforced riprap protection of the banks and the bed downstream of the ramp is recommended rather than a doubly bent cross section.

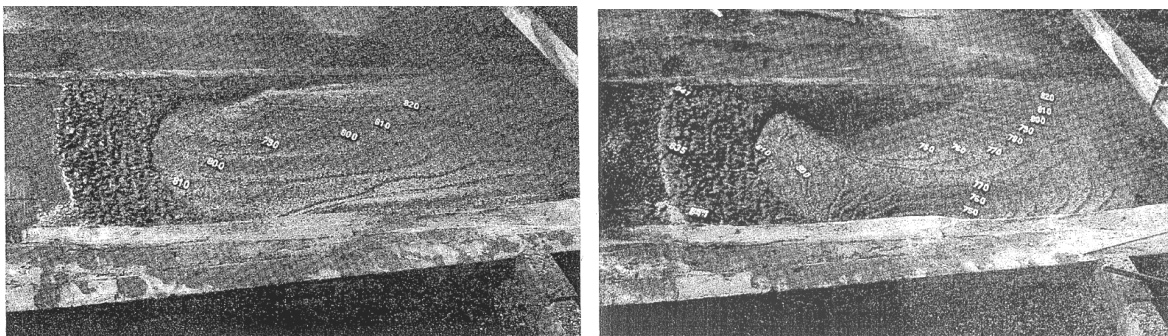


Figure 3.14 scour patterns for different ramp submergences (Niel 1960): $q = 7.7 \text{ m}^3/\text{s}/\text{m}$ (left), $q = 22 \text{ m}^3/\text{s}/\text{m}$ (right)

The current view contradicts Schauberger’s statement of the fish passability of block ramps. Assuming a specific mean flow of $0.3 \text{ m}^3/\text{sm}$, a ramp slope of 1: 10 and a block diameter of 1.0 m, then the mean velocity calculated after Scheuerlein (equation 3-4) becomes 1.7 m/s, which is too high for almost any fish species.

3.2.2 Further developments

Garbrecht (1957) analyzes the cause of the scours near the banks downstream of vertical drops, chutes and ramps and suggests Schauberger’s doubly bent crest section as a means to reduce or even prevent scouring near the banks. According to Garbrecht the reason for the scouring of the banks is the flow detachment from the banks. Eddies with a high rotational speed and a low-pressure zone in its center lead to scours near the banks that are deeper than those of the undisturbed center flow. In a series of model tests he comes to the following conclusions: bank scouring can be reduced by either preventing flow detachment or boosting it. Boosting the flow detachment means generating eddies (with a vertical axis) that serve as a bank-protecting water cushion. This can be achieved by concentrating the flow to the river center as this is the case for the doubly bent Schauberger ramp. For weirs with a steep chute and a stilling basin an arc crest does not lead to such a distinct a flow concentration in the river center because the chute is much steeper and therefore shorter than the ramp. Garbrecht suggests a connecting bank between the upstream and the downstream banks (Figure 3.15b) instead of a wing wall (Figure 3.15a).

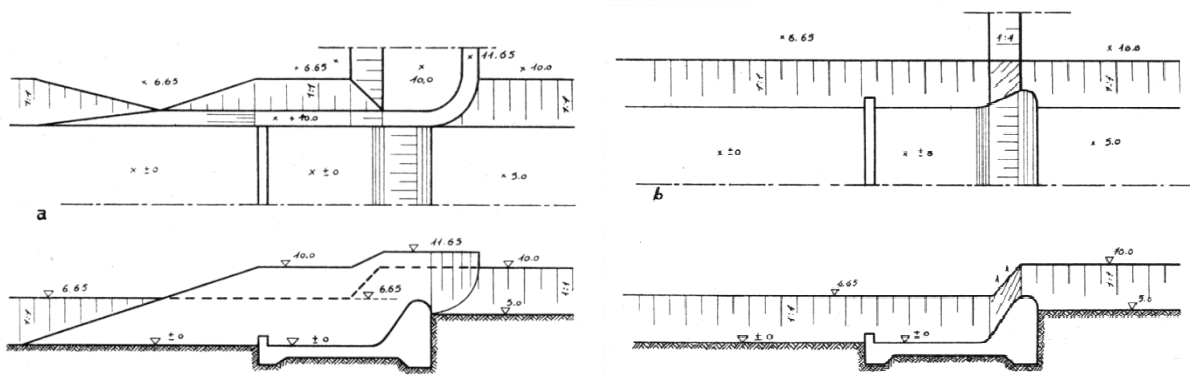


Figure 3.15 weir with wing walls (left), weir with connecting banks (right)

The construction of the end sill and the type of connection between the weir and the banks has a great effect on the scouring pattern as can be seen in Figure 3.16.

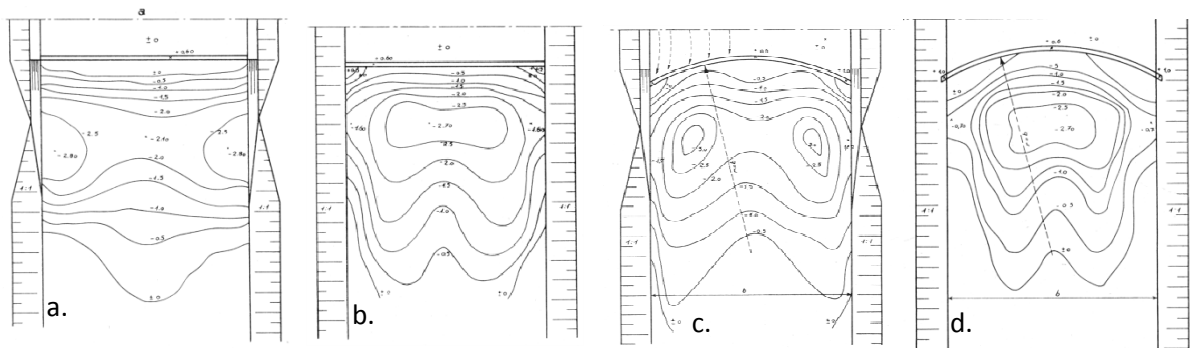


Figure 3.16 scouring pattern for different end sill constructions: a. straight end sill with wing wall b. straight end sill with connecting banks c. doubly bent end sill with wing walls d. doubly bent end sill with connecting banks (Garbrecht 1957)

Gunzelmann (1966) reports two well functioning practical examples, one of a Schauburger block ramp and one example of a chute with a stilling basin made of boulders both situated in the mountain stream Flecht in Germany. As for the block ramp he reports that the narrowing of the crest cross section to prevent lowering of the headwater would not have been necessary: The roughness of the ramp is high enough to prevent scouring of the upstream region of the ramp. For the chute (slope 1:3) he suggests a pear-shaped stilling basin to give space for the lateral recirculation zone. Gunzelmann therefore follows Garbrecht's argument of boosting the flow separation zone. Gunzelmann restricts the applicability of boulder structures to regions where boulders can be found in the vicinity of the construction site to be economical. The natural river sediment must be either cohesive enough or big enough to resist the occurring pressures in between the big boulders.

Höss (1968) describes a concrete spillway with a narrowing trapezoidal inlet made of steel to prevent scour upstream of the chute. The chute itself is doubly curved and has a maximum slope of 45° . The stilling basin is pear-shaped in plan view with the maximum expansion at the toe of the chute. It has a trough-shaped longitudinal section and a horizontal cross section. A scour protection made of boulders downstream of the stilling basin is recommended. Design rules are given in terms of y_{HW} and h referring to the maximum upstream approach depth and the drop height respectively. L_C , L_B , y_T and r refer to (horizontal) length of chute, length of stilling basin, depth of trough and radius of curved chute, respectively.

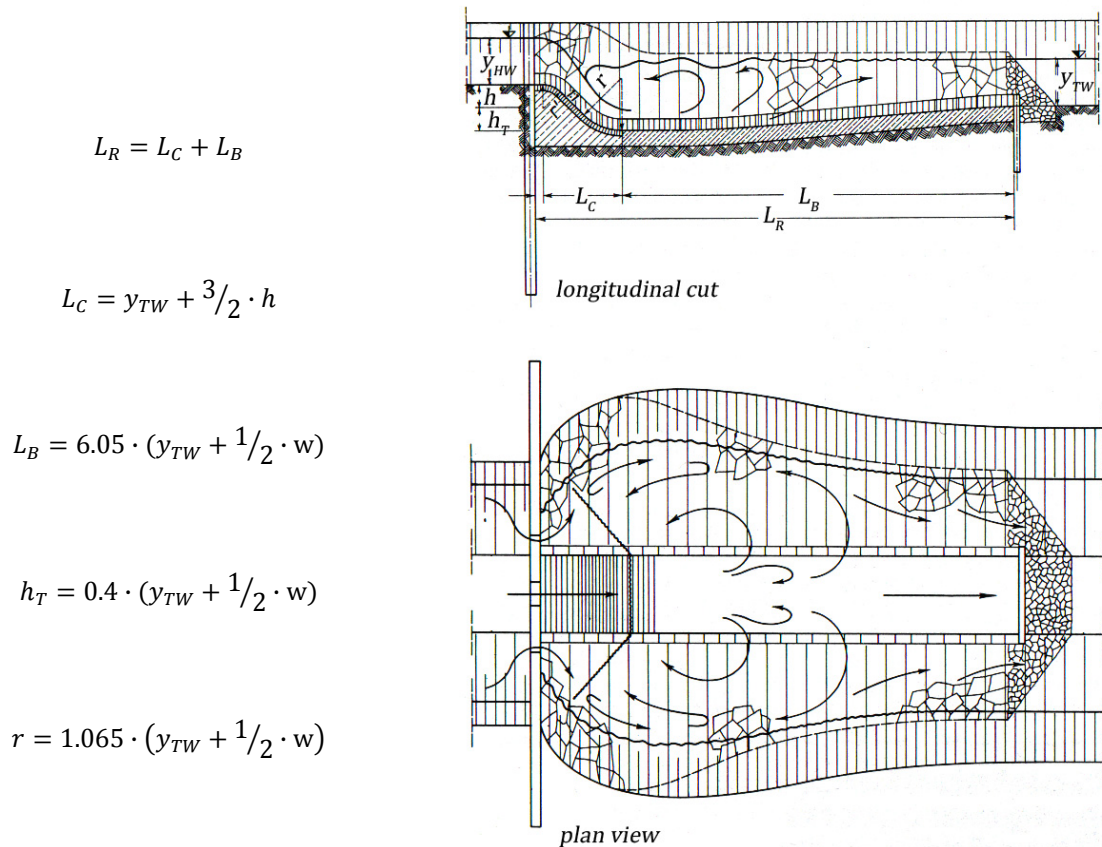


Figure 3.17 Smooth ramp after Höss (1968)

In Drobir & Simmler (1970) the results of a physical model test of a block ramp for the stream “Feistritzbach” in Styria, Austria are presented. In accordance to W. Schauberger’s design recommendations the crest has an arc shape in plan view with a radius of $5/4 B$. The slope is 1:10. The height of the ramp is 3.3 m. Unlike Schauberger’s recommendation the crest cross section is a compound profile. The aim was to find a solution where the scour downstream of the ramp does not endanger the stability of the ramp. Altogether 9 ramp designs were tested. The maximum discharge was $200 \text{ m}^3/\text{s}$ (full scale). Assuming that most of the discharge runs off within the main channel having a width of 9.8 m, this gives a specific discharge of approximately $20 \text{ m}^3/\text{sm}$. Depending on the design variant, maximum discharges from 84 to $140 \text{ m}^3/\text{s}$ ($q = 8.4 - 14.3 \text{ m}^3/\text{sm}$) were possible to prevent scouring of the downstream bed. These results support Niel’s upper limit for specific discharge of block ramps of $9 \text{ m}^3/\text{sm}$. Again in accordance to Niel, Drobir states that an undular hydraulic jump downstream of the ramp is desired and that a jump with distinct surface rollers is critical as it produces more scour downstream at the toe of the ramp (c.f. Niel 1960). For the sake of completeness it is mentioned that the final design suggestion was a vertical drop with an arc crest and a stilling basin.

3.3 Block ramps

3.3.1 Supercritical Flow Over a Rough Bed After Scheuerlein and Hartung

In a series of physical model tests Scheuerlein (1968) derives a friction formula for steep rough channels with a high relative roughness and supercritical normal flow conditions. Based on the quadratic resistance law for fully turbulent flows the mean flow depth y_m can be determined by the following equation:

$$\frac{1}{\sqrt{\lambda}} = -3.2 \log \left(c \cdot \frac{k}{4y_m} \right) \quad 3-2$$

λ ... friction factor

$$k \approx \frac{d_s}{3} \text{ mean roughness height}$$

$$c = \sigma(1.7 + 8.1 \cdot \Phi \cdot \sin \alpha)$$

σ ... air content (density of water-air mixture / density of water)

Φ ... coverage (height of roughness element / distance between two roughness elements)

α ... slope angle

Equation 3-2 is valid for slopes ranging from 1:8 to 1:15. The diameter of the roughness blocks d_s should be in the range of 0.6 – 1.2 m. Combining equation 3-2, the continuity equation $q = v_m \cdot y_m$ and the universal law of turbulent flow in open channels (equation 3-3) yields equation 3-4.

$$v_m = \frac{1}{\sqrt{\lambda}} \sqrt{2 \cdot g \cdot 4 \cdot y_m \cdot \sin \alpha} \quad 3-3$$

$$q = \sqrt{8 \cdot g \cdot I} \cdot y_m^{3/2} \cdot \log \left[\left(\frac{12}{c} \cdot \frac{y_m}{d_s} \right)^{3.2} \right] \quad 3-4$$

To derive a criterion for the maximum discharge to guarantee the stability of the steep rough channel Hartung & Scheuerlein (1970) balance the forces which act on a single boulder that is idealized as a sphere with diameter d_s and get the maximum permissible velocity v_{cr} :

$$v_{cr} = 1.2 \cdot \sqrt{\frac{2 \cdot g \cdot (\rho_s - \rho_w)}{\rho_w}} \cdot \sqrt{d_s} \quad 3-5$$

Please note: The maximum permissible velocity v_{cr} must not be confused with the critical velocity v_c which corresponds to the critical depth y_c at the flow transition from subcritical to supercritical flow.

Substituting equation 3-5 into equation 3-4 gives:

$$q_{cr} = 5 \cdot \sqrt{\frac{2 \cdot g}{\sigma} \cdot \frac{\rho_s - \rho_w}{\rho_w}} \cdot (\sigma - 1 + 1.3 \cdot \sin \alpha) \cdot \sqrt{d_s^3} \cdot \sqrt{\cos \alpha} \quad 3-6$$

Setting $\sigma = 1$ which is tolerable for slopes below 20 %, and $\sin \alpha \approx \tan \alpha = I$ and $\cos \alpha \approx 1$, respectively, simplifies equation 3-6 to

$$q_{cr} = 6.5 \cdot \sqrt{2 \cdot g \cdot \frac{\rho_s - \rho_w}{\rho_w} \cdot I} \cdot \sqrt{d_s^3} \quad 3-7$$

3.3.2 Design rules for block ramps after Knauss

Knauss (1979) takes further Hartung and Scheuerlein's investigations. Multiplying equation 3-5 with the safety factor 0.9 and taking $\rho_s = 2.7 \text{ t/m}^3$ yields:

$$v_{cr} = 6.235 \cdot \sqrt{d_s} \quad 3-8$$

Substituting equation 3-8 into equation 3-4, the latter equation can be approximated by the simpler equation

Design Rule

$$q_{cr} = \left(1.2 + \frac{0.064}{I} \right) \cdot d_s^{3/2} \cdot \sqrt{g} \quad 3-9$$

Equation 3-9 is valid for slopes ranging from 1:6 to 1:15. Some basic transformations lead to the supercritical uniform water depth y_{cr} for the maximum permissible discharge q_{cr} and the critical depth y_c at the ramp crest, respectively:

$$y_{cr} = 0.502 \cdot C \cdot d_s \quad 3-10$$

$$y_c = \sqrt[3]{\frac{q_{cr}^2}{g}} = C^{2/3} \cdot d_s \quad 3-11$$

Knauss determines the minimum required ramp height to ensure uniform flow conditions at the toe of the ramp (thus assuming a free jump that is not influenced by the tailwater). In his model tests he has found the friction coefficient to be $\zeta = 0.32$ (with $\zeta \cdot v^2/2g$ being the friction loss). Applying the energy equation to the ramp crest section and the cross section of the ramp where uniform flow has been established yields the minimum required ramp height:

$$h_{min} + 1.5 \cdot y_c = y_{max} + (1 + \zeta) \cdot \frac{v_{max}^2}{2g} \quad 3-12$$

$$h_{min} = (0.502 \cdot C - 1.5 \cdot C^{2/3} + 2.615) \cdot d_s \quad 3-13$$

For slopes from 1:6 to 1:15, h_{min} ranges from $1.4 \cdot d_s$ to $1.2 \cdot d_s$ respectively. For the standard ramp slope of 1:10 the minimum required ramp height is $h_{min} = 1.3 \cdot d_s$. If the tailwater depth t_{TW} is such that a submerged jump develops over the ramp, Knauss gives the following equation for the minimum required ramp height for a ramp slope of 1:10:

$$h_{min} = t_{TW} - d_s = t_{TW} - \frac{2}{3} \cdot y_c \quad 3-14$$

Equation 3-14 is in accordance with Franke (1970) (chapter 3.5.1).

The Froude number at the toe of a non-submerged ramp ranges from 1.91 to 2.2 (see also chapter 3.5.1). Therefore high bed shear stresses downstream of the ramp are to be expected. The river bed of the tailwater section has to be protected accordingly.

Knauss states advantages of a rough ramp over a steep smooth chute. The large roughness and the flatter slope of the rough ramp stabilize the flow and weaken the undular surface. The protection of the river bed of the tailwater section can thus be designed shorter.

3.3.3 Design rules for block ramps after Whittaker / Jäggi

Whittaker & Jäggi (1986) derive design rules for “loose block ramps” and “standing block ramps”. The former consist of multiple layers of boulders whereas the latter are comprised of a single layer of standing boulders, i.e. the longest axis is aligned vertically. If necessary the ramp must be built onto a filter layer and / or can be protected by rails. Loose block ramps can be built without dewatering of the construction site and are thus more economic than standing ramps which in turn resist higher specific discharges. The costs of a block ramp depend on some parameters like the availability of the boulders and the construction method but are about half of the costs of a concrete drop structure on average. Moreover the ramp is a flexible structure that allows settlements of the boulders. Whittaker and Jäggi mention also the advantage of the passability of the block ramp for fish and invertebrate which becomes more important because of a growing ecological consciousness. One major goal of their investigations is the detection of failure mechanisms on block ramps. They remark that the drop down curve upstream of the ramp is a serious matter as it causes scours, yet they do not consider this complex phenomenon in their investigations. Whittaker and Jäggi consider Schauburger’s design recommendations only as a rule of thumb. Besides the maximum specific discharge of $q = 9 \text{ m}^3/\text{sm}$ is too limiting.

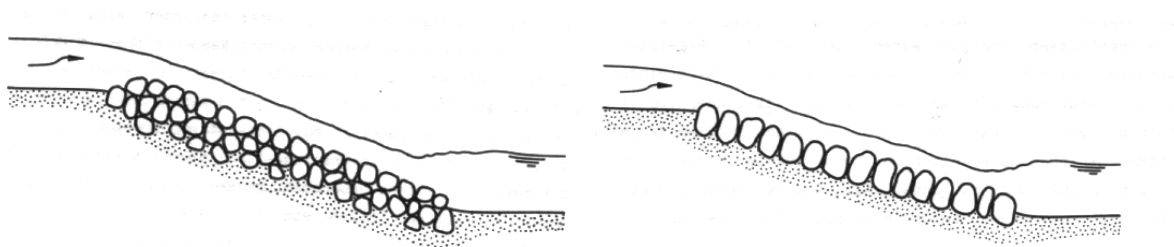


Figure 3.18 “loose ramp (left) and “standing ramp” (right) after (Whittaker, Jäggi 1986)

Whittaker and Jäggi use the Shields’ approach to determine the incipient motion of the boulders in which the dimensionless critical shields parameter τ_{*c} is almost constant for fully rough turbulent flows.

$$\text{critical shields parameter} \quad \tau_{*c} = \frac{\tau}{\rho \cdot g \cdot (s-1) \cdot D} = \frac{\rho \cdot g \cdot y \cdot I}{\rho \cdot g \cdot (s-1) \cdot D} \quad 3-15$$

$$\text{Manning-Strickler equation} \quad v = k_{st} \cdot y^{2/3} \cdot I^{1/2} \quad 3-16$$

$$\text{Strickler value to equivalent sand roughness} \quad k_{st} = \frac{a}{D^{1/6}} \quad 3-17$$

$$\text{continuity} \quad q = v \cdot y \quad 3-18$$

In the above equations τ (N/m^2), s (-), ρ (kg/m^3), g (m/s^2), D (m), y (m), I (-) and k_{st} ($\text{m}^{1/3}/\text{s}$) denote shear stress, relative density of sediment, density of sediment, gravity, characteristic sediment diameter, water depth, slope of the ramp and the Strickler value, respectively. Inserting equations 3-15 to 3-17 into equation 3-18 yields

$$q = a \cdot (t_{*c} \cdot (s - 1))^{5/3} \cdot D^{3/2} \cdot I^{-7/6} \quad \text{3-19}$$

Equation 3-19 can be rewritten in dimensionless form

$$\frac{q}{((s - 1) \cdot g \cdot D^3)^{1/2}} = \frac{a \cdot t_{*c}^{5/3} \cdot (s - 1)^{7/6}}{\sqrt{g} \cdot I^{7/6}} \quad \text{3-20}$$

In equation 3-17 the constant a is defined as 21, 24 and 26 by Strickler, Raudkivi (1967) and Meyer-Peter Müller (1948), respectively. Raudkivi suggests to take D_{65} as characteristic diameter D . Whittaker and Jäggi adopt this proposal. In their model test they find that if D_{65} is the sieve diameter and D is the longest axis of a block then the ratio $D/D_{65} = 1.55$ is constant. The following design rule is given for both loose ramps and standing ramps, where $D/D_{65} = 1.55$:

$$\text{Design Rule, direct erosion} \quad \frac{q}{\sqrt{g \cdot D_{65}^3}} = 0.257 \cdot \sqrt{s - 1} \cdot I^{-7/6} \quad \text{3-21}$$

The coefficient 0.257 is achieved for combinations:

$$a = 21, t_{*c} = 0.1 \text{ or } a = 26, t_{*c} = 0.087 \quad \text{3-22}$$

Whittaker and Jäggi report good agreement of their results to Platzer (1983) whereas their maximum discharges are significantly higher than those of Knauss. They explain the difference with the simplified balance condition Knauss adopts from Scheuerlein and Hartung.

Equation 3-21 yields a maximum discharge for a given block diameter such that the blocks of the ramp are not entrained by the flow. Whittaker and Jäggi investigate also the entrainment of bed material in between the blocks. The question of the stability of an armor layer (the block ramp can be considered as such) subject to a finer layer below has been investigated by several researchers. Raudkivi & Ettema (1982) approach this question stepwise. They analyze

- Case 1. the stability of an individual exposed grain with diameter D_1 placed on a layer of finer sediments with diameter D_2
- Case 2. the stability of a layer of grains with diameter D_1 placed on a layer of finer sediments with diameter D_2
- Case 3. the stability of non-uniform sediments

Raudkivi and Ettema distinguish four subregions for Case 1:

Case 1.1. $v_* < v_{*,i}$ and $v_* < v_{*,2}$ - no movement at all

Case 1.2. $v_{*,i} < v_* < v_{*,2}$ - the overpassing condition: Only the coarse grain moves along of the fine layer (because as it is a single exposed grain it moves before finer layer below starts to move)

Case 1.3. $v_{*,2} < v_* < v_{*,i}$ - the armoring or embedding condition: Only the fine sediments below the coarse grain move, thus causing the coarse grain to sink into the fine layer

Case 1.4. $v_* > v_{*,i} > v_{*,2}$ - all grains are in motion,

where

v_* (m/s) shear velocity of the flow, defined as $v_* = \sqrt{\tau/\rho}$

$v_{*,1}$ (m/s) critical shear velocity for the incipient motion of D_1 -grains on D_1 material

$v_{*,2}$ (m/s) critical shear velocity for the incipient motion of D_2 -grains on D_2 material

$v_{*,i}$ (m/s) critical shear velocity for the incipient motion of an individual D_1 -grain on a D_2 -layer.

The critical Shields parameters $\tau_{*,c}$, $\tau_{*,c,1}$, $\tau_{*,c,2}$, and $\tau_{*,c,i}$ are defined analogously.

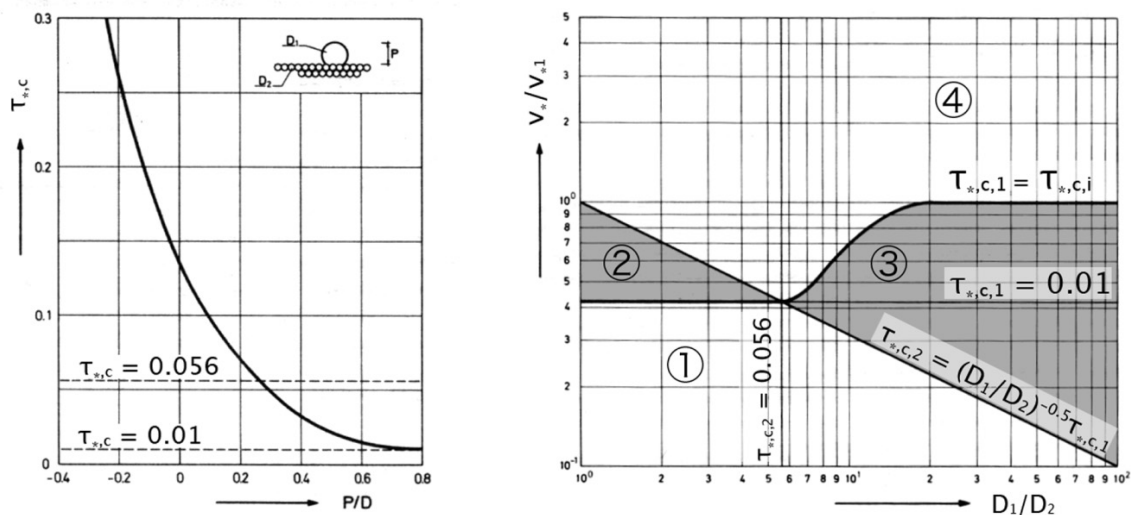


Figure 3.19 variation of $\tau_{*,c}$ in dependence of the protrusion of the grain (Fenton, Abott 1977) (left), boundaries of overpassing and embedding conditions (Raudkivi, Ettema 1982) (right), figures slightly modified after (Whittaker, Jäggi 1986)

Raudkivi and Ettema apply the findings of Fenton & Abott (1977) on how the critical Shields parameter changes as the exposure of a grain varies (Figure 3.19, left). The described cases above occur in dependence of D_1/D_2 (Figure 3.19, right and Table 3.1).

case 1.2 overpassing condition	transition between cases 1.2 and 1.3	Case 1.3 embedding condition
$1 < \frac{D_1}{D_2} < 100 \cdot \tau_{*,c,2} \approx 5.6$	$5.6 < \frac{D_1}{D_2} < 17$	$\frac{D_1}{D_2} > 17$

Table 3.1 Overpassing and embedding condition of a single exposed D_1 -grain, case 1

For case 2, that of the stability of a single particle thick armoring layer, Raudkivi and Ettema find (with $v'_{*,1}$ being the critical shear velocity for the entrainment of a D_1 -particle when $P \approx D_1$)

Case 2 unstable armor layer	Case 2 transition	Case 2 stable armor layer
$1 < \frac{D_1}{D_2} < 100 \cdot \tau_{*,c,2} \approx 5.6$	$5.6 < \frac{D_1}{D_2} < 17$	$\frac{D_1}{D_2} > 17$
$v'_{*,1} < v_* < v_{*,1}$	$v_* < v_{*,2}$ and $v_*/v_{*,2} > v_{*,i}/v_{*,1}$	$v_* < v_{*,i}$

Table 3.2 Stability of a single particle thick armor layer, case 2

Whittaker and Jäggi confirm the boundaries of the ratio of D_1/D_2 in their investigations. They report however that in one of their experiments with multiple layers of armor D_1 -particles (another description of a loose ramp) the bed material below is entrained even if $D_1/D_2 = 27$ is well in the range for a stable armor layer. They do not specify though whether or whether not the condition $v_* < v_{*,i}$ holds.

The necessary condition for a stable armor layer (Table 3.2) as proposed by Raudkivi and Ettema and as adopted by Whittaker and Jäggi is based on their experimental finding, that armor layers that tend to embed are more stable than those for which the particles of the coarse layer are entrained. In contrast, Terzaghi took the opposite approach when he developed his filter criterion (equation 2-5): His coarser top layer was designed to prevent the base material from being washed out. Another difference is that Terzaghi considers well-graded sediments whereas Raudkivi and Ettema investigated uniform materials.

Based on regression analysis Whittaker and Jäggi derive two design rules that yield the maximum discharge such that the erosion of the bed material is prevented. One criterion (equation 3-23) is given subject to the height of the block layer h_{lay} , equation 3-24 is subject to the areal coverage β (in t/m^3). D denotes the equivalent sphere diameter of the blocks, d_{65} represents the characteristic diameter of the bed material (Figure 3.20). The dimensionless variables s and n denote the relative sediment density and the porosity of the block layer, respectively.

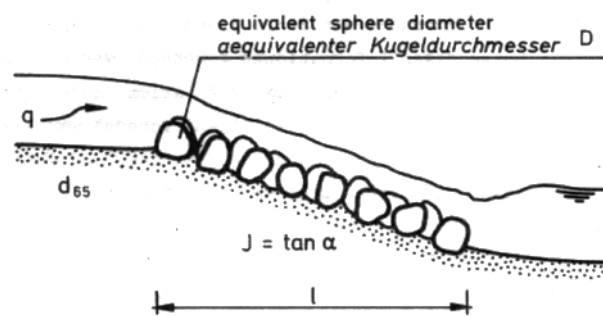


Figure 3.20 Definition sketch for the parameters used in the analysis of the effects at the interface (after Whittaker, Jäggi 1986)

Design Rule, erosion of bed material, height of the layer

$$q = 14.47 \cdot ((s - 1) \cdot (1 - n) \cdot h_{lay})^{2.35} \frac{\sqrt{g}}{l^{1.9} \cdot D^{0.85}} \cdot \left(\frac{d_{65}}{D}\right)^2 \quad 3-23$$

**Design Rule, erosion of
bed material, areal
coverage**

$$q = 14.47 \cdot \left(\frac{\beta \cdot (s - 1)}{\rho_s} \right)^{2.35} \cdot \frac{\sqrt{g}}{I^{1.9} \cdot D^{0.85}} \cdot \left(\frac{d_{65}}{D} \right)^2 \quad 3-24$$

Table 3.3 Maximum discharge to prevent erosion of bed material

The above design rules are valid for slopes $I > 0.02$ and $h_{lay} > 0.2 \cdot (n - 1) \cdot D$ and $\beta > 0.323 \cdot D$, respectively. The maximum discharge q increases with the thickness of the block layer d_{lay} resp. with the areal coverage β . The maximum discharge increases also with the ratio of the bed material and the blocks d_{65}/D . In the latter case it is advisable to increase d_{65} instead of decreasing D because the block diameter is proportional to the maximum discharge regarding the direct erosion design rule 3-21. On the other hand, according to Table 3.1 and Table 3.2, if $D/d_{65} > 5.6$, then individual blocks tend to roll or glide over the ramp thus initiating a failure of the ramp. The embedding process ($D/d_{65} > 17$) is preferable because in this case the ramp usually does not get destroyed but might sink into the bed material. Whittaker and Jäggi recommend that for $D/d_{65} \leq 6$ the areal coverage β has to be in the range of $1.44 \cdot D - 1.6 \cdot D$. They assume that similar restrictions are necessary for $6 \leq D/d_{65} \leq 10$. The parameters of the ramp have to be chosen with care.

Substituting $D = 0.8$ m, $d_{65} = 0.055$ m, $I = 0.1$, $\beta = 1.152$ into equation 3-24 yields a maximum specific discharge $q = 9$ m³/ms (as this is the case for for Schauburger block ramps, chapter 3.2.1).

Eventually Whittaker and Jäggi report that scours downstream of a ramp in combination with erosion of blocks have been a frequent cause of failure (Figure 3.45). So they identify criteria for scouring processes downstream of a block ramp. A crucial issue is the velocity v_1 at the toe of the ramp, which depends on the roughness of the ramp. Assuming normal flow conditions the roughness of the flow can be approximated by $v_1/v_* \approx 2 \cdot y_1/D_{65}$ for $0.3 \leq y_1/D_{65} \leq 7$, where y_1 denotes the water depth. v_1 can therefore be expressed as

$$v_1 = g^{0.2} \cdot q^{0.6} \cdot I^{0.2} / D_{65}^{0.4} \quad 3-25$$

Another important issue is the tailwater depth which has an influence on the position of the hydraulic jump. If it is located on the ramp, the scours are small. If it is downstream of the ramp and lowers the tailwater level such that the lowest row of block on the ramp is not submerged then the scours are deep.

Given a minimal submergence of the lowest region of the ramp the scour depth can be estimated by the scour depth criterion of Tschopp-Bisaz which has been slightly adopted by Whittaker and Jäggy.

Maximum scour depth $S = 1.31 \cdot q^{0.5} \cdot v_1^{0.5} - 7.125 \cdot d_{90} \quad 3-26$

S and d_{90} denote the scour depth the characteristic diameter of the bed material. To prevent scours downstream of the ramp Whittaker and Jäggy suggest three measures for scour protection:

- Measure 1. a horizontal layer
- Measure 2. a steep ramp
- Measure 3. rails and sheet pile walls

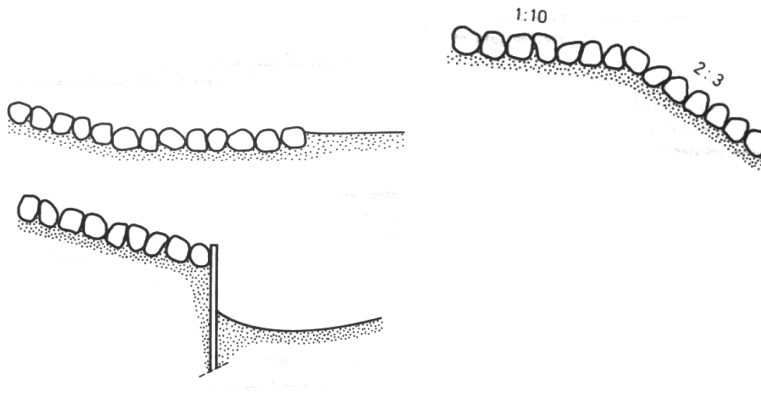


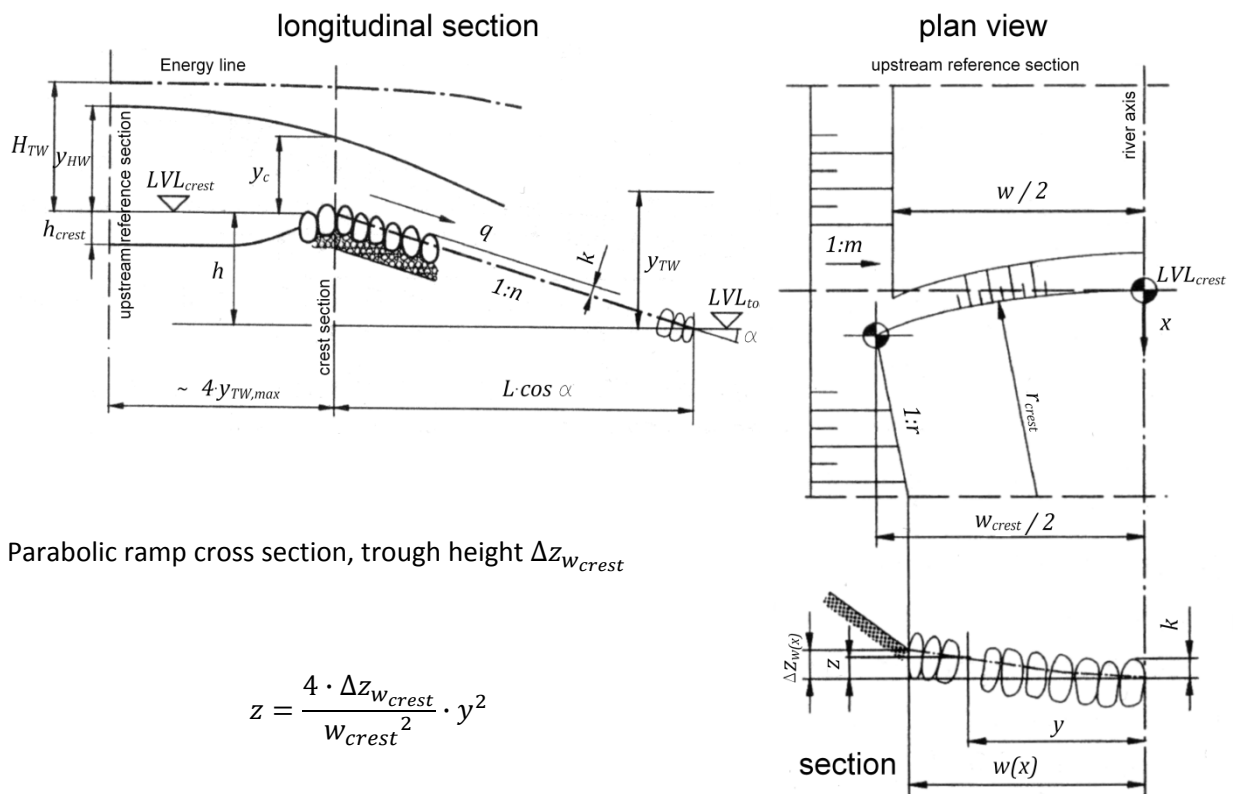
Figure 3.21 Scour protection measures (Whittaker, Jäggi 1986)

The horizontal layer must be such that the blocks may embed into the bed material, i.e. $D/d_{65} > 17$. Otherwise the scour problem is only shifted further downstream. For measure 2 the flow must separate at the edge of the steep ramp. If rails are used to enhance the stability the ramp is not flexible any longer because if some blocks settle the rails could be exposed and eventually collapse which in turn would lead to a failure of the ramp.

In their investigations Whittaker and Jäggi identify three failure mechanisms (see also 3.5.2, pp.64): direct erosion of blocks, erosion of bed material, scours downstream of the ramp. They present design rules (equations 3-21, 3-23, 3-24 and 3-26) to prevent these causes of failure.

3.3.4 Design Rules for Trough-Shaped Block Ramps After Platzter

(Platzer 2000) investigates a trough-shaped block ramp (Figure 3.22). The design criteria he derives include the scour protection downstream of the ramp. Ramp and scour protection have to be regarded as one unit. The design rules are based on a 1-dimensional analysis. Due to the trough-shaped cross sectional profile the flow is highly 3-dimensional. Platzter regards the 3-dimensionality by introducing appropriate coefficients in the 1D-equations. According to Platzter it is necessary to take into account the varied flow conditions. Assuming uniform flow yields inappropriate results. The functioning of the ramp depends on an accurate construction. Only then the design rules can be used as a prediction tool. Platzter mentions that air entrainment matters only for small discharges. For the stability of the ramp, higher discharges are relevant. In the latter case the air entrainment can be neglected. The design rules are given under the assumption of subcritical flow up- and downstream of the ramp.



Parabolic ramp cross section, trough height $\Delta z_{w_{crest}}$

$$z = \frac{4 \cdot \Delta z_{w_{crest}}}{w_{crest}^2} \cdot y^2$$

Conical shape parameter r in ramp plan view

$$r = \frac{w_{toe} - w_{crest}}{2 \cdot L \cdot \cos(\alpha)}$$

Figure 3.22 sketch of a trough-shaped ramp (modified after Platzer 2000)

w_{crest} and w_{toe} denote the width of ramp crest and ramp toe, respectively. In his investigations Platzer introduces the "Froude number of the specific discharge" which contains the roughness k of the ramp as characteristic length. k is defined as one third of the vertical axis of the blocks.

$$Fr_q = \frac{Q}{(w_{crest} \cdot \sqrt{g \cdot k^3})} = \frac{q}{(\sqrt{g \cdot k^3})} \quad 3-27$$

The trough-shaped block ramp can be used within certain ranges of ramp slope I , relative ramp height h/k , relative ramp width w/k , trough height $\Delta z_{w_{crest}}$, Froude number of the specific discharge Fr_q and type of block layer (loose or standing).

Ramp slope

The ramp slope may range from 1:8 to 1:15. Flatter ramps allow higher specific discharges and yield smaller scour depths, while steeper ramps dissipate more energy. Ramps with a slope of 1:8 will typically be installed in mountain streams. According to Platzer a ramp slope flatter than 1:10 is

economically unacceptable. The choice of the ramp slope depends also on ecological aspects and has to be adjusted to the type of the water body and the aquatic animals. As a general rule ramps should be steep in steep streams and flatter in mildly sloped rivers.

Ramp height

The minimum required ramp height must provide a sufficient tailwater depth (given by a hydrograph) to ensure the formation of a hydraulic jump at the toe of the ramp. If this is not the case the toe of the ramp has to be lowered, i.e. the ramp height increases. The minimum required ramp height has to guarantee a good energy dissipation, which implies a twofold flow transition subcritical – supercritical – subcritical. Platzter claims the latter at least for the bed building discharges, which are (according to Platzter) characterized by $Fr_q \approx 2.5$. The limiting condition for a flow transition is reached if the tailwater depth equals the ramp height plus the critical depth. The minimum required relative ramp height is given by equation 3-85, where I_{TW} denotes the tailwater slope in per mill.

$$\frac{h}{k} \geq \frac{7}{(I_{TW} + 1)^{1.1}} + \frac{(I_{TW} - 2)}{2.5} \quad 3-28$$

If the relative ramp height is smaller than proposed by the above equation then the ramp no longer serves as an energy dissipating structure but as a bottom protection structure. Platzter also reasons about the maximum ramp height. The longer (higher) a ramp the higher is the probability of entrapments that reduce the stability of the ramp. The relative maximum ramp height must not exceed

$$\frac{h}{k} \leq \frac{75}{n} \quad 3-29$$

where $1:n$ is the ramp slope. Moreover, standing ramps should exceed 3 m only in well-justified exceptional cases. In all other cases a cascade of ramps is preferable. The distance between the ramps should be at least the length of the scour of the upstream ramp. Platzter's argument is reverse to Whittaker and Jäggi who reason that once normal flow conditions are reached along a ramp it is advisable to have one long ramp instead of several shorter ramps. As the velocity at the toe of the ramp determines the magnitude of the scour, splitting one ramp into several means having to deal with the same scour several times instead of only once (Whittaker, Jäggi 1986).

According to Platzter the ramp height for loose ramps should in general be in the range of the minimum ramp height as given by equation 3-28. For mildly sloped rivers the ramp heights should not be too high in order to ensure the passability of the ramp for weak-swimming fish species.

If no scour protection is provided downstream of the ramp the maximum permissible relative ramp height is given by equation

$$\text{Clear water scour} \quad \frac{h}{k} \geq \left[\frac{1.33 \cdot n \cdot \tanh(I_{TW})}{(\Delta z_{w_{crest}} / w_{crest})^{0.3} \cdot \frac{k}{d_{90}}} \right]^{0.769} \quad 3-30$$

$$\text{Live-bed condition} \quad \frac{h}{k} \geq \left[\frac{2.76 \cdot n \cdot \tanh(I_{TW})}{(\Delta z_{w_{crest}} / w_{crest})^{0.3} \cdot \frac{k}{d_{90}}} \right]^{0.769} \quad 3-31$$

where I_{TW} denote the tailwater slope in per mill. If bed-load discharge can be expected then the maximum scour depth is reduced about 25% and equation 3-31 applies instead. Equations 3-30 and 3-31 are valid for ramps with parallel banks and relative ramp widths $w/k = 50$ and maximum relative scour depths $h_{scour}/k = 6$.

Ramp width

To determine the minimum relative ramp width the maximum scour depth and the required accuracy of the ramp as a control section are relevant. The maximum relative ramp width is subject to constructive matters. The permissible range or the relative ramp width is given by equation 3-32, where $r = 0$ for parallel bank lines and $r = -0.1$ for conical bank lines (notation see Figure 3.22). Platzer prefers parallel banks over conical banks as the former yield shorter scour holes and tolerate higher discharges. Conical banks are only recommended for restricted space conditions, or special upstream condition like drop-down curves or riverbed expansions.

$$50 - 2 \cdot r \cdot \frac{L_R}{k} \leq \frac{w}{k} \leq 150 \quad 3-32$$

For small ramp widths $w/k = 50$ a creek downstream of the ramp can be installed to prevent bank erosions. A creek makes sense in mildly sloped rivers and in river bends. The ratio of the maximum width of the creek cross section and the ramp width at the toe of the ramp should be $w_{creek}/w_{toe} = 1.2$. A sketch of the creek is given in Figure 3.23 where l_s denotes the length of the scour.

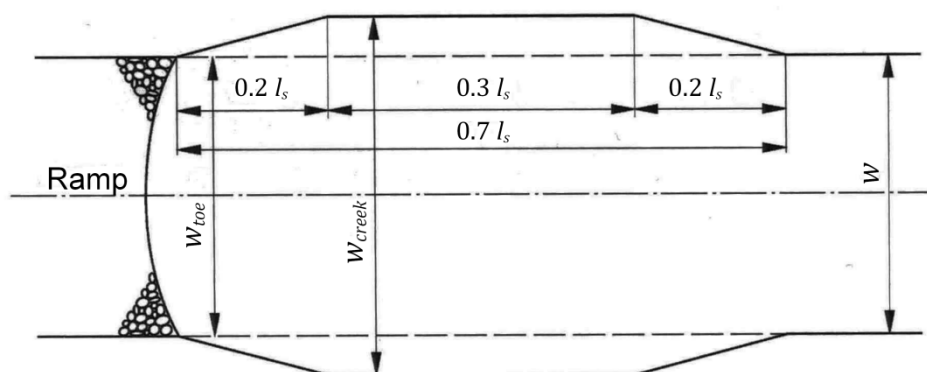


Figure 3.23 sketch of a creek (modified after Platzer, 2000)

Trough height

The trough height $\Delta z_{w_{crest}}$ of the parabolic cross section is bounded by

$$0.012 \cdot w_{crest} \leq \Delta z_{w_{crest}} \leq 0.025 \cdot w_{crest} \quad 3-33$$

For loose ramps the minimum value is $0.015 \cdot w_{crest}$. If $\Delta z_{w_{crest}}$ exceeds the maximum value, then the flow concentration is too strong. If $\Delta z_{w_{crest}}$ is too small, then asymmetric flow conditions can no longer be balanced by the flow concentration.

Choosing a relative ramp roughness k/d_{90} , the maximum permissible relative scour length l_s/k can be expressed subject to the trough height $\Delta z_{w_{crest}}$ and k/d_{90} .

$$\frac{l_s}{k} = \frac{1153}{n^{0.6}} \cdot \left(\frac{\Delta z_{w_{crest}}}{w_{crest}} \right)^{0.35} \cdot \left(\frac{k}{d_{90}} \right)^{0.75} \cdot \tanh(I_{TW}) \quad 3-34$$

Reversely, if the relative scour length l_s/k is preset, the relative ramp roughness k/d_{90} can be approximated subject to the trough height $\Delta z_{w_{crest}}$ and l_s/k .

$$\frac{k}{d_{90}} = \left(\frac{n^{0.6}}{1153} \cdot \left(\frac{\Delta z_{w_{crest}}}{w_{crest}} \right)^{-0.35} \cdot \frac{l_s}{k} \cdot \frac{1}{\tanh(I_{TW})} \right)^{1.33} \quad 3-35$$

Equations 3-34 and 3-35 are valid for ramps with parallel banks and relative ramp widths $w/k = 50$ and maximum relative scour depths $h_{scour}/k = 6$ under both clear water and live-bed conditions.

The trough height is relevant for the relative ramp roughness (equation 3-35) and should be determined in accordance to the ramp height.

For coarse bed materials small trough heights are preferable because of a better energy dissipation and smaller waves downstream of the ramp. For fine bed materials it is important to prevent asymmetric scouring. It is therefore recommended to fulfill equation 3-35 in favor of having small trough heights and a better energy dissipation. For small low water flows a large trough height leads to a flow concentration and can thus prevent the ramp from drying up.

Maximum discharge

The specific discharge expressed in terms of Fr_q depends on the ramp slope $1:n$. Different formulas apply for ramp slopes $1:n$ flatter and steeper than $1:n_0$, respectively:

$$n \geq n_0 \quad Fr_q = 6 \cdot \sqrt{h/k} \quad 3-36$$

$$n < n_0$$

$$\text{Standing ramp, parallel banks} \quad Fr_q = (1.4 + 0.59 \cdot (f - 1)^{0.7}) \cdot n - (8.1 + 0.33 \cdot f^2) \quad 3-37a$$

$$\text{Standing ramp, conical banks} \quad Fr_q = (1.3 + 0.45 \cdot (f - 1)^{0.7}) \cdot n - (8.0 + 0.3 \cdot \sqrt{f - 1}) \quad 3-37b$$

$$\text{Loose ramp, } \tau_{*c} = 0.06 \quad Fr_q = 1.48 \cdot n - 8.1 \quad 3-37c$$

$$\text{Loose ramp, } \tau_{*c} = 0.07 \quad Fr_q = 1.84 \cdot n - 9.2 \quad 3-37d$$

where $s = l_a/l_b$ is the ratio of the longest block axis to the middle axis and n_0 is calculated as follows:

<p>Standing ramp parallel banks</p> $n_0 = \frac{6 \cdot \sqrt{h/k} + 3.4 \cdot s^{0.7} + 0.5}{1.4 + 0.67 \cdot (s - 1)^{0.7}}$	<p>Standing ramp conical banks</p> $n_0 = \frac{6 \cdot \sqrt{h/k} + 0.3 \cdot \sqrt{s-1} + 8.0}{1.3 + 0.45 \cdot (s - 1)^{0.7}}$	<p>Loose ramp</p> $\tau_{*c} = 0.06$ $n_0 = 4.05 \cdot \sqrt{h/k} + 5.47$	<p>Loose ramp</p> $\tau_{*c} = 0.07$ $n_0 = 3.26 \cdot \sqrt{h/k} + 5.0$
--	--	--	---

As for the type of the block layer Platzer finds that the cost-savings are small for a loose ramp compared to a standing ramp. Thus the choice of type of the block layer depends on stability criteria hence the ramp height h and the design discharge q . Platzer recommends loose ramps only for small ramp heights and small design discharges. In contrast, Whittaker and Jäggi favor the loose block ramp as multiple layers of blocks better prevent the erosion of bed material.

Construction recommendations and dimensioning

In bed load carrying rivers or streams the blocks of the ramp should be made of granite to prevent high abrasion. A presorting of blocks is recommended. Comparing the longest axis of the blocks, the deviation of the maximum length l_{max} from the average length l_m should be $\pm 20\%$ maximum. The ratio of the longest block axis to the middle axis should exceed $l_m/b_m \geq 1.5$. For loose ramps, blocks that differ strongly from the average should be eliminated. To ensure the ramp stability the filter layer below the block layer should have a minimum diameter $5 \cdot d_{f,min} \geq 15 \cdot k/7 \cong d_s$ and should consist of at least two layers. d_s denotes the equivalent spherical diameter. Using Platzer's notation, Terzaghi's filter criterion can be re-written as

$$4 \cdot d_{f,15} > d_s > 4 \cdot d_{f,85}$$

Platzer's filter criterion is similar to the Terzaghi's left inequality. Platzer does not demand that the boulders of the ramp must be larger than a multiple of the larger filter material.

If the bed material below is fine the filter layer has to be trickle-proof, otherwise a geotextile has to be used.

Platzer discourages from installing a fish path along the ramp that is bevel to main flow direction as this causes asymmetric scours downstream. For standing ramps a water drainage is necessary because it ensures accurate construction and maximum roughness. In the end it saves maintenance costs. The bank protection along the ramp should reach as high as the highest expected water level. The ramp toe has to be secured with rails. Additional riprap should be applied as shown in Figure 3.24.

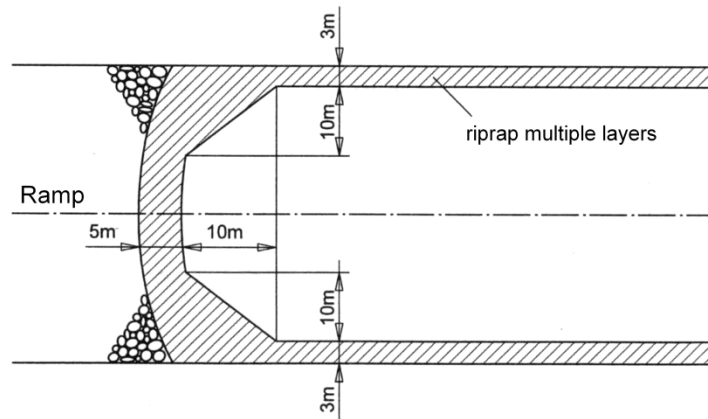


Figure 3.24 riprap protection downstream of the ramp (Platzer 2000, labels translated by author)

The design rules for the ramp are outlined in Table 3.4. The key parameters are the ramp roughness $k = l_a/3$, the ramp height h , the design discharge Q and the ramp width w . This might require a recursive application of these design rules. Platzer lists more criteria, for instance those which take into account drop-down curves upstream of the ramp. However they are omitted here.

Ramp type	Design rules	Additional design rules if no scour protection downstream of the ramp is provided
Standing ramp parallel banks	3-28, 3-29, 3-32, 3-33, 3-36 or 3-37a	3-30, 3-31, 3-34, 3-35
Standing ramp conical banks	3-28 (equality!), 3-32, 3-33, 3-36 or 3-37b	Not specified
Loose ramp, parallel banks $\tau_{*c} = 0.06$	3-28, 3-29, 3-32, 3-33, 3-36 or 3-37c	Not specified
Loose ramp, parallel banks $\tau_{*c} = 0.07$	3-28, 3-29, 3-32, 3-33, 3-36 or 3-37d	Not specified

Table 3.4 Design rules after Platzer (2000)

3.3.5 Investigations on Block Ramps by Pagliara et al.

Pagliara and Chiavaccini (2006a) investigate the energy dissipation on block ramps. In a series of physical model tests they use three flumes with different widths (0.25 m, 0.35 m and 0.8 m) and lengths (3.5 m, 6 m and 25 m) to investigate possible scale effects.

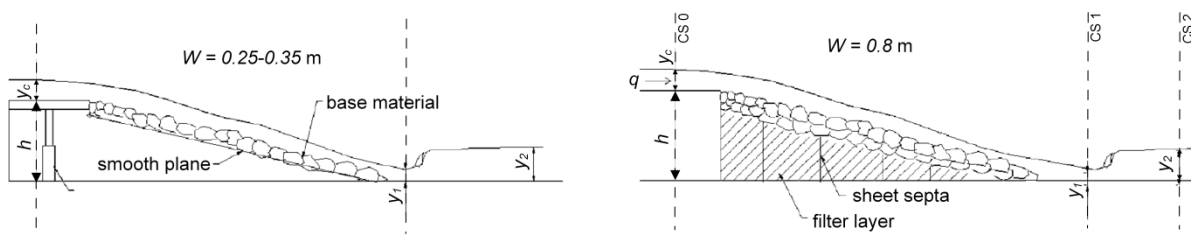


Figure 3.25 sketch of the ramp for the investigation of energy dissipation on block ramps (modified after Pagliara, Chiavaccini 2006a)

The energy loss along a ramp can be expressed as

$$\Delta E = E_0 - E_1 = h + 1.5 \cdot y_c - \left(y_1 + \frac{q^2}{2 \cdot g \cdot y_1^2} \right) \quad 3-38$$

where E_0 and E_1 denote the total energy head at a control section upstream of the ramp crest (cross section CS 0 in Figure 3.25, right) and at the toe of the ramp where the flow enters the hydraulic jump (cross section CS 1 in Figure 3.25, right). h , y_c , y_1 and q denote ramp height, critical depth, water depth of the flow entering the jump and specific discharge, respectively. Five block materials were tested with a non-uniformity coefficient $U_{60} = d_{60}/d_{10}$ close to unity. Pagliara and Chiavaccini identify the parameters that are potentially involved in the energy dissipation process, apply the Π -theorem of the dimensional analysis and get

$$F \left(\frac{\Delta E}{E_0}, \frac{y_c}{d_{50}}, \frac{y_c}{h}, I, \text{Re}, \text{We}, C_{mean}, \frac{w}{y_c} \right) = 0 \quad 3-39$$

where d_{50} , Re , We , C_{mean} , I and w denote diameter of the blocks where 50% of the block material is finer, Reynolds number, Weber number, non-dimensional air concentration, ramp slope and ramp width. Step by step Pagliara and Chiavaccini rule out certain dimensionless factors. The model tests show that the width w/y_c can be omitted as was proven in test runs with different flume widths. Viscous effects were also found to be negligible, thus the Reynolds number Re can be eliminated from the above equation. The air entrainment also proved to be insignificant, practically no white water conditions were observed. So the Weber number We and the air concentration C_{mean} are discarded. Equation 3-39 thus reduces to equation 3-40:

$$\frac{\Delta E}{E_0} = f \left(\frac{y_c}{d_{50}}, \frac{y_c}{h}, I \right) = 0 \quad 3-40$$

The dimensionless factor y_c/d_{50} is a measure for the relative submergence. Following Bathurst's classification of relative submergence into the three categories small scale roughness, intermediate scale roughness and large scale roughness, Pagliara and Chiavaccini derive a formula for each of these categories thus eliminating y_c/d_{50} from equation 3-40.

Roughness category (Bathurst 1978, Bathurst, Li et al. 1981) (Pagliara, Chiavaccini 2006a)

Large roughness scale	$y_u/d_{84} < 1.2$	$y_c/d_{50} < 2.5$
Intermediate roughness scale	$1.2 < y_u/d_{84} < 4.0$	$2.5 < y_c/d_{50} < 6.6$
Small roughness scale	$y_u/d_{84} > 4.0$	$6.6 < y_c/d_{50} < 42$

Table 3.5 Relative submergence categories

In Table 3.5 y_u and d_{84} denote the uniform flow depth and the diameter where 84% of the material is finer respectively. In their experiments Pagliara and Chiavaccini report good agreement to Bathurst's specified ranges when they calculate y_u/d_{84} instead of y_c/d_{50} in their experiments.

$$\frac{\Delta E}{E_0} = A + (1 - A) \cdot e^{(B+C \cdot I) \cdot y_c/h} \quad 3-41$$

Pagliara and Chiavaccini find that the experimental data fit equation 3-41 very well. The coefficients A , B and C are listed in Table 3.6. Equation 3-41 is valid for $0 < y_c/h < 1.2$. The relative energy dissipation increases with decreasing slopes and increasing roughness. While the latter result doesn't come unexpectedly the fact that flatter slopes dissipate more energy is surprising. The steeper the slope the smaller the relative submergence y_u/d_{84} . As the Darcy-Weisbach friction factor f increases with decreasing relative submergence y_u/d_{84} the friction loss (and thus the energy dissipation) increase with the slope. Pagliara and Chiavaccini choose y_c/d_{50} as an indicator for the relative submergence which is constant for all slopes for a given discharge. Maybe the results can be interpreted differently if y_u/d_{84} is chosen instead of y_c/d_{50} .

Roughness category	A	B	C
Large roughness scale	0.33	-1.3	-14.5
Intermediate roughness scale	0.25	-1.2	-12.0
Small roughness scale	0.15	-1.0	-11.5
Smooth ramp	0.02	-0.9	-25.0

Table 3.6 Coefficients for calculating the energy dissipation on block ramps with a free jump

Pagliara and Chiavaccini (2006b) proceed the experiments and investigate the energy dissipation on "reinforced block ramps". The reinforcement consists of boulders protruding from the bed. The protruding boulders are either placed in rows, thus making it a step-pool ramp, or are randomly placed. The aim of these experiments was to determine the increase in energy dissipation due to the protruding boulders. Thus, potential influence factors are identified, such as the boulder concentration factor Γ (equation 3-42) where N_B , D_B , w and L denote the number of the boulders, the diameter of the boulders, the ramp width and the ramp length, respectively.

$$\Gamma = \frac{N_B \cdot \pi \cdot D_B^2}{w \cdot L} \quad 3-42$$

Pagliara and Chiavaccini find the boulder concentration Γ along with the boulder roughness (crushed or smooth rounded boulders) and the boulder disposition (in rows, random) to be the key variables. All other potential parameters like the ramp slope I , Re , Fr , D_B/d_{50} and y_c/d_{50} can be neglected. On the basis of equation 3-41 the relative total head loss that takes into account the protruding boulders can be expressed as

$$\frac{\Delta E}{E_0} = A + (1 - A) e^{\left(1 + \frac{\Gamma}{E+F \cdot \Gamma}\right) \cdot (B+C \cdot I) \cdot y_c/h} \quad 3-43$$

Without protruding boulders Γ equals 0 and equation 3-43 reduces to equation 3-41. Thus equation 3-43 can be used in both, the absence or presence of protruding boulders. The coefficients E and F are listed in Table 3.7. Equation 3-43 is valid for boulder concentrations less than 0.33 and ramp slopes ranging from 0.08 to 0.33.

Roughness and disposition of protruding boulders	E	F
Smooth, random	0.6	13.3
Smooth, in rows	0.55	10.5
Rough, random	0.55	9.1
Rough, in rows	0.4	7.7

Table 3.7 Coefficients for calculating the increased energy dissipation on block ramps due to protruding boulders

As can be seen from equation 3-43 and Table 3.7 protruding boulders placed in rows are more dissipative than randomly placed boulders. Similarly rough boulders dissipate more energy than smooth boulders.

Pagliara et al. (2008) continue the experiments and investigate the influence of different tailwater levels and the presence or absence of a scour downstream of the ramp on the energy dissipation. In these experiments the total head loss is calculated between cross section CS 0 upstream of the ramp crest and cross section CS 2 downstream of the ramp toe resp. of the hydraulic jump (see Figure 3.25 right). The tailwater levels is adjusted such that the – submerged - hydraulic jump is located at 1/3 and 2/3 of the ramp length, respectively. The submergence level is expressed as the ratio L_{HJ}/L_h of the horizontal distance L_{HJ} of the location of the hydraulic jump (w.r.t. the ramp toe) and the horizontal ramp length L_h . Also a free jump ($L_{HJ}/L_h = 0$) is investigated as in the previous experiments. Moreover the energy dissipation for a smooth fixed bed and a mobile bed (with or without a scour) downstream of the ramp is compared.

As in the previous experiments the results differ with respect to the scale roughness and the relative critical depth y_c/h . While the presence or absence of a scour downstream of the ramp was found to be negligible the submergence level does effect the energy dissipation. The higher the submergence level L_{HJ}/L_H the lower the energy dissipation. For a fixed submergence level and a fixed scale roughness the energy dissipation does not depend on the ramp slope. Similar to equation 3-41 Pagliara et al. find an empirical relationship:

$$\frac{\Delta E}{E_0} = \frac{E_0 - E_1}{E_0} = A + (1 - A)e^{B \cdot y_c/h} \quad 3-44$$

The coefficients A and B are listed in Table 3.8. Equation 3-44 is valid for relative critical depths $0.1 < y_c/h < 1.2$, ramp slopes ranging from 1:4 to 1:8 and for submerged jumps $L_{HJ}/L_H < 0.7$.

Roughness category	A	B
Small roughness scale	$0.239 \cdot e^{-2.323(L_{HJ}/L_H)}$	$-(10.7 \cdot L_{HJ}/L_H + 1.729)$
Intermediate roughness scale	$0.249 \cdot e^{-1.618(L_{HJ}/L_H)}$	$-(9.95 \cdot L_{HJ}/L_H + 1.863)$
Large roughness scale	$0.256 \cdot e^{-1.245(L_{HJ}/L_H)}$	$-(8.475 \cdot L_{HJ}/L_H + 1.931)$

Table 3.8 Coefficients for calculating the energy dissipation on block ramps with a submerged jump

Aside from energy dissipation matters on block ramps Pagliara et al. also deal with scouring processes downstream of block ramps. The influence of sediment gradation on the scour geometry is investigated (Pagliara 2007, Pagliara, Palermo 2008a) as well as scour control measures such as sills

or expanding stilling basins (Pagliara, Palermo 2008a, Pagliara, Palermo 2008b, Pagliara, Palermo et al. 2009).

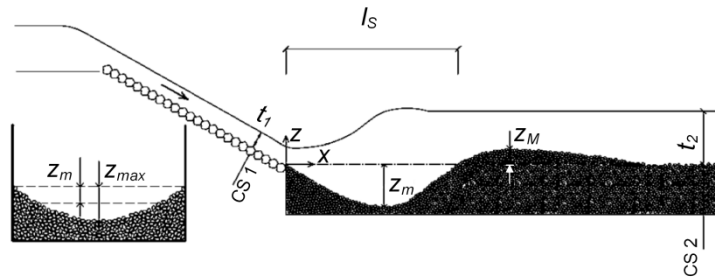


Figure 3.26 sketch of a scour downstream of a block ramp (modified after Pagliara, 2007)

Figure 3.26 illustrates the sketch of a scour downstream of a block ramp in the presence of a ridge at the end of the scour hole. The ridge protrudes from the bed level downstream of the ramp. If a ridge is formed downstream of a scour then the scour process terminates and a maximum resp. mean scour depth can be determined. There is no sediment transport downstream of the ridge. In the absence of the ridge there is a gradually eroded. The sediment transport proceeds further downstream. The erosion process does not stop. In Pagliara (2007) the influence of the sediment gradation (expressed by the non-uniformity coefficient) on the scour geometry is investigated in the presence of a ridge. The experiments were performed in two flumes with different widths (0.25 m and 0.35 m) and lengths (3.5 m, 6 m). The Reynolds number Re ranged from 15000 to 35000. For the measurement of water depth t_1 at the ramp toe the virtual ramp bed is assumed to be $0.2 \cdot D_{65}$ below the mean top of the ramp blocks. The key parameters that influence the scour geometry are:

- the densimetric Froude number $Fr_{d_{xx}} = \frac{v}{\sqrt{g' d_{xx}}}$
- the non-uniformity coefficient $U_{84} = \sqrt{d_{84}/d_{16}}$ (experimental range: 1.2, 1.8, 2.8)
- ramp slope I (experimental range 1: 4, 1: 8, 1: 12)

The mean scour hole depth is found to fit the following equations expressed by $Fr_{d_{50}}$ and $Fr_{d_{90}}$, respectively.

$$Z_m = \frac{Z_m}{t_1} = 0.58 \cdot U_{84}^{-0.55} \cdot I^{0.75} \cdot Fr_{d_{50}} \quad 3-45$$

$$Z_m = 0.58 \cdot U_{84}^{0.55} \cdot I^{0.75} \cdot Fr_{d_{90}} \quad 3-46$$

The maximum scour hole depth is independent of the ramp slope and the non-uniformity of the sediment. The ratio of the maximum and the minimum scour depth equals:

$$\frac{Z_{max}}{Z_m} = 1 + 1.75 \cdot Fr_{d_{50}}^{-1.75} \quad 3-47$$

$$\frac{Z_{max}}{Z_m} = 1 + 0.55 \cdot Fr_{d_{90}}^{-0.75} \quad 3-48$$

The dimensionless scour length $L_S = l_S/y_1$ depends on the mean scour depth, U_{84} and I . The longitudinal section of the scour hole is independent of U_{84} , I and $Fr_{d_{90}}$. Its shape can be expressed in dimensionless form by $X = x/y_1$ and $Z = z/y_1$ (see Figure 3.26)

$$L_S = 3.75 \cdot U_{84}^{0.8} \cdot I^{-0.5} \cdot Z_M^{0.8} \quad 3-49$$

$$Z = 3.5 \cdot X^3 - 9.1 \cdot X^2 + 5.6 \cdot X \quad 3-50$$

With the above equations 3-45 - 3-50 the scour geometry can be estimated. If for prototype ramps the water depth y_1 cannot be measured, Pagliara suggests to calculate it from equation 3-41.

Based on these experiments Pagliara & Palermo (2008b) investigate the effect of three sill types to control the scour downstream of the ramp for uniform sediments. The three sill types are a rock sill, a continuous sill and a dentated sill respectively. Four different scour categories are identified depending on the ramp slope and the position of the sill. In Pagliara & Palermo (2008a) the experiments are extended to non-uniform sediments resulting in a scour classification for non-uniform sediments. Only the rock sill is investigated. The scour hole geometry depends on the sill position and the sediment gradation.

plan view

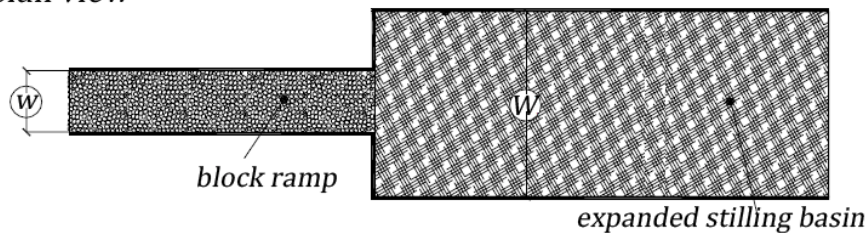


Figure 3.27 Sketch of expanded stilling basin, plan view (modified after Pagliara & Palermo, 2008b)

In Pagliara et al. (2009) study the effects of an expanding stilling basin on the scour geometry and the hydraulic jump for both uniform and non-uniform sediments. Different tailwater depths and two expansion ratios ($W/w = 1.8$ and 2.8 , respectively) are investigated and compared to the results of a prismatic stilling basin ($W/w = 1$). The experiments show that the hydrodynamics and the scour hole geometry are highly 3-dimensional. For expansions the scour depth increases. Pagliara et al. explain this with the flow recirculation in the lateral zones that deflect the main flow towards the center. (At this point it should be noted that the expansion has a similar effect on the scour hole as the doubly bent cross sectional profile of the Schauberger block ramp (see 3.2.1). The trough-shaped cross section of the latter concentrates the flow towards the river center. In the lateral zones a recirculation flow develops.) The higher the tailwater level the smaller the scour depth under otherwise constant conditions. For jump types are identified that depend on the expansion ratio W/w , the densimetric Froude number $Fr_{d_{90}}$ and on the ramp slope. For mobile beds the stilling basin expansion dissipates more energy than a non-expanded stilling basin ($W/w = 1$).

3.4 Step-pool ramps

3.4.1 Introduction

Step-pool ramps copy their design from natural step-pool systems that, under certain circumstances, develop in steep mountain streams. Step-pool systems are one of 7 morphological patterns that can be distinguished in mountain streams according to Schälchli (1991). Schälchli provides the following classification:

Pattern	Slope (%)	d_{max} (m)	Step / riffle height (m)
1: no bed forms	1.5 – 5	0.5 – 0.7	
2: riffle-pools	1.5 – 7	0.6 – 0.9	$- 0.7 \cdot d_{max}$
3: step-pools	3.5 – 12.5	0.9 – 1.2	$- 1 \cdot d_{max}$
4: boulder steps and pools	9.0 – 30	1.1 – 2.0	$1 \div 2.5 \cdot d_{max}$
5: boulder glide	12 – 35	1.3 – 2.0	
6: boulder glide	29 – 49	2.5 – 5.0	
7: rock bed	Any		

Table 3.9 Morphological patterns, classification according to Schälchli (1991)

Boulder glides of pattern 5 consist of abraded rounded material while those of pattern 6 are composed of angular stones. Rock beds may occur at all slopes. Schälchli observed pattern 7 mainly at slopes exceeding 20 %, however. In Figure 3.28 a sketch illustrates the first 4 morphological patterns.

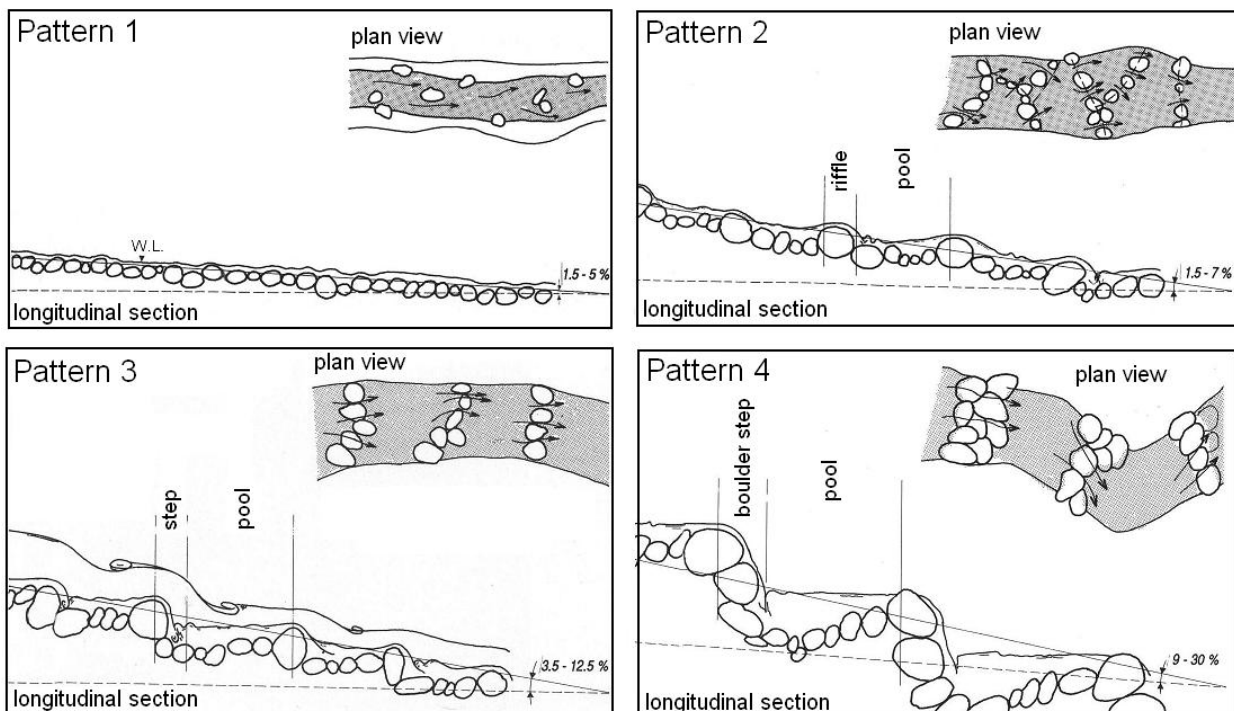


Figure 3.28 Sketches of morphological patterns 1 – 4 (Schälchli 1991, labels modified by author)

Like their natural step-pool models man-made step-pool ramps consist of laterally aligned steps of boulders (Figure 3.29). Typically the pools in between are also armored with large boulders to ensure the stability of the ramp. Different step-pool ramp designs are described in detail in the following sections.



Figure 3.29 Example of a step-pool ramp near Teisendorf, Bavaria (© Wasserwirtschaftsamt Traunstein)

It should be mentioned, although this is beyond the scope of this thesis, that the riffle pool patterns also serve as a model for ramp types that consist of a cluster of pools (e.g. Hengl, Stephan 2007, Hengl, Korger et al. 2007, Hengl, Aufleger et al. 2008). Two ramps of this kind have been successfully built recently in the Salzach river and the Saalach river located at the border between Salzburg, Austria and Bavaria, Germany (Table 3.10, Figure 3.30).

River, station	Ramp height (m)	Ramp slope (%)	Mean flow (m ³ /s)	Design discharge (m ³ /s)	Specific design discharge (m ³ /sm)
Saalach, km 4.6	2.7	2.85	34	1000	19.23
Salzach, km 51.9	3.3	2.00	250	2831	20.20

Table 3.10 Examples of cluster ramps, parameters

The design discharge of the Saalach ramp corresponds to a 100-year flood. The design discharge for the Salzach ramp corresponds to the channel discharge of a 100-year flood + 15 %. Both ramps have to resist high specific discharges. They are much flatter than the traditional block ramps (chapter 3.3) and therefore require smaller stone sizes. Moreover they are more likely to be fish-passable than the steeper block ramps.

The pools of the Salzach ramp are 1.5 m deep. The mean length of a pool is 15 m (Hengl, Aufleger et al. 2008). Assuming a pool of parabolic shape of the pools the mean pool depth is approximately 1.2 m (cf. Figure 7.6). The ratio $15/1.2 = 12.5$ lies beyond Morris' recommended range for the relative spacing. (chapter 3.6.2, pp.67). The flow transition from tumbling flow to rapid flow is a crucial loading case for the ramp as pointed out in chapter 5.4.12, pp.171. According to formulas 5-12 - 5-14 this flow transition will take place for a specific discharge of 20 m³/sm. The formulas are applied beyond the recommended range, so the result has to be treated with caution. As the ratio of lift force to drag force is extremely high for the flow transitional discharge (Table 5.15) it seems dangerous that the flow transition coincides with the design discharge. On the other hand it is likely that at design discharge conditions sediment transport will reduce the forces acting on the ramp structure.



Figure 3.30 ramps with pool cluster: Saalach river, km 4.6 at low flow conditions (left), physical model of the Salzach river ramp, km 51.9 (right)

Two different fields of research contribute to the understanding of step-pool ramps:

1. Natural step-pool systems
2. Energy dissipating structures using artificial steps (see chapter 3.6, pp. 65)

3.4.2 Natural step-pool systems

Chin & Wohl (2005) give an overview of the research on natural step-pool systems. According to her, studies on this topic were rare up until the 1989s. The research field covers questions like

1. Under which morphological and climatic circumstances do step-pool systems develop?
2. What function serve step-pool systems?
3. Are there correlations between morphological parameters, for instance step spacing, step height, slope, channel width and bed material?
4. What processes can be observed in step-pool systems?

Definition of morphological parameters

Two key parameters in step-pool systems are step height K and step spacing L . Subscripts indicate different definitions of step height and step spacing. The latter is also termed “wave length” or “step frequency”. Nickolotsky & Pavlowsky (2007) point out that there exist different definitions of K and L , which may lead to deviations in up to 30 % depending on the measure of step height.

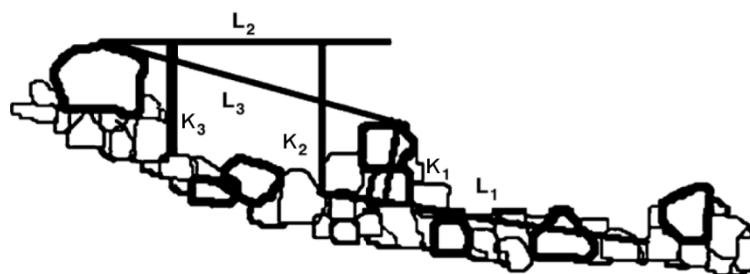


Figure 3.31 Various definitions morphological parameters step height K and step spacing in natural step-pool systems (Nickolotsky & Pavlowsky 2007, labels modified by author)

If not stated otherwise, throughout this thesis K_3 and L_3 (as in Figure 3.31) will be used as step height and step spacing, respectively. Hence, data from researchers who use different definitions

(e.g. Billi, D'Agostino et al. 1998, Chartrand, Whiting 2000) will be transformed accordingly (Figure 3.32).

Formation of step-pool systems

Chin & Wohl (2005) report that step-pool systems develop in almost all hydroclimatic environments. Necessary conditions for their development are bed slopes that exceed 2 % (cf. Table 3.9) as well as an adequate sediment gradation (gravel to boulder). Step-pool morphology develop only on high-magnitude, low-frequency flow events (return periods 20-50 years, e.g. Chin, Wohl 2005, Chartrand, Whiting 2000, Zimmermann, Church 2001, Whittaker, Jäggi 1982). There is disagreement among scientists whether or whether not step-pool formations can be described with the antidune model. Whittaker (1987) and Chartrand & Whiting (2000) support the latter. Abrahams et al. (1995) point out that the antidune model cannot be applied to step-pool systems because the Froude numbers of the step-pool systems lie well below those necessary for the formation of antidunes. Neither do Zimmermann & Church (2001) confirm the antidune model.

Function of step-pool systems

Step-pool systems function as energy-dissipating structures that provide excellent flow resistance. In narrow mountain valleys the stream cannot extend its bed laterally on high floods like in meandering or braided rivers. In step-pool systems water flows over a step, plunges into a pool and dissipates energy by producing roller eddies. Thus the vertical dimension for energy dissipation plays an important role for step-pool systems. Moreover the notion that step-pool systems can be regarded as a kind of meandering in vertical direction spreads among scientists. (Abrahams, Li et al. 1995) suggest that step-pools adjust to a maximum flow resistance. They develop if the morphological and hydrological conditions are such that the maximum flood events are just able to move the largest boulders of the stream. The largest boulders align laterally, thus prolonging the stability of the bed and increasing the resistance. To prove their maximum resistance hypothesis Abrahams et al. perform flume tests. For a given step height K and given slope I , they determine the step spacing L , such that maximum resistance is achieved. They find K , I and L to fit the following relation 3-51. Accompanying surveys of 18 natural step-pool sections show that relation 3-51 also holds true for natural step-pool systems. Abrahams et al. conclude that their maximum resistance hypothesis is verified.

***Maximum flow
resistance criterion***

$$1 \leq K/L/I \leq 2$$

3-51

Relation between morphological parameters

The inequality 3-51 relates the morphological parameters K , L and I to each other. Several other researchers try to link the morphological parameters to each other. One of the first are (Judd, Peterson 1969) who propose the following relationship

***Relation of
morphological
parameters***

$$\frac{L}{K} = \frac{C}{I^2}$$

3-52

where C and z denote constants. Whittaker (1987) reports that equation 3-52 holds true only for the step length L and the slope I . They cannot find a relationship with the step height K (see chapter 3.3.3, equation 3-69).

Researchers	Location	Range of slopes (%)	Relative Spacing L/K	Step height to step particle size
Abrahams et al. 1995	Adirondeck Mountains, NY, USA	6.3 – 21.5	4.0 – 11.3	Not investigated
Billi et al. 1998	Rio Cordon, Italy	7.1 – 18.8	4.4 – 10	$K = 2 \cdot d_{90}^+$
Chartrand & Whiting 2000	Idaho, USA	1.5 – 13.4	4.2 – 12.7	$K = 1 \div 1.5 \cdot d_{50}$
Wooldridge & Hickin 2002	Mosquito Creek, BC, Canada		5.0 – 9.0 ⁺	Not investigated
Chin 1999, Chin & Wohl 2005	Santa Monica Mountains, CA, USA	1.7 – 11.5	6.3 – 21.2 ⁺⁺	$K = 1 \div 1.5 \cdot d_{avg}^{+++}$
Nickolotsky & Pavlowsky 2007	Boston Mountains, AR, USA	4.6 – 30.2	3.0 – 19.5	No clear trend

+ cited after Chin & Wohl, 2005

++ no definition of step height K and wavelength L is provided in (Chin 1999)

+++ calculated by averaging the b-axis of the five largest rocks at each step

Table 3.11 Morphological parameters in natural step-pool systems

Data from Abrahams et al. (1995), Billi et al. (1998), Chin (1999) and Nickolotsky & Pavlowsky (2007) suggest that equation 3-52 holds true, although the constants C and z vary considerably among the scientists. Chartrand & Whiting (2000) do not confirm equation 3-52 (Figure 3.32). Consequently they argue that although step spacing can well be correlated to step height, the channel slope does not have a dominant control on step spacing. Maxwell et al. (2001) propose a logarithmic relationship of L , K (both in meter) and I of the form

Relation of morphological parameters

$$L = 7.39 \ln \frac{K}{I} - 5.52 \quad \mathbf{3-53}$$

In equation 3-53 L denotes the horizontal spacing (cf. L_2 in Figure 3.31).

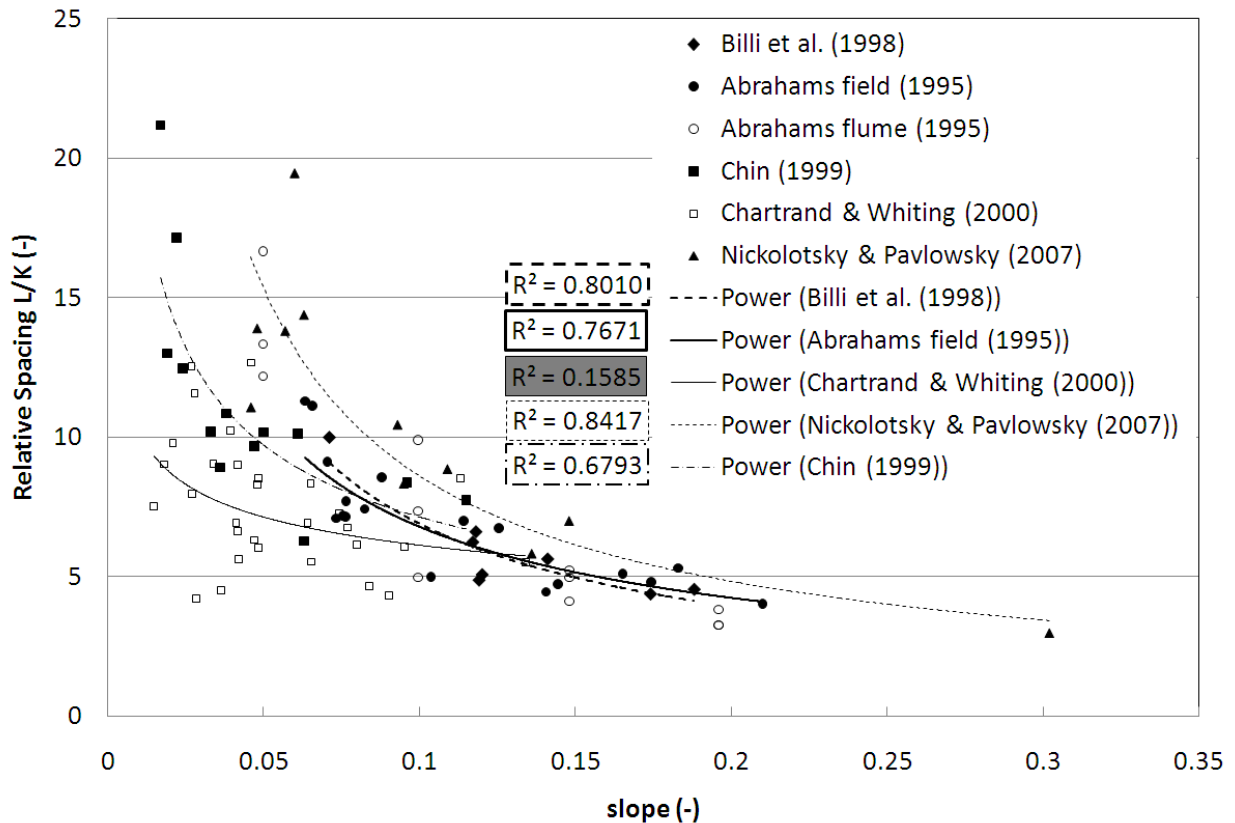


Figure 3.32 Correlation between slope and relative spacing in natural step-pool systems, R^2 is a measure for the goodness of the fitted power function ($R^2=1$ means that all data points lie on the power function)

Wooldridge & Hickin (2002) come to the conclusion that channel slope partially controls wavelength and bedform height, which in turn weakly controls the individual step spacing. Wavelength and grain size (d_{90}) do not correlate.

In contrast to those scientists who find a relationship between the morphological parameters, Zimmermann & Church (2001) claim that there does not exist any relationship and that the step-pool morphology is of random nature.

Several researchers report, that the step particle size controls the step height (Table 3.9, Table 3.11).

Processes in step-pool systems

Wohl & Thompson (2000) conducts 1D-velocity measurements in natural step-pool systems at different discharges. The velocity profiles immediately downstream of a step are dominated by wake turbulence from mid-profile shear layers. This energy dissipating process appears to be more effective than the bed-generated turbulence and skin friction as measured upstream of a step. Similarly Comiti et al. (2005) state that “flow resistance in step-pool systems is dominated by turbulent energy dissipation analogous to that of hydraulic jumps, rather than grain or form drag.” Chin & Wohl (2005) report that with increasing discharge the average longitudinal velocity also increases but does not affect the lateral and vertical components, respectively.

Comiti et al. (2005) investigate 37 natural step-pool systems and 73 artificial pools downstream of grade control structures. They find that the morphological parameters between natural and artificial pools do not differ statistically if normalized by the “energy of falling jet”. The latter is defined as the critical depth where discharge rates of the latest flood events were available due to gauging stations.

If this was not the case the bankfull water depth was taken instead. Comiti et al. thus use morphological and hydraulic parameters alike to describe the pool geometry.

3.4.3 Investigations on step-pool-ramps by Volkart

In a series of physical model tests Volkart investigates the stabilization of rivers with a sequence of sills (“Querschwellen”) (Volkart 1972). The sills are made of wood or rock. Unlike ramp structures that are typically steeper than the natural river slope the sequence of sills is a means to stabilize a river section at natural slope conditions. Nowadays, newly-built ramps often have flat slopes due to ecological reasons. The sequence of sills can thus be regarded as a modern step-pool ramp. The pools in between the steps (sills) may or may not be protected by an armor layer of coarser sediments.

The experiments are performed in a 5.5 m long and 0.3 m wide flume. The model scale is 1:30 (Froude similarity). In the case of unprotected pools formulas are provided to calculate the location ξ_s and the maximum depth Y_{max} of the scour within one pool and the minimum, mean and maximum water depths Z_{min} , \bar{Z} and Z_{max} for a given discharge q , a given pool length L and the diameter d_{90} of the bed material (see Figure 3.33). If for a given design discharge the emerging scours endanger the stability of the steps a coarser armor layer has to be installed.

For pools with an armor layer design rules are given for the incipient motion of the armor layer subject to the pool length L , the step height K , the diameter d_{90} of the armor material and the slope I (see Figure 3.34).

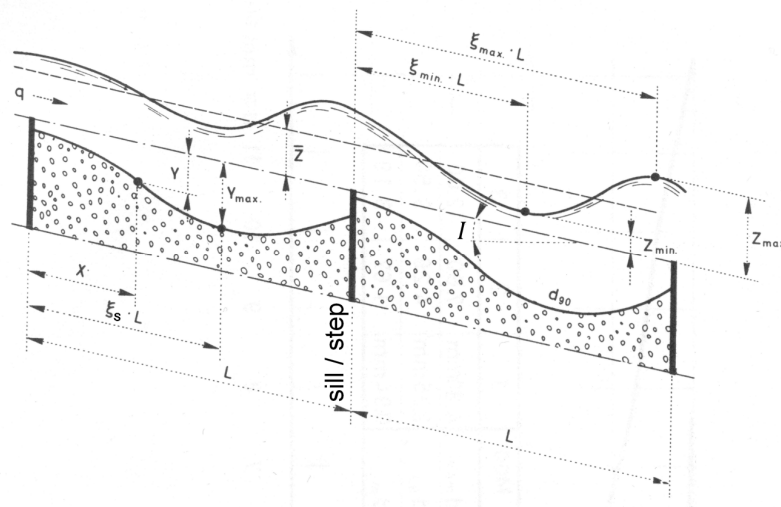


Figure 3.33 Sketch of a step-pool sequence without armor layer (modified after Volkart 1972)

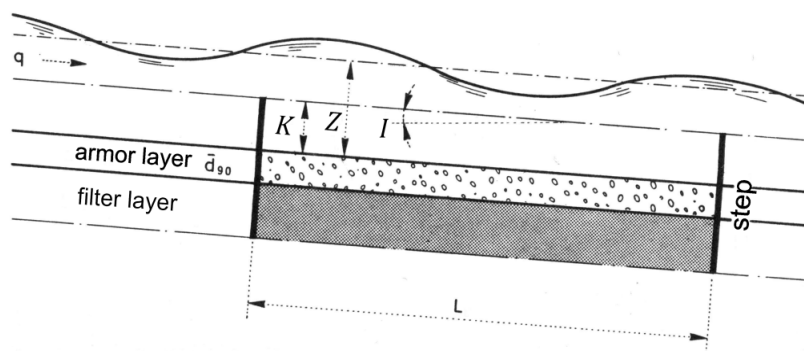


Figure 3.34 Sketch of a step-pool sequence with armor layer (modified after Volkart 1972)

Step-pool sequence without armor layer

In the experiments for the step-pool sequence without armor layer viscous effects are negligible because the Reynolds number $Re > 10^5$. Wall effects are not taken into account, a 2-dimensional flow is assumed. The experiments are carried out for the following ranges of parameters:

- slopes: $0.0075 \leq I \leq 0.07$
- bed materials: $2.35 \leq d_{90} \leq 9.5$ mm
- step spacing: $0.2 \leq L \leq 0.8$ m
- spec. discharge: $7 \leq q \leq 39.6$ l/sm
- bed-load discharge: $0 \leq q_b \leq 0.033$ kg/sm

At the beginning of each test run the pools were leveled to the top levels of the steps. Each test run took between 6 and 12 hours. During each test run the following processes occur:

1. scouring of the pools which are beginning to take a trough shape, exposition of the top levels of the steps, the bottom flow follows the bed, the surface flow is almost undisturbed
2. if the scour hole exceeds a certain longitudinal slope the steps become the starting point of a flow separation, below the separation line a clockwise vortex develops that transports finer materials to the upstream step, the point of the flow reattachment to the downstream step consists of the coarser material, thus a sorting of sediments takes place, the flow is undular, a counter-clockwise surface roller may develop in the middle of the pool
3. if the discharge is further increased and the scouring process has not been finished another clockwise vortex develops immediately before the downstream step, sediments are moved upstream, get caught by the main flow and are subsequently transported to the next downstream pool
4. a further increase of the discharge may boost the vortex described in 3. such that the pool can erode within a short time beginning from the furthest downstream part of the pool

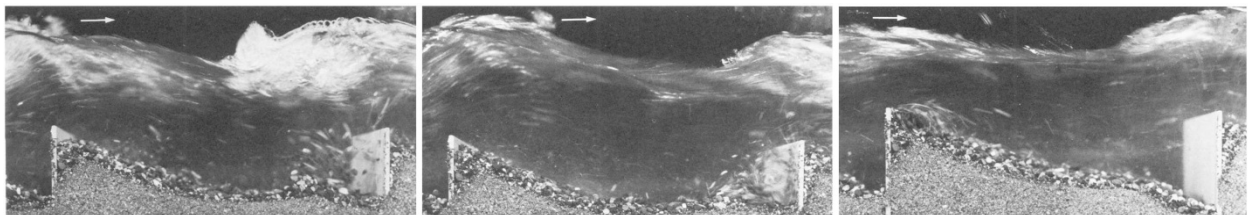


Figure 3.35 Erosion of the downstream part of the pool (Volkart 1972)

For the derivation of the maximum scour depth formula Volkart identifies the parameters that influence the scour process, applies the Π -theorem of the dimensional analysis and gets:

$$\mathbf{F} \left(\frac{d_{90}^3 \cdot g}{q^2}, \frac{L}{d_{90}}, \frac{Y_{max}}{d_{90}}, I, \frac{\rho_w}{\rho_s - \rho_w}, \frac{q_b}{q \cdot (\rho_s - \rho_w)} \right) = 0 \quad \mathbf{3-54}$$

where q_b , ρ_w and ρ_s denote the bed-load discharge (kg/ms), the density of water (kg/m^3) and the sediment density (kg/m^3) respectively. Altogether 61 experiments result in the following relationship in dimensionless form:

$$\frac{Y_{max}}{d_{90}} - 1.25 \cdot \left(\frac{d_{90}^3 \cdot g}{q^2} \right)^{-1/4} \cdot \left(\frac{L}{d_{90}} \right)^{2/3} \cdot I^{1/2} \cdot \frac{\rho_w}{\rho_s - \rho_w} = 0 \quad 3-55$$

The dimensionful explicit calculation of the maximum scour depth is given in equation 3-57. When designing a step-pool structure without an armor layer for a certain river section, the parameters q , d_{90} , ρ_w and ρ_s are usually given and cannot be changed. The only design parameters in equation 3-57 are thus the spacing L and the slope I . So formula for the maximum scour depth has the following form:

$$Y_{max} = C \cdot L^{2/3} \cdot I^{1/2} \quad 3-56$$

A multiplicative reduction factor r for the maximum scour depth can be calculated in the presence of a bed-load discharge q_b according to equation 3-58. As the presence of a bed-load discharge cannot be guaranteed, Volkart recommends to design the step-pool sequence under the assumption of clear-water conditions, i.e. equation 3-57 should be used and the reduction factor (equation 3-58) should be disregarded. By definition the location ξ_s of the maximum scour is 0 resp. 1 if the scour is located at the upstream resp. downstream step of a pool (Figure 3.33). With increasing discharge or slope the scour gets deeper and moves further downstream (Figure 3.36 a.) and b.) In the next stage (Figure 3.34 c.) the bed in the downstream third of the pool is almost parallel to the step top levels. If this condition is reached the step-pool unit is on the verge of stability. Only a slight increase in discharge or slope causes the scour to move to the downstream step of the pool ($\xi_s = 1$). The pool then begins to erode completely beginning from the downstream step to the upstream step. Throughout the experiments without bed-load discharge it was found that the turning point from a stable to an unstable condition (Figure 3.36 c.) satisfies equation 3-60 with high accuracy.

Equations 3-61 - 3-66 can be used to calculate minimum and maximum water depths and their locations, the mean water depth and the wave extent factor.

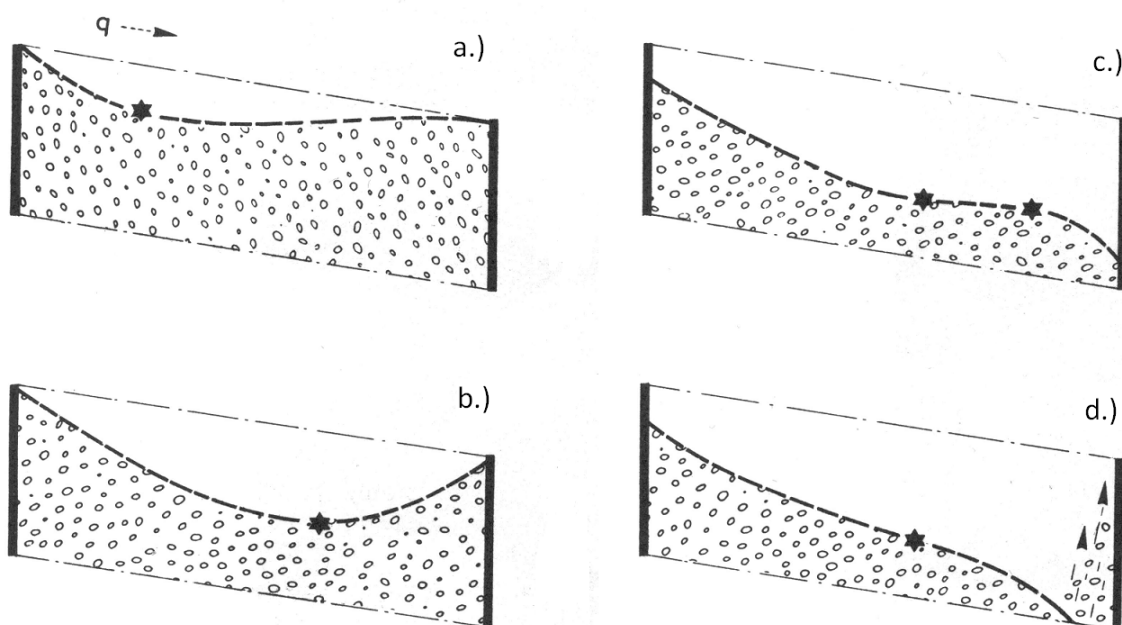


Figure 3.36 Location of the maximum scour depth within one pool (Volkart 1972)

$$\text{Maximum scour depth} \quad Y_{max} = 1.25 \cdot \frac{q^{1/2} \cdot I^{1/2} \cdot L^{2/3}}{d_{90}^{5/12}} \cdot \frac{\rho_w}{(\rho_s - \rho_w) \cdot g^{1/4}} \quad 3-57$$

$$\text{Reduction factor of the maximum scour depth in case of bed load discharge} \quad r = 1 - 0.526 \cdot \frac{I \cdot L}{d_{90}} \cdot \left(\frac{q_B}{q \cdot (\rho_s - \rho_w)} \right)^{1/8} \quad 3-58$$

$$\text{Longitudinal location of maximum scour in the pool} \quad \xi_s = \left(\frac{Y_{max}}{L} \right)^{1+15 \cdot I} \cdot (3.5 + 150 \cdot I) \quad 3-59$$

$$\text{Stable step-pool unit} \quad Y_{max} \leq 0.2 \cdot L \quad 3-60$$

$$\text{Max. water depth} \quad Z_{max} = 0.9 \cdot \frac{q^{0.88}}{L^{0.02} \cdot d_{90}^{0.3} \cdot I^{0.09}} \cdot \frac{\rho_w}{g^{0.44} \cdot \rho_s} \quad 3-61$$

$$\text{Location of max water depth} \quad \xi_{max} = 1.824 \cdot \left(\frac{Z_{max}}{L} \right)^{0.61} \quad 3-62$$

$$\text{Min. water depth} \quad Z_{min} = 0.0589 \cdot \frac{q^{1.5}}{L^{0.51} \cdot d_{90}^{0.74} \cdot I^{0.6}} \cdot \frac{\rho_w}{g^{0.75} \cdot \rho_s} \quad 3-63$$

$$\text{Location of min water depth} \quad \xi_{min} = 1.289 \cdot \left(\frac{Z_{min}}{L} \right)^{0.61} \quad 3-64$$

$$\text{Mean water depth} \quad \bar{Z} = 0.367 \cdot \frac{q^{0.9}}{L^{0.08} \cdot d_{90}^{0.27} \cdot I^{0.32}} \cdot \frac{\rho_w}{g^{0.47} \cdot \rho_s} \quad 3-65$$

$$\text{Wave extent} \quad W = \frac{Z_{max} - Z_{min}}{\bar{Z}} \quad 3-66$$

Step-pool sequence with armor layer

In these experiments the pools of a step-pool sequence was secured with an armor layer. Two different armor materials (A_1, A_2) and associated filter materials (F_1, F_2) were tested as can be seen from Table 3.12 (all data in mm). In contrast to the maximum scour experiments described in the previous section the grain size distribution is almost linear for the armor layer material. The linear distribution correlates with naturally built armoring layers in rivers.

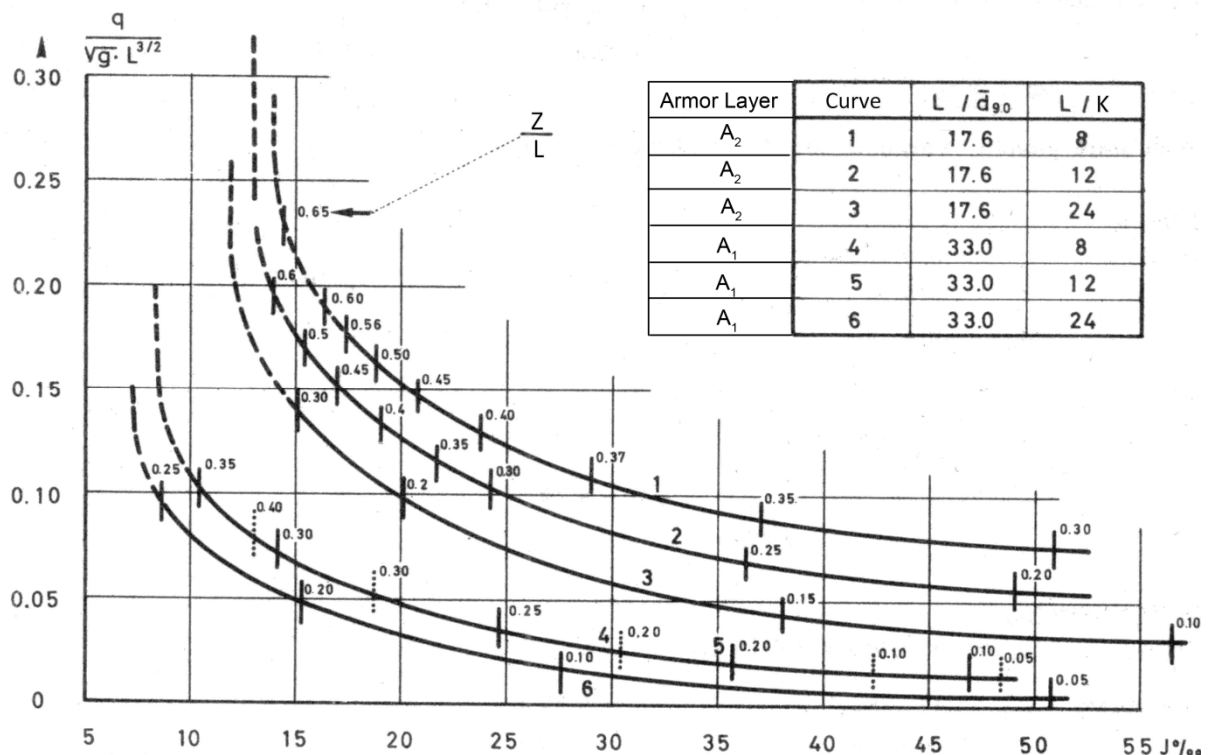
material	F_1	A_1	F_2	A_2
d_{max}	4.1	8.3	8.3	14.4
d_{90}	3.5	7.2	6.4	13.8
d_{50}	1.0	5.7	1.8	11.0

Table 3.12 Filter and armor materials for a step-pool sequence with armor layer (mm)

The aim of these experiments is to determine the incipient motion of the armor layer subject to the specific discharge q , the step spacing L and the step height K and the diameter d_{90} of the armor layer. The incipient motion condition is reached if a slight increase in discharge or slope causes an exposition of the filter layer in a larger area. Rearrangements of the bed or a marginal subsidence of the bed due to erosion of the filter layer material is tolerated and is not regarded as the incipient motion.

The experiments take one hour on average and are carried out for the following ranges of parameters:

- slopes: $0.007 \leq I \leq 0.058$
- bed materials: *see Table 3.12*
- step spacing: $L = 0.24 \text{ m}$
- step height: $K = 1, 2, 3 \text{ cm}$
- spec. discharge: $0 \leq q \leq 120 \text{ l/sm}$
- armor density: 0.83 g/cm^2 for A_1 resp. 1.65 g/cm^2 for A_2


Figure 3.37 Critical discharge for the incipient motion of a step-pool sequence with armor layer (modified after Volkart, 1972)

All over the 45 experiments the condition of the incipient motion is characterized by a strong horizontal clockwise vortex immediately downstream of the upstream step of the step-pool unit and

a surface roller in the downstream half of the pool. The location of the maximum bottom shear stress is equal to the location of the maximum scour depth as calculated from equation 3-59. An artificial armor layer behaves similar than the natural bed formed by natural armoring processes. For low slopes or high relative submergences Z/K where Z denotes the water depth, the main flow is above the top levels of the steps. Below one horizontal clockwise vortex develops that extends along the whole pool length. The armor layer is stable for very high discharges but fails abruptly e.g. due to small irregularities in the armor layer.

As expected the coarser armor material A_2 resists higher discharges than the finer armor layer A_1 . Higher slopes reduce the critical discharge for the incipient motion. Higher step heights K increase the discharge for the incipient motion. The increase is more distinct for the coarser armor material A_2 . The results for the critical discharges and the respective relative submergences Z/K is only given graphically Figure 3.37. For the quasi-smooth flow the water depths can be calculated from equation 3-67. It is valid for slopes ranging from 0.01 to 0.06, L/K ranging from 8 to 30 and for relative submergences $Z/K > 4$.

$$\text{Quasi-smooth flow} \quad Z = 0.649 \cdot \frac{q^{0.55} \cdot K^{0.24}}{L^{0.07} \cdot I^{0.26} \cdot g^{0.275}} \quad 3-67$$

The influence of the step height K on the water depth is about 2.5 times bigger than that of the spacing L . A filter layer is recommended if the diameter \bar{d}_{90} of the armor layer is too coarse in comparison to the diameter d_{90} of the natural bed material. A filter criterion is not provided.

$$\text{Filter layer recommended if} \quad d_{90} < 0.5 \cdot \bar{d}_{90} \quad 3-68$$

Volkart's recommendation concerning the filter layer is in conflict with Whittaker & Jäggi (1986) who report that finer rather than coarser sediments below an armor layer yield a stable armor layer (see Table 3.2, p. 26).

3.4.4 Sediment Transport in Step-pool Streams by Whittaker

Whittaker (1987) investigates sediment transport in step-pool streams. In steep streams sediment inputs are of bulk or unsteady nature. They vary temporarily and spatially. Sediment transport is not so much controlled by bed and hydraulic variables but by sediment supply (surface erosion, land slide, debris flow and erosion of the channel bed and banks). Evaluating field data from other researchers Whittaker finds a relation between the stream slope I and the length of a step-pool unit L but reports that no clear trend can be found for to relate the step height K or the channel width w to the slope.

$$\text{Step-pool length in natural streams} \quad L = \frac{0.3113}{I^{1.188}} \quad (R^2 = 0.6783) \quad 3-69$$

In a series of flume tests Whittaker examines the sediment transport through idealized step-pool sequences under both clear water and live bed conditions. The experiments are performed in a 10 m long, 0.132 m wide tilting flume. The steps are modeled with wooden weirs at a spacing $L = 0.5$ m and a step height $K = 0.19$ m. The width of the steps is 0.033 m. At the beginning of each test run

the steps are filled up with a uniform gravel ($d_{90} = 4.9$ mm, non-uniformity coefficient $U_{84} = 1.1$). Slopes up to 0.248 are investigated. Different combinations of slopes and specific discharges are tested. Whittaker finds that for a given slope the scour hole gets deeper as the discharge rises. This process stops as the scouring is limited by the downstream step. If the discharge is further increased the maximum scour depth reduces a bit. Whittaker does not explain this result explicitly but it can be assumed that at this point the scour extends along the whole pool thus reducing the maximum scour depth. If the specific discharge is further increased the flow becomes unstable, slug waves may occur. Whittaker's results and Figures support Volkart's description of scour development as shown in Figure 3.36 a-d. Unlike Volkart who does not classify the flow patterns of his experiments, Whittaker describes the flow through step-pool systems as tumbling flow (see chapter 3.6.1). The maximum scour depth is deeper for higher slopes, though the transition from stable to unstable tumbling flow occurs at the same specific discharge. Unstable tumbling flow can be subdued by sediment inputs. Conversely, Whittaker reports that in cases where clear water conditions yield stable tumbling flow a steady sediment input rate leads to unstable conditions. In agreement to field observations Whittaker finds that bulk sediment input is transported through the channel as long low waves.

In his laboratory experiments Whittaker reports the occurrence of upstream scours (cf. Figure 3.36 d) surmising that such a scour pattern won't occur in natural step-pool systems because of armoring processes.

3.4.5 Practical examples of step-pool-ramps by Gebler

Gebler is the head of an engineering company that deals with environmental river engineering. He has a lot of experience in the planning and installation of ramps, sills and fish passes part of which is presented in Gebler (1991). The practical examples include ramps in the style of the Schauburger ramp, loose ramps and step-pool-ramps. The standard ramp slope for block ramps has long been 1:10. To fulfill ecological requirements the ramp slope should be decreased depending on the region. To distinguish flat-sloped ramps that take into account the biological matters from the traditional block ramps (in German "Rampen") the German standard DIN 19661-2 introduces the term "Sohlegleiten" for ramps with slopes ranging from 1:15 to 1:30. Adopting to the biological continuity requirement of the Water Framework direction Gebler (2007) recommends step-pool ramps with an integrated low-flow channel for the water fauna. For higher discharges the near-bank zones provide the best fish passes. The extent of turbulence (equation 3-85) is a relevant factor for the biological continuity. It is defined as the ratio of the energy that is entrained into a pool and the pool volume. The bulletin DVWK-232 (1996) of the German Association for Water, Wastewater and Waste (short "DWA") includes recommendations for the pool geometry (pool length and width, water depth) and for the maximum extent of turbulence for different fish species resp. fish regions. According to these recommendations Gebler gives design rules for step-pool ramps regarding ecological rather than stability matters. A sketch of such a ramp is shown in Figure 3.38. The low-flow channel consists of disconnected rows of boulders. The boulders in each row are staggered transversely with those in adjacent rows. The steps and the riprap in between build a compound structure which is incorporated into the banks

Extent of turbulence
$$E = \frac{\rho \cdot g \cdot \Delta h \cdot Q}{V_P} \quad (\text{W/m}^3) \quad \mathbf{3-70}$$

In equation 3-70 Δh and V_p denote the water level difference of two adjacent pools (m) and the volume of a pool (m^3), respectively.

Gebler (2009) gives recommendations for the construction of flat-sloped ramps (Sohlegleiten). Recommendations concerning occupational safety and mandatory laws and standards are omitted here. Gebler recommends frost-resistant rocks from within the region. The excavator operator plays an important role in the success of the installation. Apart from the technical ability he or she should also develop a sense for ecological matters. Before the installation a visit of an existing similar ramp can be useful. The boulder steps of the low-flow channel should be installed at an accuracy of ± 5 cm. The boulders for the steps should have one long and two small axes. The boulders and the blocks of the riprap are installed “standing”, i.e. with the longest axis vertical. The greater platform should be at the bottom. The step boulder should be slightly inclined downwards from the vertical. During a flood event flotsam can pass over the boulders more easily.

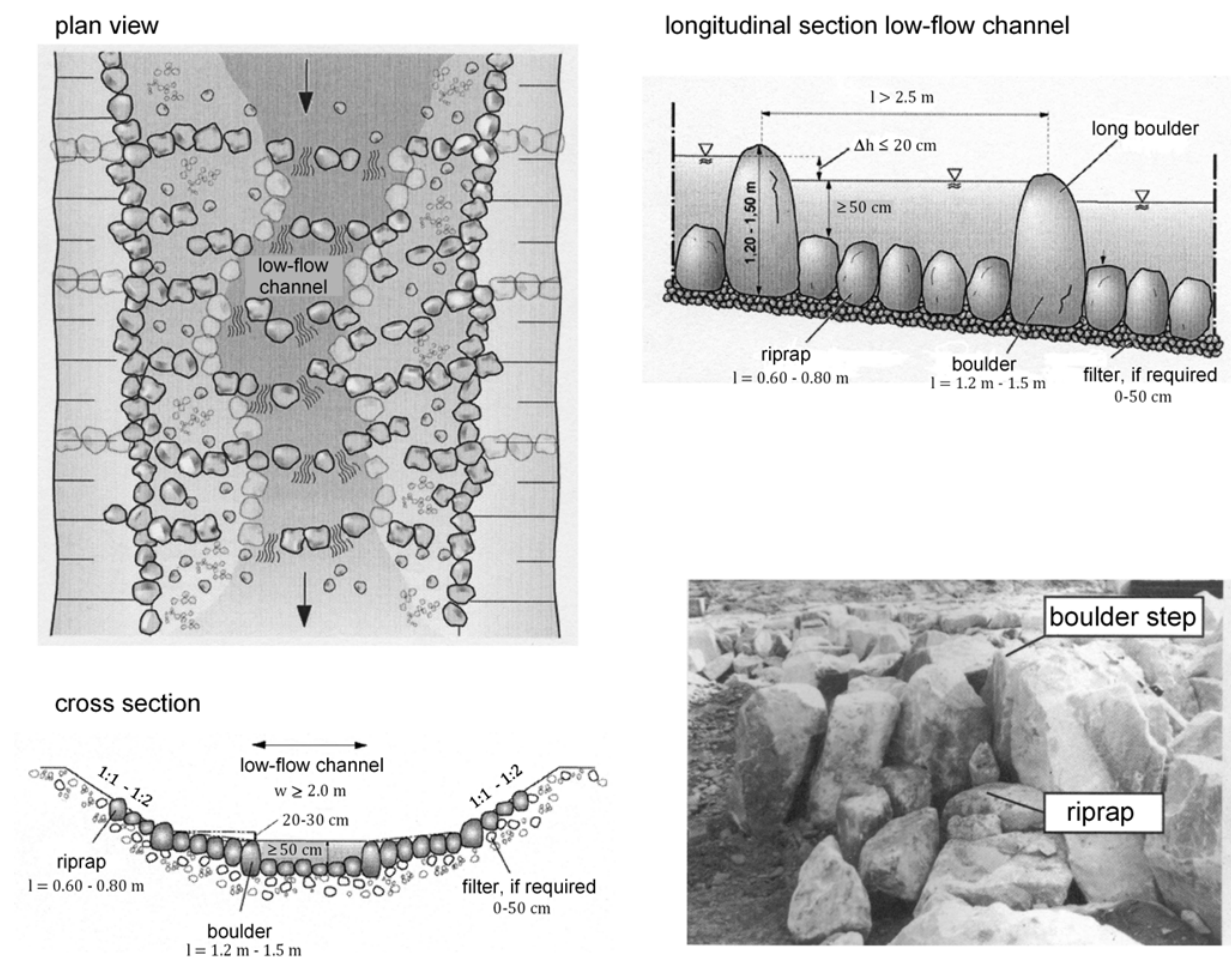


Figure 3.38 step-pool ramp with low-flow channel (sketches modified after Gebler 1991), picture bottom right from Gebler 2009)

At least half of the boulders should be embedded into the riprap. The boulder steps are installed first, the riprap comes second. The total width of the gaps of a boulder step has to be met accurately. Too large resp. small widths lead to too low resp. high water levels upstream of the step so that the required difference of water levels between two pools cannot be met. The boulders should be placed with the shortest axis transversal to the main flow. This way the fish only have to pass a short distance of high velocity. Each step should have gaps of 20 – 30 cm to provide a pass for the bigger

fish. Gaps in between the riprap should be filled up with smaller stones. The riprap surface should be rough rather than paved. All components of the structure must be tied positively together. To position a boulder it can be provided with steel brackets and lifted by a rope. An excavator with a stone grab would be best, but Gebler mentions the acquisition costs. Most ramps can be installed without open dewatering. In case of concrete work a dry construction method has to be applied. According to Gebler concrete work or the use of steel rails is necessary if the ramp has to be installed upon a fixed structure, e.g. an old weir or paved banks. The riprap bank protection should cover at least 2/3 of the bank height. Gebler recommends to build a ramp beginning upstream so as not to flood the excavation pit. On completion of the ramp construction a trial operation is recommended to check the elevation differences between the pools and the water depths. If appropriate final adjustments can be made.

3.4.6 Investigations on step-pool-ramps by Vogel

In a series of model tests Vogel (2003) derives design criteria for step-pool ramps as they are built by the water management office Rosenheim, Bavaria. An existing prototype ramp in Bavaria is re-built and tested in the model. In four further basic tests step-pool ramp configurations typical for the water management office Rosenheim are investigated for slopes of 1:10, 1:15, 1:20 and 1:30 (Figure 3.39). The scale of all the test series is 1:16. All experiments are performed in a flume with a width of 200 cm. The prototype ramp is re-built in the model with a trapezoidal cross section with a bottom width of 80 cm and a bank slope of 1:1. The ramp length 1.9 m (model scale). The basic flume tests are performed with a rectangular cross section with a width of 110 cm. The ramp length is 6 m (model scale).

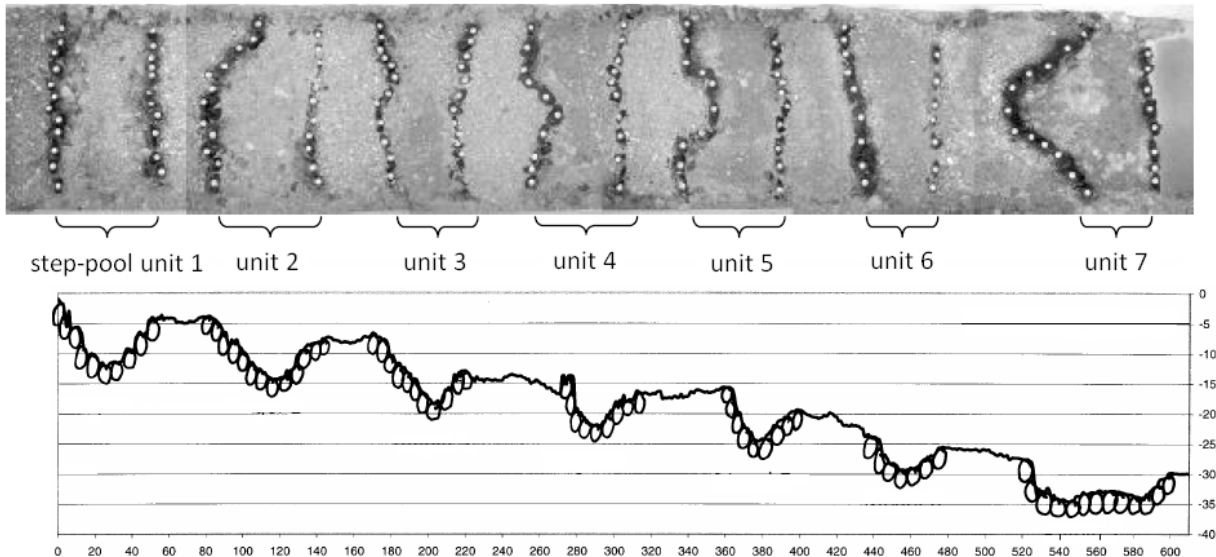


Figure 3.39 Sketch of a step-pool ramp, $I = 1:20$ (Vogel 2003)

Vogel reports that during her experiments the most likely failure mechanism is the sweep out of blocks into the scour hole downstream of a step-pool unit (see also Figure 3.45). The scour holes have developed in the naturally sloped sections between the step-pool units. As her graphical results reveal, these scours develop because of a strongly undular flow. Conversely the re-built prototype ramp (slope 1:30) with a boulder coverage $\Psi = 1$ (no unprotected section between the step-pool units) cannot be destroyed for discharges up to $q = 29 \text{ m}^3/\text{sm}$ (full scale). This specific discharge is a multiple of the design discharge.

If enough space is available Vogel recommends a ramp slope of 1:30 as a flat ramp provides a better stability and is most likely to ensure the continuity for fish, canoeists and oarsmen. As the step-pool ramps have naturally sloped unprotected sections in between, flat sloped ramps do not necessarily result in higher material consumption. The length of a prototype step-pool unit should be between 8 and 10 m. The maximum depth of the pool is 1 – 1.5 m. The vertical height between upstream and downstream step of a unit has to be chosen subject to the fish region. In plan view the steps can be shaped imaginative. The furthestmost upstream resp. downstream step should be perpendicular to the main flow to avoid asymmetric in- and outflow conditions. Equation 3-71 yields the maximum specific discharge q for a ramp subject to the ramp slope I , the equivalent sphere diameter d_s of the blocks of the step pool unit (not including the material of the unprotected naturally sloped section) and the boulder coverage Ψ which is defined as the ratio of the covering area of the step-pool units to the whole area of the ramp.

$$\text{Design rule} \quad q = \sqrt{d_s^3 g} \cdot \sqrt{\frac{\rho_s - \rho_w}{\rho_w}} \cdot (0.05 \cdot I^{-1.463} - 51.4 \cdot (1 - \Psi) \cdot e^{-48 \cdot I}) \cdot 0.774 \quad \text{3-71}$$

According to Platzer (1983) Vogel recommends that the diameter d_f of the filter material should meet equation 3-72, where k denotes the ramp roughness which is defined as one third of the boulder height (see Figure 3.22). The recommended filter criterion is contrasted with Terzaghi's filter criterion in chapter *Construction recommendations and dimensioning*, p.33

$$\text{Filter material} \quad d_f \geq (1/7 \div 3/7) \cdot k \quad \text{3-72}$$

The downstream step of the last step-pool unit should be reinforced with rails. If the downstream river bed has to be protected (Vogel does not state criteria to determine the need of such a protection), then, following Hassinger (1991), the length of the downstream protection should be 2 – 2.5 times the width of the ramp at the ramp toe. The height of this armor layer should be in the range of 1.5 times the maximum diameter of the armor material. Vogel further recommends to fill up small gaps between a boulder step with smaller stones to prevent high velocity jets between the blocks that erode the bed material below. One advantage of the step-pool ramp over the traditional block ramp is that it can be built without a water drainage. The first positioning of a boulder should be slightly below the desired elevation. If the boulder is lifted again the bed material enfolds the block. The ramp should be installed from the downstream to the upstream end (this is opposite to the advise in Gebler, 2009). The order of installing a step-pool unit is as follows: 1. Downstream step, 2. Upstream step and 3. Scour blocks. Thus the required vertical height of a step-pool unit can be ensured. Vogel dissuades from installing individual blocks protruding from the ramp.

Apart from the biological continuity of step-pool ramps Vogel mentions further advantages for canoeists. Removing drops by step-pool ramps reestablishes the navigability of a river. On the other hand the risk of being drowned in a subsurface roller with horizontal axis downstream of the drop vanishes. Drops with heights as small as 30 cm are already considered a safety hazard.

3.4.7 Investigations on step-pool-ramps by Korecky

Korecky (2007) investigates vey flat sloped step-pool ramps in flume experiments. The slopes range from 1:30 to 1:83. A step consists of three boulder rows. Particular attention is paid to the influence of the grouping of the boulder rows (e.g. roof-tile style), the shape of the filter material (rounded or cruhsed) and the sediment gradation (non-graded, graded). The experiments are carried out in a tilting rectangular flume with a length of 15 m and a width of 54 cm. The ramp configurations consist of upstream and downstream reference sections and the ramp itself. The ramp length is either 1.25 m or 2 m. A formula (equation 3-73) for the required mass of stones M (kg) subject to a given specific discharge q , the ramp slope I and a tolerance parameter Ω is derived from these experiments. The tolerance parameter specifies the proportion of moving step stones that is tolerated. If a movement of 2% of the stones is acceptable, then $\Omega = 0.02$. Equation 3-73 can be re-written as a formula for the maximum discharge in terms of the equivalent sphere diameter d_s (equation 3-74).

Design rule – required mass

$$M = \frac{\rho_s}{g} \cdot \frac{q^2}{(-3.238 \cdot \Omega^{-0.035} \cdot \ln I - 4.520 \cdot \Omega^{-0.129})^2} \quad \mathbf{3-73}$$

Design rule – maximum discharge

$$q = \sqrt{d_s^3 g \cdot (-2.343 \cdot \Omega^{-0.035} \cdot \ln I - 3.271 \cdot \Omega^{-0.129})} \quad \mathbf{3-74}$$

Equations 3-73 and 3-74 are valid ramp slopes ranging from 1:330 to 1:30, for a roof-tile grouping of the three boulder rows that build a step and for a crushed filter material. The filter material is chosen such that $d_{s,f} = 0.2 d_s$ where $d_{s,f}$ and d_s denote the equivalent sphere diameter of the filter and step material, respectively. Coefficients that either reduce or increase the calculated mass for different groupings and shapes are listed in Table 3.13.

Grouping, shape	Coefficient
Rounded filter material, grouping other than roof-tile	1.42 – 1.58
Rounded filter material, grouping other than roof-tile, supporting wedge (consisting of filter material) downstream of the step	< 1.40
Crushed filter material, grouping other than roof-tile	1.18 – 1.20

Table 3.13 Coefficients to reduce or increase the calculated mass of stones from equation 3-73

Final test series are performed in 18 m long and 1 m wide horizontal flume to determine the necessary bank and bed protection downstream of the ramp. Therefore a half model with a trapezoidal cross section (bank slopes 1:1.5 or 1:2) is installed. It consists of upstream and downstream reference sections and a ramp itself. The banks and the downstream reference sections are mobile. The sediments of the upstream reference section and the bed of the ramp are glued to the bottom. The experiments prove that a single layer of bank boulders with a mass of about 30 % of the step stones is sufficient to protect the banks. This is more economic than the common practice of a two-layer bank protection. Direct erosion of bank boulders is not observed during the experiments. The bank toe must not be washed out to prevent the bank from sliding. Therefore an additional row of bank stones (in longitudinal direction) level with the river bed is recommended. The stones of the bed protection downstream of the ramp should have 10 % of the mass of the step stones and cover 50 % of the river bed.

3.4.8 Investigations on step-pool-systems by Rosport and Aberle

Step-pool systems offer a vast field of research (e.g. Whittaker, Jäggi 1982, Abrahams, Li et al. 1995, Chin 2002, Valle, Pasternack 2006, without intending to be exhaustive). Key questions are to identify the parameters that influence the development of step-pool systems, the maximum resistance and the periodicity (spacing, step height) of step-pool systems. In connection with step-pool ramps the genesis of step-pool systems is not so important as the step-pool structure is built artificially. In contrast knowledge of the maximum resistance and the periodic nature of step-pool systems can be applied in the planning and installation of step-pool ramps.

Rosport (1998) investigates the flow resistance and the bed stability of steep streams, particularly step-pool structures. Flume experiments are conducted in a 12 m long and 0.2 m wide rectangular tilting flume which can be adjusted to slopes ranging from 0 – 9.6 ‰. The slopes are classified as “flat” ($I = 2 - 4\%$) and “steep” ($I = 8 - 9.6\%$). Two different sediment materials of a rather spherical shape are used having the same characteristic diameter d_{50} . For one material the large grain sizes are removed, resulting in smaller d_{84} and non-uniformity parameter U_{84} . The scale of the experiments is 1:8. Rosport finds that the equivalent sand roughness k_s does not only depend on geometrical properties of the sediments (i.e. the grain size distribution) but also on bed forms and the Froude number. Similar to Knight & Macdonald (1979) (see chapter 3.6) a geometrical shape parameter K'_s is defined, which is composed of the standard deviation s (m) of the rough bed and a roughness arrangement parameter γ (m). Rosport finds that the shape parameter K'_s can be related uniquely to the Nikuradse roughness k_s (equation 3-76).

**Geometrical shape
parameter**

$$K'_s = 3.71 \cdot s \cdot \gamma^{-13.43 \cdot I^{1.66}} \quad 3-75$$

**Relation to Nikuradse
roughness**

$$\frac{k_s}{K'_s} = 0.23 \cdot e^{1.85 \cdot Fr} \cdot \left(\frac{R_s}{s}\right)^{(-2.55 \cdot Fr + 2.4)} \quad 3-76$$

Knowing k_s the friction factor λ can be calculated via the Colebrook-White formula for fully turbulent flows (equation 3-77), where f denotes a form parameter. Moreover the dimensionless critical shear stress $\tau_{*,c}$ can be determined via K'_s and the characteristic diameter d_m of the armor layer.

**Semi-empirical Colebrook-
White formula for fully
turbulent flows**

$$\sqrt{\frac{8}{\lambda}} = 2.5 \cdot \ln \frac{R}{k_s} + 2.5 \cdot \ln(14.84 \cdot f) \quad 3-77$$

**Dimensionless critical shear
stress**

$$\tau_{*,c} = 0.013 \cdot \frac{K'_s}{d_m} + 0.017 \quad 3-78$$

Afzalimehr & Anctil (1998) also try to ameliorate the prediction of the friction factor by expanding the semi-logarithmic law with the Froude number. Aberle et al. (1999) (for Rosport, 2008 and Afzalimehr & Anctil, 2007) and Rennie & Millar (1999) (for Afzalimehr & Anctil, 2007) show however that the enhanced predictability arises from the fact that the mean velocity \bar{u} is known and the Froude number is calculated from \bar{u} . If the mean velocity is known, however, the friction factor λ can be calculated directly from equation 3-79.

Relation of friction factor and mean velocity

$$\lambda = 8 \cdot g \cdot h \cdot I \cdot \bar{u}^{-2} = \frac{8 \cdot I}{Fr^2} \quad 3-79$$

Using the known mean velocity U to calculate Froude leads to a spurious self-correlation (Aberle, Dittrich et al. 1999, Rennie, Millar 1999). If on the other hand \bar{u} is unknown then the Froude number Fr has to be calculated iteratively by the following procedure:

1. estimate Fr
2. calculate friction factor λ from equation 3-77
3. calculate Fr from 3-79 with λ (from step 2)
4. if estimated Froude number Fr (step 1) and calculated Froude number Fr (step 3) do not match, goto step 1.

Aberle (2000) shows that if the Froude number is calculated iteratively in Rosport's experiments then the given formula 3-77 does not improve the predicted friction factor. Therefore Aberle re-analyzes Rosport's data and finds a semi-empirical relationship (equation 3-80) for the friction factor λ subject to y/s (equation 3-80) where y denotes the mean water depth (m). Aberle also derives equations for the critical discharge and the critical depth (equations 3-81 and 3-82).

Semi-empirical Colebrook-White formula for fully turbulent flows

$$\sqrt{\frac{8}{\lambda}} = 3.83 \cdot \ln \frac{y}{s} - 1.18 \quad 3-80$$

Critical discharge

$$\frac{q_{cr}}{\sqrt{g \cdot s^3}} = 0.2 \cdot \sin \alpha^{-1.3} \quad 3-81$$

Critical depth

$$\frac{y_{cr}}{s} = 0.45 \cdot \sin \alpha^{-0.77} \quad 3-82$$

Equations 3-80 - 3-82 are expressed in terms of the standard deviation s of the rough bed. As the standard deviation of the rough bed includes morphological structures like step-pool structures it is better suited to determine λ , q_{cr} and y_{cr} than any characteristic diameter d_{xx} . Nonetheless Aberle also provides a criterion that is based on the mean diameter d_m :

$$\frac{q_{cr}}{\sqrt{g \cdot d_m^3}} = 0.079 \cdot \sin \alpha^{-1.11} \quad 3-83$$

3.4.9 The Meandering Ramp by O. Grober

The "meandering ramp" is a special kind of a step-pool ramp. The steps of a "meandering ramp" are alternately inclined to the left and the right bank. This lateral inclination induces a meandering flow on low discharges which leads to reduced velocities along the ramp (Figure 3.40). Seen from above the steps of the meandering ramp are arc-shaped. This serves a twofold purpose: the first is the force transmission into the banks. Secondly, the step can be interpreted as two deflecting submerged groins ("inklinante Buhnen") which induce two counter-rotating secondary currents. Transported

sediments move from the center towards the banks thus protecting them (Figure 3.41, left). If possible the pools of the ramp consist of the natural river bed material. No additional armoring is needed. This enables natural processes of scouring and deposition. The steps are made of large boulders with a diameter of 1 - 1.5 m. Approximately 4/5 of a boulder are embedded into the natural river bed (Figure 3.41, Figure 3.41). The meandering ramp has been installed three times in Austria and once in Switzerland so far (Table 3.14).

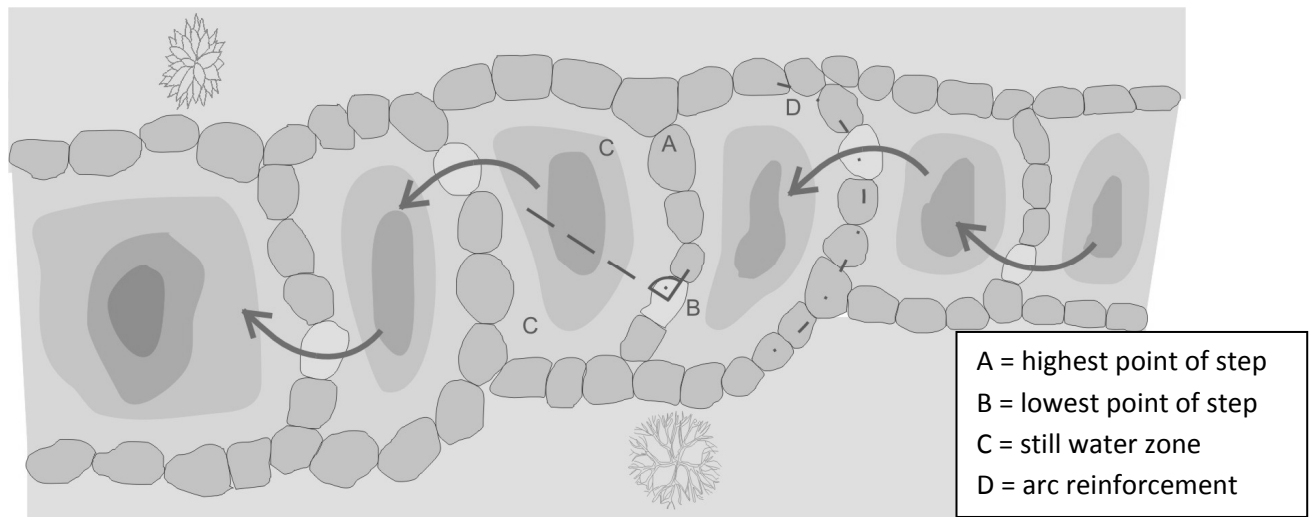


Figure 3.40 Sketch of a meandering ramp, plan view (Mende, Gassmann 2009, labels translated by author)

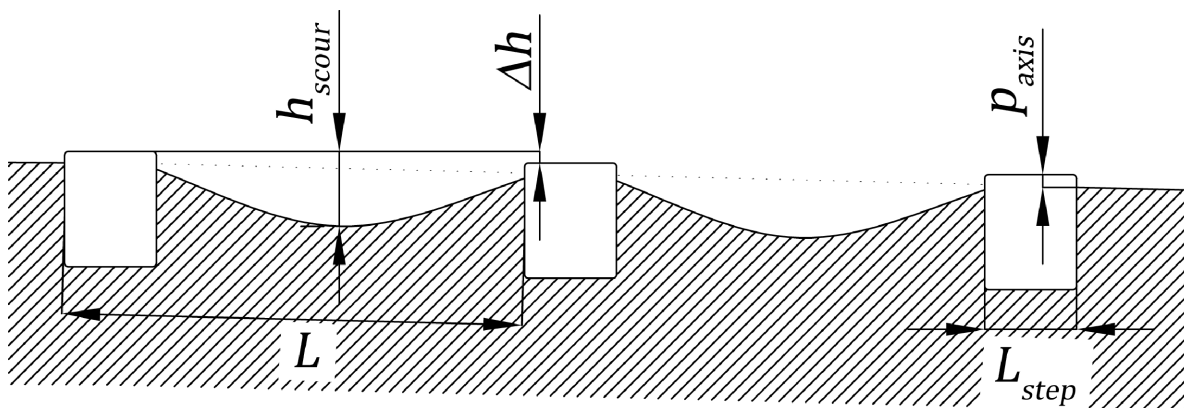


Figure 3.41 Sketch of a longitudinal section of a meandering ramp in river axis

The meandering ramp has been developed by the Austrian engineer Otmar Grober. A mountain stream served as a natural role model. Figure 3.42 shows photographs of the natural model and the prototype meandering ramp. On the latter picture the meandering flow is well visible.

Location, year of installation	Ramp height (m)	Ramp slope (%)	Stream slope (%)
Grünauerbach, near Rasing, Austria, 2004	2.15	6.9	2.0
Stübmingbach, near Turnau, Austria, 2004	2.26	6.8	3.9
Salza, near Gusswerk, Austria, 2010	1.0	2.5	-
Scherlibach near Köniz, Switzerland, 2008	3.17	4.2	2.0

Table 3.14 Existing meandering ramps



Figure 3.42 Natural model for the meandering ramp (left), first prototype meandering ramp, Stübmingbach (right)

3.4.10 Advantages of a Meandering Ramp over Conventional Step-Pool Ramps

When step-pool ramps are properly designed the tumbling flow regime (and thus very good energy dissipation) occurs for a certain range of discharges. The residual energy at the toe of the ramp is minimized. Normally the pools of a step-pool ramp are armored. This prevents scouring processes in the pools. If possible the pools of the meandering ramp do not need additional armoring. Natural processes of scouring and deposition are possible. The meandering ramp as a special kind of step-pool ramp provides further advantages.

1. Material and cost savings
2. Ecological benefit: scouring and deposition processes, sediment sorting, variance in depth and (spatial) flow variability improve the habitats of aquatic life.
3. Hydraulic benefit: the higher the discharge the deeper gets the scour hole. A deeper scour hole prolongs the tumbling flow regime (very good energy dissipation). On the falling limb of the flood wave sediments deposit and fill up the scour holes again because of the reduced bed shear stresses.
4. The steps of a meandering ramp are laterally inclined. Energy dissipation takes place also in lateral direction. It is therefore assumed that the total energy dissipation is higher for laterally inclined steps than for non-inclined steps. For three dimensional stilling basins this advantage over two dimensional stilling basins is well known.

3.5 Key Features of Ramps

3.5.1 Hydraulic Efficiency of Drop Structures and Ramps

The first step should be at the crest of the ramp to prevent high approach velocities to the first step due to the fast acceleration on the ramp (see chapter 3.1.5).

A baffle pier of the Chute Spillway Basin III (see chapter 3.1.4) has a vertical upstream face. The hydraulic jump takes place in the cross section of this upstream face. The water surface is almost vertical.

For a drop structure with a stilling basin the potential of the drop height which is transformed to kinetic energy along the drop structure should be dissipated within the stilling basin. A hydraulic jump with surface rollers should develop. This requires a Froude number minimum of the flow entering the jump. An undular jump should be avoided because its oscillating jet may propagate far downstream the stilling basin causing bed scouring and bank damages. The scouring of the river bed may eventually endanger the structure itself.

Bleines (1951) explains why small drop heights are often preferable, for instance to ensure balanced groundwater levels up- and downstream of the structure. He argues though that there is a lower limit of a drop height in order to guarantee the hydraulic efficiency of the drop structure. Bleines distinguishes a free overfall with a flow transition from sub- to supercritical and a hydraulic jump with surface rollers downstream of the structure from a submerged overfall with an undular jump.

For Bleines a drop structure is hydraulic efficient if the drop height is high enough to avoid an undular jump even for the highest flood event.

According to Bleines the transition from a free to a submerged overfall arises when the critical depth y_c is reached at the drop crest. Applying the momentum equation to the drop cross section and a cross section downstream of the drop with depth y_2 yields the minimum possible drop height h_{min} :

$$h_{min} = y_c \cdot \left(-1 + \sqrt{\left(\frac{y_2}{y_c}\right)^2 + 2\frac{y_c}{y_2} - 2} \right) \quad 3-84$$

He reports however that equation 3-84 underestimates the minimum possible drop height for vertical or almost vertical drops as shown field and model tests. Bleines therefore suggests the empirical formula which he gains from evaluating own model tests and those described in literature (h_{min} as defined in equation 3-84):

$$h_{min,vert} = y_c \cdot \left(-3.97 + \sqrt{\left(\frac{h_{min}}{y_c} + 5.47\right)^2 - 14.15} \right) \quad 3-85$$

For all of Bleines' 59 measured minimum drop heights, equation 3-85 yields a good approximation below the measured value, thus the results are on the safe side.

The reason why the theoretically derived equation 3-84 needs corrections is because Bleines does not take into account the fact that the undular jump does not only occur for the singular condition of critical depth at the drop crest section but for a range of entrance conditions. Nowadays, the upstream control section for momentum considerations is taken at the point where the flow enters the jump (e.g. Peterka 1964, Montes, Chanson 1998). Re-analyzing Bleines' data and expressing the minimum possible drop height in terms of a lower limit for the Froude number Fr_1 of the flow entering the jump yields values $Fr_1 = 1.21 - 1.67$ (assuming that the flow enters the jump at the drop crest section).

Interestingly enough Bleines finds that equation 3-84 is valid for chutes with slopes ranging from 1:4 to 1:12 including chutes with a rough bottom and chutes with a deepened stilling basin with end sill.

As $h_{min} < h_{min,vert}$, chutes allow smaller drop heights than vertical drops.

Niel (1960) argues that for block ramps a hydraulic jump with surface rollers should be avoided so as not to endanger the ramp because of scouring processes downstream of the ramp. Instead of a hydraulic jump with surface rollers he requests an undular jump downstream of the ramp. To distinguish the type of hydraulic jump he suggests Bleines' equation 3-84 which he states in terms of the Froude number Fr_2 downstream of the ramp.

$$\frac{y_2 - h_r}{y_2} = 1 - Fr_2^{2/3} \left(\sqrt{Fr_2^{-4/3} + 2Fr_2^{2/3} - 2} - 1 \right) \quad \text{3-86}$$

Franke (1970) distinguishes between four flow regimes for vertical drop structures:

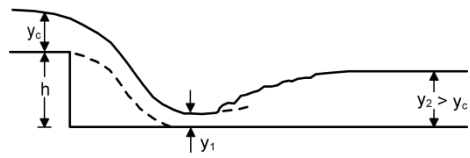

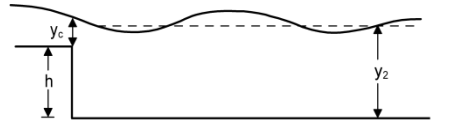

	Flow Trans.	Upstream condition	Downstream condition
<p>Free jump with surface rollers</p> 	YES		
<p>Submerged jump with surface rollers</p> 	YES	$\frac{2}{3}y_c < y_1 < \frac{3}{4}y_c$	$h < y_2 < h + \frac{2}{3}y_c$
<p>Undular jump</p> 	YES	$\frac{3}{4}y_c \leq y_1 \leq y_c$	$h + \frac{2}{3}y_c \leq y_2 \leq h + y_c$
<p>Permanently subcritical flow</p> 	NO	$y_1 > y_c$	$y_2 > h + y_c$

Table 3.15 Flow Regimes for vertical drop structures according to Franke (1970)

Franke's criteria can be expressed in terms of the Froude number Fr_1 using the relation $q = \sqrt{g \cdot y_c^3}$ and $Fr_1 = q / \sqrt{g \cdot y_1^3}$:

- Jump with surface roller 3.87
 $1.54 < Fr_1 < 1.84$
- Undular jump 3.88
 $1 \leq Fr_1 \leq 1.54$
- Subcritical flow 3.89
 $Fr_1 < 1$

The highest amplitude of the waves of the undular flow is at the lower limit of the region.

For Hartung (1973) a drop structure must have a flow transition to be hydraulic efficient. The Froude number Fr_1 entering the jump should be at least 3.0.

Knauss (1979) states criteria for the hydraulic efficiency of a ramp for different purposes:

Hydraulic efficiency as ...

a drop structure
$$y_2 \leq h + \frac{2}{3} \cdot y_c$$
 3.90

a ground swell
$$h + \frac{2}{3} \cdot y_c < y_2 < h + y_c$$
 3.91

**a bottom protection structure
(level with the river bed)**
$$y_2 \geq h + y_c$$
 3.92

From equations 3-8 and 3-10 it follows that the Froude numbers Fr_1 entering the jump at the toe of the ramp can be expressed as

$$Fr_1 = \frac{2.81}{\sqrt{C}} \quad \mathbf{3-93}$$

where the parameter C is defined as in equation 3-9.

The Froude numbers Fr_1 thus range from 2.23 to 1.91 for slopes from 1: 6 to 1: 15, respectively. For the standard ramp slope 1: 10 the Froude number $Fr_1 = 2.07$.

Bleines requirement to ensure hydraulic efficiency for **all** discharges is considered as possibly too strict by Knauss. He argues that the maximum discharges last only a short time and that a continuous subcritical flow over the ramp can be accepted for such peak flow situations. Instead he recommends to guarantee hydraulic efficiency of a ramp as a drop structure for the bed building discharges.

Whittaker & Jäggi (1986) propose to require hydraulic efficiency for discharges from a 2-year-flood up to a 20-year flood.

Platzer (2000) claims the hydraulic efficiency at least for the bed building discharges.

As criteria for hydraulic efficiency the German standard for ramps (DIN 19661-2) requires a twofold flow transition (subcritical – supercritical – subcritical) along the ramp and a Froude minimum at the toe of the ramp of $Fr \geq 1.7$.

Criteria for the hydraulic efficiency of ramps have been adopted from those of drop structures with a stilling basin and are therefore inappropriate. For a drop structure with a stilling basin the potential of the drop height which is transformed to kinetic energy along the drop structure should be dissipated within the stilling basin. A hydraulic jump with surface rollers should develop. This requires a Froude number minimum of the flow entering the jump. An undular jump should be avoided because its oscillating jet may propagate far downstream the stilling basin causing bed scouring and bank damages. Otherwise there is the danger of scouring the river bed downstream of the structure which may eventually endanger the structure itself.

To determine the energy dissipating ability of a ramp Pagliara & Chiavaccini propose the calculation of the total head loss $E_0 - E_1$ between an upstream control section 0 (critical depth y_c is assumed) and a downstream section 1 (Figure 3.25, right). The relative energy dissipation ΔE_r is defined as the

total head loss divided by the total energy head at the upstream control section, i.e. $\Delta E_r = (E_0 - E_1)/E_0$ (cf. equation 3-43, Table 3.7).

What is confusing about the above definition is that the relative energy dissipation cannot become 1. For a discharge q the minimum possible energy level at the toe of the ramp is $E_1 = 1.5 \cdot y_c$. This is the best performance a ramp can provide. In this case the above definition yields

$$\Delta E_r = \frac{h}{h + 1.5y_c} < 1$$

Another approach would be the following (as proposed by the author): The ramp is considered to work optimal if the potential energy of the ramp height h can be dissipated along the ramp, i.e. if the specific energy level of the ramp crest and the ramp toe is the same. It makes sense that in this case the relative energy loss should be 1. Thus the definition of the relative energy dissipation ΔE_r is proposed to satisfy equation 3-94:

$$\Delta E_r := \frac{E_0 - E_1}{h} \tag{3-94}$$

With this definition a step-pool ramp works optimally as long as the tumbling flow regime can be preserved (definition of tumbling flow, see chapter 3.6.1).

3.5.2 Failure Mechanisms

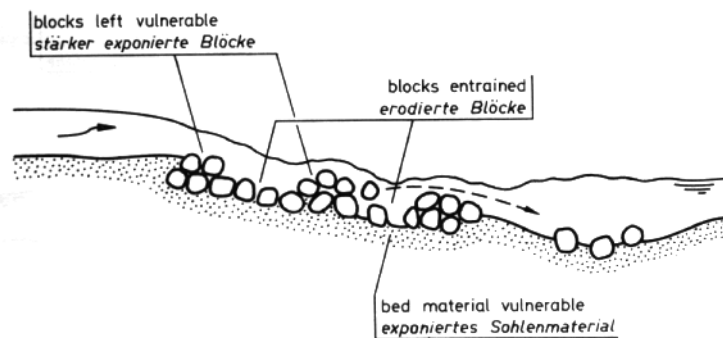


Figure 3.43 direct erosion of blocks (Whittaker, Jäggi 1986)

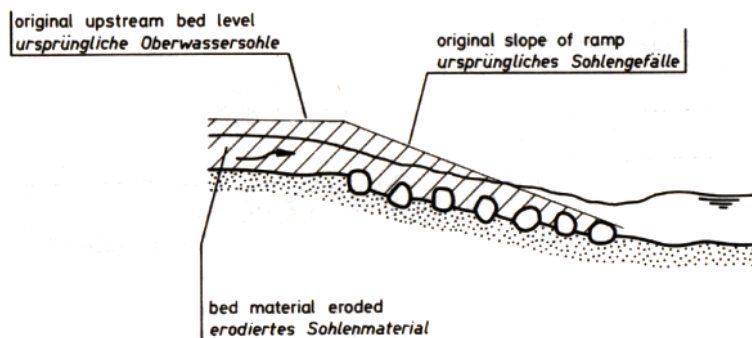


Figure 3.44 Erosion of bed material (Whittaker, Jäggi 1986)

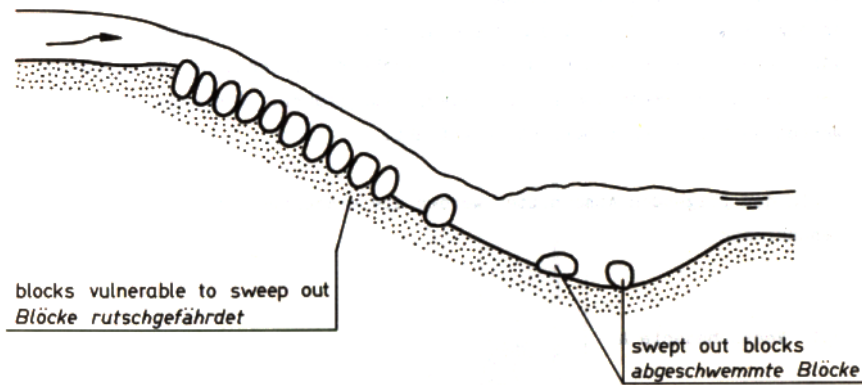


Figure 3.45 Blocks are swept away into the scour hole downstream of the ramp (Whittaker, Jäggi 1986)

Hassinger (1991) lists two further failure mechanisms for block ramps with a reinforced ramp toe (e.g. with rails):

1. failure of the reinforcement (e.g. rails); causes the blocks to slip downstream
2. erosion of the blocks due to compressive stress applied to the armor layer by the flow. The armor layer cannot resist the compressive stress as it is pressed against the fixed reinforcement at the ramp toe.

According to Donnelly & Blaisdell (1965) states, that for $y_2 \geq h + \frac{2}{3}y_c$ the jet impinging the tailwater does not reach the river bottom. Discharges with tailwater levels fulfilling the above equation can be neglected.

3.6 Artificial Roughness Elements

3.6.1 Classification of Flow Regimes Over Roughness Elements by Peterson & Mohanty

Peterson & Mohanty (1960) investigate flow patterns over artificial roughness elements. They distinguish three flow regimes:

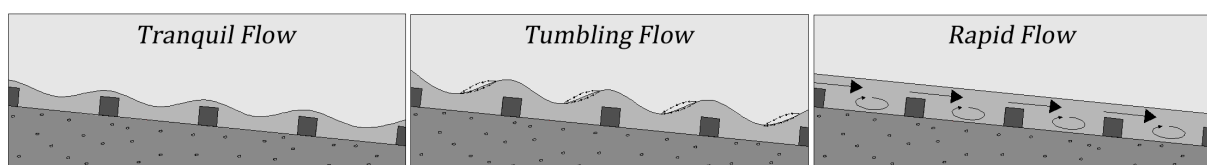


Figure 3.46 Flow regimes over artificial roughness elements according to Peterson & Mohanty (1960)

The tranquil flow regime is characterized by a smooth, subcritical flow even over the tops of the roughness elements. No hydraulic jump is observed. The tumbling flow regime is identified by an alternate succession of subcritical and supercritical flow through critical flow over each roughness element. Between the elements a hydraulic jump develops. At higher discharges the rapid flow regime appears in which the flow skims over the roughness elements at supercritical conditions.

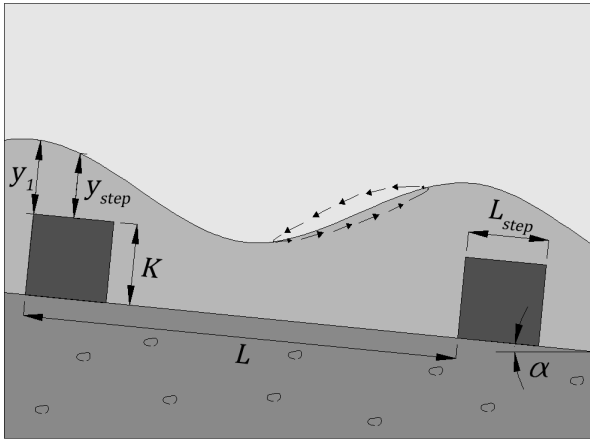


Figure 3.47 Design parameters for large roughness elements

Peterson and Mohanty identify parameters that influence the flow pattern:

- K (m) height of the roughness element
- L (m) spacing of roughness elements
- y_1 (m) water depth above upstream crest of roughness element
- v_1 (m/s) velocity at upstream roughness crest
- $I = \tan \alpha$ (–) slope
- g (m/s²) gravity

From these 6 dimensionful parameters 4 dimensionless parameters can be found:

$$f\left(\text{Fr}_1, \frac{K}{y_1}, \frac{L}{y_1}, I\right) = 0 \quad 3-95$$

Fr_1 denotes the Froude number above the upstream crest of a roughness element.

For the tranquil and the rapid flow regime a relationship as given by equation 3-95 can be found in several experiments and is presented graphically. Peterson and Mohanty report that within the same flow regime (tranquil or rapid) different discharges q may yield the same flow depth y_1 for varying L/K . This is explained by different flow patterns as classified by Morris (1995). Conversely if for one and the same flow depth y_1 the ratio L/K is such that quasi-smooth flow occurs, the discharge is greater than it is for wake-interference flow. The maximum discharge occurs at isolated roughness flow conditions.

For the tumbling flow regime Peterson and Mohanty cannot find a relationship as given by equation 3-95. The flow depth over the upstream crest of a roughness element satisfies equation 3-96, where $c = 1.13$ and y_c denote a constant and the critical depth respectively.

$$y_1 = c \cdot y_c \quad 3-96$$

Morris (1968) reports the same relationship with $c = 10/9$.

Equation 3-96 merely states that in the tumbling flow regime the flow depth over the upstream crest of a roughness element is slightly larger than the critical depth. It would be desirable though to relate

the occurrence of tumbling flow with the roughness geometry, i.e. with L/K and the slope I . Peterson and Mohanty presume the existence but are unsuccessful in finding such a correlation in their experiments.

According to Peterson and Mohanty roughness elements can be used as an energy dissipating structure. A chute with a large stilling basin is expensive. Using roughness elements the costs can be reduced or the slope of the chute can be increased. Roughness elements are also a means to enhance the sediment transport due to increased turbulence. Moreover they can be used for stream measurements particularly in streams with a high temporal variability of bed load transport. A tumbling-flow chute having the same slope as the stream can serve as an overfall weir avoiding problems in connection with stilling basins and sediment drop outs.

3.6.2 Design Rules for Channels With Artificial Roughness Elements after Morris

In a series of model tests Morris investigates the hydraulics of energy dissipation in steep channels with roughness elements (Morris 1969, Morris 1968). The experiments are conducted in a 9.14 m long and 0.61 m wide tilting flume with a maximum slope of 30 %. Objectives of the studies are to determine characteristics and limitations of the tumbling flow phenomenon. In order to serve as an energy dissipating structure an optimal design of the roughness geometry (height, spacing, shape) is sought. Finally design criteria for practical engineering design of steep channels for effective energy dissipation are provided. The various roughness configurations include roughness heights K ranging from 13 – 102 mm, spacing varying between 0.1 and 0.5 m. Mostly square bars are investigated. In connection with the roll waves phenomenon (see next paragraph) different shapes of the cross section of the lateral bars are tested: square with rounded edges, rectangle with a triangle top, triangle, rectangle with trapezoidal top (Figure 3.48).

Morris expands Peterson & Mohanty's flow classification and distinguishes a stable from an unstable tumbling flow regime. In the unstable tumbling flow regimes roll waves superimposed on the main flow may occur which move downstream at a lower velocity than the main flow. The wave amplitude increases as the waves propagate downstream. Apart from the freeboard problem these waves may even endanger the stability of the channel and should thus be avoided. Usually the unstable tumbling flow regime occurs at higher discharges than the stable tumbling flow phenomenon.

Unlike Peterson & Mohanty who choose the velocity v_1 (m/s) and the water depth y_1 (m) to be influencing parameters of the flow regimes, Morris selects the specific discharge q (m²/s) as independent variable. The dimensional analysis yields dimensionless terms $K \cdot \sqrt[3]{g/q^2}$ and the relative spacing L/K instead of the Froude number, K/y_1 and L/y_1 as in equation 3-95. Consequently a relationship as given by 3-97 is sought in Morris' experiments.

$$\mathbf{f} \left(K \cdot \sqrt[3]{\frac{g}{q^2}}, \frac{L}{K}, I \right) = 0 \quad \mathbf{3-97}$$

Morris however cannot find a functional relationship of the relative spacing L/K and the tumbling flow regime. According to Morris the relative spacing plays an important role with respect to the roll wave phenomenon. Relative spacings smaller than $L/K \leq 5$ produce rapid flow even at very low discharges. For relative spacings ranging from $5 < L/K < 8,5$ roll waves may occur. For $L/K > 10$ the acceleration of the flow between to roughness elements is large enough as to shift the location of the hydraulic jump towards the downstream roughness element which can be regarded as a form

of rapid flow. Morris therefore recommends the following range for the relative spacing (equation 3-98):

$$\text{Recommended relative spacing} \quad \frac{L}{K} \doteq 8.5 - 10 \quad 3-98$$

By doing so the relative spacing is eliminated from equation 3-97. Morris finds a criterion that relates the maximum specific discharge q (m^2/s) for which tumbling flow can be preserved to the roughness height K (m) and the slope I (-).

$$\text{Required roughness height to ensure tumbling flow} \quad K = \left(\frac{q}{(3 - 3.7 \cdot I)\sqrt{g}} \right)^{2/3} = \left(\frac{1}{3 - 3.7 \cdot I} \right)^{2/3} \cdot y_c \quad 3-99$$

$$\text{Maximum discharge at tumbling flow conditions} \quad q = K^{3/2} \cdot (3 - 3.7 \cdot I)\sqrt{g} \quad 3-100$$

Equations 3-99 and 3-100 are valid for 2-dimensional square bars and slopes ranging from 1.9 to 30 %. Only four rows of roughness elements are necessary to establish a cyclical uniform flow. This is in accordance with Peterka's baffled apron (see Peterka (1964) and chapter 3.1.5). Additional experiments in both a 30.5 cm wide rectangular channel and a trapezoidal channel (bank slope 1: 1, bed width 61 cm) suggest that the results are independent of channel width and bank inclination, although too little experiments are conducted to get significant results.

To prevent roll waves Morris tests different shapes of the cross sectional profile of the 2-dimensional roughness elements (Figure 3.48). As the roll waves phenomenon is most severe for square bars and relative spacings $L/K = 5$, all other shapes are also tested with this relative spacing. All shapes different from the square reduce the roll wave phenomenon although none of them can prevent it entirely. The triangle shape works best. On the other hand all the non-squared shapes reduce the maximum discharge for which tumbling flow can be preserved. Rather than using a non-squared shape Morris recommends a squared cross section in connection with equation 3-98 to prevent roll waves.

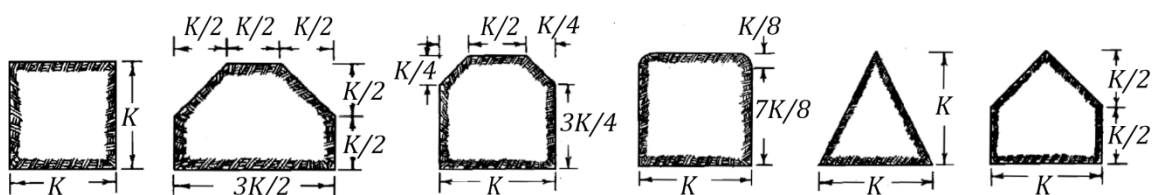


Figure 3.48 cross sectional shapes of roughness elements (Morris 1986)

Morris also determines the drag force acting on a roughness element by integrating the pressure distribution around the roughness element, the latter being measured by a piezometer bank on an inclined manometer board. From the drag force he further calculates the drag coefficient. Morris provides empirical formulas for two roughness shapes: square cross section (leftmost picture in Figure 3.48) and triangle top (rightmost picture in Figure 3.48). Experimental data ranged from $L/K = 7.5 \div 10$, $I = 2.5 \div 12.5 \%$ and $q = 16 \div 139 \text{ l/sm}$ for the derivation the formula for the square element. For the triangle top element experimental data ranged from $L/K = 5 \div 10$,

$I = 4 \div 23 \%$ and $q = 54 \div 71 \text{ l/sm}$. The triangle top element has a constant height of $K = 2 \text{ in}$. So caution is advised when applying formula 3-102 to different roughness heights.

$$\text{Drag coefficient square } (-) \quad c_D = 0.88 \cdot I^{3/4} \cdot \left(\frac{L}{K}\right) \cdot \left(1 + \frac{K}{y_1}\right)^2 \cdot \left(\frac{K}{y_1}\right)^{1/2} \quad \text{3-101}$$

$$\text{Drag coefficient triangle top } (-) \quad c_D = 0.75 \cdot I^{2/5} \cdot \left(\frac{L}{K}\right)^{1/3} \cdot \left(\frac{K}{y_c}\right)^{3/4} \quad \text{3-102}$$

Apart from the 2-dimensional bars Morris also investigates the performance of cubical elements. An additional design parameter is introduced: the lateral spacing of the roughness elements T . The cubical elements of each row are staggered transversally with those in adjacent rows. The undesired roll wave phenomenon does not occur with the cubical elements. Morris gives the following design recommendations for cubical roughness elements:

$$\text{Recommended relative spacings} \quad \frac{L}{K} = 10, \quad \frac{T}{K} = 1.5 \quad \text{3-103}$$

$$\text{Required roughness height to ensure tumbling flow} \quad K = 0.7 \cdot \left(\frac{q}{\sqrt{g}}\right)^{2/3} = 0.7 \cdot y_c \quad \text{3-104}$$

$$\text{Maximum discharge at tumbling flow conditions} \quad q = 0.586 \cdot K^{3/2} \cdot \sqrt{g} \quad \text{3-105}$$

For cubical elements the maximum specific discharge for which the tumbling flow regime can be preserved is independent of the slope.

Knight & Macdonald (1979) determine the flow resistance of an artificial strip roughness. Experiments are conducted in a 15.25 m long and 0.46 m wide flume with a constant slope $I = 0.958 \cdot 10^{-3}$. Discharges up to 180 l/s are investigated. The artificial strip roughness consists of bars with a 3 mm squared cross section, i.e. the roughness height is $K = 0.003 \text{ m}$. The spacing L of the roughness elements varies from $L = 0.014 \text{ m}$ to $L = 1 \text{ m}$. Based on Morris' flow classification over roughness elements (Morris 1955), namely "isolated roughness", "wake-interference" and "quasi-smooth flow", Knight & Macdonald distinguish two more flow patterns and relate their occurrence with the relative spacing L/K (Figure 3.49).

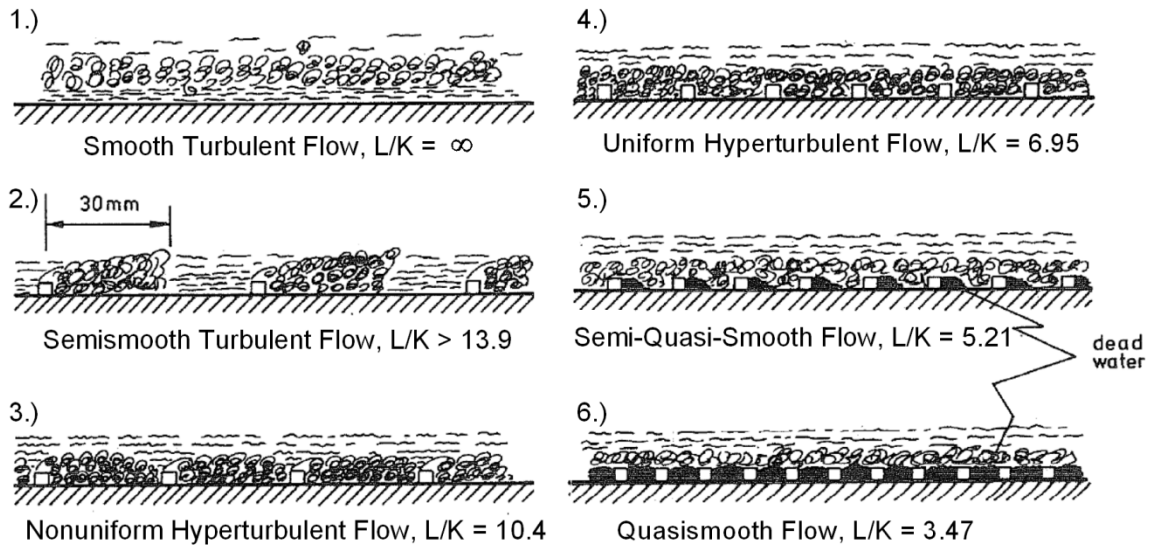


Figure 3.49 Flow patterns over roughness elements (Knight, Macdonald 1979)

The semi-quasi-smooth flow observed by Knight et al. refutes Morris' claim that a smooth flow pattern can only develop if the groove length (= clear length between roughness elements) approaches the roughness height. The maximum flow resistance for $y/w = 0.2$ is observed at $L/K = 8$, where y/w denotes the ratio of water depth y to flume width w . Knight & Macdonald point out that the equivalent sand roughness after Nikuradse is not a good measure for the roughness parameter if large isolated roughness elements are present. Equation 3-106 can be used to calculate the 2-dimensional resistance factor f_b subject to the water depth y and a parameter χ that covers shape, size and spacing of the roughness elements. A graphical solution for the determination of χ is presented in Figure 3.50.

$$\sqrt{\frac{2}{f_b}} = \frac{u}{u_*} = 6.06 \cdot \log \frac{y}{\chi} \tag{3-106}$$

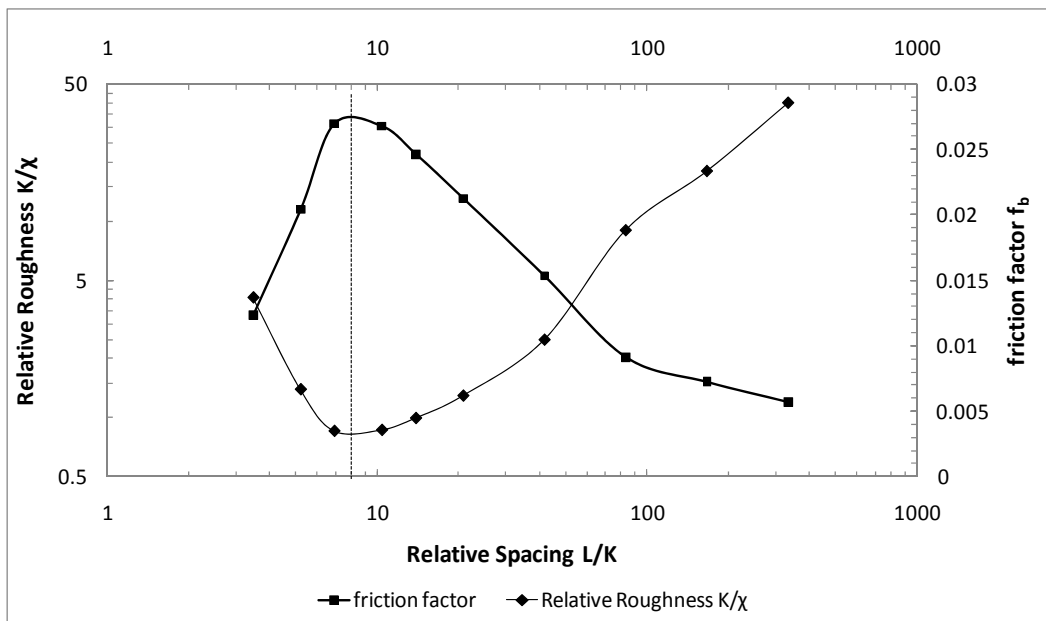


Figure 3.50 Graphical determination of Roughness parameter χ and flow resistance (Knight, Macdonald 1979)

While it seems logical that the roughness decreases with the increase of the relative spacing L/K it is somewhat surprising that the roughness also decreases as the relative spacing becomes sufficiently small, i.e. $L/K < 8$. This can be explained by the dead water zones (Figure 3.49, 5.) and 6.) that do not intermingle with the flow over the tops of the roughness elements and thus do not produce momentum exchange. As only one flat slope ($I = 0.000958$) and large relative submergences are examined it is questionable whether the results can be transferred to steeper slopes. Knight & Macdonald do not report the appearance of the water surface. As Figure 3.50 has been developed for $y/w = 0.2$, i.e. $y = 0.092$ m, the relative submergence y/K is large and therefore, presumably, the water surface is flat.

3.7 Concluding Remarks

Increasing ecological demands in river engineering have turned structures for overcoming an excess height from concrete vertical drops through block ramps to step-pool ramps.

All design rules presented in this literature review determine the maximum specific discharge q subject to some characteristic diameter d_{xx} of the boulders of the ramp. Dimensional analysis yields a dimensionless term for these parameters. All design rules thus have the same left-hand side:

$$\text{General design rule structure} \quad \frac{q}{\sqrt{g \cdot d_x^3}} = \mathbf{f}(I, \Psi, \Omega, \sigma, \dots) \quad \mathbf{3-107}$$

The design rules only differ in the right-hand side which is a dimensionless function \mathbf{f} of the ramp slope I and – optionally – other dimensionless parameters such as air content σ (Scheuerlein), boulder coverage Ψ (Vogel 2003) or a tolerance parameter Ω (Korecky 2007), to name a few.

Figure 3.51 illustrates the different design rules for a boulder size $d_{xx} = 1$ m. Different researchers use different characteristic boulder sizes. The non-filled and filled symbols label block ramps and symbols step-pool ramps, respectively. As a tendency, block ramps resist higher discharges than step-pool ramps. The downside of block ramps is their reduced fish passability and the fact that the major part of the energy dissipating process takes place in the tailwater section of the ramp. This often requires expensive riprap protection of the tailwater section.

Conversely, major advantages of a step-pool ramp are an enhanced fish passability and a very good energy dissipation along the ramp – as long as the tumbling flow regime is preserved. As a consequence, the remaining excess energy at the ramp toe is small. The scour protection downstream of the ramp can thus be reduced. As can be concluded from investigations on artificial roughness elements (chapter 3.6) the energy dissipation along step-pool ramps is the better the deeper the pools are. Vogel's step-pool ramp design consists of deep pools. Therefore the energy dissipation along the ramp is expected to be very good as long as the tumbling flow regime can be preserved. Vogel's design rule includes a boulder coverage parameter Ψ that strongly influences the result. This parameter allows a great freedom in the design of the ramp. Hence, it seems daring that the design rule is derived from a physical model test that covered only 4 ramp configurations, each one for a different ramp slope.

Korecky's ramp design does not have deep pools. The boulders of a "step" do not protrude much from the plane pool bed. Therefore the steps increase the roughness of the ramp only slightly as Korecky admits in her work. As a consequence the flow regime along the ramp cannot be described

as a tumbling flow pattern. A hydraulic jump will not develop in the pools. From an energy dissipating point of view Korecky's step-pool ramp rather acts like a traditional block ramp.

While the tumbling flow regime is a desired flow regime along step-pool ramps the flow transition to the rapid flow regime presents a significant challenge for the stability of the ramp as will be discussed in detail in the following chapters. Neither of the researchers (Hengl, Korger et al. 2007, Hengl, Aufleger et al. 2008, Gebler 2009, Vogel 2003, Korecky 2007) who deal with step-pool ramps address this problem.

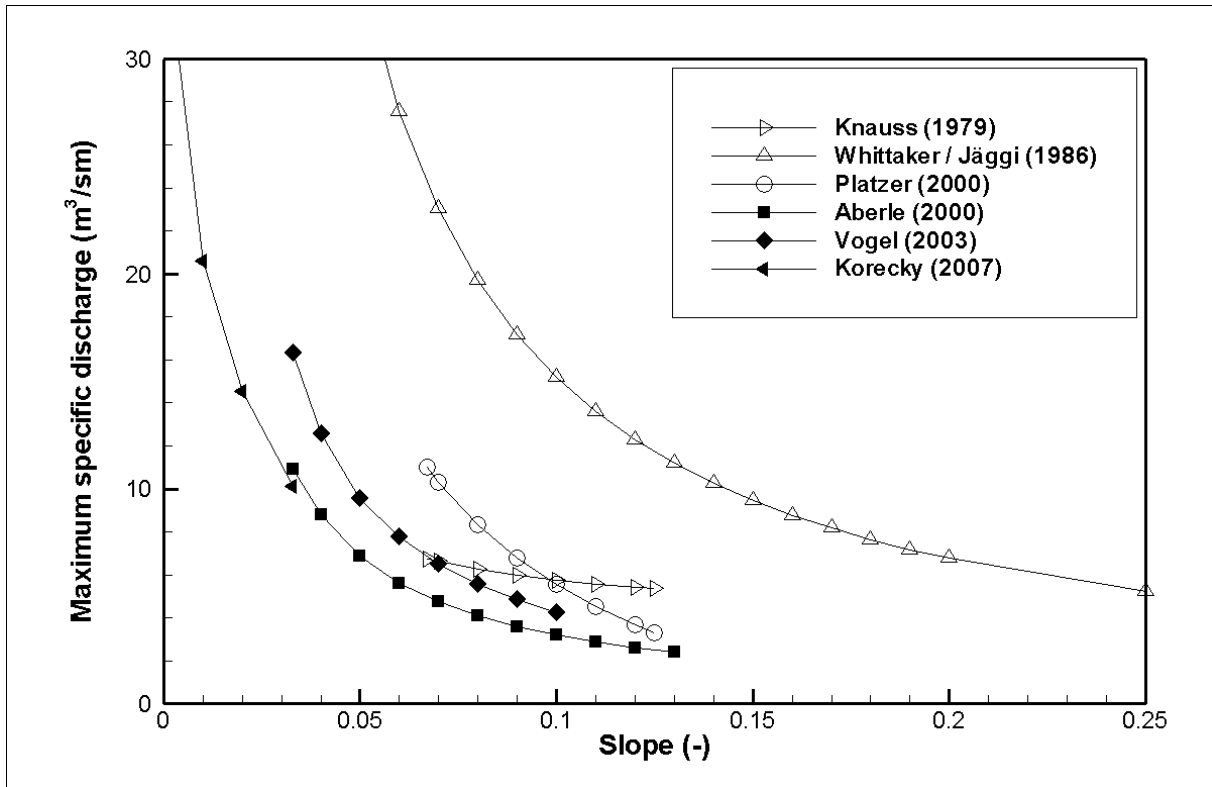


Figure 3.51 Comparison of different design rules, non-filled symbols: traditional block ramps, filled symbols: step-pool ramps for $d_{xx} = 1 \text{ m}$, $\rho_s = 2650 \text{ kg/m}^3$, $\rho_w = 1000 \text{ kg/m}^3$

Researcher	Design rule equation	Optional parameters	Not considered
Knauss 1979	3-9		
Whittaker / Jäggi 1986	3-21		equations 3-23 and 3-24
Platzer 2000	3-37d		Further design rules (Table 3.4)
Aberle 2000	3-83		
Vogel 2003	3-71	$\Psi = 0.8$	
Korecky 2007	3-74	$\Omega = 0.06$	

Table 3.16 Design rules used for Figure 3.51

4 Physical Model Test for a Meandering Ramp for the “Große Tulln” River

The aim of the physical model test is to find a design for a meandering ramp (chapter 3.4.9, pp. 58) for the „Große Tulln“ river. The stability of the ramp should be guaranteed for a 100-year flood.

If not otherwise stated all measures are given in full scale dimensions.

4.1 Project Area

The river “Große Tulln” is a tributary to the Danube River with its mouth 22 km northwest of Vienna. The project area “Neulengbach” is located 18 km south of the confluence. The catchment area of the “Große Tulln” river is about 93 km². Neulengbach is situated in the flysch zone. Typical for that zone are layers of sediments that are almost water impermeable. The flood events are thus characterized by an abrupt rise. Figure 4.2 shows a 100-year flood hydrograph that was calculated from a rainfall runoff simulation model. Within just 3 hours the discharge rises from mean flow to the peak flow. During the 100-year flood wave the discharge lies above the 1-year flood discharge for only 5.5 hours.

The Große Tulln river has been channelized and straightened in the 1970es. It has a uniform cross sectional profile and many vertical drops due to the straightening. Within the major part of the project area it is not possible to give the river more space because of populated and agricultural areas.

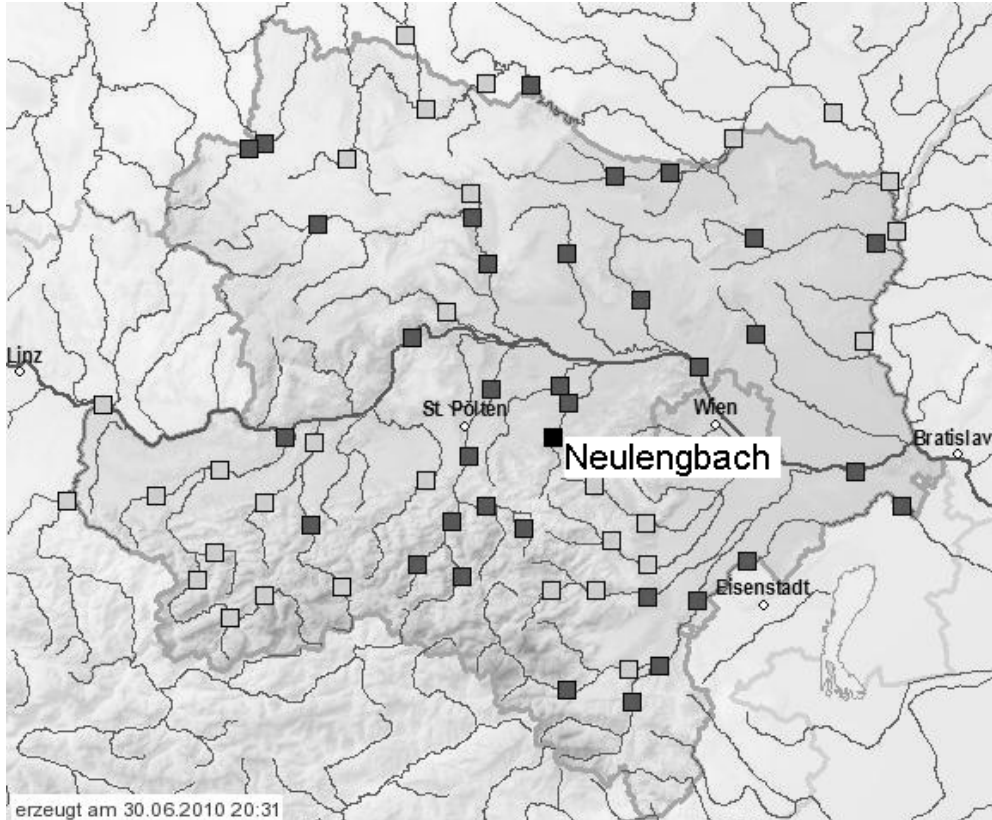


Figure 4.1 Project area: Neulengbach – Große Tulln river

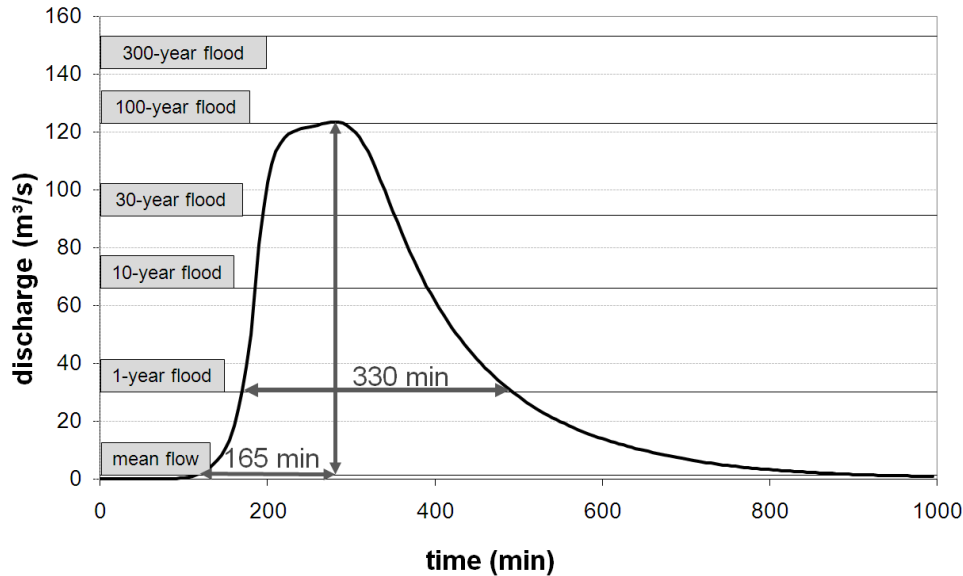


Figure 4.2 100-year flood hydrograph in the project area calculated from a rainfall runoff simulation model

Hydrological properties of the project area have been provided by the engineering consultancy “Pieler ZT”. The data has been established by flood risk assessment data (“HORA-Daten“) and hydrological expertise of the hydrographic division of the Office of the Provincial Government of Lower Austria. As no discharge was provided for the mean flow, the value was adopted from the gauging station in Siegersdorf, which is located 7 km downstream (north) of the project area.

discharge	m ³ /s	Roughness k_{st}	m ^{1/3} /s
Mean flow (Siegersdorf)	1.22	Channel	26
1-year flood	30	Banks	11 – 14
10-year flood	66	Morphology	
30-year flood	91	bed slope	0.58 %
100-year flood	123	bed width	10 m
300-year flood	153	bank slope	1:3

Table 4.1 Morphology and hydrology

The original idea was to build a scaled physical model of the meandering ramp for a specific location of the Große Tulln river, namely the area of an old unused weir in the city of Neulengbach at km 23.5 (Figure 4.3). The old weir should be replaced by a meandering ramp.

As an alternative location the engineering consultant Pieler ZT proposed the location „Furt Unterthurm“ at km 27.175, where a ground sill should have been replaced by a meandering ramp. Both proposals would have required site-specific plannings (freeboard considerations of bridges, relocation of bridges, lowering of the water level after the removal of the weir, ...), which would not have contributed to the understanding of the meandering ramp. As there are many vertical drops to be replaced in the project area it was desirable to make the result of the model test applicable to several locations. This is possible because of the uniformity of the bed geometry throughout the project area. Therefore a straight physical model was built having the typical morphological properties of this area.

For the determination of the geometry the river regulation project „Große Tulln (Laabenbach) Neulengbach – St. Christophen – Altenglengbach, km 24.26 - 33.28“ of the Office of the Provincial Government of Lower Austria, division B/3 of 1969 was available. Bed slope $I = 0.0058$, channel width of 10 m, bank slope of 1:3 and the top level of the banks of 2 m above the channel bed were adopted from the regulation project.



Figure 4.3 Old weir, Neulengbach, Große Tulln river, km 23.5

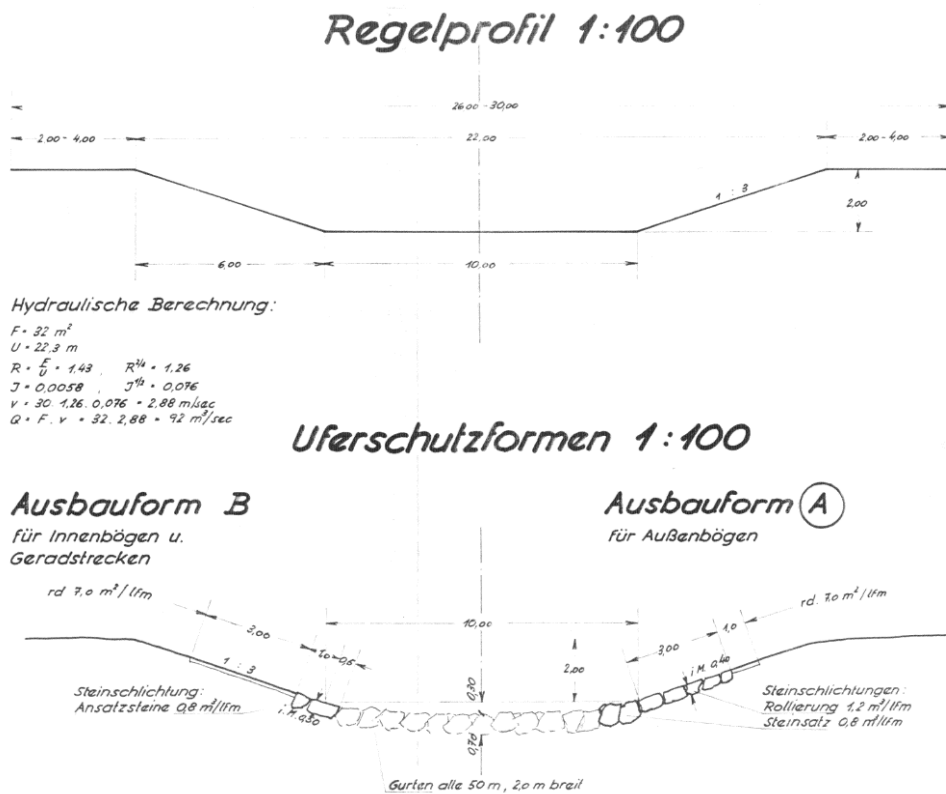


Figure 4.4 facsimile of the river regulation project 1969, standard section

4.2 Initial Design of the Meandering Ramp

The initial ramp design was provided by O. Grober whose experimental knowledge of the already existing meandering ramps was invaluable. The initial ramp consists of 12 step-pool sequences with a length L of 6 m each and a vertical distance between two steps Δh of 0.15 m. This ramp slope is $I = 0.025$ (Figure 3.41). Between the first and the last six pools two horizontal pools of 8 m length are arranged (see Figure 4.5). The first and the last six pools will be referred to as ramp 1 and ramp 2, respectively. Six meters downstream of the ramp toe a boulder step level with the bed stabilizes the structure.

The pools are separated by boulder steps. The steps are alternately inclined to the left and the right bank. The dimensions of the boulders of the steps are approximately $1 \text{ m} \times 1 \text{ m} \times 1.5 \text{ m}$. The boulders are embedded into the bed. In the initial ramp design they protrude $\Delta h = 0\text{--}15 \text{ cm}$ from the bed surface. In plan view one step has an S-shape and connects to the banks at half length of the pool where it joins the next downstream step seamlessly. The steps thus form a continuous sinuous line. The lowest point of a step is aligned with the bed level and is located a quarter distance from one bank to the other. The upper part of each step (which is alternately located near the left and right bank) is reinforced with boulders downstream of the step (Figure 4.5).

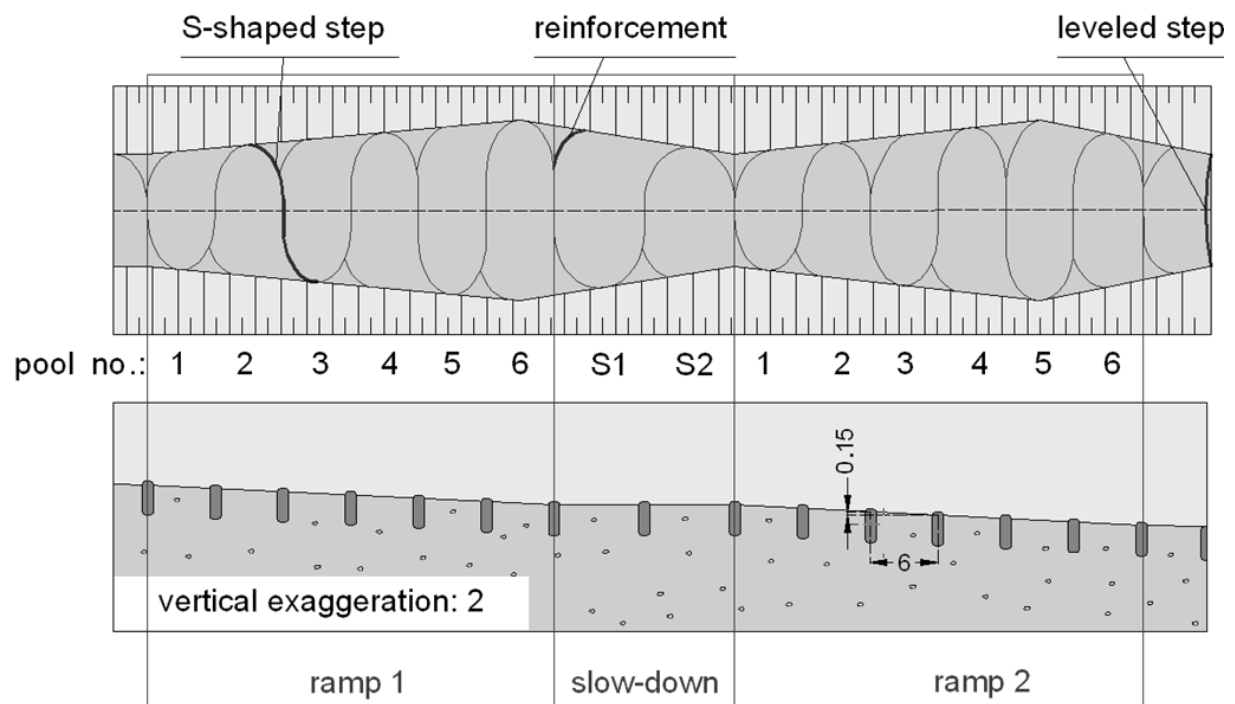


Figure 4.5 sketch of the initial ramp design by O. Grober, units in (m)

Along ramp 1 the channel widens continuously from 10 m to 16 m. The bank top lines remain parallel to the center line. Therefore the bank inclination changes from 1:3 to 2:3 at a channel width of 16 m. The slow down area between the two ramp sections reduces the channel width back to 10 m. Within the following 5 step-pool unit the channel widens again. Until the final leveled step the channel eventually narrows down to 10 m width (Figure 4.5).

One major question of the model test was, whether it was possible to build a stable ramp without armoring the pools. This enables energy dissipation due to scouring. A key parameter in the experiments therefore was to determine the maximum scour depth h_{scour} (Figure 3.41, right).

Table 4.2 summarizes important parameters of the initial ramp design.

Channel width w	10 – 16 m
Bank slope	1:3 – 2:3
Step spacing L	6 m
Vertical step distance Δh	0.15 m
Ramp slope I	2,50 % (slow down excluded)
Protrusion of the boulders from the bed (in centerline) p_{axis}	0.075 m
Maximum protrusion of the boulders from the bed p_{max}	0.225 m
Ramp height	1.8 m
Length of the structure	88 m (slow down included)

Table 4.2 parameters of the initial ramp design

4.3 Sediment Samples Of the Große Tulln and Model Sediments

On June, 5th 2007 sediment samples were taken from the Große Tulln river by the company Hochgerner Ges.m.b.H. from Innermanzing. O. Grober, R. Hohenauer and C. Sindelar were also on the spot. At four locations (km 23.4, km 23.9, km 24.25 and km 25.15) two samples were taken: one of the top layer of the river bed and another one of a layer 1 m below the channel bed. The sediment samples were analyzed by the Institute of Urban Water Management and Landscape Water Engineering of the University of Technology Graz according to the Austrian standard ÖNORM B4412. When sieving the largest mesh size was 70 mm. The largest particle of each sediment sample was determined. The two largest axis were measured. The middle axis of the largest particle is taken as the maximum particle size of each sampe.

Some characteristic diameters of the sediments are presented in Table 4.3. The mean diameter d_m and the non-uniformity parameters U_{60} and U_{84} are defined in chapter 2.3.1.

Sediment samples	Characteristic diameter (mm)									
	d_{90}	d_{84}	d_{65}	d_m	d_{60}	d_{50}	d_{16}	d_{10}	U_{60}	U_{84}
Averaged	105	87	50	41	43	30	3	1	45.2	5.7
Km 23.4 sub layer	125	110	65	51	58	42	1	1	92.0	9.6
Km 23.4 top layer	80	67	46	32	40	24	1	0	86.1	9.8
Km 23.9 sub layer	72	62	39	33	34	25	6	4	9.4	3.2
Km 23.9 top layer	73	63	39	31	33	23	5	4	9.2	3.5
Km 24.25 sub layer	167	143	69	63	56	41	6	2	25.8	5.1
Km 24.25 top layer	85	68	51	40	46	35	7	3	14.3	3.2
Km 25.15 sub layer	141	124	71	57	61	43	3	2	38.0	6.0
Km 25.15 top layer	86	72	32	29	25	14	1	1	38.5	8.8

Table 4.3 Sediment samples of the Große Tulln river

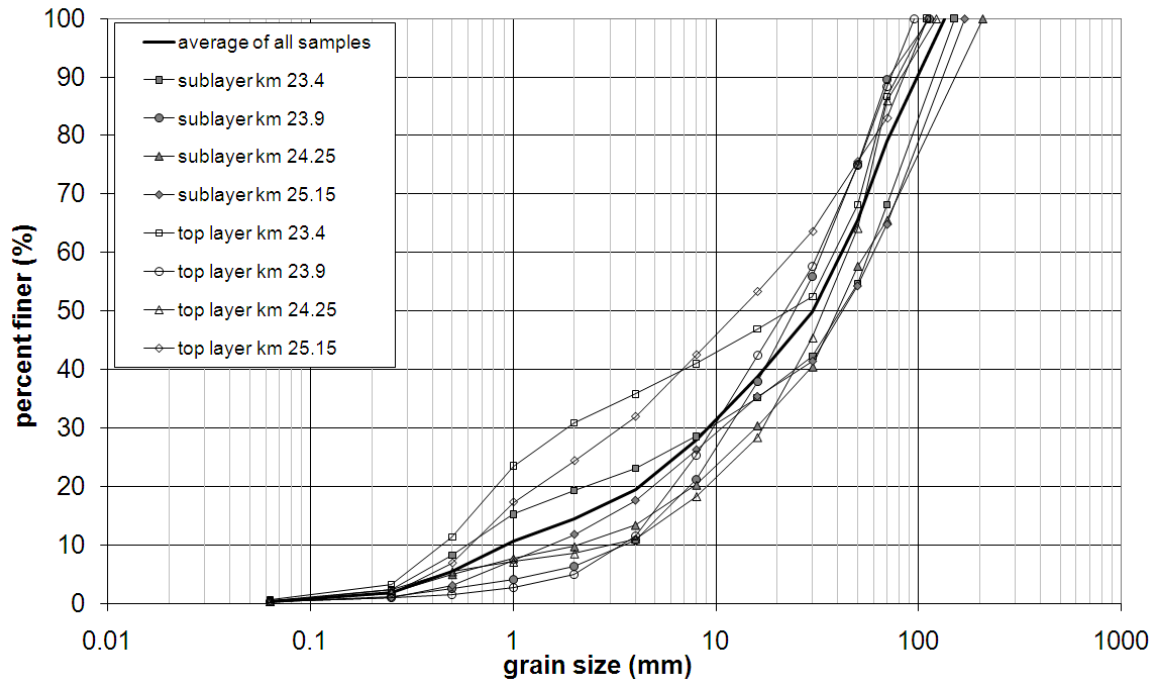


Figure 4.6 Sediment samples of the Große Tulln river

Three different model sediment mixtures from the company “Scherf GmbH und CO KG” from Hartberg were tested. According to the supplier the two rounded gravel mixtures range from 4-8 mm and 8 – 16 mm, respectively. The crushed gravel mixture ranges from 0 – 15 mm. A sieve analysis was performed for the rounded gravel 4 – 8 mm and for the crushed gravel. For the rounded gravel 8-16 mm the particle size specification of the supplier was adopted.

Compared to the field sediments the rounded gravel S1 (see Table 4.4) misses the fine parts of the particle size distribution. The diameter d_{90} of the rounded gravel converted to full scale is smaller than those of the averaged field samples. The coarser rounded gravel S2 has a diameter d_{90} that is well above the d_{90} of the averaged field samples if converted to full scale. The non-conformity parameters U_{60} and U_{84} are small for both rounded sediments S1 and S2.

Model sediments (full scale)	Abbr	Characteristic diameter (mm)				
		d_{90}	d_m	d_{50}	U_{60}	U_{84}
Rounded gravel 4-8 mm	S1	78	61	61	1.5	1.3
Rounded gravel 8-16 mm	S2	152	N.V.	120	1.5	1.3
Crushed gravel mixture	S3	N.V.	N.V.	N.V.	N.V.	N.V.
Crushed gravel 0-15 mm	S4	145	76	62	11.0	3.0
<i>Crushed gravel 0-15 mm, 4-fold fine</i>	<i>S5</i>	<i>139</i>	<i>59</i>	<i>45</i>	<i>70.4</i>	<i>8.2</i>
Averaged field samples		105	41	30	45.2	5.7

Table 4.4 Model sediments (converted to full scale)

As the crushed gravel 0 – 15 mm (S4) converted to full scale is coarser than the averaged field samples, a company was instructed to provide a sediment mixture S3 according the particle size distribution of the averaged field samples. On delivery of sediment S3 however it was visible to the naked eye that the mixture misses the coarse fractions. Besides the sediment mixture was very dirty. Therefore a sieve analysis of S3 became unnecessary.

Experiments were performed with model sediments S1 – S4. The rounded gravel proved to be inappropriate. The rounded shape prevents a wedging and blocking of the particles. The sediment gradation is poor, thus no armoring or sorting processes are to be expected. Moreover the shape of the rounded gravel does not resemble the field sediments of the Große Tulln river which are mostly angular shaped. The experiments also showed that under the same conditions the rounded gravel 8 – 16 mm produces deeper scour holes than the crushed gravel 0 – 15 mm. Experiments using S3 confirmed that this material was inappropriate because of the missing coarse fractions and the contamination.

Very fine sediment fractions are to be avoided if possible. The water gets turbid and affects other model tests. Comparing gravel S4 to the grain size distribution of the Große Tulln samples shows that the fine grain sizes are missing in S4. Quadrupling the fine grain sizes up to 0.25 mm of gravel S4 then the resulting gravel S5 lies within the range of the Große Tulln samples. Assuming that this procedure does neither enlarge the volume of the gravel nor ameliorate the bed stability then gravel S4 can be used instead of gravel S5.

After completion of the model sediment tests all following experiments (beginning from no. 16, see Table 4.11) were performed with crushed gravel 0 – 15 mm (S4). This way the grain size distribution of the Große Tulln river samples was best modeled. There is no information of the grain size distribution and the amount of the sediments transported on high floods. The findings of this physical model test are valid for the grain size distribution of the crushed gravel S4.

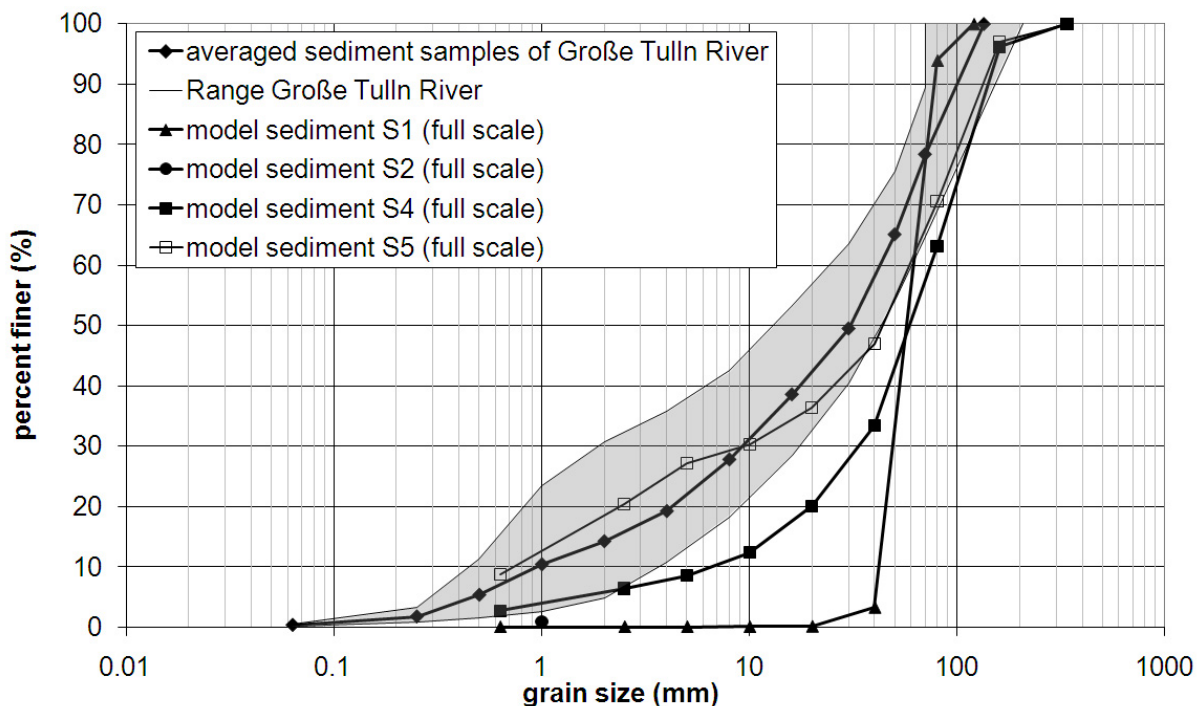


Figure 4.7 Model sediments (transformed to full scale) and averaged field samples, shaded area marks the range of the field samples

4.4 Bed Load Transport – Calculations

To calculate the bed load transport Meyer-Peter Müller's formula was used (Meyer-Peter, Müller 1948). This half-empirical formula had been developed in extensive experiments with sediments of different particle sizes and specific weight. The experiments took place at the ETH Zürich and were conducted by Meyer-Peter and Müller.

$$M_G = \frac{\rho_S}{\rho_S - \rho_W} \frac{8}{g} \sqrt{\frac{1}{\rho_W}} \cdot [\rho_W \cdot g \cdot I \cdot R_S - 0.047 \cdot (\rho_S - \rho_W) \cdot g \cdot d_m]^{3/2} \quad \left(\frac{\text{kg}}{\text{ms}} \right) \quad 4-1$$

M_G (kg/ms), ρ_W and ρ_S (kg/m³) denote the transported bed load rate per unit width, the density of water and sediment, respectively. g (m/s²), I (–), R_S (m) and d_m denote gravitational acceleration, slope, hydraulic radius and the mean diameter (equation 2-2).

As can be seen from equation 4-1 the bed load rate is a function of the difference of actual and critical shear stress. The formula for the actual shear stress is derived from mechanical considerations.

$$\text{Critical shear stress} \quad \tau_{cr} = 0,047 \cdot (\rho_S - \rho_W) \cdot g \cdot d_m \quad (\text{N/m}^2) \quad 4-2$$

$$\text{Actual shear stress} \quad \tau_{act} = \rho_W \cdot g \cdot I \cdot R_S \quad (\text{N/m}^2) \quad 4-3$$

4.5 Measurement Variables and Equipment

4.5.1 Water Levels

The water levels were measured with a hook gauge which was mounted to the crane cage of the laboratory. The crane cage was put into the desired horizontal position. By means of an automatic control the hook gauge positioned itself to the water level which was manually read using a leveler.

Water levels were measured when the model was calibrated (chapter 4.7, pp. 88).

4.5.2 Discharge

The discharge was measured with a magnetic flowmeter from the company “Bailey Fischer & Porter” (Model number 10DX3311D). It has a maximum deviation of 0.5 % of the measured value.

4.5.3 3D Velocity Measurements with ADV-probe

For the velocity measurements the high-resolution ADV-probe (Acoustic Doppler Velocimeter) Vectrino⁺ (Nortek AS) was used. The basis measurement technology is coherent Doppler processing.

The ADV-probe measures the frequency shift of a transmitted sound wave that is being reflected by very small particles in the water and is received by four beams of the probe. The frequency shift can be transformed to get 3D velocities of the moving particles. Under the assumption that the small

particles move approximately at the same speed as the surrounding water, these velocities correspond to the water velocities within the sampling volume (Figure 4.8, left).

Two probes are available, a down-looking probe and a side-looking probe. In order to measure velocities at low water depths the side-looking probe (Figure 4.8, right) is appropriate.

Technical data	
Water Velocities	
Range (user selectable)	$\pm 0.01, 0.1, 0.3, 1, 2, 4$ m/s
Accuracy	$\pm 0.5\%$ of measured value ± 1 mm/s
Sampling rate (output)	1–25 Hz 1–200 Hz (Vectrino firmware)
Sampling Volume	
Distance from probe	0.05 m
Diameter	6 mm
Height (user selectable)	3–15 mm
Echo Intensity	
Acoustic frequency	10 MHz
Resolution	Linear scale
Dynamic range	25 dB

Table 4.5 Technical data of ADV-probe Vectrino⁺

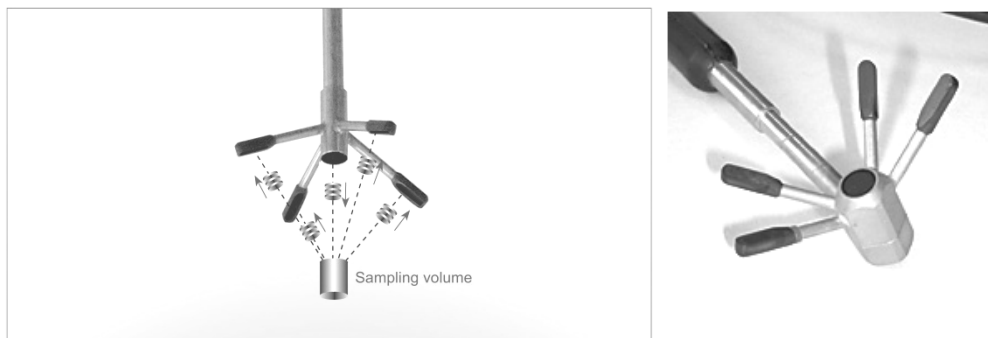


Figure 4.8 Nortek-ADV-probe: measuring principle (left), side-looking probe (right)

A carriage for the ADV-probe was prepared that could be moved manually on rails parallel and transverse to the centerline of the model. The vertical positioning was carried out with an electrical drive (Figure 4.9).



Figure 4.9 Carriage for ADV-probe moving on rails

The mean velocity of a vertical profile was determined using just one measuring point. (“Einpunktmethode”, Austrian standard: ÖNORM B 2403). The measuring point is located in 40 % of the water depth above the bed. Under the assumption of a parabolic vertical velocity distribution the measured velocity at this location represents the mean velocity v_m (Figure 4.10).

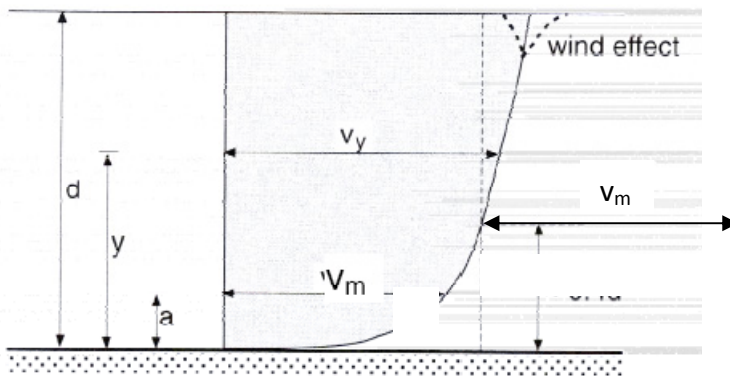


Figure 4.10 Determination of the mean velocity using 1 measuring point (ÖNORM B 2403)

4.5.4 1D-Velocity Measurements with a Hydrometric Impeller

Velocities were also measured with a hydrometric impeller “FA incl. μ P-Flowtherm-display unit” from the company “Höntzsch”. According to the manufacturer the hydrometric impeller has an accuracy of 1.5 %.

4.5.5 Digital Elevation Model by Means of Digital Photogrammetry

Digital photogrammetry is a measuring technique that allows the modeling of a 3D space using 2D digital images. Similar to the stereoscopic vision of the human eye 3D objects can be reconstructed because of the diversity of two images of one and the same object. Of an object that needs to be surveyed two images from different perspectives have to be taken. The 3D coordinates of the camera and the camera angle, the so called “outer orientation”, have to be known. A software recognizes the

overlapping area of the two images. The space coordinates of each pixel of the stereoscopic overlap are determined by a spatial forward intersection (Figure 4.11).

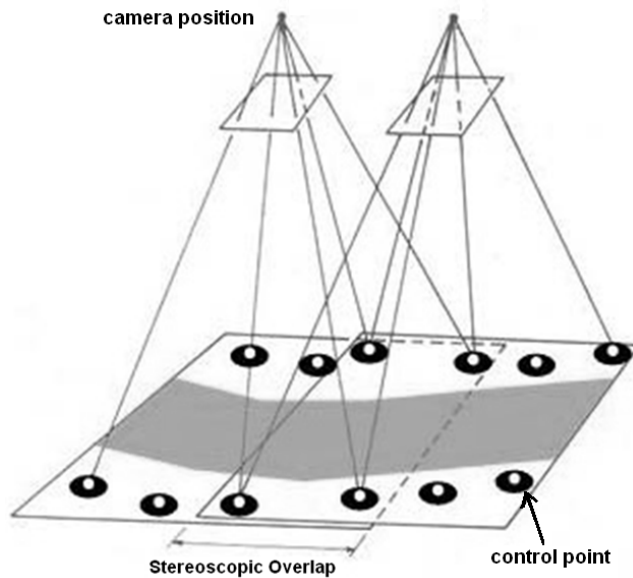


Figure 4.11 Principle of the stereoscopic image evaluation

In this physical model test the outer orientation was determined via spherical control points lined on both sides of the model (Figure 4.9, Figure 4.11). The control points were measured at an accuracy of 0.1 mm by the Institute of Engineering Geodesy and Measurement Systems of the University of Technology Graz. On each image 10 to 12 control points had to be visible. By means of a spatial backward intersection the outer orientation can be determined. With 10 to 12 control points the spatial backward intersection is over-determined. This way it is possible to estimate the quality of the calculated outer orientation.

The images were taken with a digital reflex camera (NIKON D 70) with a 35mm fixed-focus lens. Before the beginning of the experiments the camera had to be calibrated, i.e. all camera data that influence the projective imaging between space and image plane had to be determined. This includes the pixel coordinates of the principle point and the focal length dimensions and lens distortion parameters. These parameters are termed the “inner orientation” of a camera.

The pictures were taken from the crane bridge of the laboratory (Figure 4.12). The distance of the camera to the channel bed was about 4 m. After each image the crane moved parallel to the centerline of the model such that two adjacent pictures have an overlap of approximately 60 %. To photograph the whole model 20 images were necessary.



Figure 4.12 Images for digital photogrammetry taken from the crane bridge

The subsequent processing of the images was carried out with the software DIBIT that had been developed by the Institute “DIGITAL-Remote Sensing and Geoinformation” of the Joanneum Research Graz. For each image the software corrects it from lens distortion and calculates the external parameters of the camera. Every two adjacent images are checked against each other. Then the space coordinates are calculated for the overlapping area. Eventually the overlaps are put together to one orthophoto that is geometrically corrected (“orthorectified”). The resolution of the resulting digital elevation model (DEM) was 5×5 mm (model scale). The results allow for appealing visualizations and extensive evaluation of the gained data.

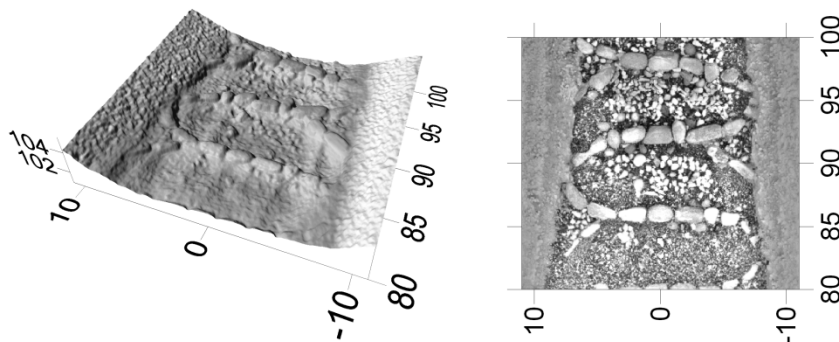


Figure 4.13 3D surface (left) and orthorectified image (right) of the model resulting from digital photogrammetry

To determine the accuracy of the digital photogrammetry for the physical model described in this chapter four control cross sections were measured with a hook gauge and compared with the DEM from the photogrammetry (Table 4.6). For the leveling the hook gauge was positioned manually to each measurement point. For each control section 29 measurement points at distance of 5 cm (model scale) were measured. The accuracy of the digital photogrammetry depends on the roughness of the bed. If only measurement values are compared that were measured on a concrete surface (22 points at control section $X = 86$) the standard deviation between leveling and photogrammetry is 1.1 mm (Table 4.6). For all other control sections the channel bed was covered with stones that had a diameter of 50 – 70 mm. The high roughness of the bed resulted in uncertainties concerning the correct positioning of the hook gauge. A positioning error of 2 – 3 mm could lead to vertical differences of several millimeters. It can be assumed that the results of the leveling had been more accurate if the hook gauge were positioned automatically. Nonetheless the results agree well with those of Lane et al. (2001) who compare the digital photogrammetry with the laser distance method. Lane and Chandler find that the standard deviation of the height differences ranges from 1.5 mm for a sand bed to 5.9 mm for a sand-gravel bed. Rosier et al. (2004) report that their digital elevation model of a sand bed that was gained from digital photogrammetry has a standard deviation of 2.5 mm.

Control section	Standard deviation (mm)
$X = 99.3$	6.0
$X = 97.0$	5.9
$X = 93.3$	7.8
$X = 86.0$	3.6
$X = 86.0$ (only concrete)	1.1

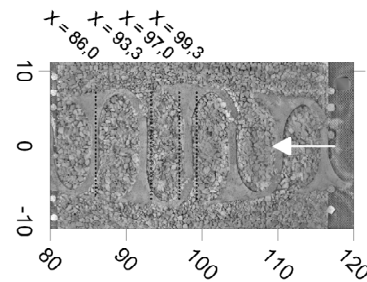


Table 4.6 Comparison of digital photogrammetry and leveling, standard deviation, measured control sections

4.6 Experimental Setup

4.6.1 Model Laws

The dimensionless Froude number Fr determines the flow regime of a free surface flow.

$$Fr = \frac{v}{\sqrt{g \cdot y}} \quad (-) \quad 4-4$$

In equation 4-4 v (m/s), g (m/s^2) and y (m) denote mean velocity, gravitational acceleration and water depth, respectively. For $Fr < 1$ the flow is subcritical, for $Fr > 1$ the flow is supercritical, for $Fr \approx 1$ the transition from subcritical to supercritical flow takes place. For physical models with a free surface one usually requires that the Froude number in the model and in the prototype must match to guarantee that the correct flow regimes in the model. In the present model test this so called "Froude similitude" was used. For the model length scale L_R the following laws are valid:

	Model	Prototype
discharge (m^3/s)	Q_M	$Q_P = L_R^{5/2} \cdot Q_M$
velocity (m/s)	v_M	$v_P = \sqrt{L_R} \cdot v_M$
time (s)	t_M	$t_P = \sqrt{L_R} \cdot t_M$

Table 4.7 Model laws using Froude similitude

The scale of the model is 1: $L_R = 1:10$. For the length scale factor $L_R = 10$ the following conversion factors apply: $L_R^{5/2} = 316.23$ for discharges and $\sqrt{L_R} = 3.16$ for velocities and the time. The relation between model discharge and prototype discharge is summarized in Table 4.8.

discharge	Model (l/s)	Prototype (m^3/s)
Mean flow (Siegersdorf)	3.9	1.22
1-year flood	94.9	30
10-year flood	208.7	66
30-year flood	287.8	91
100-year flood	389.0	123
300-year flood	483.8	153

Table 4.8 Relation between model and prototype discharge

4.6.2 Model plan

Apart from the ramp itself reference sections up and downstream of the ramp are also represented in the model which are referred to as headwater and tailwater section, respectively. The reference sections have the same slope ($I = 0.0058$) as Große Tulln river in the project area. The model further consists of an inlet tank, a flow straightener of bricks, a sand trap at the downstream end of the model and a flap to regulate the water levels. The resulting physical model has a length of 19.2 m.

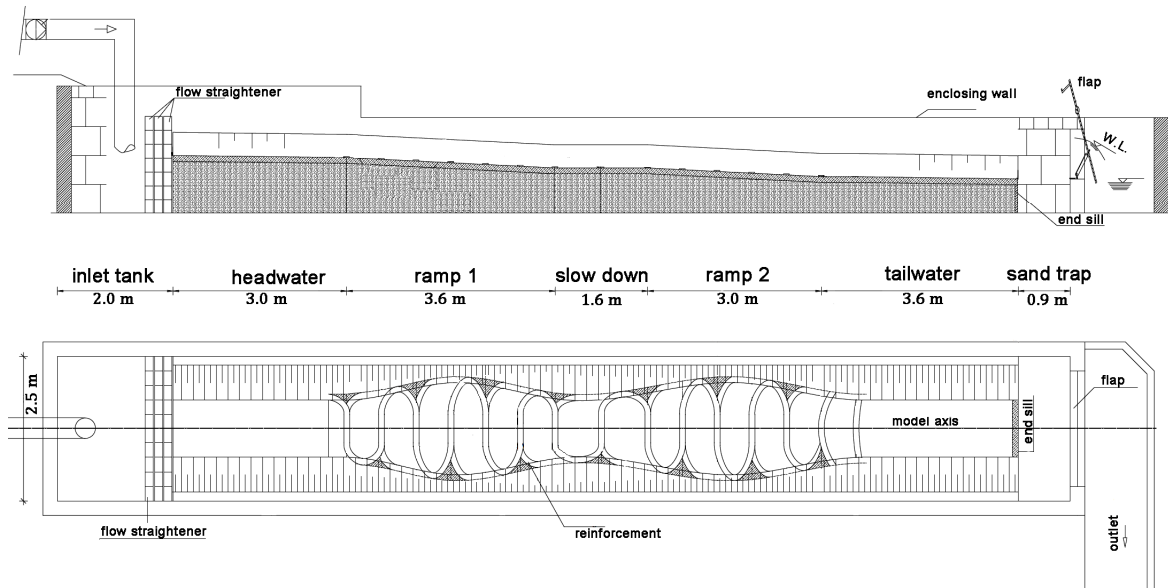


Figure 4.14 Longitudinal section (top) and plan view (bottom) of the initial model (dimensions in model scale)

The headwater section serves the purpose of providing uniform flow conditions without surface waves. The tailwater section should be long enough to prevent an influence of the flap. During the experiments it turned out that the experiments are better performed without the use of the flap (chapter 4.9, pp. 103).

To get sufficiently large reference sections the original plan of the meandering ramp provided by O. Grober (Figure 4.5) was reduced by one pool. The initial model consists of a 3 m long headwater section, a ramp section divided into two parts (with 6 and 5 pools, respectively, with a pool length of 0.6 m), two pools for slow down in between the two ramp parts and a 3.6 m long tailwater section. The reference sections are made of concrete, the ramp section is paved with coarse gravel (50 – 70 mm).



Figure 4.15 Construction of the model: view from the downstream end of the model (left), pavement of the bed with coarse gravel (right)

4.7 PHASE 1 – Model Calibration

In PHASE 1 the model was calibrated. A 1D numerical calculation with HEC-RAS was performed using the above mentioned geometry and roughness values (Table 4.1). The geometry for the HEC-RAS calculation represented the model geometry without the steps in full scale. It was the aim to adjust the roughness in the model such that the calculated water levels for the discharges mean flow, 1-year, 10-year, 30-year and 100-year flood concur the water levels in the model.

The calibration tests firstly were carried out for a 1-year flood. As expected the initial variant 0 (Table 4.9) with its reference sections made of concrete was too smooth and the water levels too low accordingly (Figure 4.17). In the slow-down area the water levels were also well below the calculated values despite the rough bed.

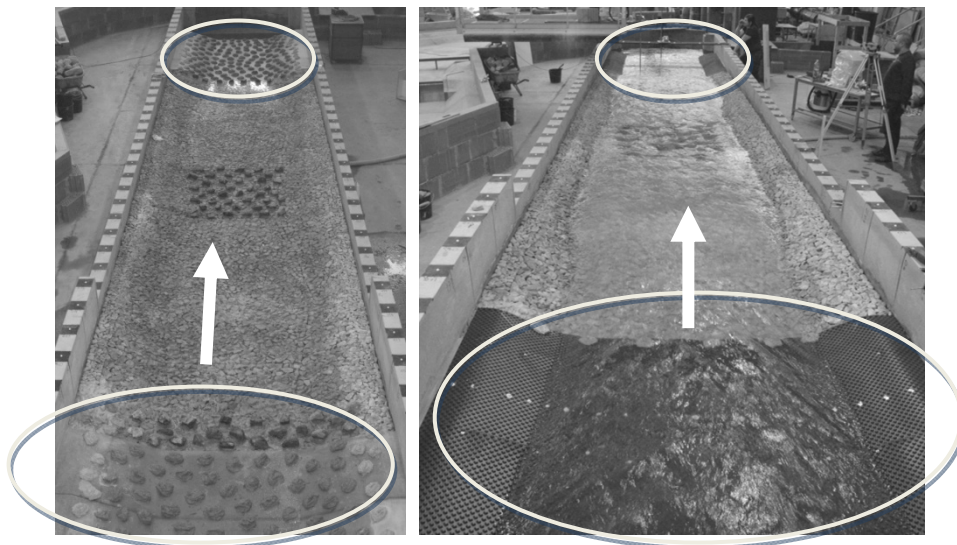


Figure 4.16 Increase of roughness by means of mortar elements (variant 1, left) and pimple mat (variant 3, right)

Variant	Headwater section	Slow-down area	Tailwater section
Var 0	concrete	rough bed	concrete
Var 1	mortar elements	stones	mortar elements
Var 2	pimple mat	stones	mortar elements
Var 3	pimple mat	stones	pimple mat

Table 4.9 Roughness variants in the model

For the roughness variant 1 the roughness within the reference sections was increased by means of mortar elements (diameter 10 cm, height about 5 – 8 cm). In the slow-down area stones were glued to the rough bed because the removal of the mortar elements would have damaged or destroyed the rough bed below. It turned out that the mortar elements in the headwater section are too rough (Figure 4.17). Moreover due to their height they negatively affect the flow especially on low discharges.

The headwater section of roughness variant 2 is therefore lined with a pimple mat instead of the mortar elements. The pimples have a height of 2 cm (Figure 4.16, right). As the pimple mat yielded the desired roughness and did not affect the flow the tailwater section was also covered with a pimple mat (variant 3). In each cross sectional profile the water levels were measured in the centerline of the model and above the left resp. right bank toe. Figure 4.17 shows the calculated

water levels for a 1-year flood and the measured water levels averaged in lateral direction. All values are displayed in full scale.

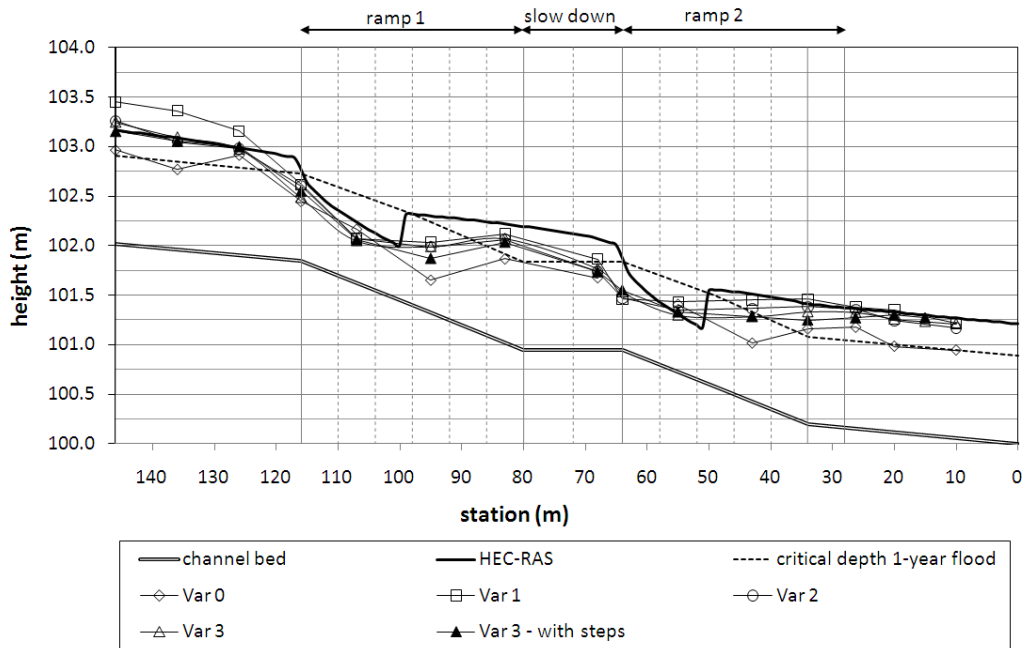


Figure 4.17 Model calibration, roughness variants: 1-year flood, HEC-RAS calculation vs. water level measurements (averaged in lateral direction)

Figure 4.18 shows the water level measurements for the roughness variant 3 including the steps made of concrete. The steps that protrude only 1.5 cm from the bed do not raise the water levels compared with the measurements of variant 3 without the steps. Nonetheless the steps do have an influence on the inclination of the water level in lateral direction.

A complete compilation of the water level measurements for other discharges (mean flow – 100-year flood) can be found in the appendix A.1.

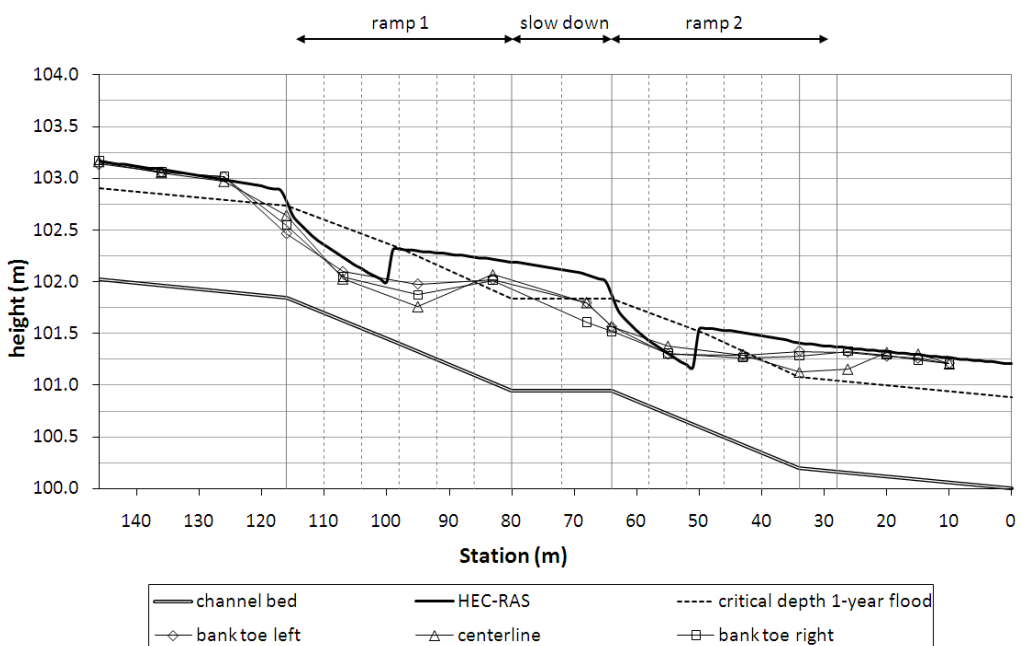


Figure 4.18 Water level measurement 1-year flood: lateral inclination of water level

4.8 PHASE 2 – mobile bed experiments

The experiments in PHASE 2 were carried out with a mobile bed within the ramp section under both clear water and live bed conditions. The channel bed from PHASE 1 was filled up 15 cm with rounded gravel S1 (4 – 8 mm, see Table 4.4). While the gravel in the reference sections was fixed with a very thin layer of mortar the gravel filling up the ramp section remained mobile and was eventually replaced by different model sediments (Table 4.4). Altogether 8 different ramp designs were tested in PHASE 2.

4.8.1 Development of the ramp design

All ramps designs investigated in PHASE 2 had a step length of 6 m and a vertical distance between to steps of 0.15 m. In Table 4.10 the gradual development of an appropriate ramp design is summarized. The bold outlined cells mark the changes compared to the preceding ramp design. “ID” denotes the initial ramp design. In the direction of the flow the reinforcement slopes downward (dwn) for the first designs. Since design D5 the reinforcement slopes upward (up).

Ramp desin	Step protruding from the bed in the centerline Δh (mm)	Material of the steps	Maximum channel width Middle / End of ramp	Number of pools in slow-down area	Inclination of reinforcement (in direction of flow)	Leveled step	Step properties
ID	15	concrete	M	2	dwn	-	
D1	15	stone	M	2	dwn	-	
D2	30	concrete	M	2	dwn	-	
D3	30	cobblestone	E	2	dwn	-	Joints between cobblestones filled
D4	30	cobblestone	E	2	dwn	Y	Joints between cobblestones partly filled
D5	30	cobblestone	E	2	Up	Y	Joints between cobblestones partly filled
D6	30	cobblestone	E	1	up	Y	Joints not filled, top edges of cobblestones abraded
D7	30	cobblestone	E	1	up	Y	top edges of cobblestones abraded, gaps not filled, except for the cobblestones upstream of the reinforcement
D8	30	cobblestone, casted concrete	E	1	up	Y	top edges of cobblestones abraded, gaps not filled, except for the cobblestones upstream of the reinforcement

Table 4.10 Gradual development of a final ramp design

For ramp design D1 and D2 only the first three step-pool units of ramp 1 were built. At the end of the third pool was a steep almost vertical drop to the original channel bed of PHASE 1 (Figure 4.19). For the ramp designs D3 to D7 the first ramp including the slow-down area was constructed. Ramp design D8 consisted of the whole ramp, i.e. 6 step-pool units of ramp 1, slow-down area and 5 step-pool units of ramp 2.

4.8.2 Experiments PHASE 2

In PHASE 2 altogether 17 test runs including 8 ramp designs and 5 different model sediments (Table 4.4) were carried out which are summarized in Table 4.11. Key findings are described within this chapter. A complete documentation of the results can be found in the appendix A.2.

No.	Ramp design	Model sediment	discharge	Sediment addition	Duration (model scale)
1	D1	S1	1-year flood	-	2h15min
2	D2	S1	1-year flood	-	2h15min
3	D3	S1	1-year flood	-	2h15min
4	D3	S1	1-year flood	-	2h15min
5	D3	S1 ⁺	1-year flood	-	2h15min
6	D3	S1 ⁺	30-year flood	-	30min
7	D4	S1 ⁺	1-year flood	-	2h15min
8	D4	S2	1-year flood	-	2h15min
9	D4	S4	1-year flood	-	2h15min
10	D5	S4	1-year flood	-	2h15min
11	D6	S4	1-year flood	-	2h15min
12	D6	S4	30-year flood	100 l/h	2h15min
13	D6	S4	30-year flood	200 l/h	2h15min
14	D7	S4	30-year flood wave	Varying	2h15min
15	D8	S3	1-year flood wave	-	2h15min
16	D8	S4	30-year flood	200 l/h	2h15min
17	D8	S4	100-year flood wave	Varying	3h

⁺ with fine parts

Table 4.11 Complete list of test runs in PHASE 2 in chronological order



Figure 4.19 Ramp design D2

Prior to each test run the channel bed was leveled and then surveyed photogrammetrically. During a test run a flood event was simulated under live bed or clear water conditions. For the live-bed experiments the sediments were supplied manually at the upstream end of the model. During the live-bed experiments no velocity measurements were possible so as not to endanger the measurement devices by the moving sediments. Water levels were measured in the centerline of the model. Due to the high turbidity of the water the sediment movements could not be observed during a test run. After a test run the bed was again surveyed photogrammetrically.

In the experiments 5-7 the rounded gravel 4 – 8 mm (S1) was mixed with very fine parts according to the prototype particle size to see if the fine parts had an adhesive effect which was not the case. For the test runs 14 and 17 a flood wave was simulated. The sediment addition depended on the discharge. The development of the optimal ramp design took place mainly for a 1-year flood simulation. The duration of a test run of 2h15min corresponds to approximately 7h in full scale. As can be seen from the 100-year flood hydrograph (Figure 4.2) the duration of a test run was chosen to be on the safe side. All results are presented in full scale.

4.8.3 Upstream Scours

Throughout the experiments one major concern was the development of scours upstream of a step (Figure 3.36 d.). This was unexpected because such upstream scour patterns have not been observed at the prototype ramp in the Stübmingbach (Table 3.14, chapter 6, pp.191). Two surveys (Stübmingbach, Dec. 2007 & Dec. 2009) of the bed levels show scour patterns as in Figure 3.36 a.). Undoubtedly the grain size distribution of the pool material is a crucial point in the appearance of the scour pattern. The same experiment as shown in Figure 4.22 a.) does not yield upstream scour holes if the coarser sediment S3 is taken instead of sediment S1 (Figure 4.22 b.)). Increasing the discharge from a 1-year-flood to a 30-year flood (Figure 4.22 c.) then upstream scour holes develop also for sediment S3.

The following reasons for the development of upstream scours were presumed:

- Scale effect because of the surface tension

(Kobus 1984) demands that the water depth at the crest of a sharp-crested weir must be at least 6 cm in the model to minimize the surface tension scale effect.

Assuming that the steps of the ramp model act as little weirs and that the water depth above the steps corresponds approximately to the critical depth, the required depth is fulfilled in the model for all flood discharges because the critical depth for a 1-year flood in the model is $y_c = 7.9$ cm. For non sharp-crested weirs Kobus suggests a water depth of at least 2 cm. This can be guaranteed in the model for all discharges.

- The model does not map the prototype situation properly
 - Cobblestone top edges are sharp edged compared to the natural boulders
 - Joints between the cobblestones in the model are filled, whereas there are gaps between the boulders of the prototype ramp

The major part of the ramp development aimed at eliminating the upstream scours:

- Removing the filling between the cobblestones → since D4
- Ground sill at half pool length for the first three pools → since D4

- Abrasion of the cobblestones → since D6

These measures reduced the upstream scours only slightly.

Some other researchers report the occurrence of upstream scours:

Korecky (2007) (see also chapter 3.4.7, pp. 56) reports the occurrence of upstream scours in a physical model test on flat sloped step-pool ramps where the diameter of the pool sediments was a fifth of the diameter of the steps. No further explanation is given. Korecky concludes that in these cases the pool sediments should be coarser.

In his diploma thesis Hackl (2008) performs basic flume experiments on the effect of so called micro groins. The experiments were carried out at the laboratory of the Institute of Hydraulic Engineering and Water Resources Management of the University of Technology Graz. Micro groins are submerged groins have a small relative depth (groin height / water depth). During the mobile bed experiments with a relative groin depth of 0.2 upstream scours developed (Figure 4.20) which could be reduced significantly if the groin crest was inclined such that the tip of the groin was leveled with the initial bed surface (Figure 4.20 b.). As the groins did not extend across the whole flume width a comparison to the submerged steps of the meandering ramp can be drawn only to a limited extent.

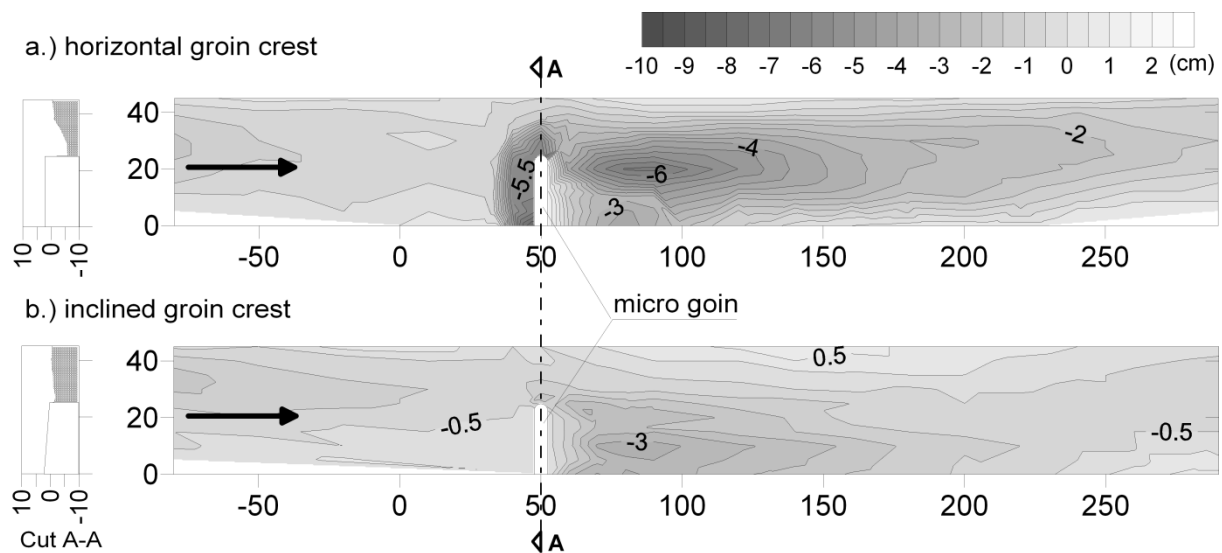


Figure 4.20 Bed changes around submerged groins with a.) horizontal and b.) inclined crest, station and height in (cm)

Upstream scours are well known for bridge piers. As bridge piers are non-submerged structures which do not extend across the whole channel width they can only be compared with caution to the steps of the meandering ramp. It is assumed however that the upstream scours of the steps of the meandering ramp and of the micro groins also develop because of a downward pointing flow. This notion suggests that upstream scours develop if the particle size of the pool material is such that the particles can be mobilized by the downward flow (Figure 4.21).

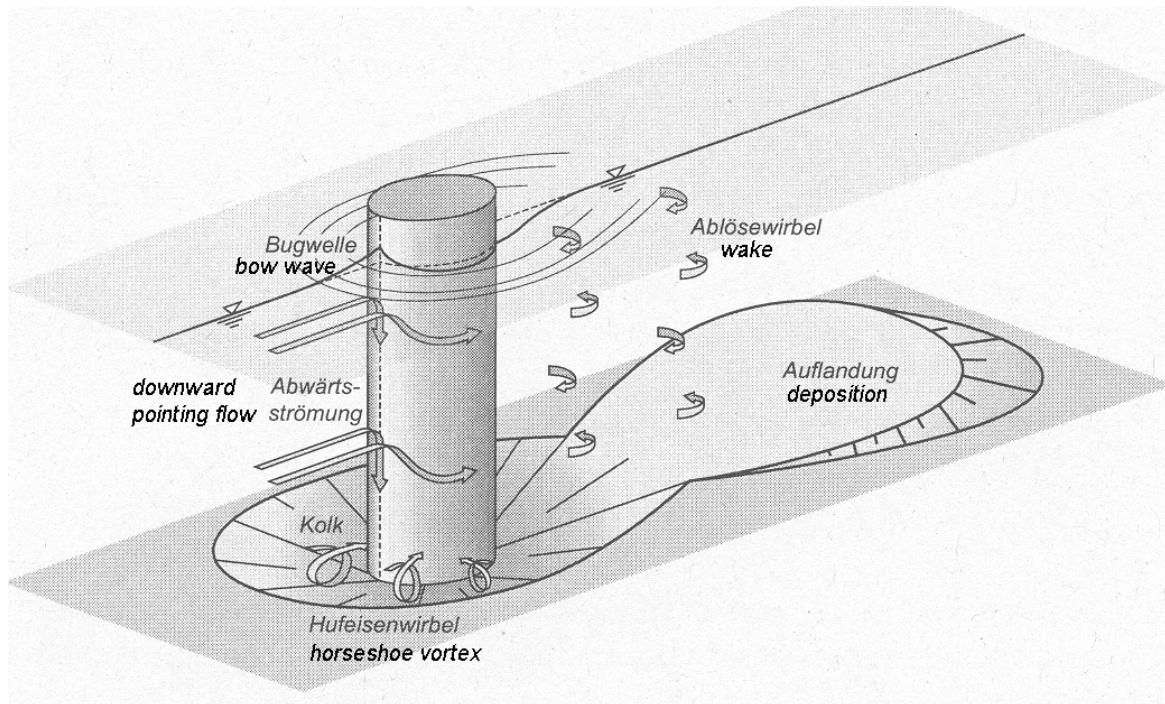


Figure 4.21 Scour around a bridge pier (Bezzola, 2004)

Morris' report on the design of roughness elements for drainage chutes (see chapter 3.6.2, pp. 67) give rise to the assumption that upstream scours develop on the transition from tumbling flow to rapid flow (Morris 1969). This assumption is supported by Volkart's findings (see chapter 3.4.3, pp. 46): Although Volkart does not distinguish the flow regimes tumbling flow and rapid flow the photo sequence in Figure 3.35 marks the transition from tumbling to rapid flow. In the left picture the upstream scour starts to develop. Due to the long exposure the direction of the vortex is well visible. On the right picture the flow is in the rapid regime.

None of the publications on natural step-pool systems dealt with in this thesis reports the occurrence of upstream scours in the field. The question whether the formation of upstream scours is a phenomenon that occurs only in the lab (possibly due to scale effects) is not yet answered. The fact that they do not occur at the prototype ramp in the Stübmingbach stream may be related to different framework conditions of the model ramp for the Große Tulln river and the prototype ramp (e.g. ramp slope, particle size distribution). Moreover there is no gauging station close to the prototype ramp. Therefore reliable conclusions on the return periods of the flood events that have occurred in the past since the ramp has been constructed cannot be drawn. It seems possible that upstream scours would also develop for the prototype ramp on very high flood events.

4.8.4 Results PHASE 2

Development of Upstream scour holes

Figure 4.22 shows the bed changes of ramp 1 for different model sediments after a flood event. (1-year flood resp. 30-year flood). For the rounded gravel 4 – 8 mm (S1) upstream scour holes in the first two pools develop already on a 1-year flood (Figure 4.22 a.). Presumably these scour holes form because of the downward pointing flow upstream of the step. If the pools are filled with crushed gravel 0 – 15 mm (S4) the same 1-year flood event does not lead to upstream scours (Figure 4.22 b.). Increasing the discharge up to a 30-year flood the upstream scours in the pools 4 and 5 also develop for the crushed gravel (Figure 4.22 c.). In this test run the first three pools were additionally

armored with a ground sill halfway of the pool length which slightly reduced the upstream scours within these pools.

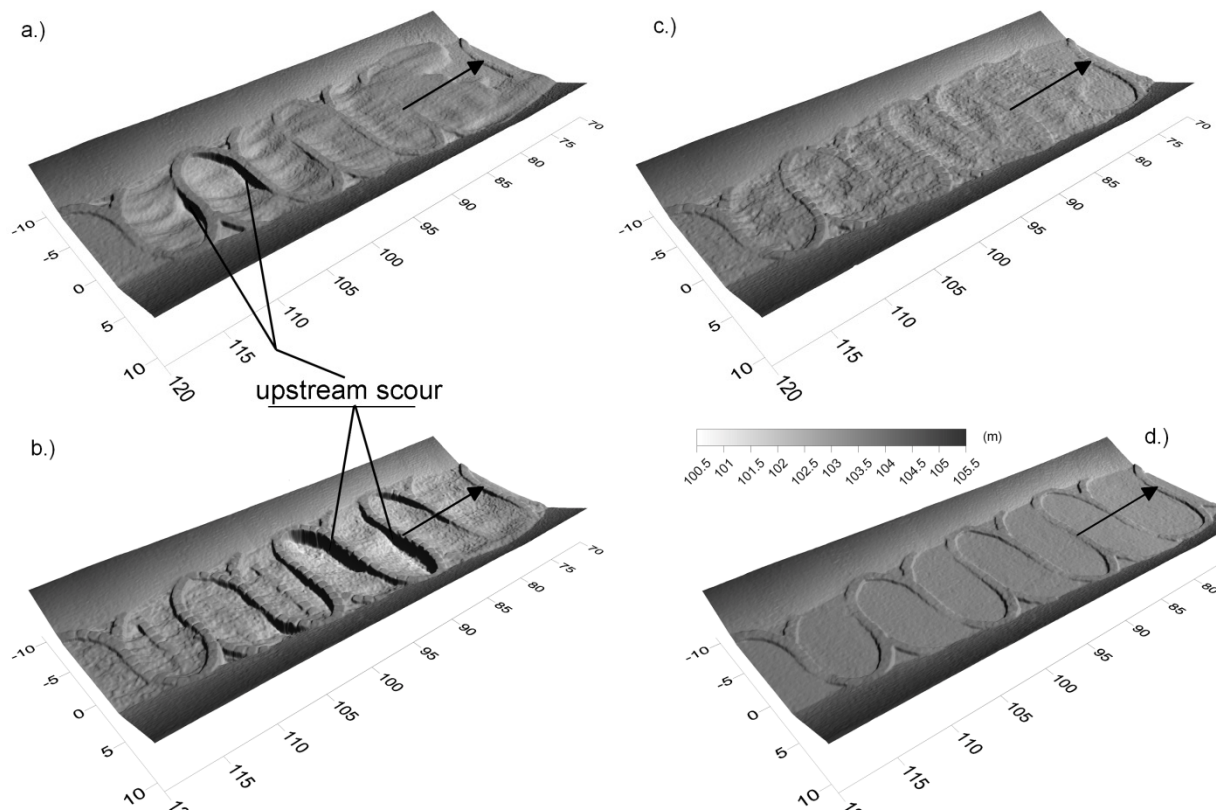


Figure 4.22 Upstream scours: a.) test run no. 3: 1-year flood, S1 b.) test run no. 11: 1-year flood, S4 c.) test run no. 12: 30-year flood, S4 d.) initial bed surface prior to each test run

Ramp Designs D1 – D7

Up until the ramp design D7 the following insights were gained:

- The 1-year flood event yields satisfactory results with respect to scour depths and the stability of the ramp
- During test run no. 11 (D6) the maximum scour depth occurred in the second pool with a mean depth of 40 cm and a maximum depth of 61 cm (Figure 4.22 b.).
- Ground sills (cf. Figure 4.24) halfway of the pool length reduce the development of upstream scours but do not prevent them completely.
- One slow-down pool between the two ramp sections is sufficient
- During test run no. 12 (D6) where a 30-year flood was simulated upstream scours developed in the pools 4 and 5 ((Figure 4.22 c.)

Construction of Ramp Design D8

Up until ramp design D7 only the first ramp section including the slow-down pool was constructed. The design D8 included also the second ramp section with 5 step-pool units. The test runs before design D8 had shown that 1 slow-down pool is sufficient to achieve the desired flow calming. The initial design consisted of 2 horizontal step-pool units for calming the flow. The steps of the ramp 1 were made of cubic-shaped cobblestones which did not well model the prototype boulders because of their sharp edges. As it was assumed that the sharp-edged cobblestones support the development of upstream scours the steps of ramp 2 were made of casted concrete. A boulder (model scale) of the

desired shape was used to form a cavity in a sand box thus yielding a sand mold. Figure 4.23 shows the erection of ramp design D8 with the cobblestone steps on ramp 1 and the casted concrete stones on ramp 2.

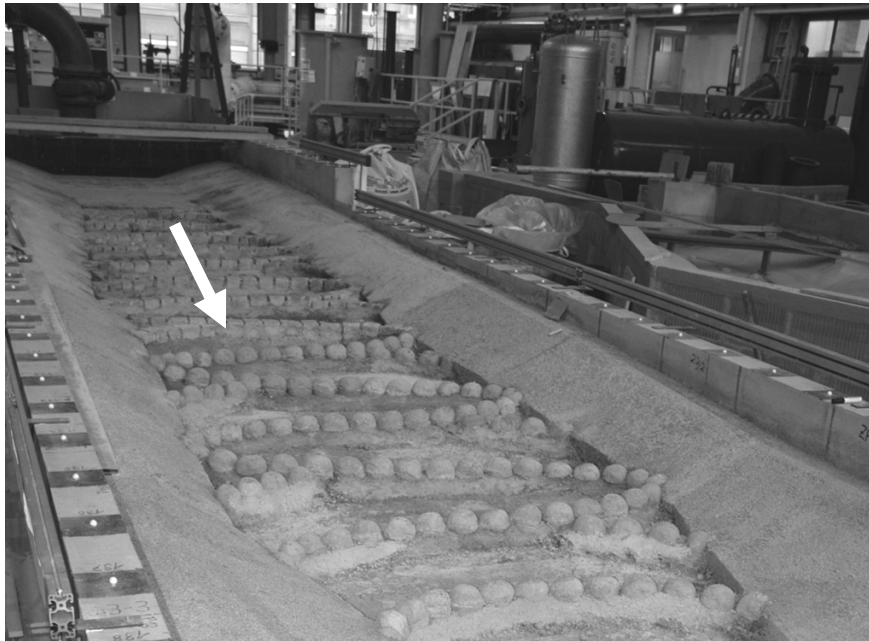


Figure 4.23 Erection of design variant D8, viewing direction: upstream

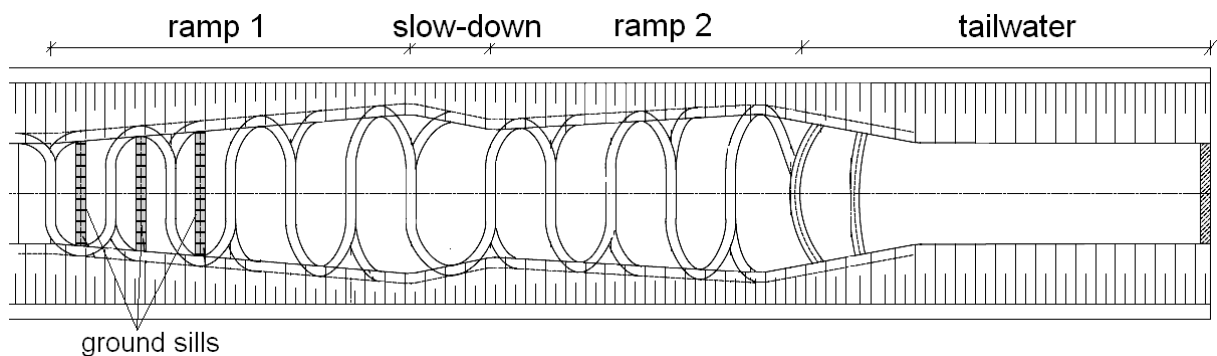


Figure 4.24 Plan view ramp design D8

Ramp Design D8 – Results 1-year flood

In test run 15 (Table 4.11) the ramp design D8 filled up with model sediment S3 (Table 4.4) a 1-year flood lasting for 7 hrs (full scale) was simulated. Figure 4.25 shows the ramp immediately after the beginning of (0 hrs) and right before the end (7 hrs) of test run 15. On ramp 1 a hydraulic jump is clearly visible in the first 5 pools. This is known as the tumbling flow regime. The backwater from the slow-down pool prevents the formation of a hydraulic jump in pool 6. The flow pattern does not change significantly during the test run except for the sixth pool in ramp 1. About 3.5 hours after the beginning of the test run a hydraulic jump develops on the right side of the pool (marked in Figure 4.25, bottom). As the scour holes in the pools upstream get deeper the water surface undulations become more pronounced. The water depth above step 6 increases and is not completely submerged by the backwater of the slow-down pool any longer. This way supercritical flow occurs right below the step. With the subsequent hydraulic jump the flow is subcritical again.

On the second ramp below the slow-down pool a hydraulic jump forms only in the first two pools. Due to the high roughness of the channel (Table 4.1) the water level in the tailwater section very high, thus backing up the water up until the third pool of ramp 2. The backwater is supported by the widening of the channel (Figure 4.24).

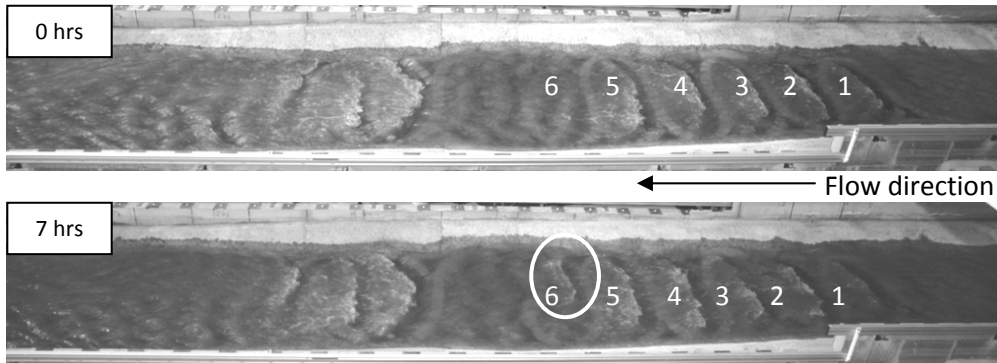


Figure 4.25 1-year flood for ramp design D8, direction of flow from right to left, pools of ramp 1 are labeled

The model sediment S3 that was used for test run 15 should have been mixed according to the prototype particle size distribution. It was visible to the naked eye that the sediment mixture contained too much fine particles and missed the coarse parts (chapter 4.3, pp. 77). The scour holes are much deeper for this model sediment which confirms this assumption. Nonetheless the analysis of the bed changes after test run 15 show already the tendency that the backwater from the tailwater section leads to depositions in the area of the ramp 2.

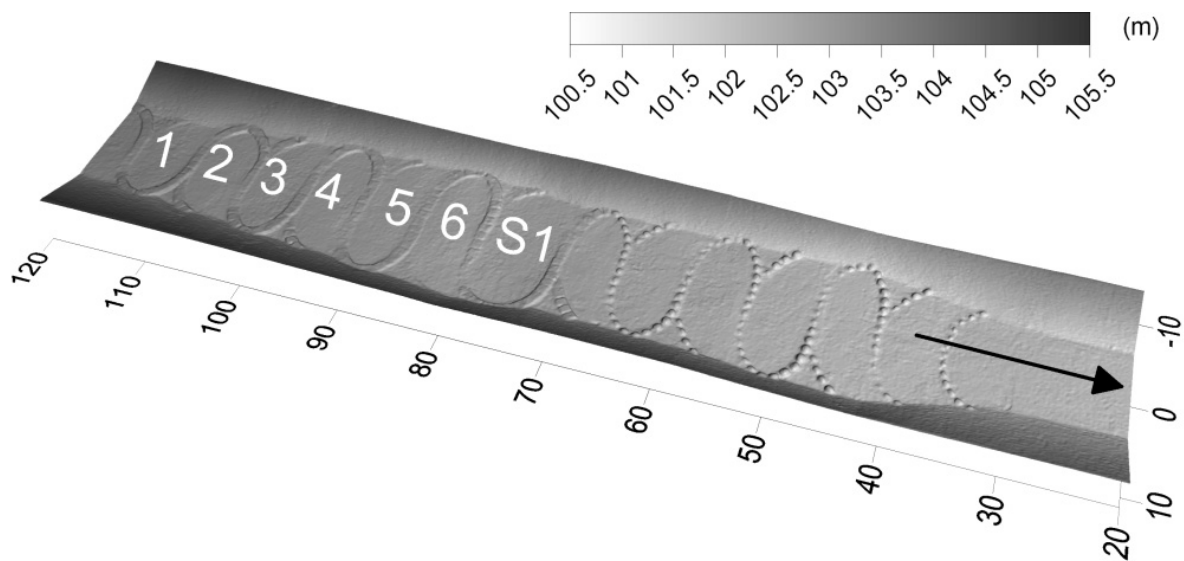


Figure 4.26 Ramp design D8: initial bed surface, pools of ramp 1 and slow-down pool labeled

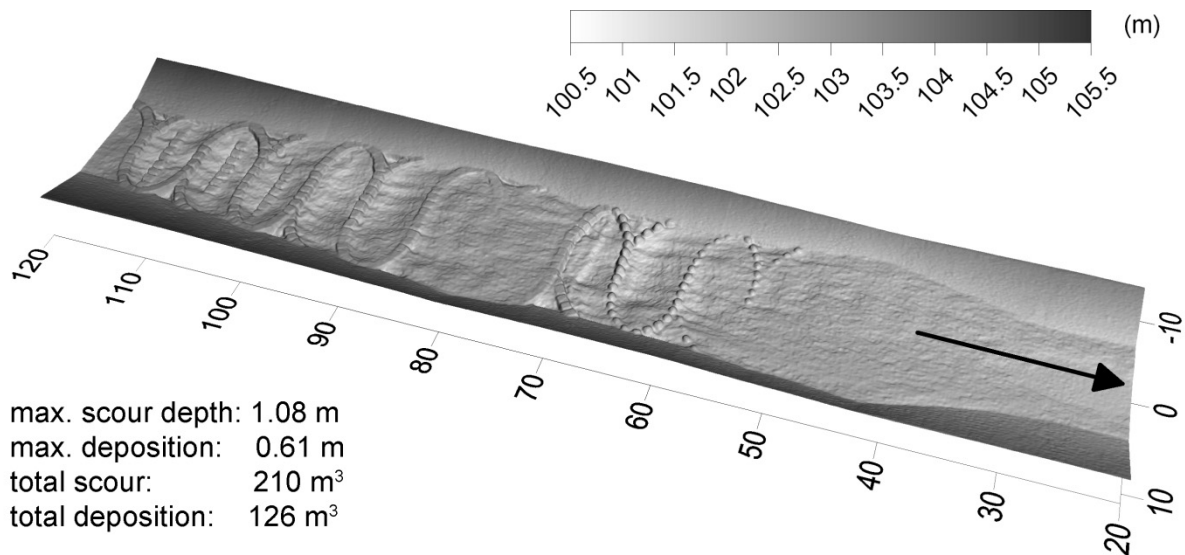


Figure 4.27 ramp design D8: bed changes after a 1-year flood

Ramp Design D8- Results 30-year flood

In test run 16 (Table 4.11) the ramp design D8 filled up with model sediment S3 (Table 4.4) a 30-year flood lasting for 7 hrs (full scale) was simulated. Sediment S3 was supplied manually at the upstream end of the model at a rate of 200 l/h (model scale). This corresponds to a full scale bed load transport rate of 3.16 kg/ms according to Meyer-Peter Müller’s formula (4-1) with values as given in Table 4.12. The bulk density was defined in the technical data sheet. By means of the flap the water depth at the downstream end of the model was adjusted to 22.5 cm, which corresponds to the normal flow depth for a 30-year flood for the standard section (Figure 4.4) as calculated by HEC-RAS.

Density water (kg/m ³)	ρ_w	998.21
Density sediments (kg/m ³)	ρ_s	2650
Bulk density sediments (kg/m ³)	$\rho_{s,b}$	1800
Gravitational acceleration (m/s ²)	g	9.81
Bed slope (–)	I	0.0058
Hydraulic radius (m) for a 30-year flood (HEC-RAS)	R_s	1.4
Mean diameter (m)	d_m	0.08
Shields parameter (–)	Fr_*	0.047
Channel width (m)	B	10

Table 4.12 Choice of parameters for MPM’s formula for a 30-year flood

The bed changes after the 30-year flood show (Figure 4.28, initial surface: Figure 4.26) that some parts of the added sediments have deposited in the pools. The first three pools of ramp 1 have less deep scour holes than after the 1-year flood without sediment addition. The high tailwater level has lead to large areas of deposition on ramp 2 below the slow-down pool. Only in the first two pools of ramp 2 scours have developed. All other pools have higher bed levels compared to the initial bed levels. It is well visible that the sediments have deposited more on the right side.

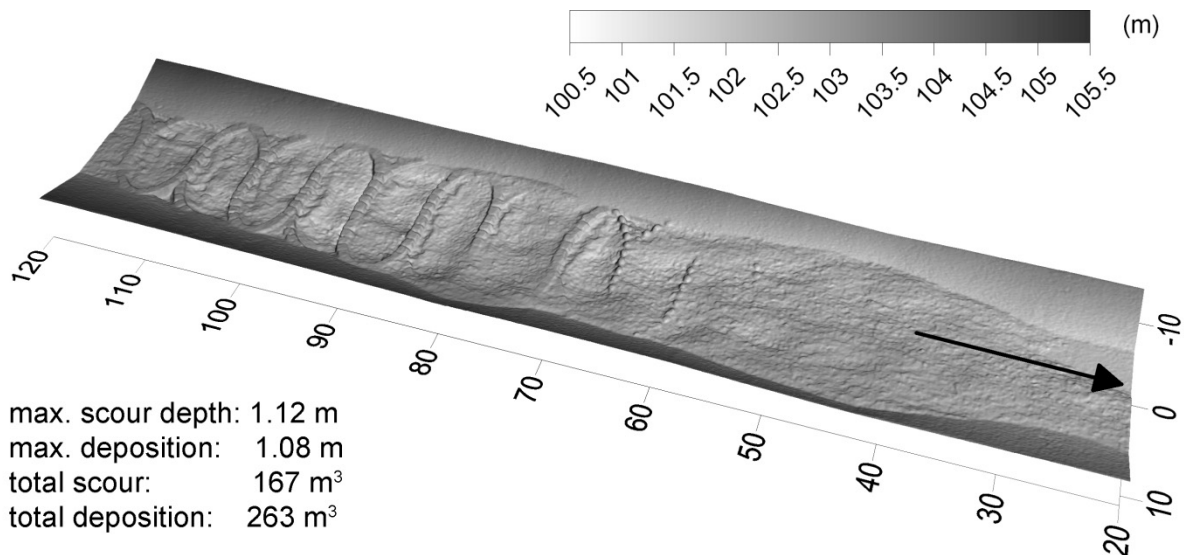


Figure 4.28 Ramp Design D8 - bed changes after a 30-year flood

Ramp Design D8 – Results 100-year flood wave

In test run 17 (Table 4.4) the ramp design D8 filled up with model sediment S3 (Table 4.4) a 100-year flood wave with a peak flow of 123 m³/s lasting for 9.5 hrs (full scale) was simulated. The discharge was adjusted automatically by the frequency-controlled pumps of the laboratory.

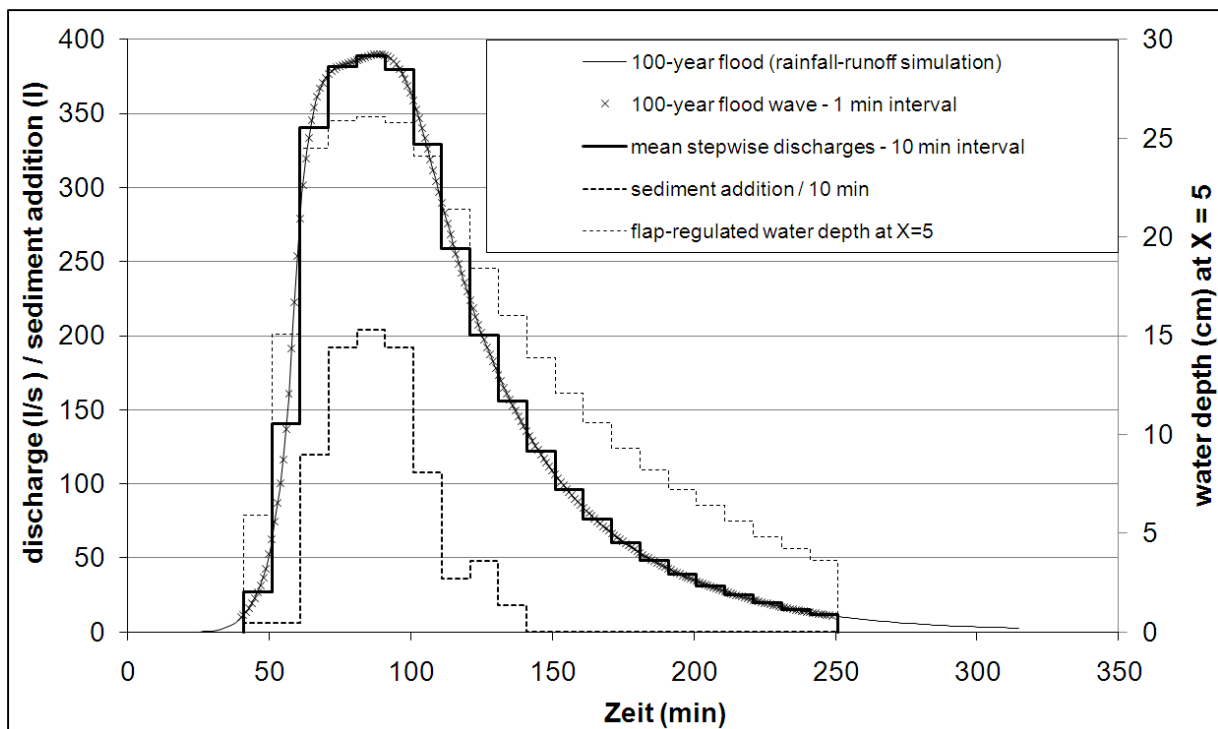


Figure 4.29 100-year flood hydrograph, sediment addition and water depths - model scale!

Depending on the current discharge sediment S3 was supplied manually at the upstream end of the model. For the bed load calculation the model scale hydrograph was approximated by a step function (10 min steps). For each averaged 10min discharge value the hydraulic radius and the water depth was calculated using HEC-RAS. The water depth at control section X=5 located 50 cm upstream of the sand trap was regulated via the flap (Figure 4.14).

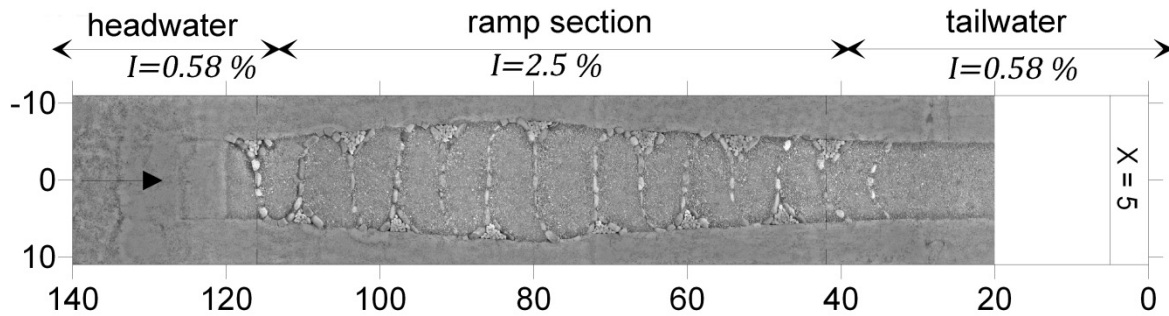


Figure 4.30 Control section X=5 for water level regulation via flap

The full scale bed load transport rate according to Meyer-Peter Müller’s formula (4-1) was calculated with the values given in Table 4.12. The corresponding hydraulic radius was calculated with HEC-RAS.

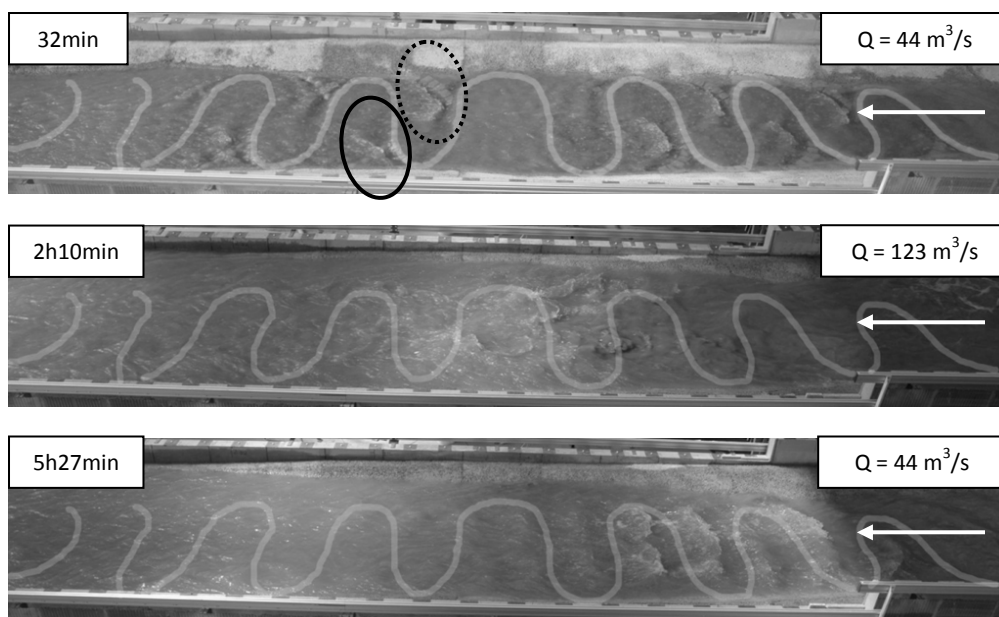


Figure 4.31 Ramp Design D8: 100-year flood wave, flow direction from right to left!

Figure 4.31 shows the ramp after 32 minutes (top), at peak flow after 2h10min (middle) and after 5h27min (bottom) at the same discharge ($44 \text{ m}^3/\text{s}$) as after 32 minutes. The position of the steps in Figure 4.31 is drawn as half-transparent line.

At the beginning of the flood wave (after 32 min) a hydraulic jump develops alternately close to the right resp. left bank. The lateral position of the hydraulic jump is indicative of the lateral inclination of the steps: Each step is aligned with the bed level near one side of the banks. On the other bank the step protrudes Δh from the bed. The step on this side of the banks acts like a little weir. A flow transition from subcritical to supercritical and a subsequent hydraulic jump in the pool below occur. In the sixth pool of ramp 1 no hydraulic jump is visible. This is due to the backwater effect of the slow-down pool.

On ramp 2 below the slow-down pool a hydraulic jump develops until the fourth pool. Back water effects from the tailwater extend to the fifth pool of ramp 2. The location of the hydraulic jump of the first pool of ramp 2 is downstream of the reinforcement (encircled with dots). The hydraulic jump of the second pool of ramp 2 (encircled) is located immediately downstream of the main step. The shape of the stones of the steps makes the difference. The reinforcement of the first pool is made of

cobblestones whereas the reinforcement of the second pool is made of casted concrete stones which have a spherical shape. Obviously the reinforcement made of cobblestones is able to direct the flow towards the centerline. The reinforcement made of spherically shaped concrete stones does not act as a single structure because the spacing between two steps is too large. The hydraulic jump there takes place immediately downstream of the main step. The reinforcement made of the concrete stones only serves to disturb the flow so that the hydraulic jump cannot develop properly.

When constructing the prototype ramp great care must be taken to place the boulders properly. The boulders should not act as single elements but as one structure.

After 2h10min the peak flow is reached. As can be seen from Figure 4.31 (middle) no hydraulic jump is visible. Due to the high turbidity of the water the sediment movements could not be observed during the test run. No conclusion can therefore be drawn whether the white water between pool 5 and 6 of ramp 1 is visible because of a scour below or because of a sediment wave traveling through the ramp.

After 5h27min on the falling limb of the hydrograph the discharge reaches $44 \text{ m}^3/\text{s}$ again. In comparison to the same discharge on the rising limb of the hydrograph after **32** minutes the water levels are much higher because of sediment depositions. On ramp 1 the hydraulic jumps coincide with the scour holes in the pools 2 (only right side) 4 and 5 (Figure 4.32, initial bed surface: Figure 4.26).

Figure 4.32 shows that parts of the added sediments have deposited in the ramp pools. The scour holes of the first three pools of ramp 1 are less deep than after a 1-year flood without sediment addition. Similar as for the 30-year flood (pp. 98) the high tailwater level has lead to large areas of deposition on ramp 2 below the slow-down pool. All the pools of ramp 2 have higher bed levels compared to the initial bed levels. It is well visible that the sediments have deposited more on the right side.

During the testing of ramp design D8 the following insights were gained:

- The high tailwater level leads to backwater effects along the ramp. The channel widening of ramp 2 is therefore counterproductive
- The boulders for the prototype construction should not be spherically shaped. The spacing between two adjacent boulders must be small such that the boulders may act as a single structure
- The edges of the cobblestones are too sharp. Boulders of a shape halfway between the cobblestones and the spherically shaped casted concrete stones should be preferred.

For all test runs in PHASE 2 the stones of the steps were glued to the channel bed with mortar. As the construction of the ramp design was time-consuming it was aimed at not destroying the ramp during the experiments.

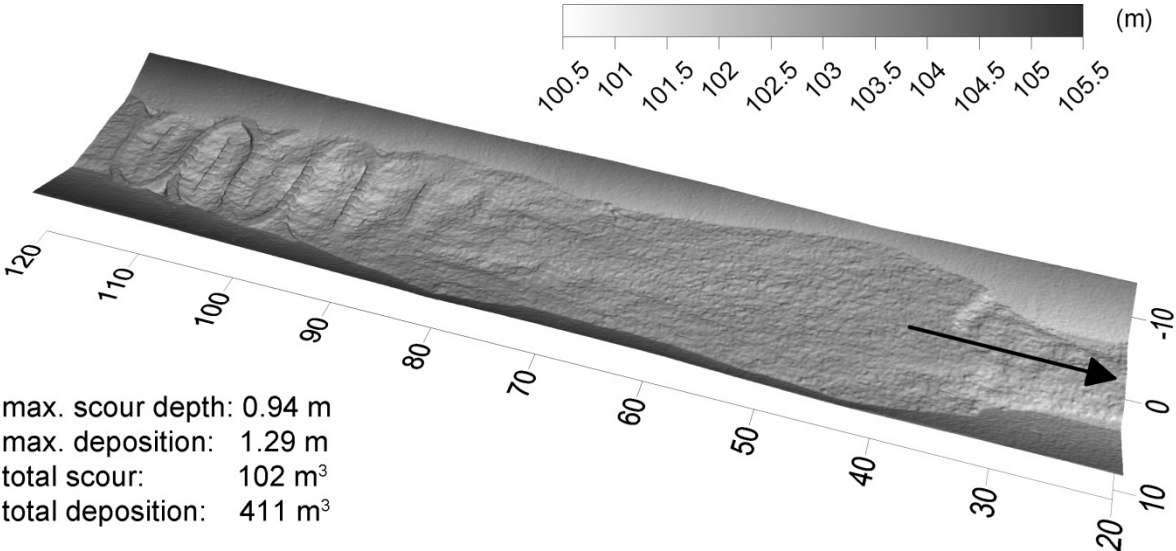


Figure 4.32 Ramp Design D8, bed changes after a 100-year flood wave

4.9 PHASE 3 – Mobile Bed Experiments – Final Design

For the final PHASE 3 Dr. Michael Hengl, head of the “Institut für Wasserbau und hydrometrische Prüfung” of the “Bundesamt für Wasserwirtschaft”, Vienna, Austria, was asked to act as an external expert. Based on the results from PHASE 2 a ramp with steps made of natural stones without channel widening in the second ramp section was constructed in PHASE 3.

4.9.1 Results PHASE 3

In PHASE 3 altogether 21 experiments with ramp design D9 and the resulting final design were performed. All experiments in this PHASE 3 were carried out with crushed gravel 0 – 15 mm (S4). Key findings are described within this chapter. A complete documentation of the results can be found in the appendix A.2.

The individual experiments in PHASE 3 are summarized in Table 4.13. For the experiments with the flap regulated water level the normal depth was calculated via HEC-RAS from the given geometry and roughness values (Table 4.1). The flap regulated experiments lead to massive depositions in the tailwater section. To make sure that these depositions were not caused by the influence of the flap gate the experiments were eventually performed without the flap gate. This way critical depth occurred at the downstream end of the model, so the energy gradient was steeper than the bed slope in the tailwater section. If the stability of the ramp could be achieved under these conditions it would also prove stable for normal flow conditions.

Since experiment number 21 the bank roughness was highly increased by gluing 25 – 50 mm stones (model scale) to the banks.

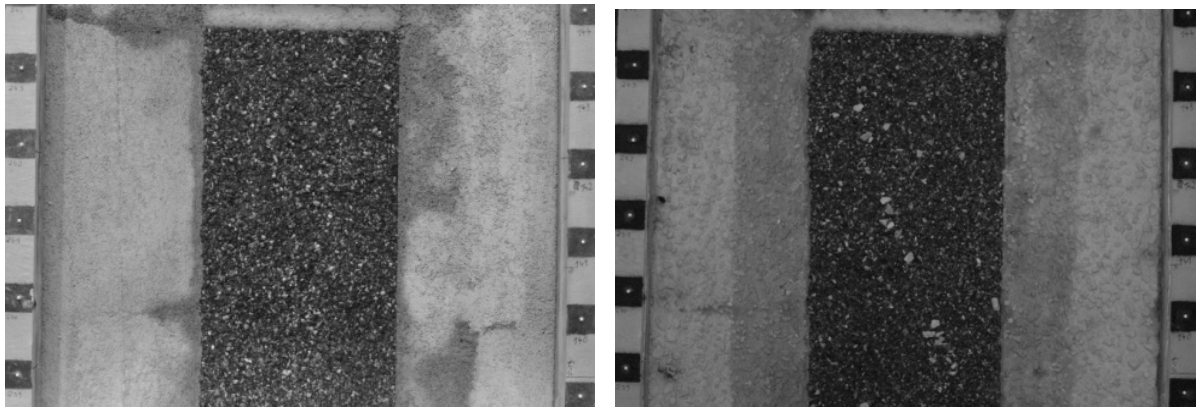


Figure 4.33 Bank roughness before (left) and after experiment no. 21, tailwater section with end sill

Since experiment no. 24 the initial bed level was not rebuilt prior to each test run. Instead the experiments were started with bed levels from the preceding test run. This series aimed at simulating several flood events.

No.	Ramp design	Flap regulated water level	discharge	Sediment addition	duration (model scale)
18	D9	Yes	1-year flood	-	2h15min
19	D9	No	30-year flood	-	2h15min
20	D9	Yes	100-year flood wave	varying	1h25min
21	D9	Yes	30-year flood	720 l/h	1h05min
22	D9	No	30-year flood	720 l/h	2h15min
23	Final design	No	100-year flood wave	varying	3h
24	Final design	No	1-year flood	-	4h
25	Final design	No	5-year flood	72 l/h	4h
26	Final design	No	10-year flood	144 l/h	4h
27	Final design	No	5-year flood	-	1h
28	Final design	No	5-year flood	-	1h
29	Final design	No	5-year flood	-	1h
30	Final design	No	5-year flood	-	1h
31	Final design	No	5-year flood	-	2h
32	Final design	No	5-year flood	-	2h
33	Final design	No	5-year flood	-	2h
34	Final design	No	10-year flood	-	2h
35	Final design	No	10-year flood	-	2h
36	Final design	No	10-year flood	-	2h
37	Final design	No	10-year flood	-	2h
38	Final design	No	10-year flood	-	2h

Table 4.13 Complete list of test runs in PHASE 3 in chronological order

Results Ramp Design D9

For PHASE 3 the ramp was newly constructed. The steps were made of natural stones. Unlike in PHASE 2 the stones were not glued to the channel bed in PHASE 3. The ramp construction should reflect the prototype construction. The configuration of a step is shown in Figure 4.35. A step consists of natural stones ($a \times b \cong 10 \times 15$ cm – model scale!) for the step itself and stones for the scour protection up- and downstream of the step ($a \times b \cong 8 \times 5$ cm – model scale!). The scour protection stones are installed in between two adjacent step stones. To further support the stability of the steps the remaining gaps of the scour protection are filled with smaller stones ($a \times b \cong 4 \times 2$ cm – model scale).

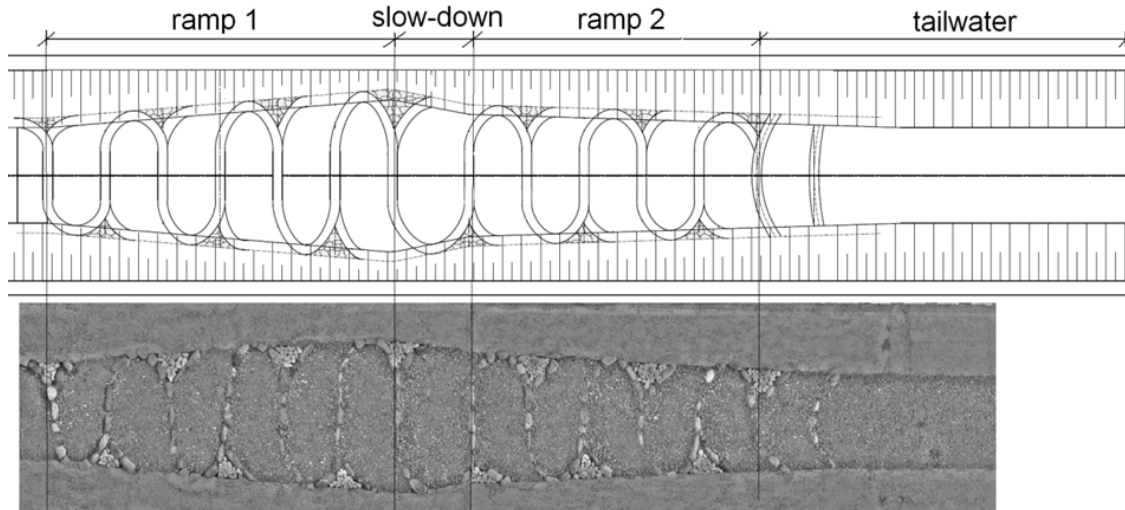


Figure 4.34 Plan view ramp design D9 - ramp area and tailwater section

As the triangular shaped area between step, reinforcement and bank often eroded during the experiments in PHASE 2 this area was armored with stones $a \times b \cong 4 \times 2$ cm in ramp design D9.

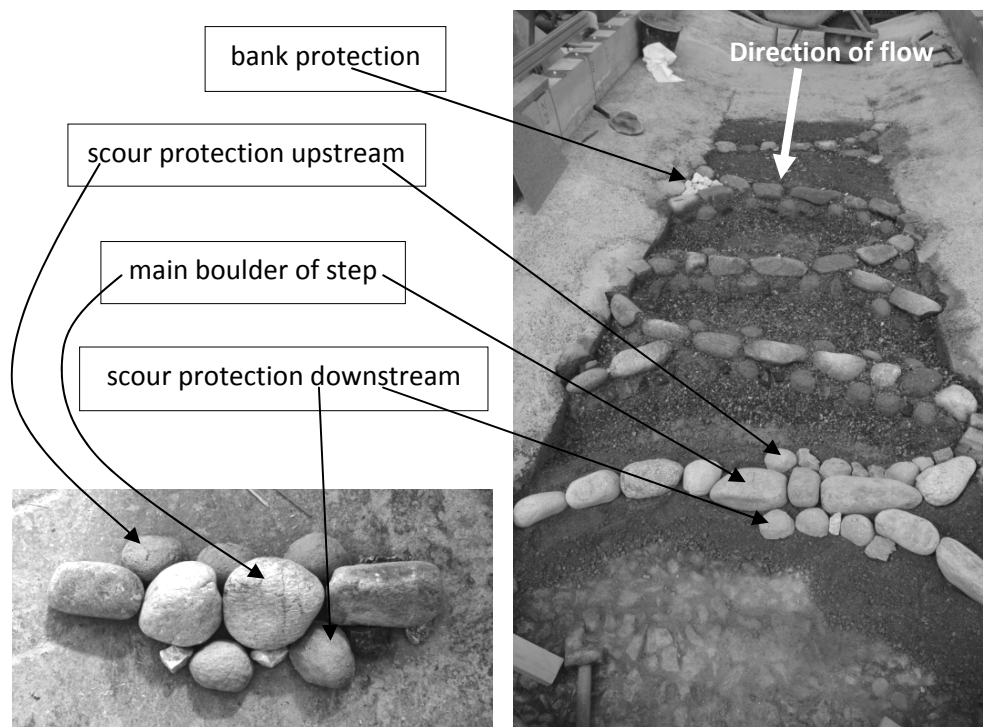


Figure 4.35 Configuration of a step, ramp design D9

The channel widening of ramp two was omitted in ramp design D9. The tailwater section was completed with a mobile bed. The banks were fixed in the whole model. The ground sills halfway between two steps were omitted.

Results Ramp Design D9 before Increase of Roughness

After a 1-year flood simulation for 7 hours (full scale) of ramp design D9 the maximum scour depth is 1.3 m in the second pool of ramp 2. No upstream scours have developed. The bed sediments eroding in the upper pool tend to deposit on the right hand side of the channel further downstream (Figure 4.37).

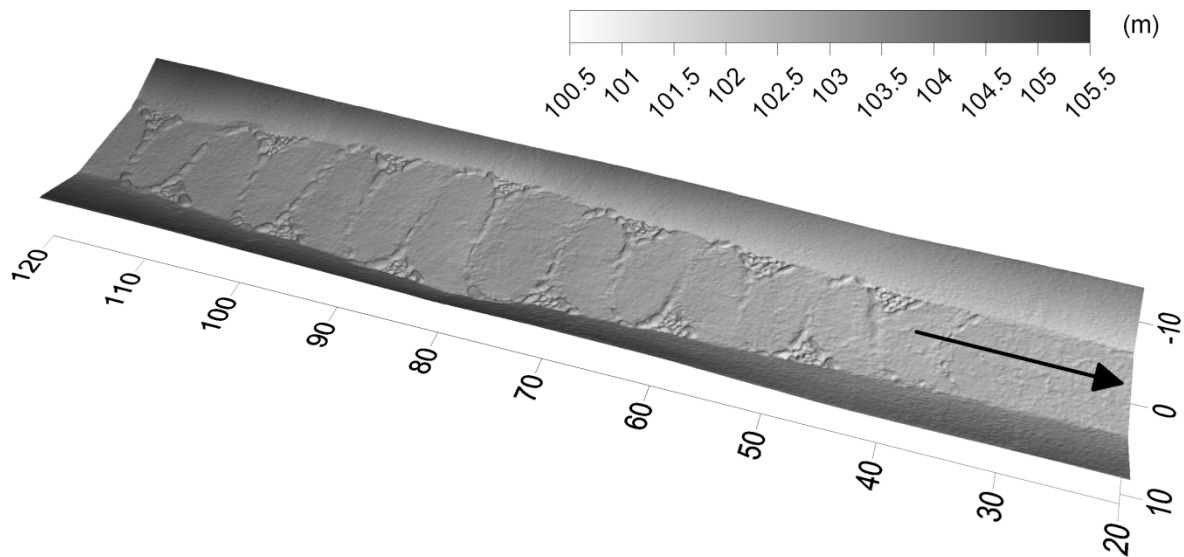


Figure 4.36 Ramp Design D9 - initial bed surface

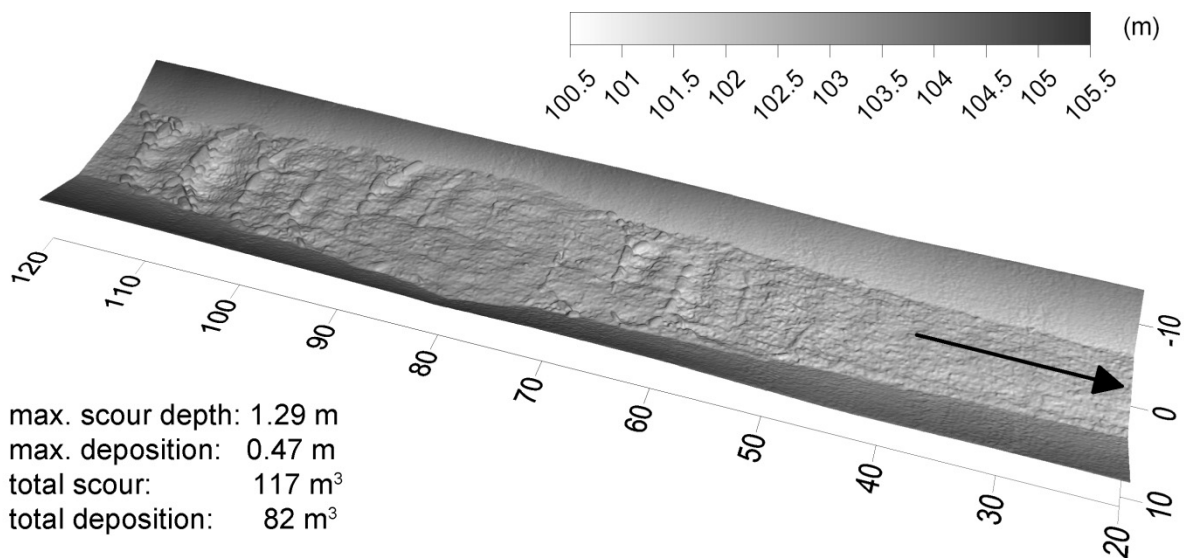


Figure 4.37 Ramp Design D9 - bed levels after a 1-year flood, (test run 18)

In test run 19 a 30-year flood ($91 \text{ m}^3/\text{s}$) was simulated for 7 hours (full scale). No sediments were added. For the first time of the mobile bed experiments the water levels were not regulated using the flap. Figure 4.38 shows very deep scours that have developed during the test run. (initial bed: Figure 4.36). In the fourth pool of ramp 1 the maximum scour depth of 1.66 m occurs. The maximum scour depth was determined by subtracting the DEM of the initial bed from the DEM of the bed levels after the test run. The DEM's are calculated digital photogrammetry. Before the test run the upstream scour protection must have protruded from the initial bed level. Because the mobile bed layer is only 15 cm thick. Therefore the maximum possible scour depth in the model is 1.5 m (full scale). Almost all pools have eroded all the way to the channel bed from PHASE 1. Some scour protection stones were washed away as can be seen in Figure 4.38. The steps itself were not mobilized. The tailwater section with a slope of $I = 0.0058$ eroded severely.

Figure 4.38 shows the influence of the leveled step at the end of the ramp structure (initial bed: Figure 4.36). The leveled step is U-shaped in plan view and is aligned with the channel bed in the

centerline. Near the banks the step protrudes 15 cm from the bed. The small protrusion of the leveled step near the banks causes a scour in the channel center that does not endanger the banks.

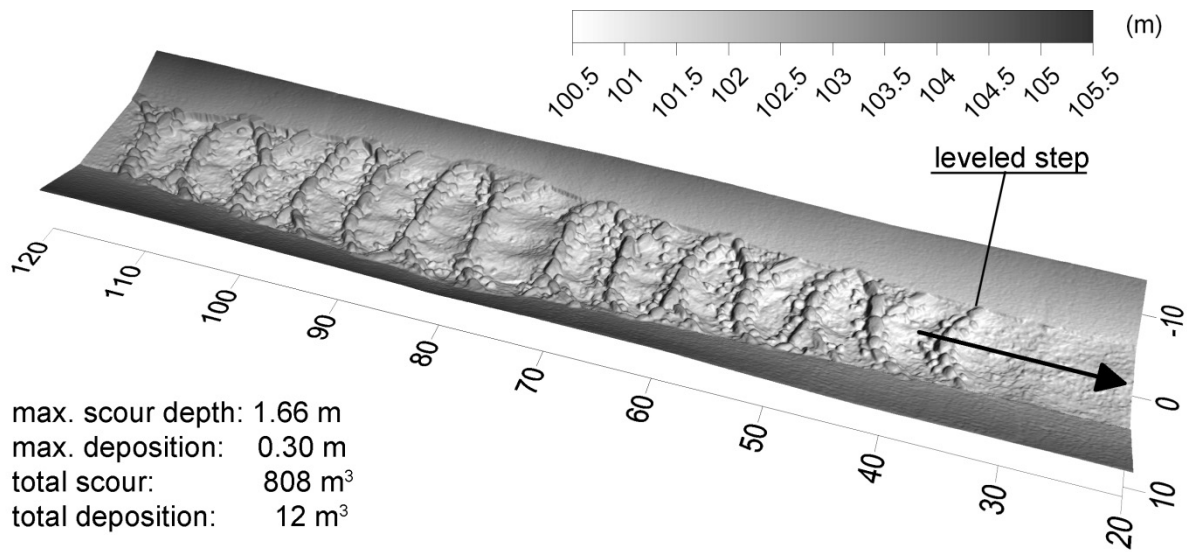


Figure 4.38 Ramp design D9 - bed levels after a 30-year flood, no flap (test run 19)

As the water levels were not regulated with the flap critical depth occurred at the downstream end of the model. The energy gradient was steeper than the bed slope in the tailwater section, resulting in higher shear stresses which in turn promote the severe erosion of the mobile bed.

In the subsequent test run 20 a 100-year flood wave was carried out (Figure 4.41).

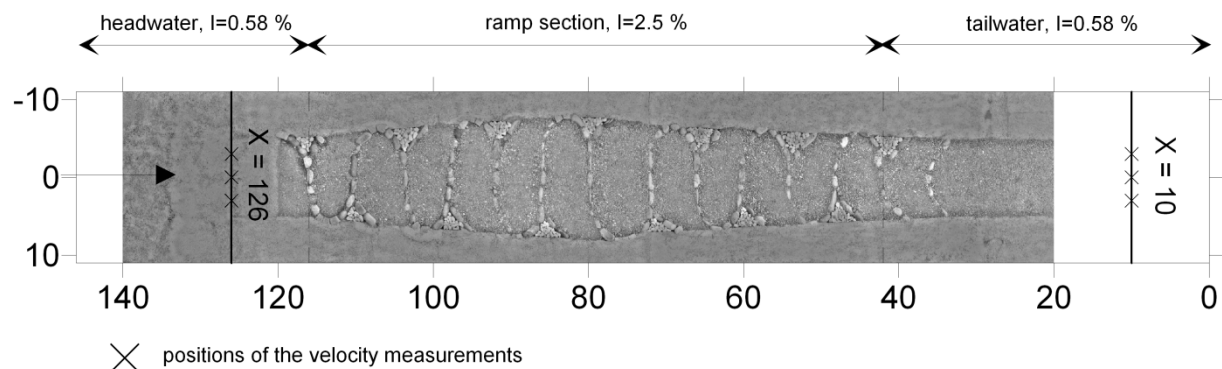


Figure 4.39 Check of the model roughness, position of the water level measurements $X=126$

For this test run the water levels were flap-regulated again. During the experiment water level measurements were taken for different discharges at a control profile ($X = 126$) of the headwater section (Figure 4.39). The mean velocity was calculated by application of the continuity principle. These velocities transformed to full scale were compared to those of the HEC-RAS calculation for the given roughness values (Table 4.1). As can be seen from Figure 4.40 the actual velocities in the model are higher than the velocities resulting from the set roughness of the HEC-RAS calculation. Accordingly, the water depths in the model are smaller than the set water depths of the numerical calculation. When the set velocities are multiplied by the factor 1.5 (dashed line in Figure 4.40) the resulting velocities correspond approximately to those of the physical model transformed to full scale. Hence, the model is too smooth.

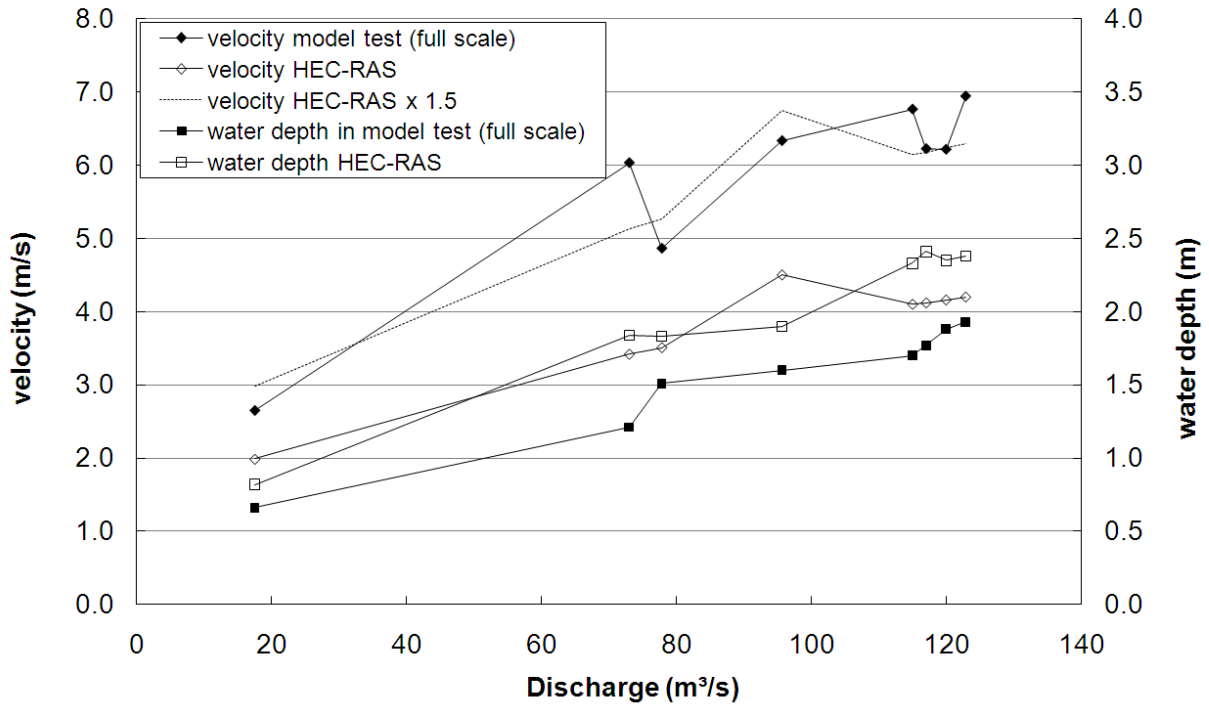


Figure 4.40 Check of the model roughness, velocities and water depths (test run 20)

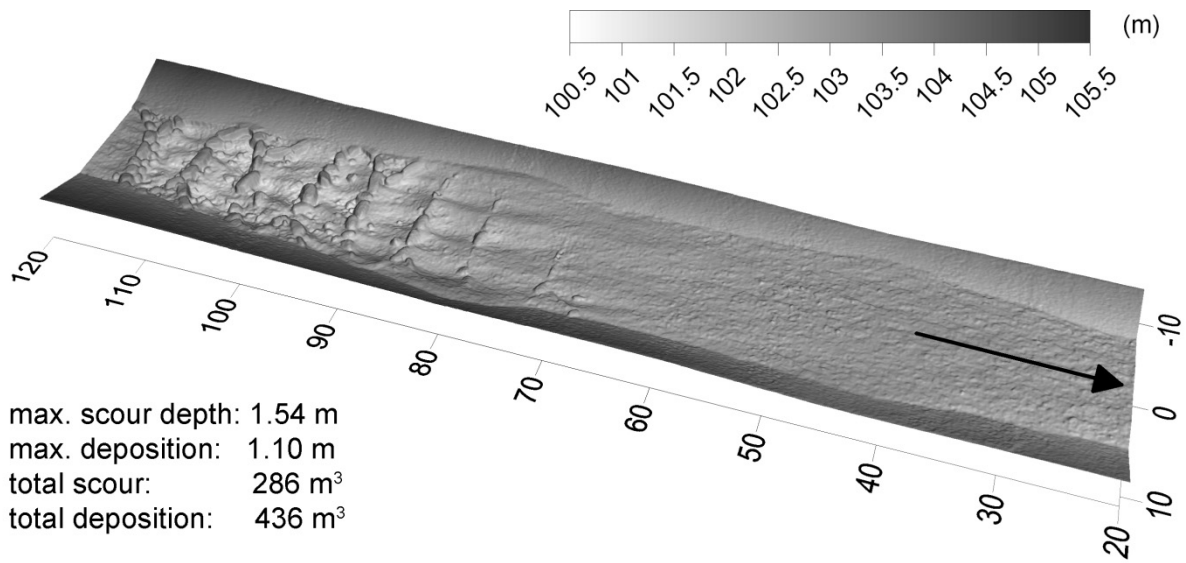


Figure 4.41 Ramp Design D9 - bed levels after a 100-year flood, flap-regulated (test run 20)

Test run 20 had to be interrupted after 85 min model time because of an error in the pump control. The peak flow of the wave was already exceeded. Figure 4.41 demonstrates that the pools of the upper part of the model bed eroded severely while there are depositions further downstream. (initial bed: Figure 4.36). A stone of the step of the third pool has been washed out. Conversely the tailwater section exhibits depositions up to 0.6 m. In the headwater section (not shown in Figure 4.41) which has the same slope as the tailwater section no sediments have deposited. The reason for this discrepancy is that for the tailwater section the set water levels were flap-regulated while in the headwater section water levels according to the model roughness had adjusted.

Increase of Roughness in the Model

As the bed of the ramp section and the tailwater section was mobile in PHASE 3 with sediments corresponding approximately to the prototype particle size distribution the channel roughness could not be increased anymore. It was possible though to increase the roughness of the fixed bed of the headwater section and of the banks. Until test run 20 these sections were made of rounded gravel 4 – 8 mm that was fixed with a thin layer of mortar.

The banks of the Große Tulln river in the project area are heavily overgrown and thus very rough. They have a mean bank Strickler roughness of $k_{st,B} = 12.5 \text{ m}^{1/3}/\text{s}$ (Table 4.1). As a consequence to the results of test run 20 the bank roughness was increased by gluing stones onto the banks ($a \times b \cong 5 \times 2.5 \text{ cm}$). The roughness of the headwater section was increased by applying grit onto the channel bed that was fixed with mortar. Finally the initial bed surface of the mobile bed sections (ramp and outlet) was reconstructed.

Before and after the increase of roughness velocity measurements were carried out for a 1-year flood and a 30-year flood with a hydrometric impeller. Two control cross sections, one in the headwater section and one in the tailwater section were measured (Figure 4.39) to see the influence of the increase of roughness on the velocities and water depths.

From it becomes clear that the increase of roughness resulted also in higher water depths. Nonetheless the water depths after the increase of roughness lie well below the set water depths according to the normal depths given by the prototype roughness values (Table 4.1). The mean velocity decreases accordingly. Within the channel the mean velocities were partly higher after the increase of roughness than before. This can be explained as follows: Due to the increase of roughness the cross sectional area has diminished. Additionally the increased roughness results in a reduced discharge rate within the bank areas.

	1-year flood	30-year flood
Water levels set	1.21 m	2.25 m
Actual water levels in the model (full scale) before the increase of roughness	0.77 m	1.45 m
Actual water levels in the model (full scale) after the increase of roughness	0.85 m	1.65 m

Table 4.14 Water depths before and after the increase of roughness

The results of the velocity measurements can be found in appendix A.3.

Results Ramp Design D9 after Increase of Roughness

After the increase of roughness two further test runs (no. 20 and 21) for ramp design D9 were carried out both simulating a 30-year flood. The sediment addition was 720 l/h (model scale). In the preceding test runs no. 13 and no. 16 the sediment addition for a 30-year flood was only 100 l/h (model scale). The increase for the test runs 20 and 21 was in accordance with the client and was motivated on one hand by the statement of the head of the local water association “Große Tulln” who claimed that during a “major” flood event about 5000 m³/s of bed load deposit upstream of a weir. On the other hand the calculated bed load rate increases strongly if instead of the hydraulic radius of the trapezoidal cross section the hydraulic radius of the channel (\equiv water depth) is inserted into Meyer-Peter Müller’s equation 4-1. The hydraulic radius of the whole cross sectional area for a 30-year flood and the given roughness values is 1.4 m. The water depth (\equiv hydraulic radius of the

channel) is 2.0 m which increases the bed load rate by a factor of 3.6. This leads to the above mentioned sediment addition of 720 l/h in the model which corresponds to a total bed load of 1620 m³ in 7.1 h (full scale) during a 30-year flood.

For test run 21 the water levels were flap-regulated. For test run 22 the flap was not used. All other conditions were the same in both test runs. When the water is not regulated with a flap critical depth occurs at the downstream end of the model which results in a drop-down of the water levels in the tailwater section. To keep the influence of the drop-down short within the tailwater section a wooden board was installed at the downstream end of the sand trap. The board had the shape of the control cross section. It was leveled such that the board continues the slope of the tailwater section. Figure 4.42 (right) shows the sand trap including the wooden board shaped like the control cross section after a test run. The model sediments that were washed out of the model during a test run has deposited in the sand trap in such a way that it prolongs the channel bed until the wooden board. The critical depth occurs above the wooden board and not at the end of the channel. This way the drop-down curve of the water levels could be shifted further downstream by the length of the sand trap.



Figure 4.42 No flap, overfall into the sand trap (left) wooden board at the downstream end of the sand trap (right)

In both test runs 21 and 22 severe erosions occurred in the first pools despite the increased sediment addition of 720 l/h (model scale). During test run 22 a stone of the step between the first and the second pool has been washed out (arrow indicates the stone in Figure 4.43).

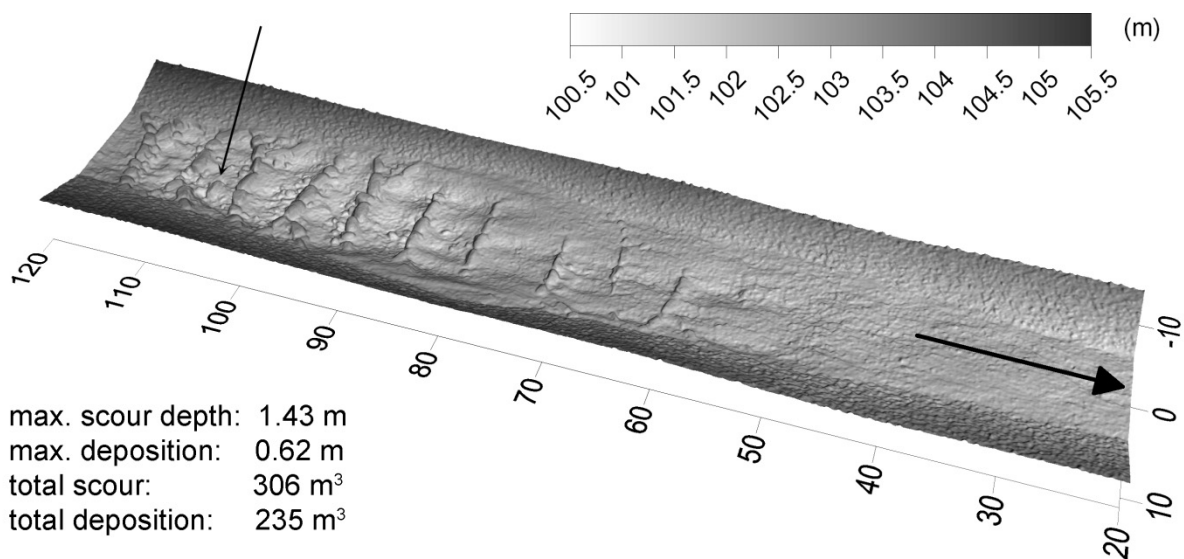


Figure 4.43 Ramp Design D9, bed levels after a 30-year flood, no flap (test run 22)

Pool Armoring

It turned out that the first pools of ramp 1 are exposed to severe stresses. The original idea to build a ramp without pool armoring had to be abandoned. For the final design the first four pools of ramp 1 were armored. Similar to the ground sills of the ramp designs D4 – D8 the armor layer was leveled 0.5 m below the initial surface halfway of the pool. The armor layer has the shape of a trough, i.e. it connects seamlessly with the scour protection of the steps up- and downstream and with the banks. The armor layer consists of one single layer of stones with a size of $a \times b \cong 5 \times 2.5$ cm (model scale). The armor layer is filled with model sediments up to the initial bed surface (Figure 4.44).

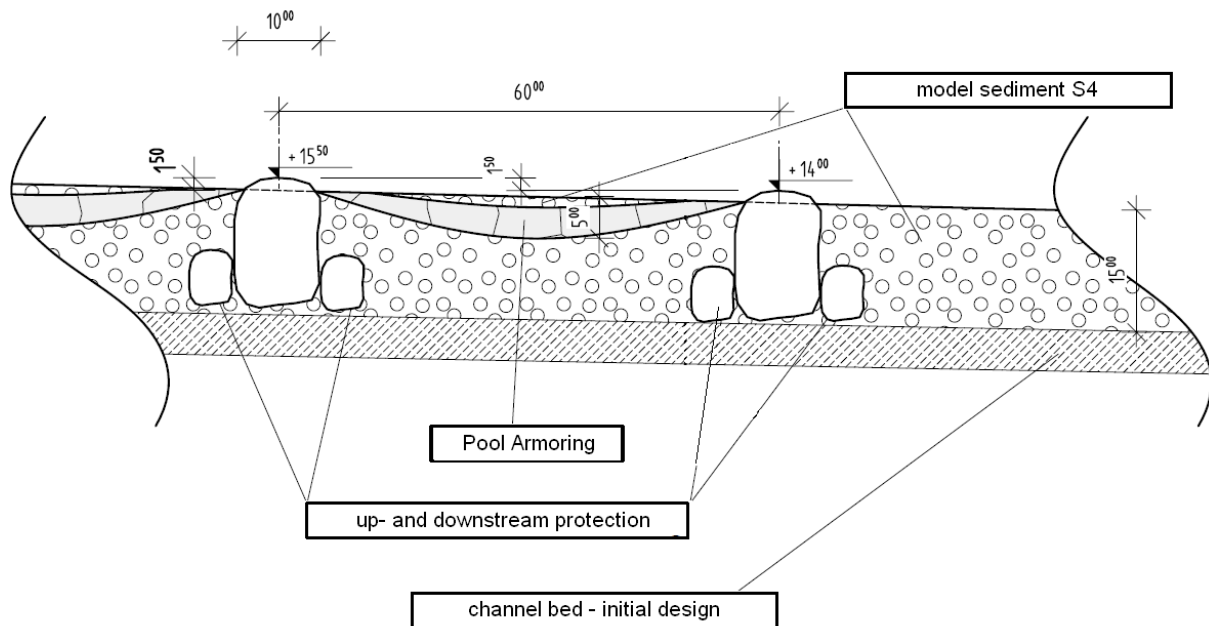


Figure 4.44 Pool armoring, longitudinal cut in the centerline (model scale, dimensions in cm)

To determine the diameter of the armor layer Terzaghi’s filter criterion 2-5 should be applied. Assuming a uniform boulder size d_a , Terzaghi’s criterion can be rewritten as:

$$4 \cdot d_{15,b} < d_a < 4 \cdot d_{85,b}$$

where $d_{15,b}$ and $d_{85,b}$ denote the characteristic diameters of the natural river sediment. Choosing the characteristic diameter $d_{90,b} = 140$ mm (Table 7.1) one can further conclude that the diameter of the armor layer must not exceed 560 mm.

$$d_a < 4 \cdot d_{85,b} < 4 \cdot d_{90,b} = 560 \text{ mm}$$

4.9.2 Final Design

The only difference between ramp design D9 and the final design is the armor layer of the first four pools of ramp 1. The plans for the final design can be found in appendix A.4.

Altogether 16 test runs were performed with the final design. The flap was not used in neither of these experiments.

Results Final Design - 100-Year Flood

The 100-year flood wave was simulated according to the specification in Figure 4.45. Unlike test runs 17 and 20 the bed load rate after Meyer-Peter Müller was calculated with a hydraulic radius that equals $0.9 \times$ water depth and a mead diameter d_m of 72 mm. This results in a higher bed load rate. All other parameters for the MPM-formula are summarized in (Table 4.12).

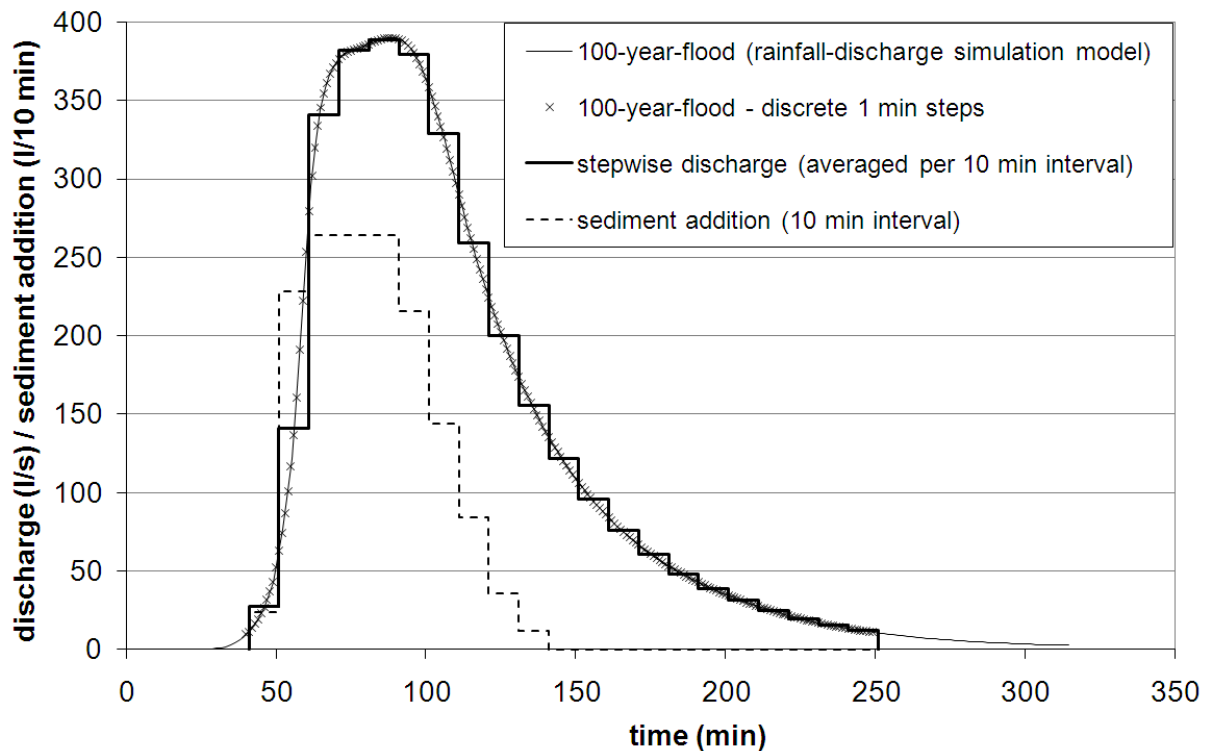


Figure 4.45 Final design, 100-year flood hydrograph, sediment addition (model scale)

After the 100-year flood wave the steps remained unchanged in position and height (Figure 4.47, initial bed levels: Figure 4.46). Some stones from the armor layer have been washed out and have deposited in the pools further downstream. In the slow-down pool sediments have deposited near the banks. The pools 4 and 5 of ramp 1 show the most severe erosions. The armor layer of pool 4 is still intact but the is 0.5 m below its original position before the test run. In the tailwater section the left channel bed is eroded up to 0.4 m maximum.

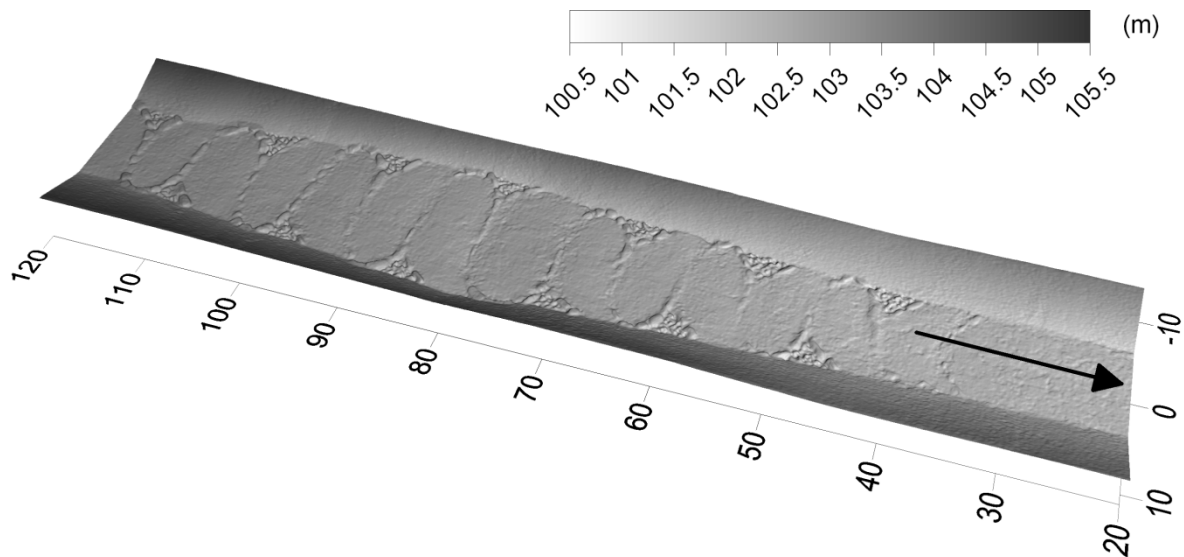


Figure 4.46 Final design, initial bed surface

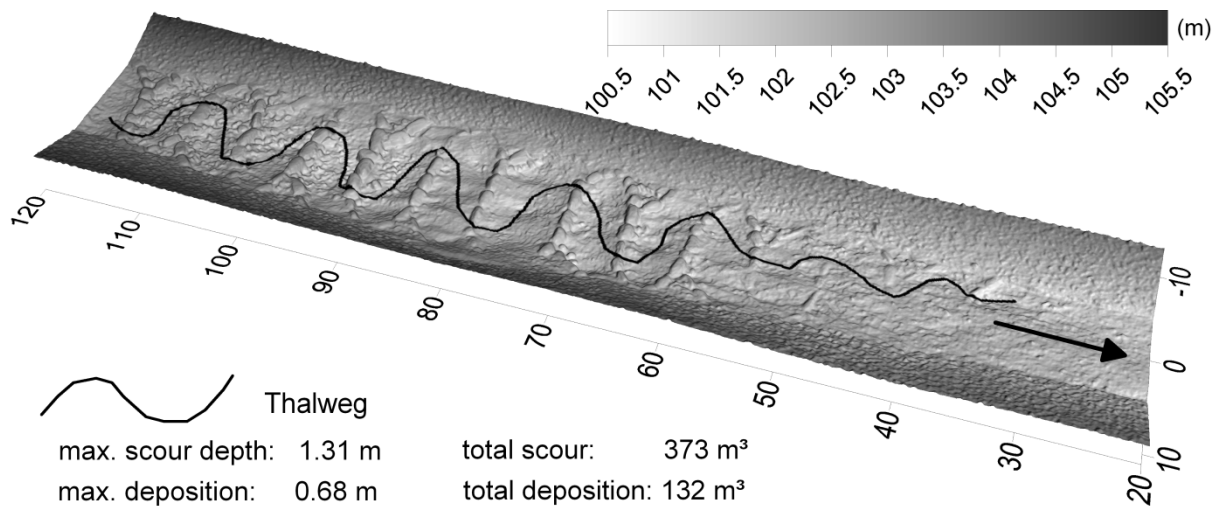


Figure 4.47 Final design, bed levels after the 100-year flood wave (test run 23)

The result of test run 23 is satisfactory with respect to the ramp stability.

- The armor layer of the first four pools of ramp 1 could resist the stresses of the 100-year flood wave
- The scour patterns of ramp 2 resemble those of the prototype ramp in the Stübmingbach: The maximum scour depth is located in the center of a pool. Until the next downstream step the bed constantly rises.
- No upstream scours have developed

Final Design – Stability of the Ramp

As the pool armoring proved to be an efficient means to guarantee the stability of the ramp it was decided in consultation with the external expert Dr. Hengl to carry out further stability tests based on the channel bed after the 100-year flood (test run 23, Figure 4.47).

For the stability of the ramp those discharges are decisive where the hydraulic jump in a pool moves towards the downstream bed thus producing upstream scours. This is the case for discharges of a return period of 10-15 years.

For this range of discharges an extensive series of stability tests was performed.

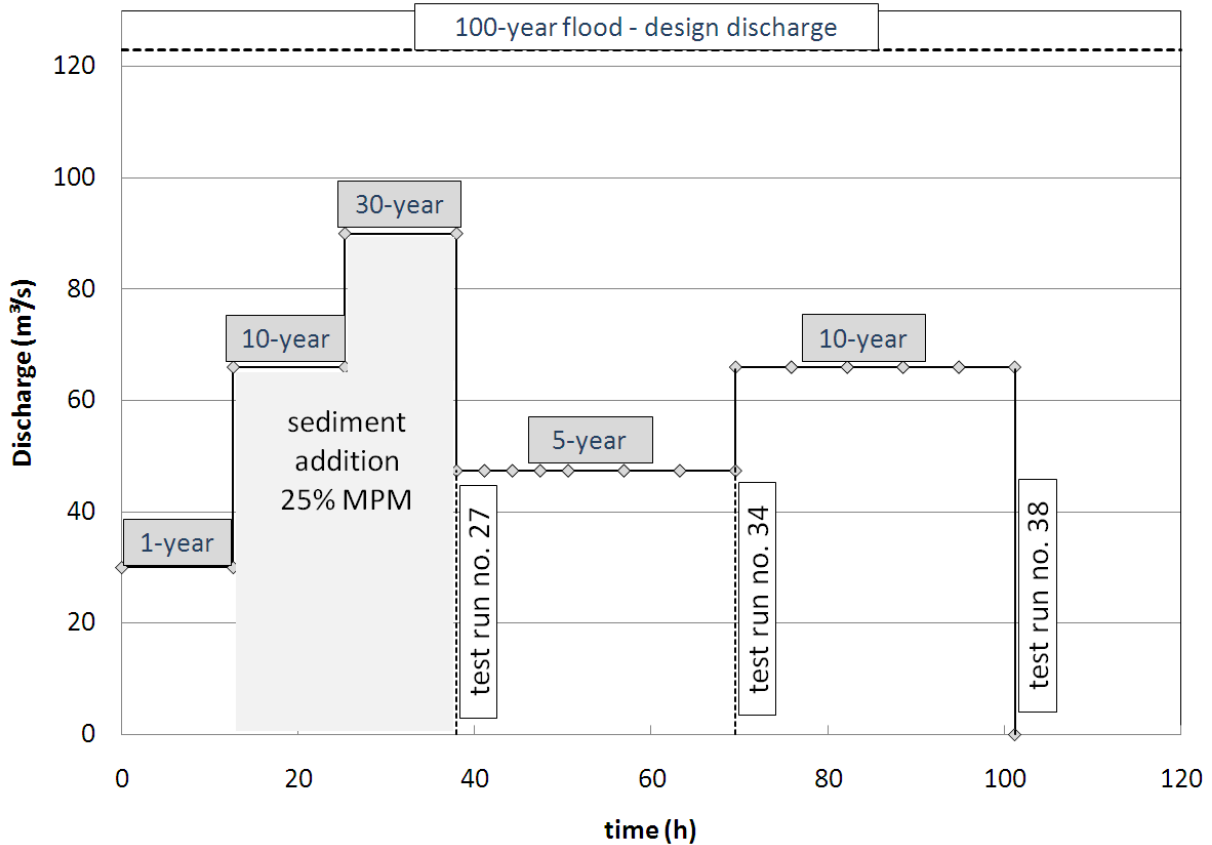


Figure 4.48 Final design, stability test series

During the stability tests the ramp was exposed to a flood discharge (HQ1-HQ30) for more than 100 h (full scale). The stability series were divided into 15 test runs (Number 24-38) which are shown in Figure 4.48 and are bounded by rhombuses. After each test run the channel bed was surveyed photogrammetrically. The initial bed of each test run was the eroded bed from the preceding test run.

Only test run 25 and 26 (Table 4.13) of the stability series was carried out with sediment addition. In the calculation of the bed load rate after Meyer-Peter-Müller the hydraulic radius R_s was $0,9 \times$ water depth and the mean diameter d_m was 72 mm. All other parameters for the MPM-formula are summarized in (Table 4.12). 25% of the calculated bed load rate was added during test run 25 and 26.

A complete documentation of the results of the stability test series can be found in the appendix A.2.

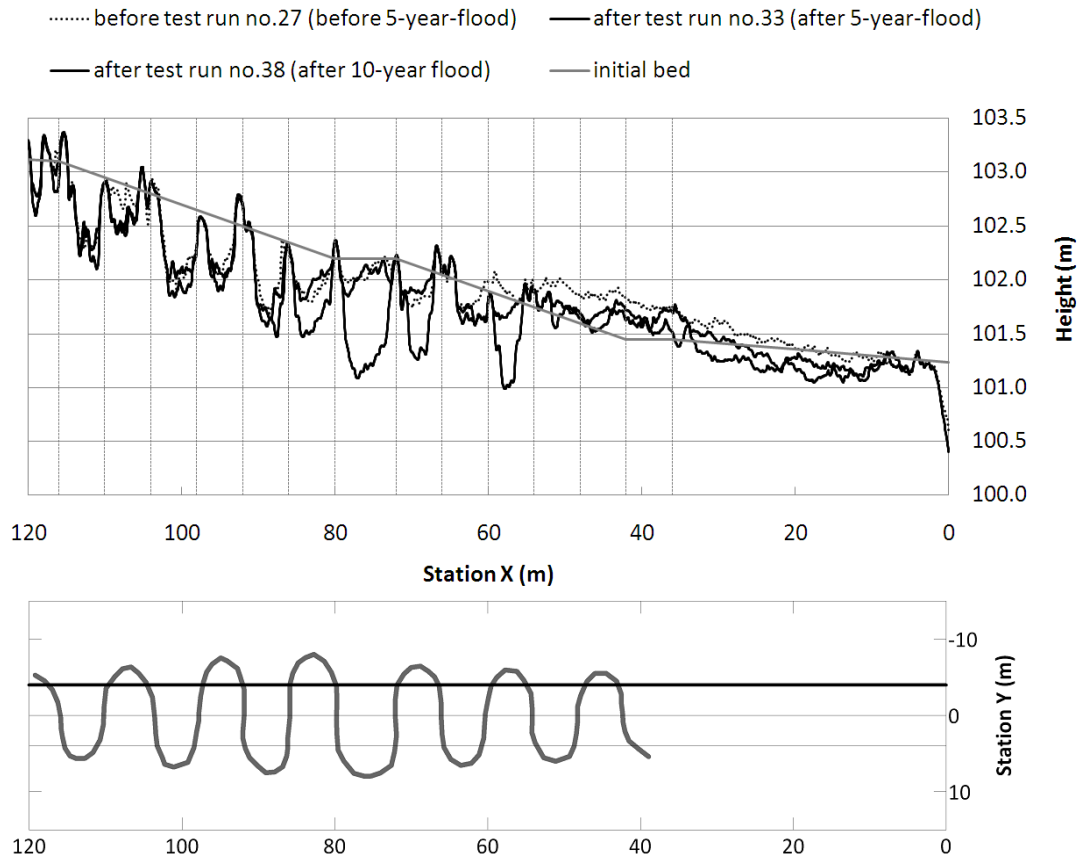


Figure 4.49 Stability test series, bed changes, longitudinal cut Y=-4

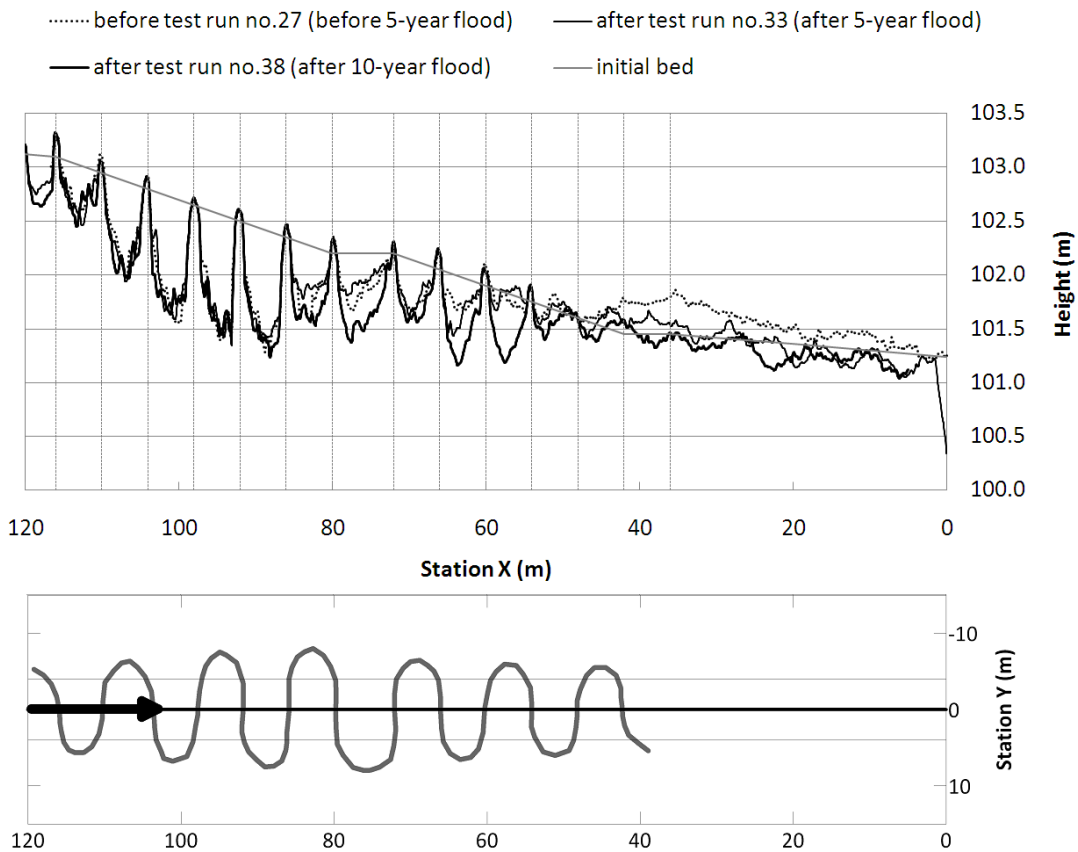


Figure 4.50 Stability test series, bed changes, longitudinal cut Y=0

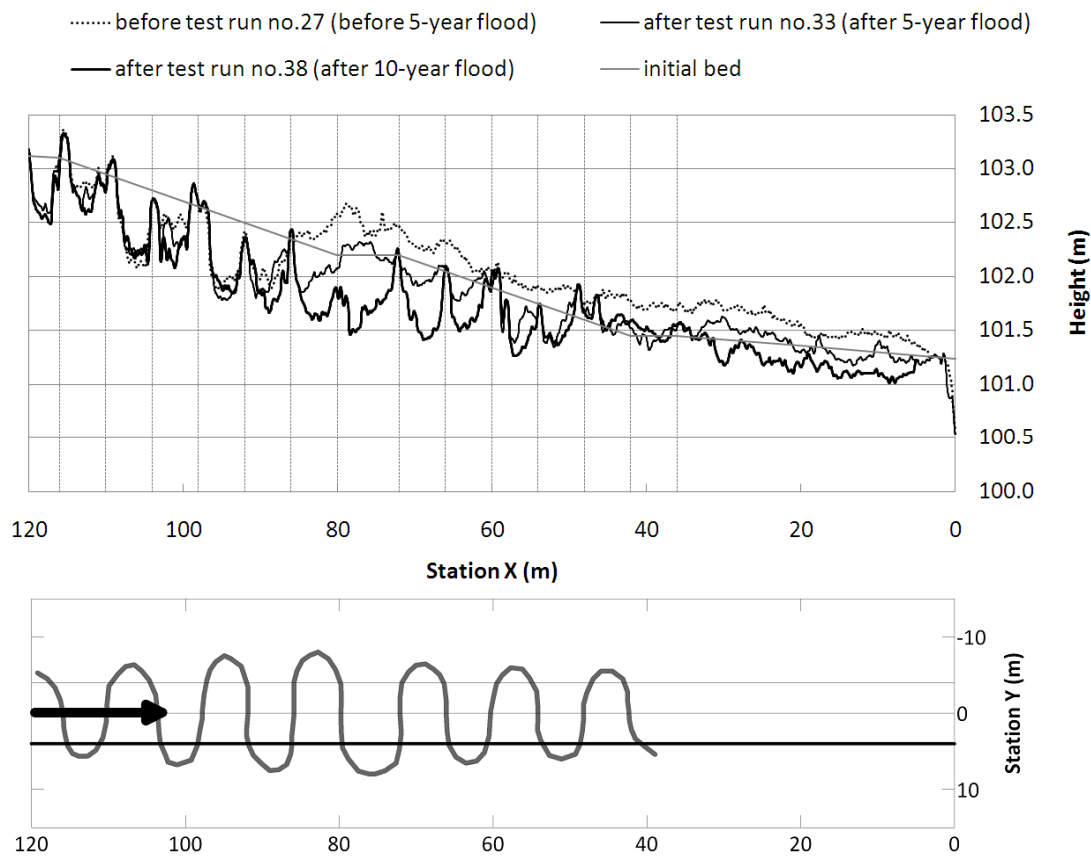


Figure 4.51 Stability test series, bed changes, longitudinal cut Y=+4

Figure 4.49 - Figure 4.51 show the bed changes during the stability tests. The bed levels of the first four pools of ramp 1 have changed scarcely at all. Despite the severe stress and without sediment addition a stable steady bed has developed. The non armored pools further downstream have eroded to different degrees. No upstream scours have developed but scour patterns that are optimal with respect to ecological and technical aspects. The pools 4 and 5 of ramp 2, which are the furthestmost downstream pools, are prevented from scouring due to backwater effects from the tailwater section. The depositions on the right side of the slow-down pool and those in the tailwater section have degraded during the stability tests.

During the test series some stones of the armor layer of the first four pools of ramp 1 were washed out. and partly have deposited in the pools below or in the tailwater section. This is a pleasant side effect that had not been considered before.

4.9.3 Construction Costs of the Meandering Ramp Große Tulln in Neulengbach

Final Design: Stone masses for the Model Ramp

For the estimation of the required stones masses for the final design in the model a sample of 17 stones that build the steps of the ramp were weighed. The three axes of each stone was measured. A step stone has an average mass of 3.61 kg (model scale, Table 4.15). The band width is 2.06 bis 5.45 kg in the model and 2.06 bis 5.45 t transformed to full scale.

Step stone sample	<i>a</i> (cm)	<i>b</i> (cm)	<i>c</i> (cm)	Mass (kg)
1	16	14	10	4.12
2	21	14	11	4.17
3	26	5	11	5.46
4	25	12	13	5.19
5	18	11	8	3.25
6	24	13	11	5.24
7	15	13	10	2.67
8	27	12	13	5.08
9	12	14	11	3.83
10	18	13	12	3.72
11	16	14	9	2.37
12	12	15	10	3.13
13	16	11	8	2.06
14	14	13	10	2.43
15	16	17	10	3.48
16	11	14	11	3.05
17	14	12	9	2.19
Average	17.7	12.3	10.4	3.61

Table 4.15 Measures of the step stone sample, model scale

The 17 stones placed next to each other have a total length of 3.1 m. This gives a standard value of the stone mass per (step) meter of 19.8 kg. The model meandering ramp consists of 27.2 step meters. This results in a total stone mass for the step stones of 539 kg (model scale).

Step	Total length (m)	Estimated mass (kg)
Main step	20.9	414
Reinforcement	5.1	101
Leveled step	1.2	24
Sum	27.2	539

Table 4.16 Lengths of the steps and stones masses

The required stone mass for the scour protection was calculated as follows: The scour protection up- and downstream of each step consists of the casted concrete stones of ramp design D8. They have a mass of 0.6 kg each. The meandering ramp consists of 131 step stones (including reinforcement and leveled step). There are as much up- resp. downstream scour protection stones, i.e. a total of 262 scour protection stones.

This results in a stone mass for the scour protection of 158 kg (model scale).

The first four pools of ramp 1 and the reinforced triangles (bank – step – reinforcement) were armored with stones of size $a \times b \cong 2.5 \text{ cm} \times 5 \text{ cm}$. A single-layer sample of these stones had a stone mass of 58.4 kg/m^2 . In the model ramp altogether 2.8 m^2 need armoring. This results in a stone mass for the pool armor and the reinforced triangles of about 164 kg (model scale).

In the model the toe of the ramp was fixed and did not need to be protected.

For the final design of the meandering ramp in the model stone masses of altogether 861 kg were needed.

Stone Masses for the Prototype Ramp in Neulengbach

The engineer Otmar Grober recommends to protect the bank toe along the whole ramp.

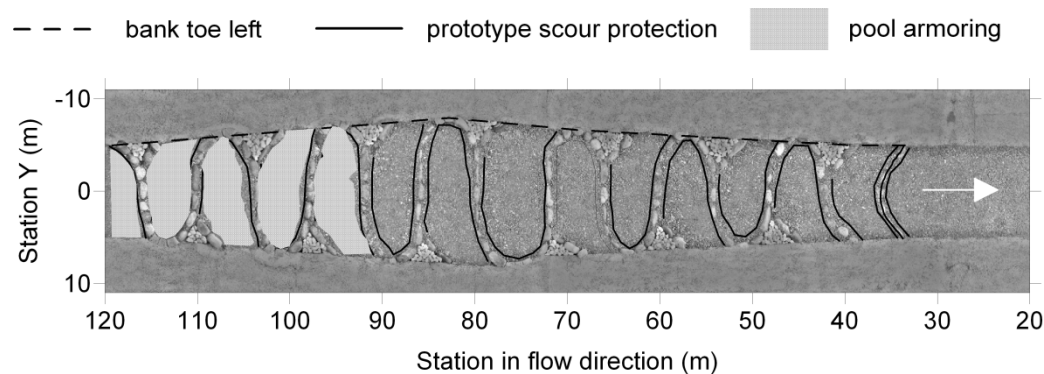


Figure 4.52 Prototype Ramp: Reinforced areas

The boulders for the steps, the reinforcement, the leveled step and for the bank toe protection should have dimensions of $a \times b \times c \cong 2 \times 1.2 \times 1.7 \text{ m}^3$.

Required boulders	Total length (rm ⁺)	Volume (m ³)
Main step	221	451
Reinforcement	51	104
Bank toe left	86	175
Bank toe right	86	175
<i>Total</i>	<i>444</i>	<i>905</i>

⁺ running meter

Table 4.17 Steps: lengths and volume, full scale

In the area of the reinforcement the scour protection can be omitted. The boulder connecting the reinforcement with the bank should be braced with an additional boulder. The dimensions of a scour protection stones should be $1 \times 1 \times 1 \text{ m}^3$. The total length of the scour protection is 324 rm (Figure 4.52). As a boulder is about 2 m long altogether 162 scour protection boulder are required. Additionally 13 boulder for the bracing of the reinforcement is needed. Thus the scour protection requires a total of 150 m³.

Scour protection	Number of boulders	Volume (m ³)
Up- and downstream	162	162
Bracing reinforcement	13	13
<i>Total</i>	<i>175</i>	<i>175</i>

Table 4.18 Scour protection: number of boulders and volume, full scale

The pool armoring of the first four pools of ramp 1 and the filling of the reinforcement triangles (bank – step – reinforcement) cover an area of 280.6 m². This area should be filled with coarse gravel 250 – 500 mm with a height of 0.5 m. This results in a volume of about 140 m³.

Pool armoring	Area (m ²)	Volume (m ³)
Pools 1 – 4 of ramp 1	241.6	120.8
Reinforcements triangles	39	19.5
<i>Total</i>	<i>280.6</i>	<i>140.3</i>

Table 4.19 Pool armoring: areas and volume, full scale

Items According to the Description Service „River Engineering“

According the description service "river engineering" of the Austrian Federal Ministry of Agriculture, Forestry, Environment and Water Management (Leistungsbeschreibung für den Flussbau. 2003) the following items are necessary for the construction of the ramp. The required stone masses in tons are roughly estimated by volume x 2:

Item		
2.210 Excavation ⁺		1221 m ³
3.103b Stone supply filling		282 t
3.103c boulders	dimensions 2 × 1.2 × 1.7 m ³	1810 t
3.103c boulders	dimensions 1 × 1 × 1 m ³	350 t
3.203 Filling*	Installation height: 0.5 m diameter: $d = 0.25 - 0.5$ m	141 m ³
3.212 Bruchsteinschichtung		1080 m ³
⁺ depends on the local conditions [*] dumped rockfill		

Table 4.20 Items of the description service "river engineering"

4.10 Recommendations

In the physical model test the upper bank edge was fixed because of space restrictions in the vicinity of the Große Tulln river in Neulengbach. In the area of the channel widening the banks thus become steeper. If the field conditions allow it the original bank slope should be kept in channel widening sections.

The experiments have shown that the pools of ramp 1 are exposed to particular strain. Due to channel widening and channel narrowing along the ramp normal flow conditions did not develop. Therefore more investigations are required to check if the above observation is also valid for a meandering ramp with a constant cross sectional profile.

The armoring of the first pools has proven to be a suitable means to ensure the stability of the ramp. If resp. how many pools need armoring in general depends, inter alia, on the ratio bed slope reference/ramp slope.

As the slow-down pool eroded severely during the stability test series it serves a hydraulic purpose. Moreover the slow-down pool also has an ecological profit as it provides a rest area particularly for the weak-swimming fish. It is therefore recommendable.

A scour protection up- and downstream of the main step is recommended. It is not advisable to disclaim the upstream scour protection in favor of heavier boulders for the main step. The upstream scour protection also serves the purpose to direct the strong current in severely eroded pools upwards instead of directly into the main step.

It is advisable to further investigate the scour development subject to ramp slope, step height, bed material and discharge including investigations of potential scale effects.

4.11 Conclusions

The final design of the meandering ramp consists of step-pool units with a step spacing of 6 m and a vertical distance between two steps of 0.15 m (slope $I = 1:40$). After the first six step-pool units a slow-down pool is arranged. Five further step-pool units are following. The main steps are S-shaped and protrude from the bed 0.3 m maximum. The lowest point of a step is aligned with the bed. The steps alternate inclined to the left and right bank, respectively. In the area of the first six step-pool units the channel widens from 10 m to 16 m, the top bank edge remains unchanged because of restricted space. This way the bank slope steepens. The ramp is 72 m long and overcomes a height of 1.65 m. A leveled step completes the structure.

The first four pools have a trough-shaped armor layer consisting of stones of size 0.25 – 0.5 m and an installation height of 0.5 m. The small stone diameters have the desired effect that during flood events parts of the armor layer are washed out and deposit further downstream. There these stones stabilize the bed like an armor layer with a sparse coverage.

The bank protection rip rap should be oriented on the original bank protection. It should be about 1.5 m high. Following the bank protection the planting of limber trees and bushes adapted to the location should, e.g. hazelnut, snowball bush, elder, is recommended. For the upper third of the banks the planting of tall trees adapted to the location should guarantee sufficient shadowing (e.g. alder, elm). One has to take care that the planting of the trees does not affect the flood discharge negatively.

The recommended volume and stone masses include a safety factor of 2 compared to the required masses in the model. On one hand the safety factor contains the bank toe protection along the ramp which was not necessary in the model because of fixed banks. On the other hand it is based on practical experience of the engineer Otmar Grober. The safety factor further includes variations in the particle size distribution and the total bed load during flood events. Bed load transport discontinuities need to be balanced with increased armoring.

Comparing the used model sediment to the grain size distribution of the Große Tulln samples, it shows that the model sediment misses the fine grain sizes. Nonetheless the stability of the ramp is proven only for the coarser model sediment. Before the construction of the ramp it is recommended to take representative sediment samples.

During the installation of the ramp the boulders of the step should be positioned by means of a theodolite or a GPS. The craftsman should be trained accordingly.

After the installation of the ramp monitorings are recommended to survey the scours that have been developed after flood events.

5 Basic Flume Test for Step-Pool Ramps

5.1 Introduction

This flume test was carried out in the laboratory of the Institute of Hydraulic Engineering and Water Resources Management of the University of Technology Graz, Austria.

5.1.1 Purpose and Scope of Investigation

The physical model test for the meandering ramp (chapter 1, pp.73) has shown that the flow transition from tumbling flow to rapid flow is critical for the stability of the ramp as upstream scours may develop that may in turn cause the destruction of the step. Besides the energy dissipation is better in the tumbling flow regime than in the rapid flow regime. Thus it is desirable to know the transitional discharge from tumbling flow to rapid flow. Such a criterion has been found by Morris (1968) for highway drainage chutes (with slopes ranging from 5 to 30 %). The question is whether it is applicable for the milder sloped step pool ramps. The meandering ramp imposes complex three dimensional flow patterns which are also reflected in the scour patterns (Figure 4.47). It is assumed that 3-dimensional energy dissipating processes are more effective than their 2-dimensional counterparts. The scale of the flume test is the same as for the model test of the meandering ramp, namely 1:10.

The flume test pursues four aims:

1. Find a functional relationship for the transitional discharge from tumbling flow to rapid flow q subject to the step height K , the ramp slope $I = \tan \alpha$ and the step spacing L : $q_{crit} = f(K, L, I)$

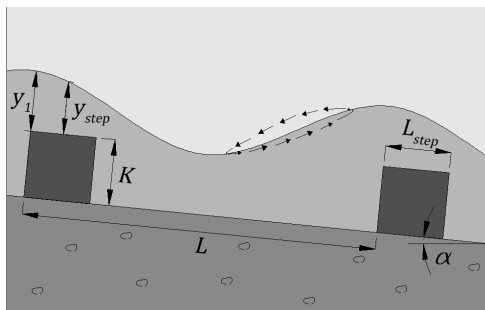


Figure 5.1 Design parameter

2. Check Morris' criterion for the transitional flow (see equation 3-100): $q_{crit} = K^{3/2} \cdot (3 - 3.7 \cdot I) \sqrt{g}$
3. Check assumption: laterally inclined steps dissipate less energy than horizontal steps
4. Determine the pressure distribution around a roughness element for different flow regimes

The experiments are performed with a fixed bed. Therefore they will not provide information about scouring processes. Ramp slopes range from $I = 2.5\%$ to $I = 6.5\%$. The lower limit is chosen to provide comparability to the model test of the meandering ramp. The upper slope limit is chosen close to the limiting slope for mildly sloped ramps according to the German standard DIN 19661-2 (2000): herein mildly sloped ramps (so-called "Sohlengleiten") that ensure continuity for aquatic life are distinguished from steep ramps ("Sohlenrampen"). The limiting slope is 1:15. For convenience, the two limiting ramp slopes will be referred to in the text as "mild slope" and "steep slope".

5.2 Experimental Setup

Apart from minor changes the description of the experimental setup has been adopted from the diploma thesis of Gomerski (2010).

5.2.1 Flume and Ramp Construction

Wide Test Flume

The experimental study was carried out in a rectangular horizontal flume which is a steel framed bolted construction. It has a 2.5 m long inlet section with flow straighteners and a 10 m long experimental area. The outlet section consists of a tail gate and a vertical drop to the laboratory's return system. The flume has a width of 76 cm and a height of 93 cm (Figure 5.2). The walls of the left hand side of the flume consist of 2 m steel sheets and one 2 m long glass window (the second last), the walls of the right hand side of the flume consist of 2 m long glass windows.

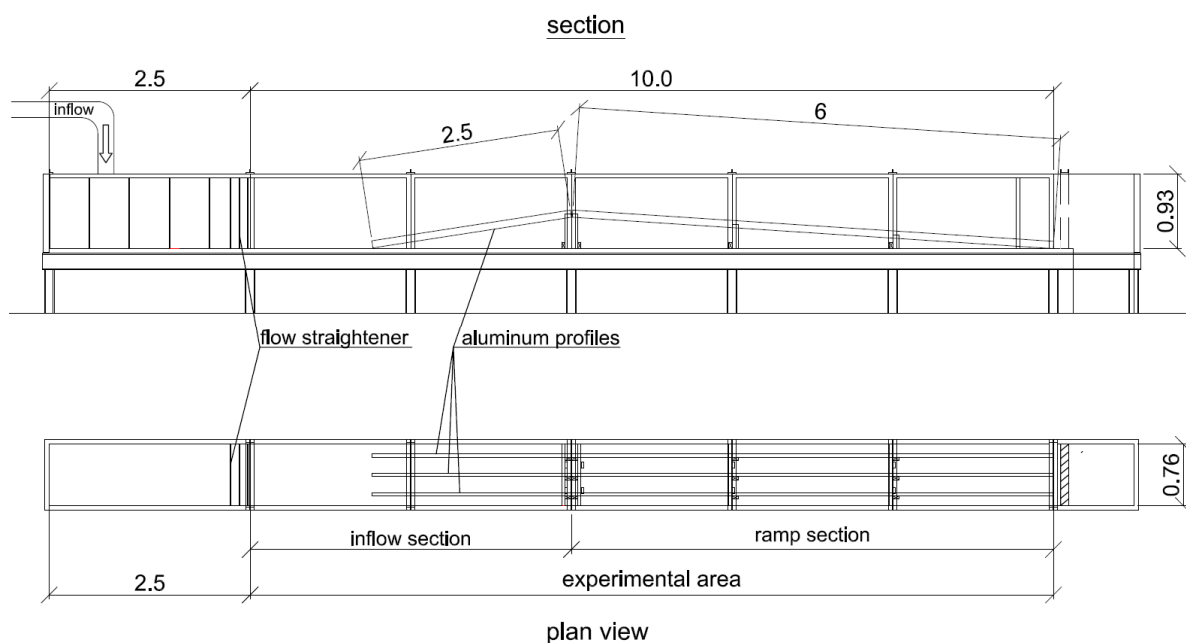


Figure 5.2 Section (top) and plan view (bottom) of the flume, dimensions in (m)

The water supply of the laboratory consists of one elevated head tank with a capacity of 70 m³, a piping system and a central pump station with four simultaneous units with a pumping capacity up to 1000 l/s. For the flume test a supply pipe (DN250) extends vertically into the inlet section such that the pipe is being submerged when the flume is in operation. The water enters the flume at very high velocities. For the maximum discharge of 240 l/s during the experiments the velocity of the inflow pipe is 4.89 m/s. The inlet section had to be equipped with spray shielding panels on top of the flume. The high velocity flow jet generates waves and strong secondary currents. To secure a uniform flow distribution three sheets of flow straighteners were installed at the downstream end of the inlet section covering a length of 1.05 m. (Figure 5.3).

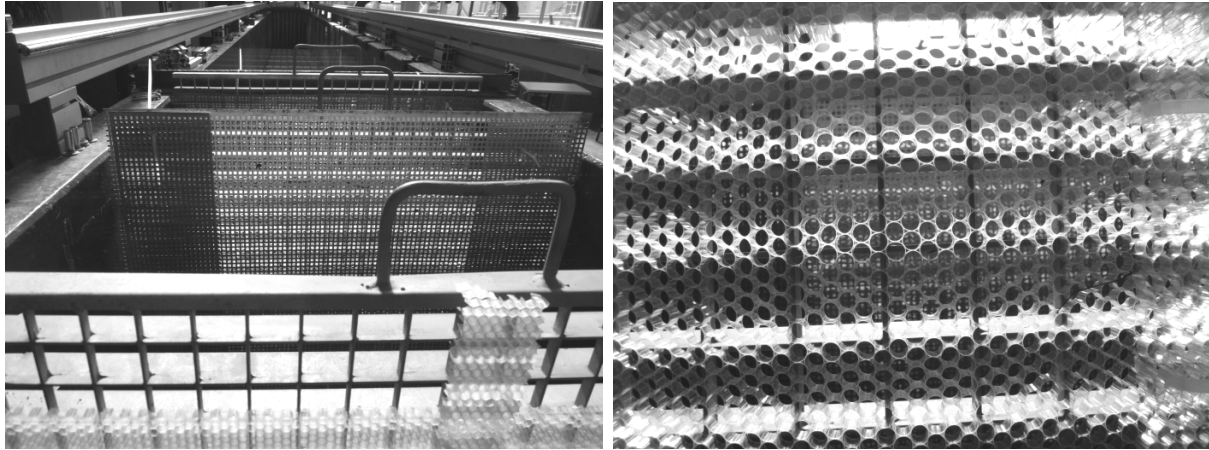


Figure 5.3 Flow straightener: steel grates and perforated sheet (left), plastic honeycombs (right)

A flow straightener consists of a steel grid (4 cm thick, outer diameter 4 cm) to which a sheet of plastic honeycombs (7 mm thick, cell diameter: 6.5 mm) is attached. The two downstream flow straighteners additionally consist of two perforated sheets on either side of the flume to get rid of the secondary flow (Figure 5.3, left). At the downstream flow straightener a floating body made of polystyrene is mounted to eliminate the surface waves.

A tail gate consisting of vertical lamellae that can be opened and closed manually provide a convenient way to control the profile of the water surface in the flume. Behind the tail gate a vertical drop is situated. There the water plunges into the return system of the laboratory which passes approximately 2 m below the flume bottom.

As the flume bottom is horizontal and cannot be tilted the desired slope of the ramp had to be constructed appropriately (chapter *Ramp Frame*, pp. 124). The experimental area consists of a 4 m long inflow section and a 6 m long ramp section. (Figure 5.2) The adversely sloped inflow section serves to continuously raise the bed to the level of the ramp crest. A sudden leap would have produced undesired vortices and secondary currents. It was decided to forgo a flatter tailwater section downstream of the ramp. This provides a longer ramp area on one hand. On the other hand, as the results of the model test of the meandering ramp for the Große Tulln river had confirmed, the tailwater level has a significant influence on flow and erosion processes along the ramp. Omitting the tailwater section is synonymous with assuming the worst case scenario with respect to stability demands of a ramp as no backwater effects from a potential flatter tailwater section reduce the velocities along the ramp.

During the preliminary experiments it turned out that the lamellae generate slight backwater effects even when fully opened. These effects reach at maximum to the second step of the step-pool ramp (counted from the downstream end). In this area no velocity measurements were performed. When completely closed the lamellae served the purpose to fill the flume with water to eliminate air (bubbles) from the experimental area which were located at the rear side of the ramp sheets.

Narrow Test Flume

Additional experiments were performed in a 12 m long, 20 cm wide an 50 cm high tilting flume which is described in detail in chapter 5.4.10, pp.161.

Ramp Frame

The ramp was constructed such that it allows for easy adjustments of different slopes and step spacings at low material costs and in little time. The ramp frame consists of three parallel longitudinal profiles made of aluminum that form the ramp slope and the adverse slope of the inflow section (Figure 5.2, Figure 5.4). The profiles are mounted to vertical columns of appropriate height which in turn are bolted down to the flume bottom. Plastic plates are mounted onto the profiles by means of slot nuts. The plates serve as the inclined channel bottom (chapter Roughness Element for Pressure Measurements, pp. 127). Wooden roughness elements that are bolted to the plates form the steps of the step-pool ramp (chapter *Roughness Elements*, 125).



Figure 5.4 Ramp frame constructed from aluminum profiles

The aluminum profiles have a cross section of size 8×4 cm with two resp. one longitudinal slot(s) on the longer resp. smaller sides. The ramp area and the inflow area consist of three 6 m and 2.5 m long profiles, respectively. Each ramp area profile is mounted to three vertical columns of appropriate height and to an angle bracket that is welded to the flume bottom at the downstream end of the flume. Each inflow profile is mounted to an angle bracket on the flume bottom and one vertical column (Figure 5.4).

During the experiments the whole ramp frame is submerged even at the rear side of the plastic plates. This water cushion below eliminates the weight forces acting on the plastic plates and the ramp frame. At the toe of the ramp a detachable vertical steel sheet prevents the water cushion below the ramp bottom from flowing out of the flume. After the preliminary tests (chapter 5.3.1, pp. 139) a plastic sheet was mounted to the steel sheet. The plastic sheet protrudes from the ramp bottom by the height of the roughness elements. This sheet serves to eliminate the drop-down curve caused by the vertical drop.



Figure 5.5 Elements comprising the ramp construction (side view): longitudinal profile, vertical column, roughness elements, panels with gravel, rubber seal

Roughness Elements

The roughness elements represent the boulders of a step. Each step in the flume experiments consists of 7 roughness elements (Figure 5.7). They are made of pine wood. Each roughness element has a base area of 100×100 mm. The top area is inclined at an angle of 3.58 deg with the smaller vertical side being the upstream face. The vertical edges are rounded with a corner radius of 5 mm. The rounded edges of the top area have a radius of 10 mm (Figure 5.6).

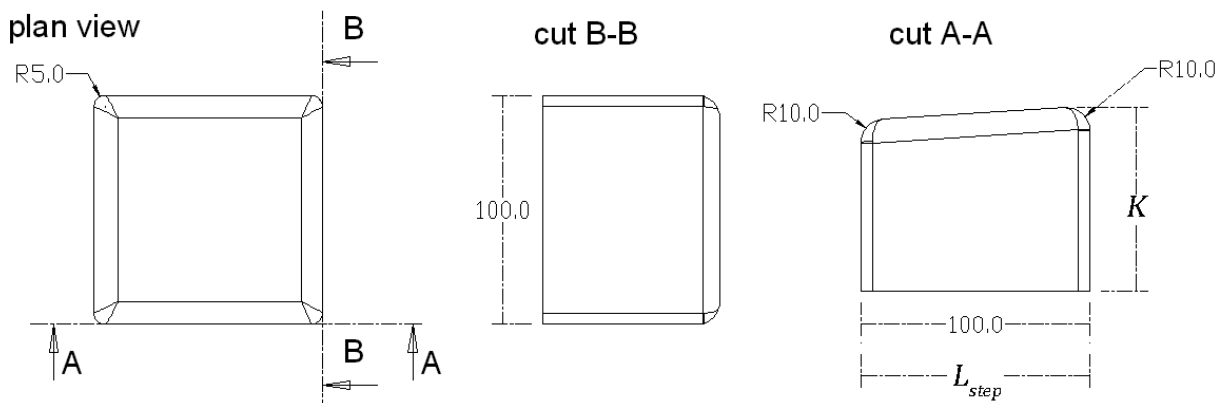


Figure 5.6 Roughness element: dimensions (mm)

Experiments were performed for both horizontal steps, i.e. the roughness elements are horizontally aligned, and laterally inclined steps. It was one aim to check whether inclined steps provide a better energy dissipation than the horizontal steps. To make these two step designs comparable the inclined step must have the same mean height as the horizontal step. For the horizontal steps two heights were investigated: 75 mm and 95 mm (measured at the higher downstream face). For the 95 mm height an inclined step was designed with 4 different heights (Figure 5.7). To distinguish the different roughness elements during the experiments, on the photos and on the videos they were colored according to their height. A boat varnish was used which also served to reduce the water

absorption of the wooden elements. In the course of the experiments however, some elements have developed small cracks due to swelling. This caused a dimensional change up to 1 mm in height and longitudinal direction.

A set of 70 roughness elements was made for both the blue (75 mm high) and the yellow (95 mm) elements. This way 10 steps consisting of 7 elements each can be built. For an inclined step of the meandering ramp 4 different heights are necessary: 80 mm, 90 mm, 95 mm and 100 cm (4 times). The meandering ramp was investigated for maximum 9 steps, resulting in the required number of elements summarized in Table 5.1.

Height (mm)	100	95	90	80	75
Color	red	yellow	grey	green	blue
Number	36	70	9	9	70

Table 5.1 Color, height and number of roughness elements

The elements were either mounted to smooth or to rough panels (see Roughness Element for Pressure Measurements, pp. 127). For the rough panels the effective height of the elements is reduced by the thickness of the roughness layer of the panel, i.e. 15 mm. The step height K corresponds to this effective element height.

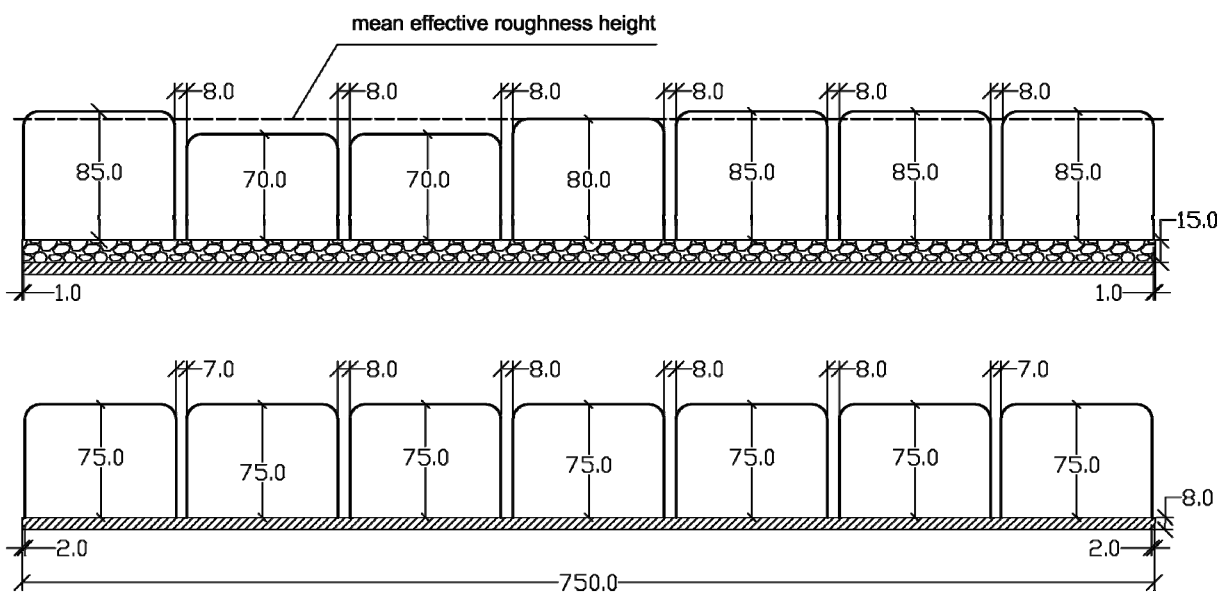


Figure 5.7 Step cross section of the meandering ramp on a gravel panel, effective element height (top), step cross section of a horizontal step on a smooth panel (bottom), dimensions in (mm)

Legend:

The gravel panel cross section corresponds to cut D-D of Figure 5.10

The smooth panel cross section corresponds to cut C-C of Figure 5.10

The roughness elements allow for three different step variants:

- 75 mm height
- 95 mm height
- 95 mm mean height (inclined)

Roughness Element for Pressure Measurements

For the pressure measurements on the surface of a roughness element a specially designed roughness element was fabricated from an aluminum square tube 100 x 100 mm with a thickness of 4 mm. On top of the tube a 12 mm thick aluminum plate was welded. A CNC-milling cutter accomplished the exact geometry of the roughness element. The geometry equals that of the yellow wooden counterpart (Figure 5.6, Table 5.1). Altogether 149 bore holes were drilled into which the pressure transducers were mounted from the inside of the roughness element (Figure 5.8). At the bottom of the roughness element a forked adapter is located which is screw on the plastic panel. The plane surfaces of the roughness element were sealed by means of an adhesive foil (~ 0.1 mm). For those bore holes which carried the pressure transducers the foil was punched out. This way the transducers had a direct contact to the flowing water (Geiger 2010).

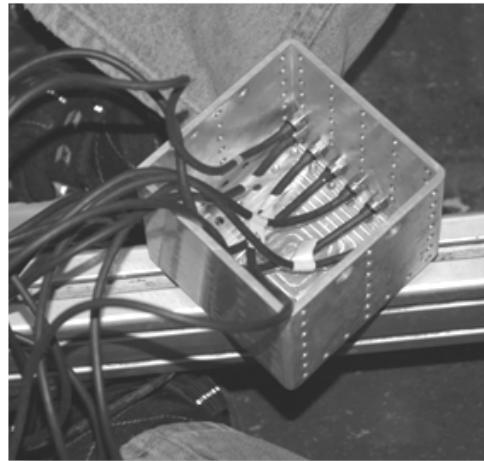
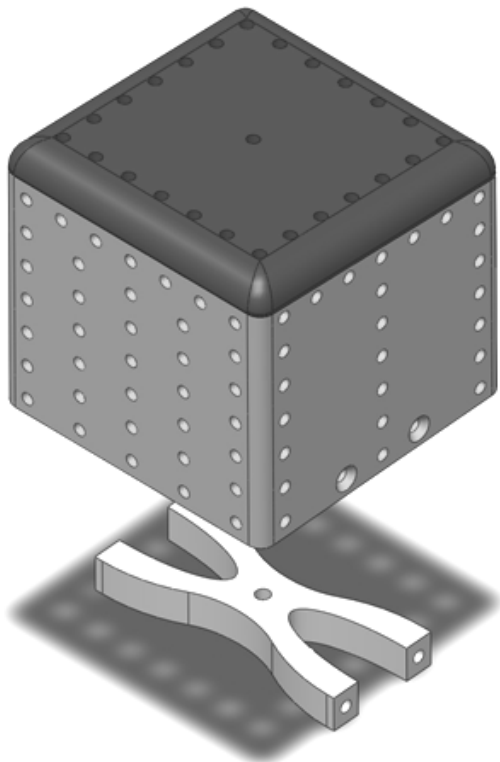


Figure 5.8 Roughness element for pressure measurements: sketch (left), original upside-down with mounted pressure transducers (right), Geiger (2010)

Panels

Plastic panels that are mounted to the ramp frame form the channel bottom of the experimental area. A modular design allowed for the variation of the step spacing with little material costs. The plastic panels are 8 mm thick and have a width of 75 cm, i.e. they are 1 cm shorter than the flume width. This way the panels could be assembled without being tilted. Between the panels and the flume walls a rubber seal was mounted to close the gaps and to balance variations of the flume width (Figure 5.5). Each panel has 3 to 7 bore holes each one above the longitudinal slot of a profile. Screws fix the panels to the profiles via the slot nuts.

Two sets of panels were cut: a “smooth panel set” and a “gravel panel set”. The smooth panel set uses the surface of the panels as a smooth bed, while rounded gravel of size 8-16 mm was glued to the gravel panel set to simulate a rough bed. For both sets there are so called “step panels” and

“pool panels” (Figure 5.9). The mean bed level is assumed to be located 15 mm above the panel. The panels of different roughness served to investigate whether the roughness of the pool had an influence on the flow transition from tumbling to rapid flow (chapters 5.4.5 and 5.4.8). Figure 5.7 illustrates cross sections of a gravel panel and a smooth panel, respectively.



Figure 5.9 step panel without roughness elements (left), pool panel (middle) and smooth panel (right)

On each step panel 7 roughness elements are mounted to the rear side of the panel by means of countersunk screws. The remaining part of the panel serves as pool part. Except for the furthest downstream step panel all other step panels have the same length. The pool panels are of varying length (Table 5.2).

Panels	Step panel downstream	Step panels (all others)	Pool Panels		
Length (mm)	400	467	155	233	333
Width (mm)	750	750	750	750	750
Color	Cyan	Red	Green	Yellow	Blue
Code	1	5	2	3	4

Table 5.2 Panel set, dimensions (mm)

The reason why the step panels consist also of a pool area is because the bore holes are easier accessible within the pool area. The pool panels only serve the variation of the step spacing. Three different pool panel lengths result in four different step spacings as the pool panels of length 233 mm are either used once or twice within just one pool (Figure 5.10).

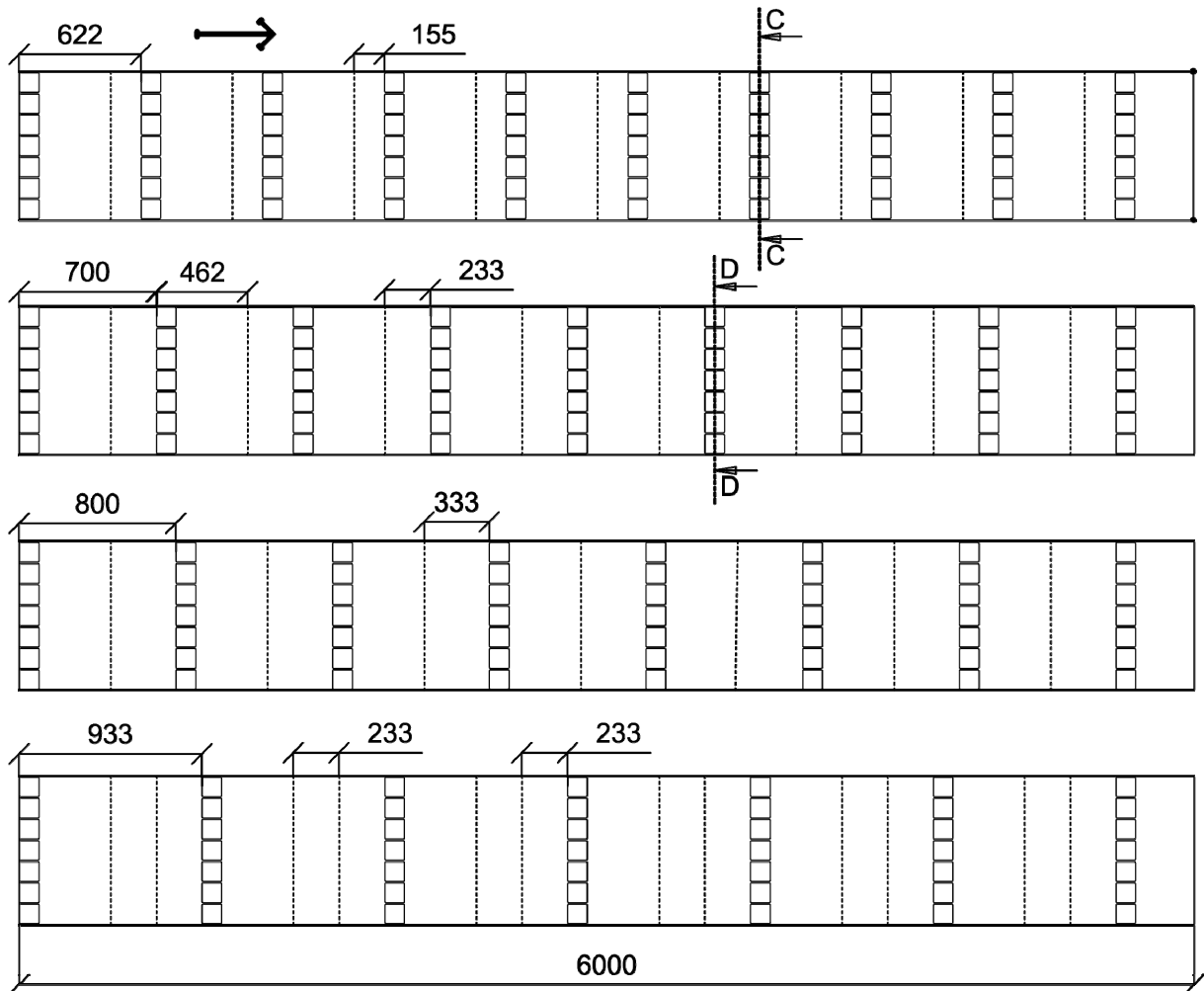


Figure 5.10 Overview of four ramp configurations resulting from three different pool panels

Legend:

Cut C-C: cross section of a horizontal step on a smooth panel (Figure 5.7, bottom)

Cut D-D: cross section of a step of the meandering ramp on a gravel panel (Figure 5.7, top)

For the rough panel the 7 elements of a step are mounted at a distance of 8 mm which leaves 1 mm between the side edges of the panel and the left and the right outer element, respectively (Figure 5.7). This outer distance proved too short to install the rubber seal appropriately. For the smooth plates, which were made later, the distance of the two outermost elements was reduced to 7 mm, so the outer distance became 2 mm (Figure 5.7, bottom).

For one set of roughness elements four different step spacings and two bed roughness types can be chosen resulting in altogether 8 configurations (Figure 5.10). As there are 3 different set of roughness elements altogether 24 configurations can be tested for a fixed ramp slope.

5.2.2 Measuring Equipment and Methods

Water Level Measurements with Ultrasonic Probes

For the water level measurements ultrasonic probes were used. Two types of probes were available at the laboratory: three probes of the brand Honeywell and four probes of the brand Microsonic (Table 5.3). As the probes were mounted to the horizontal positioning system of the flume which could not be tilted, it had to be checked whether the ultrasonic probes were able to measure inclined

water surfaces correctly. Preliminary tests in the flume with a weir overfall showed that the probes failed to yield measurement values for water surface slopes exceeding 20 degrees. An additional probe of the company Siemens was borrowed and tested but failed to yield improved results.

Producer	Type	Number	Distance range (mm)
Honeywell	947-F4V-2D-1C0-300E	3	100 - 600
Microsonic	Mic+25/IU/TC	4	50 - 350
Siemens	Sonar Bero 3RG6233-3LS00	1	150 - 1000

Table 5.3 Ultrasonic probes

The sensors work with an ultrasonic transducer used for both transmitting and receiving. In each cycle, ultrasonic pulses are transmitted. The pulses are then reflected back from the target, and received by the sensor. By means of the temperature compensated measurement of the elapsed time of the acoustic signal, the target distance is determined. The resulting measurement output is analogue.

The sensors were calibrated by mounting the probe to the vertical axis of the positioning system of the flume (chapter 5.2.3). Below the probe a box filled with water was placed. The distance from the probe to the horizontal water level was measured with a measuring tape. Then the vertical axis with the probe was shifted upwards stepwise by 50 mm. This way, at each step, the distance to the water level was known. The distance was then measured with the ultrasonic probe. These measurements were used to find the linear equation that transforms the analogue output signal (voltage) to the desired distance. After that the accuracy of each probe was tested in the physical model of the meandering ramp of the Große Tulln river (chapter 1), where tumbling flow conditions were established to test different water surface inclinations. The results of the ultrasonic measurements were compared to measurements performed with a hook gauge and a level at the same positions. It turned out that the Honeywell sensor had the smallest mean deviations from the hook gauge measurements, followed by the Siemens probe and the Microsonic probe (Table 5.4).

Ultrasonic probe	Mean deviation from point gauge (mm)
Honeywell	1.66
Microsonic	4.00
Siemens, Sonar Bero	3.11

Table 5.4 Ultrasonic probes, accuracy test

In the physical model of the meandering ramp water surface inclinations up to 50° could be determined correctly with the ultrasonic probes. This was far above the limit for the weir overfall tests in the flume (maximum surface inclination < 20°). At first this result was stunning, but it became plausible by regarding the smoothness / roughness of the water surface: If a smooth, flat target is inclined at more than half of the nominal beam angle to the normal beam axis, the echo may be deflected so far that no signal is received by the sensor. In the case of targets with a rough surface, the acoustic beam is reflected diffusely. The angle of inclination to the beam may therefore be up to 50°.

Eventually it was decided to use the available probes of the lab, namely the three Honeywell sensors and one Microsonic sensor as the Siemens sensor was only slightly better than the Honeywell probe. The Microsonic sensor had the advantage over the Siemens sensor of displaying the measured distance during the measurements. The probes were aligned with the cross sectional profile (Figure 5.11). One Honeywell probe was mounted in the flume axis, two probes 300 mm left and right of the

flume axis, respectively. The Microsonic probe was placed 150 mm right of the flume axis (in the direction of the flow).

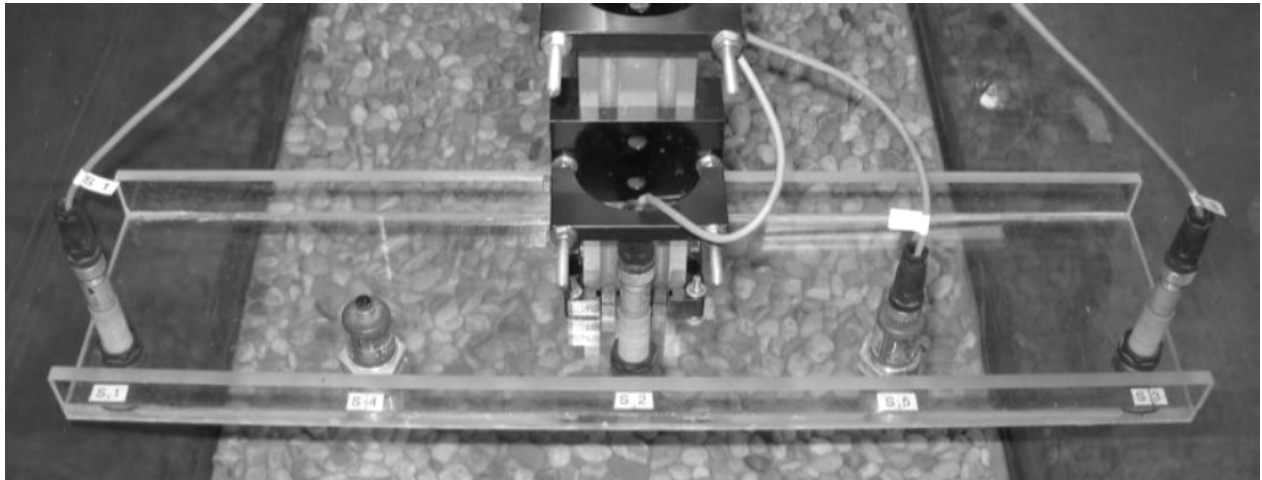


Figure 5.11 Ultrasonic probes on measurement carriage

Although five sensors can be mounted to the measurement carriage only four sensors could be recorded simultaneously. The hardware allowed for the saving 1000 values to a file for each probe and measurement (*Data Acquisition*, pp.136). The sampling rate could be chosen freely within this limit (e.g. 50 Hz for 20 seconds, 100 Hz for 10 s). As high frequency changes of the water levels were not expected a frequency of 20 Hz and a recording time of 50 seconds were chosen for the water surface measurements.

To check the accuracy of the ultrasonic probes for the 6.5 % ramp configuration additional point gauge measurements were performed.

Velocity Measurements with ADV-probe

The measurement technique of ADV-probes, especially of the Nortek Vectrino⁺, is described in chapter 4.5.3, pp. 80. In the flume velocities can be recorded with Nortek's software Vectrino Plus which processes the analogue signal and displays the velocities and other parameters (e.g. signal to noise ratio) on recording and saves them to binary files. There is no limit of sampling values per measurement but the Nortek's software and the positioning system cannot interact, so automated measurements are not possible. Therefore another method was performed: The analogue signal of the Vectrino⁺ probe is sampled and saved directly by the control unit of the flume (*Data Acquisition*, pp.136). This data is then processed in own MatLab routines. With this method the velocity samplings are subject to the same limitations of 1000 sampling values per measurement as the water level measurements. The appropriate sampling rate was determined by recording velocities simultaneously with Nortek's software at 200 Hz and the flume's data acquisition tool at 20 Hz for 50 s (resp. 50 Hz – 20 s and 100 Hz – 10 s). The time series and the mean velocity were compared. It turned out that the 50 Hz – 20 s combination achieves a good compromise between accuracy of the signal and longest possible recording time.

For the velocity measurements the ADV probe was mounted to the vertical axis of the positioning system (Figure 5.12). For each ramp configuration and each discharge at least to cross sectional profiles were measured, each above a step. For each cross section about 100 positions were measured.



Figure 5.12 Side-looking ADV-probe “Vectrino” on positioning system at the downstream end of the flume

As illustrated in Figure 5.12 the side-looking probe points to the left side of the flume. The measuring point is located 50 mm left of the probe head. Thus the furthestmost right (left) point that can be measured is 80 mm (10 mm) away from the flume wall.

Pressure Measurements with Pressure Transducers

Pressure measurements were performed with piezoresistive gauge pressure transducers from Kulite-Semiconductor Products, Inc.. The model name of the used transducers is *XTL 123C 190 SG* (Figure 5.13). They use a flush metal diaphragm as a force collector. A solid state piezoresistive sensing element is located immediately behind this metal diaphragm which is protected by a metal screen. Force transfer is accomplished via an intervening film of non-compressible silicon oil. This sensing sub assembly is welded to a stainless steel body. The transducers are temperature compensated in a range of -40°C to $+175^{\circ}\text{C}$.

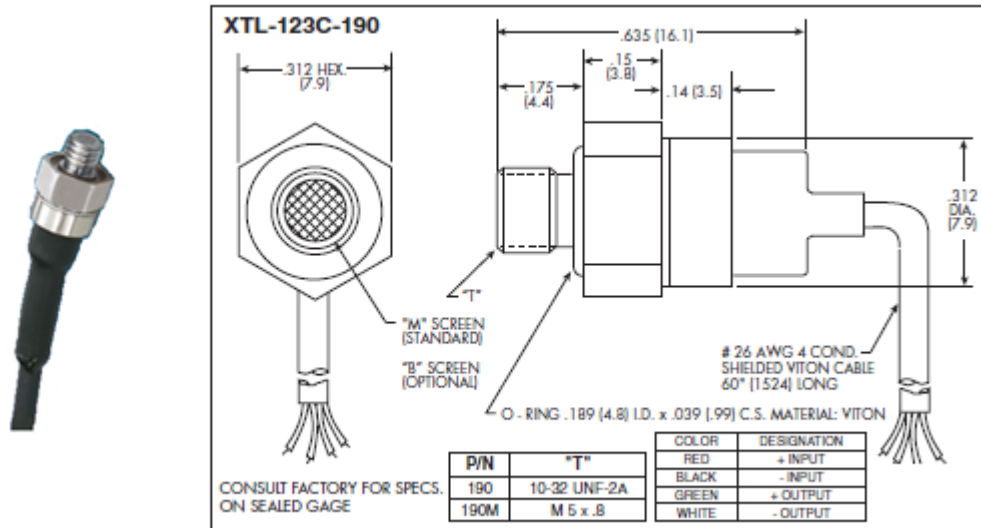


Figure 5.13 Kulite-Pressure Transducer XTL-123C-190, dimensions in inch and mm (in parenthesis), respectively

Transducer XTL-123C-190	
Pressure Range	0.35 bar
Sensitivity	~ 127 mV / bar
Combined Non-Linearity, Hysteresis and Repeatability	±0.1%

Table 5.5 Kulite-Pressure Transducer XTL-123C-190, key features

Altogether 14 pressure transducers *XTL 123C 190 SG* were available. The data acquisition device from National Instruments used to control the transducers and record the pressure data is described in detail in Geiger (2010). The software control was accomplished by a LabView program.

The 14 transducers were mounted to a specially designed roughness element (see chapter *Roughness Element for Pressure Measurements*, pp.127).

Typically pressure measurements were performed for 60 s at a sample rate of 1000 Hz. The data was saved to an Ascii-file.

5.2.3 Automatic Positioning and Data Acquisition

Positioning

The flume is equipped with a 3-dimensional positioning system. On top of the side walls of the flume longitudinal horizontal profiles are mounted. A toothed rack is fixed on this guide profiles. Guide tables are mounted to the guide profiles. A transverse profile fixed to these guide tables can be moved in longitudinal direction by means of a rack and pinion drive. A vertical axis is mounted to the transverse profile. Two additional motors can move the vertical axis in transverse and vertical direction. This way any arbitrary spatial point in the flume can be headed for (Figure 5.14, left).



Figure 5.14 positioning system (left), measurement cabinet with control unit (right)

A control unit performs the positioning and the data acquisition. The control unit is located in a measurement cabinet (Figure 5.14, right). The software of the control unit is operated via a VNC-client (virtual network computing) on a laptop.

Coordinate Systems

Two different coordinate systems have to be distinguished: The coordinate system of the positioning system “CSP” and that of the ramp construction in the flume, termed “CSR”. The axes of CSP and CSR will be distinguished with capital and small letters, respectively. The longitudinal, transverse and vertical axis will be referred to as X-, Y- and Z-axis resp. x-, y- and z-axis. Corresponding axes of CSP and CSR lie on the same line but have different origins and orientations (Figure 5.15). The positive X-axes of CSP and CSR point against the flow direction as is customary with the stationing of rivers. Both transverse positive “Y”-axes point towards the right side wall of the flume (in the direction of the flow). The positive vertical Z-axis of CSP points downwards, the z-axis of CSR points upwards. The origin of CSR was determined to be located in the center of the cross section of the ramp toe.

To head for a desired spatial point in the flume the respective coordinates have to be specified in the CSP. The offset of the origins of CSP and CSR are have to be specified individually for each measurement device which is mounted to the vertical axis of the positioning system (Table 5.6). Figure 5.15 illustrates the offset of the coordinate system of the positioning system for the ultrasonic probe in the centerline and the ramp coordinate system.

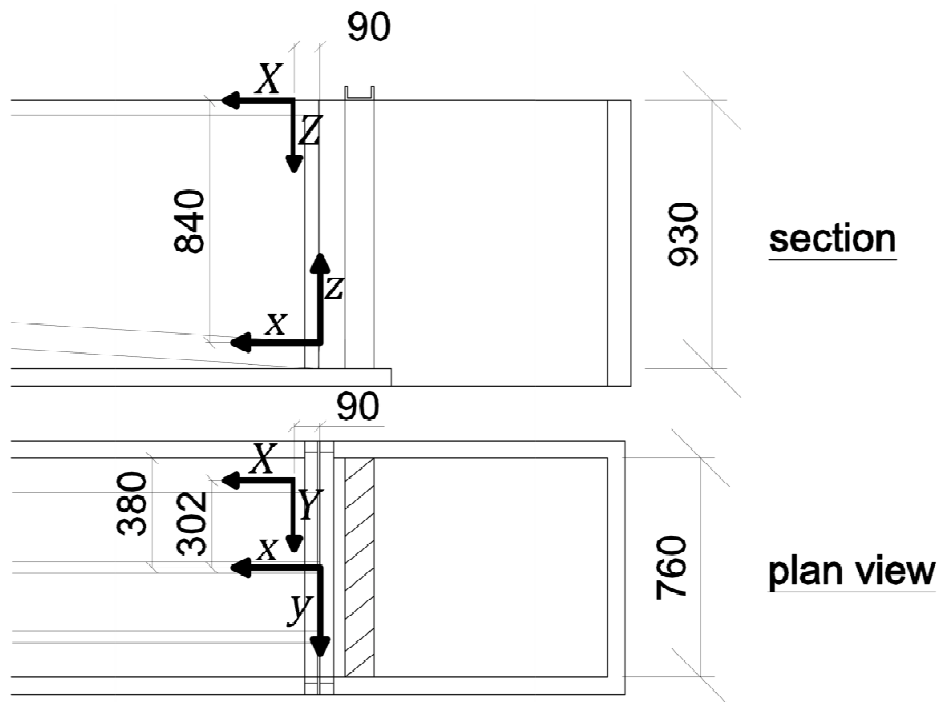


Figure 5.15 Coordinate systems CSP for ultrasonic probe in the centerline and CSR, dimensions in (mm)

Measurement device	X- x_{device}	Y- y_{device}	Z- z_{device}	
Ultrasonic sensors	90	2, 152, ± 302	Honeywell: 100	Microsonic: 50, 127
ADV probe	100	0	Determined by visual inspection at each step	

Table 5.6 Offset of measurement devices with respect to the profiles of the positioning system

The ultrasonic probes of Microsonic have a small measurement range (50-350 mm), but can measure objects at a minimum distance of 50 mm, in contrast to the Honeywell probes that have a wide measurement range (100-600 mm) but require a minimum distance to the measured object of 100 mm. Therefore the Microsonic probes were not aligned vertically with the Honeywell probes but were mounted 23 mm closer to the flume bottom (Figure 5.16).

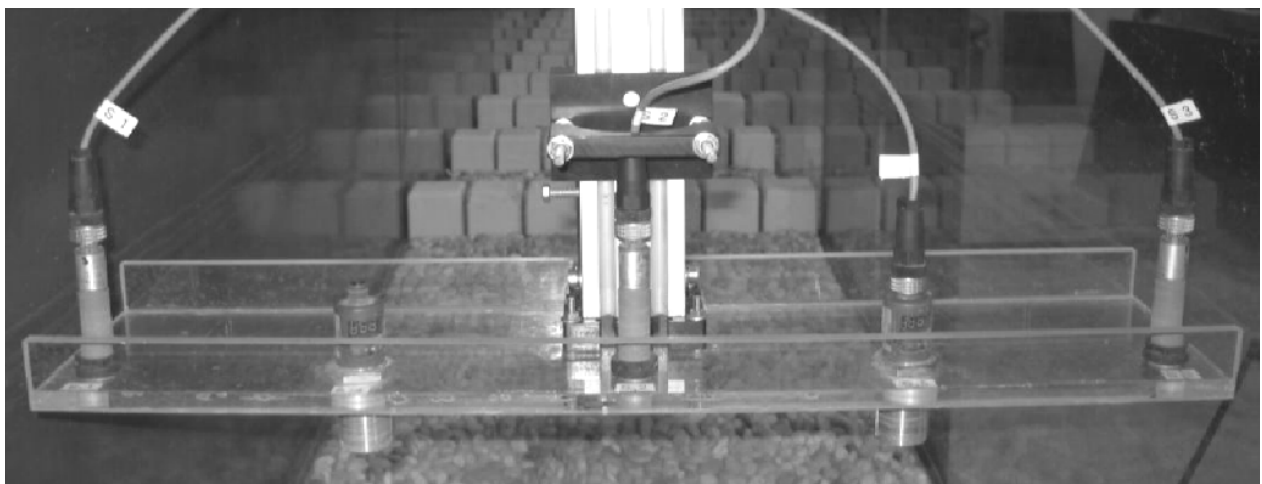


Figure 5.16 Carriage with ultrasonic probes aligned differently in vertical direction

A 100 x 100 mm grid of the ramp coordinate system was drawn onto the glass walls of the flume together with a longitudinal and vertical stationing (Figure 5.5). All results in this physical model test are displayed in the ramp coordinate system.

Data Acquisition

The control unit from the company “B&R automation” performs the data acquisition (Figure 5.14, right). The ultrasonic probes and the ADV probe yield analogue output signals in voltage. During each measurement the output signals are stored in a cache. After each measurement this data is saved to a USB-stick. The cache of the control unit is limited therefore only 1000 values per measurement could be saved.

5.2.4 Post Processing

The analogue output signal of both, the water level and the velocity measurements had to be analyzed to detect spikes. This “despiking” was performed by own MatLab routines. The results are illustrated in charts which were generated automatically by own routines using *Scripter*, a built-in Visual Basic compatible programming environment of *Golden Surfer Software 8.05*.

Despiking Algorithms for Ultrasonic Measurements

For the detection of spikes three steps were necessary. Each step was repeated recursively until no further spikes could be found. The detected spikes were removed and not replaced by a substitute. Prior to each step the mean and the standard deviation of the remaining values was calculated.

The first step compared a measurement value $m(i)$ and eliminated it if the gradient to its adjacent values $m(i - 1)$ and $m(i + 1)$ was greater than a multiple of the standard deviation σ . If all equations 5-1, 5-2 and 5-3 were fulfilled the measurement value $m(i)$ was removed by assigning the value NaN (“not a number”) to it.

$$\text{Central difference quotient} \quad \frac{1}{2} |m(i - 1) + 2m(i) + m(i + 1)| > 3 \cdot \sigma \quad \text{5-1}$$

$$\text{Backward difference quotient} \quad |m(i) - m(i - 1)| > 3 \cdot \sigma \quad \text{5-2}$$

$$\text{Forward difference quotient} \quad |m(i + 1) - m(i)| > 3 \cdot \sigma \quad \text{5-3}$$

The second step is a magnitude threshold criterion (equation 5-4). If the difference between a measurement value $m(i)$ and the mean of all valid measurement values was greater than the 3.5-fold standard deviation σ , than this value became NaN (not a number). In equation 5-4 n denotes the number of the remaining measurement values.

$$\left| m(i + 1) - \frac{1}{n} \sum_{j=1}^n m(j) \right| > 3.5 \cdot \sigma \quad \text{5-4}$$

In the final third step the difference of measurement value and mean must not exceed the threefold standard deviation σ . In addition the distance of two adjacent measurement values must not exceed σ (equations 5-5, 5-6 and 5-7).

$$\left| m(i) - \frac{1}{n} \sum_{j=1}^n m(j) \right| > 3 \cdot \sigma \quad 5-5$$

$$|m(i) - m(i - 1)| > 3 \cdot \sigma \quad 5-6$$

$$|m(i + 1) - m(i)| > 3 \cdot \sigma \quad 5-7$$

If a transmitted signal could not be received back by a probe (as was often the case for the Microsonic probe) the maximum value was written to the output file instead. If there are too many of such outliers and the mean value of the signal is well below the maximum value then the above described steps fail to identify the outliers because the standard deviation is too large in the first step. Figure 5.17 illustrates the unfiltered signal (left) and the signal filtered by values equaling the upper range bound (right). The filtered signal still contains some spikes but these can be detected by the above described algorithm (equations 5-5, 5-6 and 5-7).

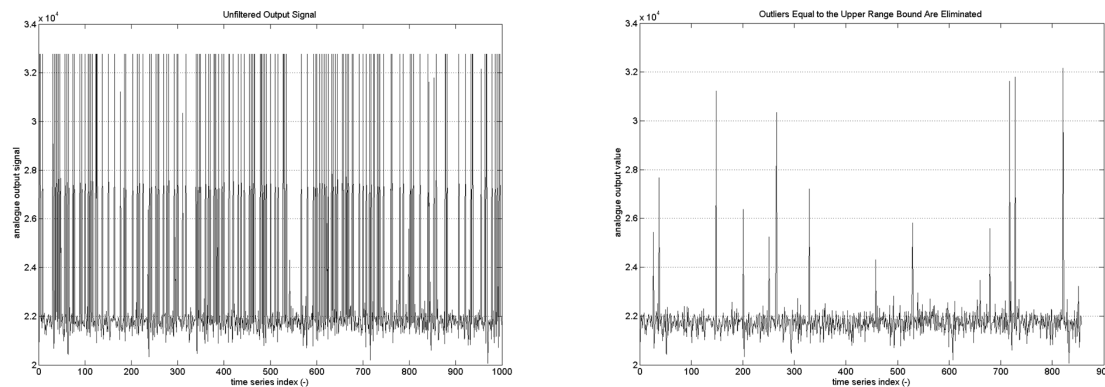


Figure 5.17 Unfiltered output signal (left), elimination of outliers equaling the upper range bound (right)

Filter Algorithms for ADV Measurements

The analogue output signal of the ADV measurements were filtered by applying the “phase space algorithm” (Goring, Nikora 2002). For a detected spike a cubic polynomial function of best fit through 12 data points on either side of the spike was determined. The spike was then replaced by the value of this cubic function. After the application of the phase space algorithm it was checked whether the acceleration of two successive data points exceeds $2 \cdot g$ (gravitational acceleration).

Automated Charts Generation with Surfer

The charts were generated automated using own routines of the Scripting Language (Visual Basic derivative) of *Golden Surfer Software 8.05*. For each test run charts illustrating the water and bed levels (longitudinal cut, cross section) were generated. The longitudinal cut displays the measured water levels of each of the 4 ultrasonic probes, the mean cross sectional water level the bed levels and the critical depth. For the calculation of the mean water level a weighted average was calculated assuming that the water level at the half-left position coincides with the measured water level at the half-right position. The cross sectional charts illustrates the water depths and the standard deviation of the measurements. Again the half-left position has been mirrored from the half-right

measurement. The mean water depth, the mean velocity and the averaged Froude number are also displayed.

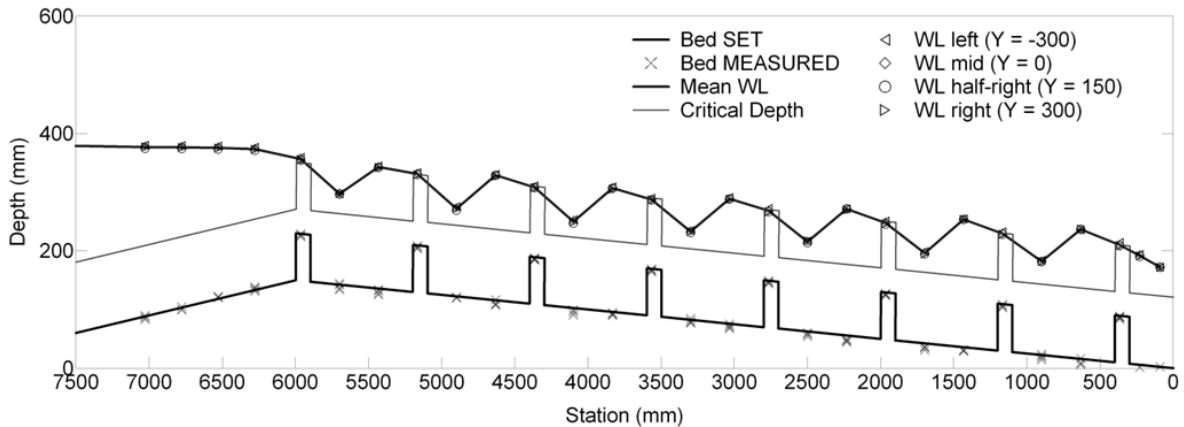


Figure 5.18 Example illustration, longitudinal cut of water levels

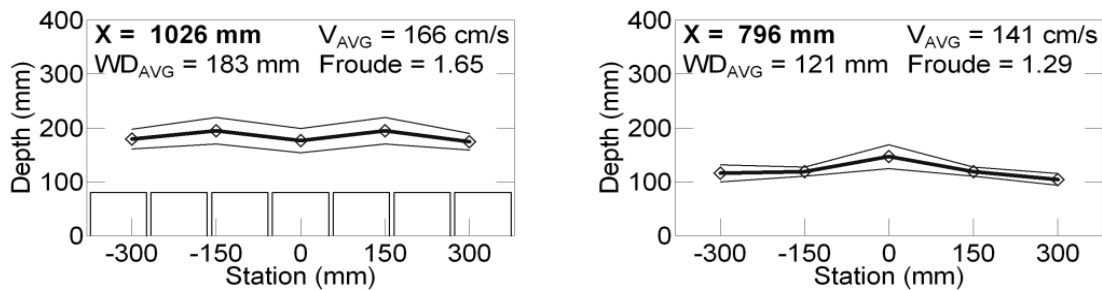


Figure 5.19 Example illustrations, water levels in cross section

Typically, ADV measurements were performed for a cross sectional profile above a step. 7 vertical columns with 10-13 measurement points each were measured (positions indicated by cross symbols in Figure 5.20).

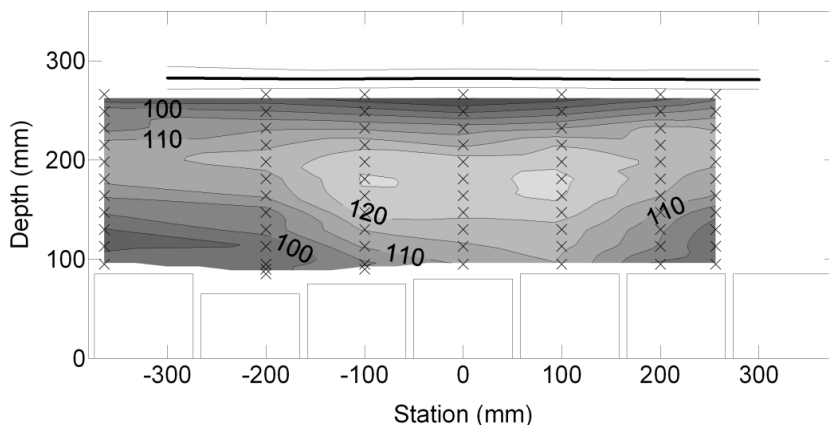


Figure 5.20 Example illustration, ADV-measurement, streamwise velocities u (cm/s)

For each ADV measurement three charts were generated (cross sectional profile).

1. Contour plot of streamwise velocities u (cm/s)
2. Vector plot of secondary flow (lateral and vertical velocities v and w , respectively)
3. Contour plot of the normalized turbulent kinetic energy per mass unit k/u_{max}^2 (-)

A complete compilation of the measurement charts can be found in appendix A.6.

5.2.5 Documentation

Photos were taken with the camera *Nikon D70*. For each tested ramp configuration a representative step-pool unit was selected for which the flow pattern was captured for stepwise increasing discharges (Figure 5.21).

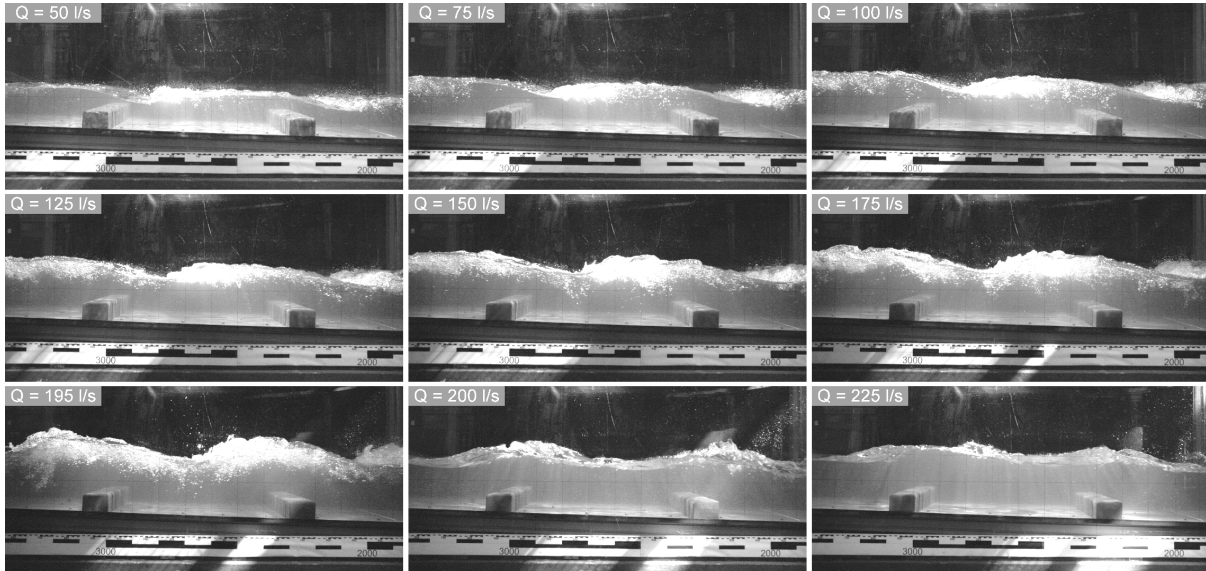


Figure 5.21: Example photo documentation

The appropriate modus operandi for the photo documentation emerged during the first experiments. Therefore the photo documentation is somewhat limited for the first two ramp configurations (Table 5.7).

For each tested ramp configuration a video of the flow transition from tumbling flow to rapid flow was recorded using Sony's camcorder *DVR SR90E*. The video documentation is available beginning from the fourth ramp configuration (Table 5.7).

5.3 Test Procedure

The described test procedure in this chapter does not include the pressure measurements which were performed separately and are documented in chapter 5.4.12, pp. 171.

5.3.1 Preliminary Tests

Preliminary tests aimed at getting a uniform flow profile. Steel grates, perforated steel sheets and plastic honeycombs served as flow straighteners. Different combinations of flow straighteners were tested. Three sheets of flow straighteners at the downstream end of the inlet section covering a length of 1.05 m finally proved to ensure a uniform flow profile (Figure 5.3).

In the experiments the ramp section had a length of 6000 mm. While the step spacings varied during the experiments (chapter *Panels*, pp. 127) the total length of the steps (5700 mm) was kept constant throughout the experiments. The remaining 300 mm of the ramp section were intended to guarantee flow conditions along the step-pools that are not influenced by the downstream conditions. The absence of backwater effects from downstream was considered to be the worst case scenario for the step-pools. In the preliminary tests it turned out however that the vertical drop behind the lamella results in a drop-down curve that reaches back to the step-pools. To eliminate the drop-down curve a plastic sheet was mounted to the steel sheet blocking the area below the ramp bottom. This can be regarded as a kind of additional step as the plastic sheet protrudes from the

ramp bottom by the height of the roughness elements. However, the step spacing between the last real step and the plastic sheet is only about half as long. In retrospect, it would have been better if the step-pools had covered the total ramp length of 6000 mm.

5.3.2 Test Procedure

For a certain ramp configuration the test procedure was as follows:

1. Determine the flow transitional discharge from tumbling flow to rapid flow by visual inspection
2. Determine the flow transitional discharge from rapid flow to tumbling flow by visual inspection (repeat steps 1 and 2 three times to validate the result)
3. Select four representative discharges
 - a. Discharge in the tumbling flow regime
 - b. Maximum discharge where tumbling flow can be preserved
 - c. Minimum discharge for which rapid flow conditions are present (if possible – due to hysteresis effects – the same discharge as in b. should be chosen)
 - d. Discharge in the rapid flow regime
4. For the four selected discharges
 - a. Measure the water levels: two cross sections for each step, two cross sections for each pool, for each cross section four water levels are measured (Figure 5.11)
 - b. Measure the velocities above the first step and a step where a cyclic uniform discharge has developed (optional)
5. Photo documentation
 - a. Select one step-pool unit where cyclic uniform flow has developed (typically 4th -6th unit)
 - i. Starting from 50 l/s, increase the discharge step-wise by 25 l/s and take a picture, additionally include representative discharges (as in 3.)
 - b. From the lab's crane take pictures of the whole ramp section, one for each representative discharge (as in 3.)
6. Video documentation
 - a. From the lab's crane record the flow transition from tumbling flow to rapid flow

5.3.3 Test Program

Altogether 20 different ramp configurations were tested: 14 each in the wide flume and 6 variants in the narrow flume. A ramp configuration is defined by the ramp slope I , the step height K and the step spacing L . The name of each variant thus is:

$I_{xx_Ky_Lzz}$

where xx , y and zz denote slope (‰), step height (cm) and step spacing (cm), respectively.

For both tested slopes in the wide flume the water levels were measured without step installations prior to the step-pool configurations. Table 5.7 lists the complete test program for the wide flume ordered by I , K and L . The chronological order of the experiments is documented in the rightmost column.

Test Program Wide Flume					
Variant	Bed	Q (l/s)	Flow Regime	ADV-position	chron. Order
I25_K0_L62	smooth	200	Supercritical	X = 1590	1
		100	trans		
		150	trans		
		200	trans		
		250	trans		
I25_K6_L62	rough	300	trans	s1 & s10 s1 & s10	3
		95	TF		
		115	TF		
		115	RF		
I25_K6_L70	rough	200	RF		9
		100	TF		
		130	TF		
		130	RF		
I25_K6_L80	rough	Determination of flow transitional discharge only			11
I25_K6_L93	rough	100	TF		10
		155	TF		
		155	RF		
		200	RF		
I25_K8_L62	rough	100	TF	s1 & s7 s1 & s7	2
		125	TF		
I25_K8_L70	rough	200	RF		8
		100	TF		
		158	TF		
		158	RF		
I25_K8_L80	Rough	200	RF	s1 & s5 s1 & s5 s1 & s5 s1 & s5	4
		100	TF		
		178	TF		
		178	RF		
I25_K8_L80	smooth	200	RF	s1 & s5 s1 & s5 s1 & s5 s1 & s5	5
		100	TF		
		178	TF		
		178	RF		
I25_K8_L80 meander	rough	200	RF	s1 & s5 s1 & s5 & s6 & s7 s1 & s5 s1 & s4 & s5 & s6 & s7	6
		100	TF		
		178	TF		
		178	RF		

I25_K8_L93	rough	100	TF	s1 & s4 & s5 & s6 s1 & s4 & s5 & s6 s1 & s4 & s5 & s6	7
		210	TF		
		210	RF		
		240	RF		
I65_K0_L93	rough	75	super		12
		100	super		
		150	super		
		170	super		
I65_K8_L62	rough	75	TF	3 x p6 2 x p6 2 x p6	15
		100	TF		
		150	RF		
		170	RF		
I65_K8_L70	rough	70	TF		14
		75	TF		
		100	TF		
		130	RF		
		170	RF		
I65_K8_L80	rough	75	TF		13
		100	TF		
		120	RF		
		170	RF		
I65_K8_L93	rough	75	TF	2 x p2, 2 x p4	16
		100	TF		
		150	RF		
		170	RF		

Table 5.7: Test program wide flume

The 6 variants in the tilting narrow flume were performed for a fixed step height $K = 80$ mm and a fixed spacing $L = 700$ mm. Only the slope was varied.

Test Program Narrow Flume					
Variant	Bed	Q (l/s)	Flow Regime	Point gauge	chron. Order
I25_K8_L70	Smooth	26.3	TF	s5, s6, s7	17
		35			
I30_K8_L70	Smooth	26.3	TF	s5, s6, s7	18
		35			
I35_K8_L70	Smooth	26.3	TF	s5, s6, s7	19
		35			
I40_K8_L70	Smooth	26.3	TF	s5, s6, s7	20
		33			
I45_K8_L70	Smooth	26.3	TF	s5, s6, s7	21
		32			
I52_K8_L70	Smooth	26.3	TF	s5, s6, s7	22
		30			

Table 5.8: Test program narrow flume

5.4 Results and Discussion

In this chapter lots of comparisons are drawn between with large roughness elements and step-pool ramps. For this flume test the terms “step” and “large roughness element” can be used interchangeably. The discharge marking the flow transition from tumbling flow to rapid flow will shortly be referred to as “transitional discharge”.

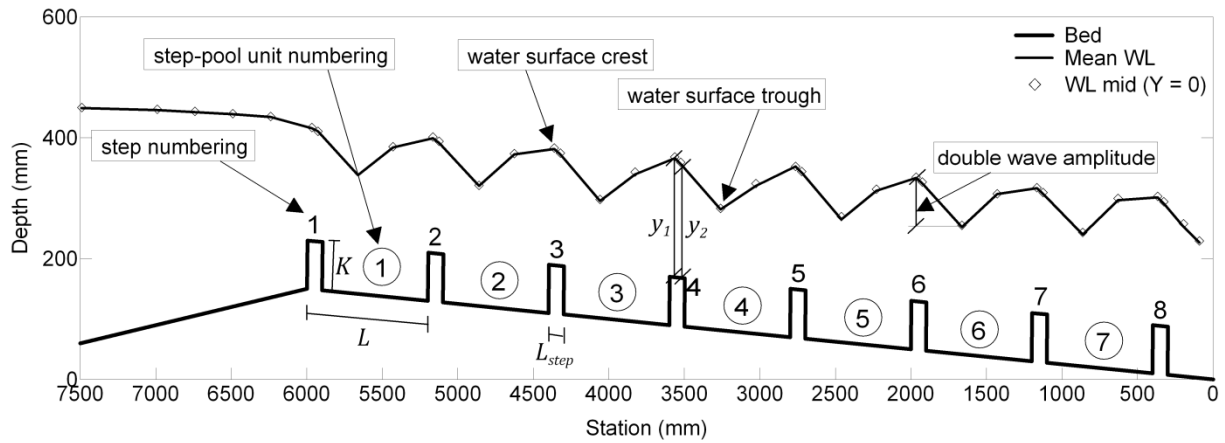


Figure 5.22 Design parameters, step-pool unit numbering, step numbering and water surface properties

Figure 5.22 illustrates the design parameters and other denotations that will be used throughout this chapter, such as the numbering of the step-pool units and of the steps and the water wave amplitude. The two water depths that are measured above each step are denoted with y_1 and y_2 , respectively. The mean value of these two water depths is denoted as y_{step} (cf. Figure 5.1). The tumbling flow and the rapid flow regime will be abbreviated as “TF” and “RF”, respectively.

The three orthogonal components of the 3D-velocity vector are denoted as:

Streamwise direction (horizontal): u
 Lateral direction: v
 Vertical direction: w

5.4.1 Water levels without step installations

For the mild slope with the smooth bed the water level was only measured for the discharge $Q = 200$ l/s. The flow at this discharge is well in the supercritical flow regime ($Fr = 1.97$). For the mild slope with the rough bed it turned out that the bed is extremely rough such that it takes 5 m to get water levels parallel to the bed. The Froude numbers for the tested discharges are near 1 so the flow is in the transitional regime. For the step slope the Froude number is about 2 (Table 5.9). The water level profiles of these experiments can be found in Appendix A.5.

Discharge (l/s)	2.5 % smooth	2.5 % rough	6.5 % rough
75			2.11
100		0.98	2.04
150		1.07	2.07
170			2.12
200	1.97	1.13	
250		1.17	
300		1.20	

Table 5.9: Froude numbers without step installations

As described in chapter 3.6 the idea of large roughness elements in steep channels is to establish tumbling flow with defined flow conditions over the steps, i.e. $Fr = 1$. A high Froude number flow can be slowed down to critical flow (and thus the minimal possible energy level at the toe of the structure) by means of large roughness elements. This way the stilling basin downstream of the structure can be smaller. The Froude number for the mildly sloped rough bed is already near 1 without step installations so that the roughness elements are not necessary. The experiments with the step installations showed however that the flow is dominated by the large roughness elements. The bed roughness has little influence. As for the mildly sloped smooth bed the Froude number is about 2 (Table 5.9) it can be argued the large roughness elements manage to decelerate the flow from $Fr = 2$ to $Fr = 1$ for the mild sloped ramp as long as the tumbling flow can be preserved.

5.4.2 Tumbling Flow Regime

Per definition (Peterson & Mohanty (1960), chapter 3.6.1) the tumbling flow regime is characterized by a cyclic succession of subcritical to supercritical flow. Critical flow conditions occur above the large roughness elements. In the experiments with the mild slope the tumbling flow regime appeared as defined. The flow transition from subcritical to supercritical flow occurs above the step. The surface wave amplitude remains constant along the ramp. With rising discharge the wavy surface increases its amplitude. Moreover the water depths increase as the flow travels downstream, i.e. the slope of the wave crests is milder than that of the bed. This increase in water depth depends on how close the discharge is to the transitional discharge. It is not a backwater effect. As the discharge approaches the transitional discharge the crest of the water surface moves from the lower part of a pool towards the next step. The flow is two-dimensional, i.e. the water levels in each measured cross section are horizontal. The described flow behavior is valid for all tested ramp variants with the mild slope. Figure 5.23 illustrates the tumbling flow pattern for the meandering ramp variant.

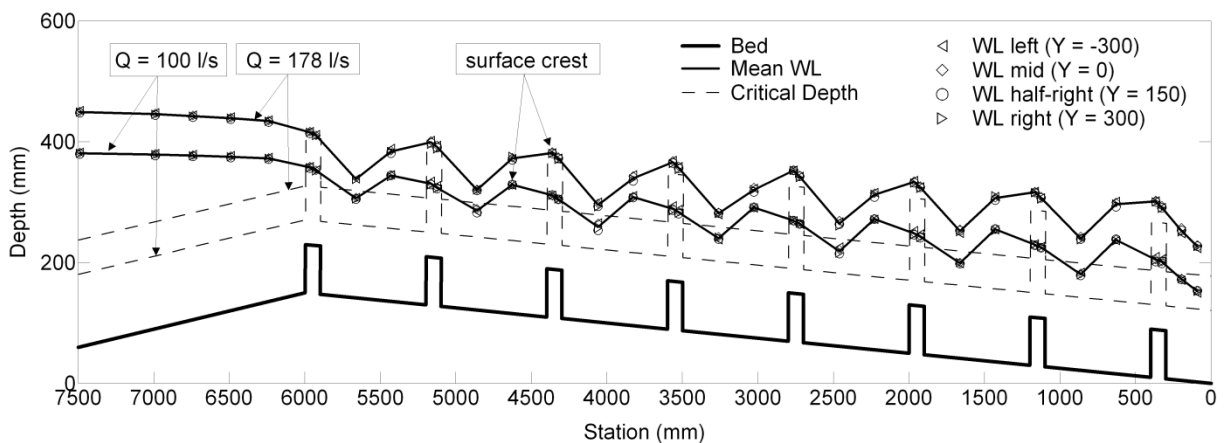


Figure 5.23 Example of tumbling flow patterns for slope $I = 2.5\%$: Variant I25_K8_L80, rough, meander

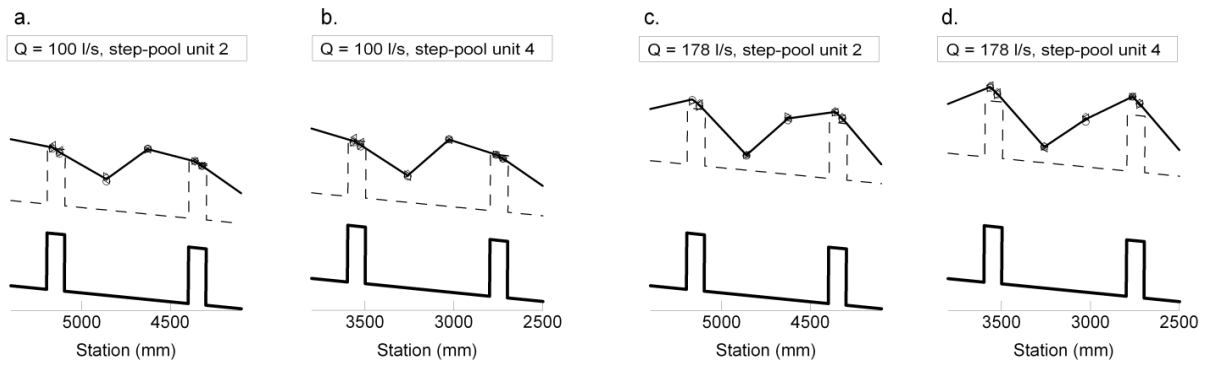


Figure 5.24 Detail of Figure 5.23: critical flow over steps (a., b., c.), rising water depth (cf. c. and d.)

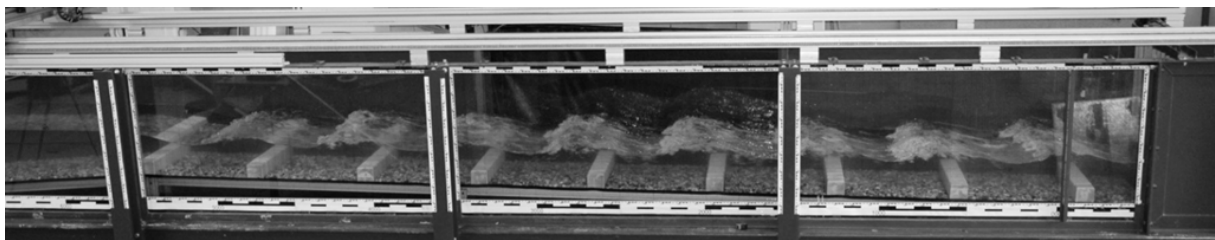


Figure 5.25 Tumbling Flow Pattern, variant: I25_K8_L70, rough bed, $Q = 158 \text{ l/s}$

As for the steep slope $I = 6.5 \%$ the surface wave amplitude remains constant along the ramp. With rising discharge the wavy surface increases its amplitude. The flow is two-dimensional. Other than for the mild slope an increase in water depth cannot be observed as the flow travels downstream. Figure 5.26 illustrates the typical tumbling flow patterns for the steep ramp configurations.

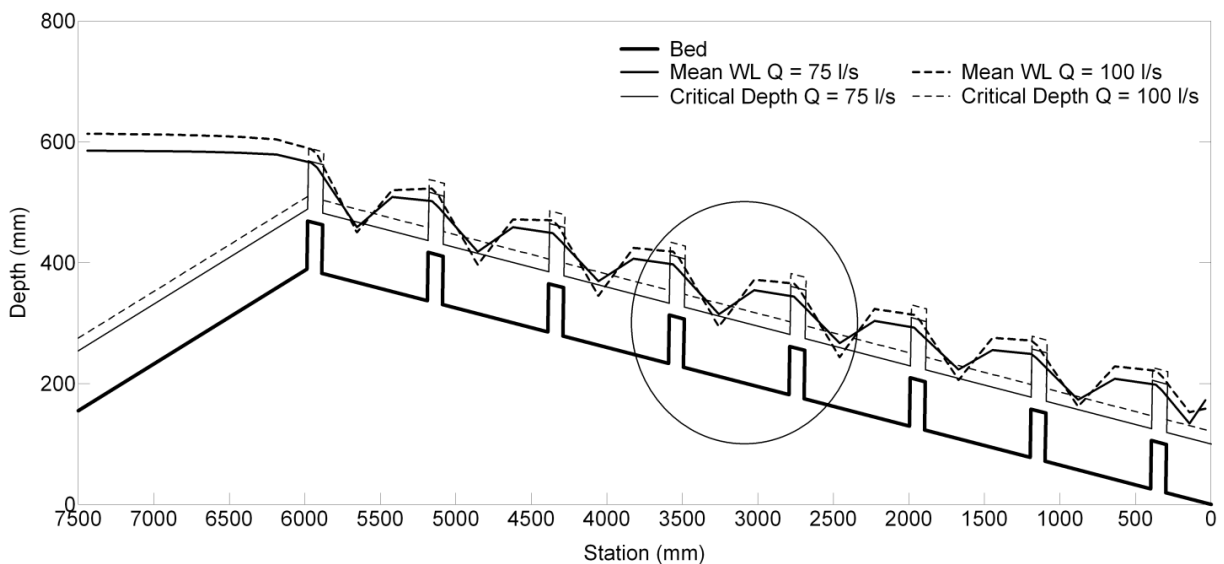


Figure 5.26 Example of tumbling flow patterns for slope $I = 6.5 \%$: Variant I65_K8_L80, rough

In contrast to the mild slope experiments and to the definition of tumbling flow (Peterson, Mohanty 1960) critical flow conditions do not occur above the steps. Throughout the ramp there is supercritical flow over the steps (Figure 5.27). This result was confirmed by additional water level measurements with a point gauge.

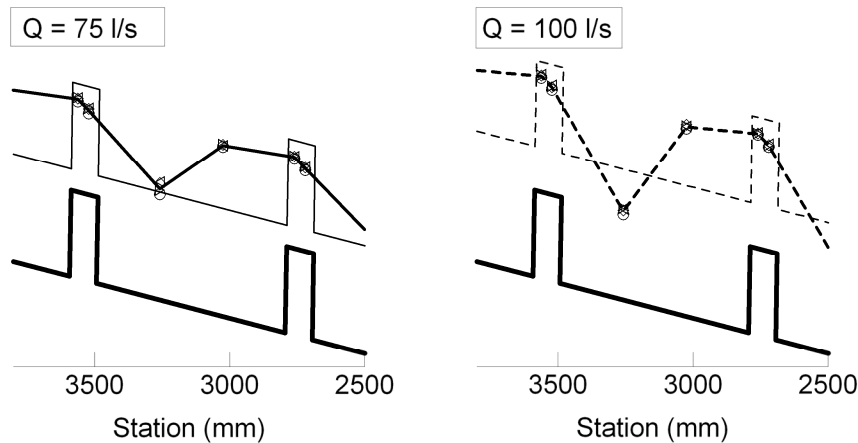


Figure 5.27 Detail of Figure 5.26: supercritical flow over steps, step-pool unit 4

Experiment	q (m ² /s)	I (%)	K (cm)	L/K	y_1/y_c
Peterson & Mohanty, 2D bar	0.154	5	9	15	1.05
Peterson & Mohanty, 2D bar	0.118	8.3	9	10	1.16
Peterson & Mohanty, 2D bar	0.138	8.3	9	15	1.04
This study, wide flume, 3D cubes	0.132	6.5	8	11.67	0.76
This study, wide flume, 3D cubes	0.099	6.5	8	10	0.82
This study, wide flume, 3D cubes	0.132	6.5	8	10	0.86
This study, wide flume, 3D cubes	0.132	6.5	8	8.75	0.88
This study, wide flume, 3D cubes	0.132	6.5	8	7.78	0.87

 Table 5.10: Comparison of present study with Peterson & Mohanty: flow depths (TF) above steps as multiples of the critical flow depth, y_1 denotes the flow depth above upstream crest of the step

As can be seen from Table 5.10 the flow depth y_1 above the upstream crest of the step normalized by the critical flow depth y_c is around 0.8 (i.e. supercritical flow) in the present study while it is close to 1 in the study of Peterson & Mohanty. Even for the 8.3 % slope Peterson & Mohanty reach critical depth above the steps than in this present study for similar specific discharges and relative spacings. The diverse results of the two studies may be explained by differences in step height, bed roughness and shape of the roughness element (2D-bars vs 3D cubes) but don't become fully coherent, though.

5.4.3 Unstable Flow and Rapid Flow Regime

The rapid flow regimes occur on discharges higher than the tumbling flow regime. On the flow transition from tumbling flow to rapid flow there is a range of discharges where the flow is unstable and the water surface is 3-dimensional (Figure 5.28, Figure 5.30). The pure stable rapid flow (SRF) is 2-dimensional again, i.e. the cross sectional water surface is horizontal (Figure 5.31, Figure 5.32). When the discharge is in the unstable range the flow in the first step-pool units typically is in the rapid flow regime. As the flow travels downstream rooster tails appear immediately upstream of a step which increase in amplitude as the flow propagates downstream. One explanation for the development of the rooster tails is that the supercritical flow over the steps (that act as a drop) generates crossing waves. At the intersection of these waves rooster tails develop. However, this does not explain the existence of two rooster tails in one cross section that could also be observed in our experiments (Figure 5.28). In his investigations on "Stationary Waves and Antidunes in Alluvial Channels", Kennedy also denies that wall effects are a necessary condition to produce rooster tails (Kennedy 1961). He supports this statement by two photographs (Kennedy 1961): one of which

illustrating a single train of rooster tails in the middle of a 2.4 m (8 ft) wide channel, which were “certainly not influenced by the flume walls”; the other photo illustrating multiple rooster tails per cross section. In Volkart’s investigations on sills three rooster tails are clearly visible per cross section at unstable flow conditions (Volkart 1972, Figure 5.29).

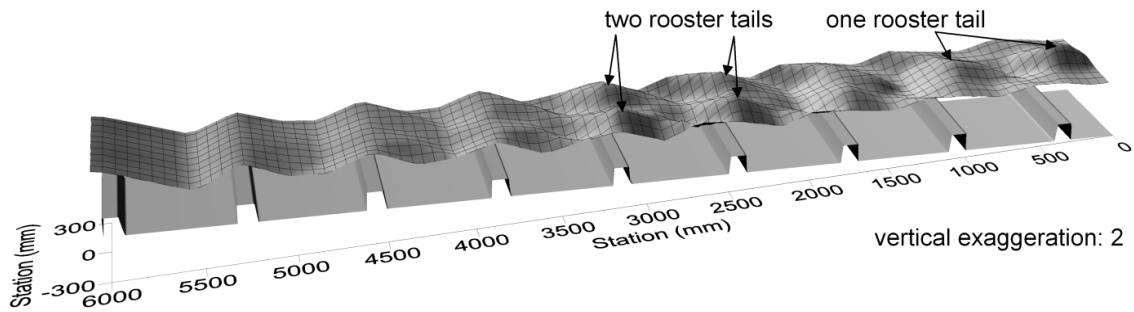


Figure 5.28 Example water surface for instable flow, variant: I25_K6_L70, rough, $Q = 130$ l/s, rooster tails

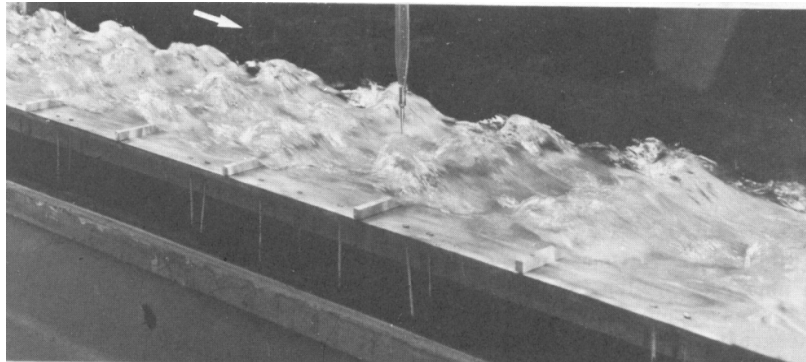


Figure 5.29 water surface instable Flow, 3 rooster tails per cross section (Volkart 1972)

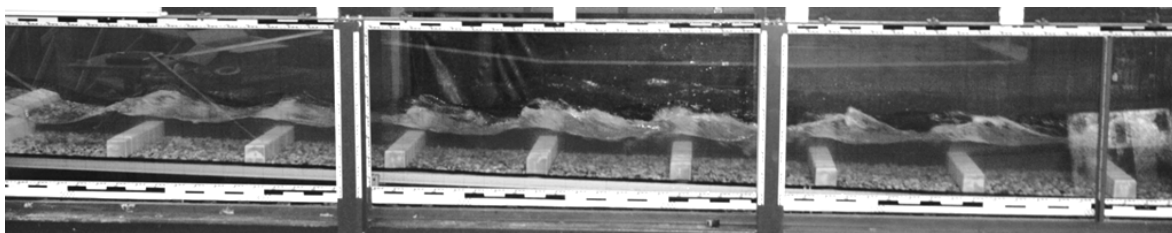


Figure 5.30 Instable flow pattern, variant: I25_K8_L70, rough bed, $Q = 158$ l/s

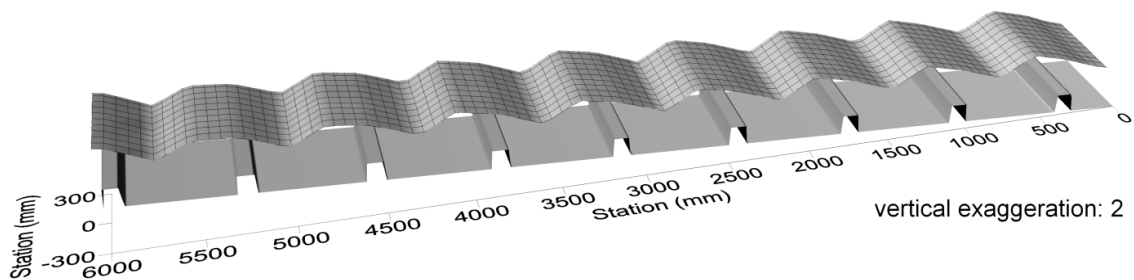


Figure 5.31 Water surface for stable rapid flow, variant: I25_K6_L70, rough, $Q = 200$ l/s, horizontal water levels in cross section

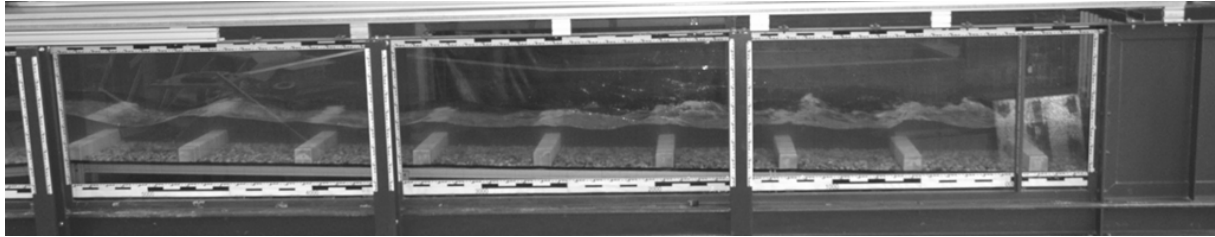


Figure 5.32 Stable rapid flow pattern, variant: I25_K8_L70, rough bed, $Q = 200 \text{ l/s}$

For some ramp configurations the highest tested discharge was still in the unstable regime, i.e. a stable rapid flow regime was not reached for some lower step-pool units.

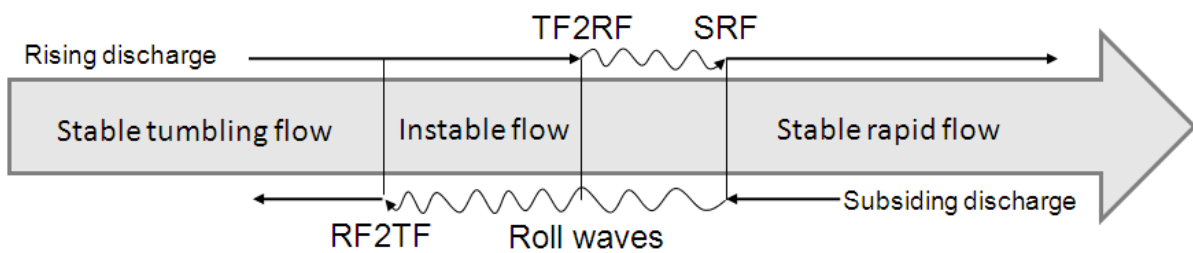


Figure 5.33 Flow regimes and transitional discharges TF2RF and RF2TF

The flow transitional discharge underlies a hysteresis effect, i.e. the transition from tumbling flow to rapid flow (TF2RF) occurs on higher discharges than the transition from rapid flow to tumbling flow (RF2TF, Figure 5.33). Within the borders of these two transitional discharges the flow is very instable. A sudden change of the flow system (e.g. small discharge fluctuations) may cause the flow to swap from tumbling flow to rapid flow and vice versa. Within this discharge range the flow can be manipulated to the desired flow regime by either blocking the flow above a step temporarily to re-establish a hydraulic jump in the pool above or by accelerating the flow momentarily in order to “wash” the jump over the step. The different flow regimes can be explained by different pressure distributions. Outside this instable range of discharges the flow is either stable tumbling or rapid (Figure 5.33). It cannot be changed by manipulation.

For tumbling flow situations the Froude number above the step is about 1. For the rapid flow regime the Froude number above the step for the mild slope is less than 1.5 for all tested discharges and spacings. The range of Froude numbers above a step for the steep slope is $2 \div 2.3$ (Figure 5.34). Different symbol shapes correspond to different step spacings. The fill color of the symbol (white, grey, black) indicate different slopes and roughness heights.

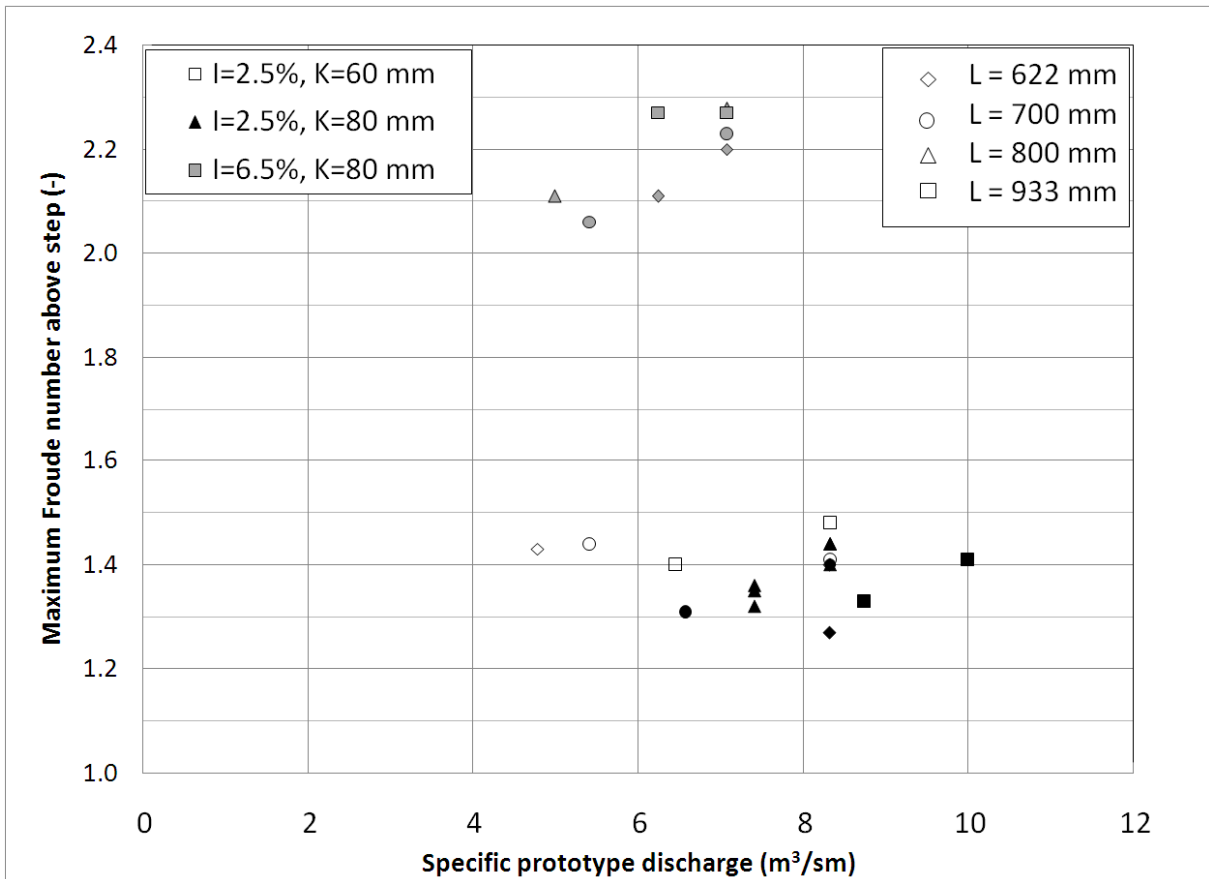


Figure 5.34 Maximum Froude numbers above step for the rapid flow regimes

5.4.4 Velocity and Turbulence Profiles

ADV-measurements were performed for the mild slope above the first step and above one or more selected steps further downstream. The latter step was chosen at a location where cyclic uniform flow conditions had established. From the ADV-data streamwise velocity profiles, secondary flow patterns and turbulent kinetic energy (TKE) plots were evaluated and analyzed. The streamwise velocity plots are displayed in cm/s. Two adjacent contour levels have a distance of 5 cm/s. The “x”-symbols mark the measurement points used to generate the contour plot. The bold and the fine solid lines on top of the contour plot indicate the mean water level and its standard deviations, respectively.

Some general trends can be observed:

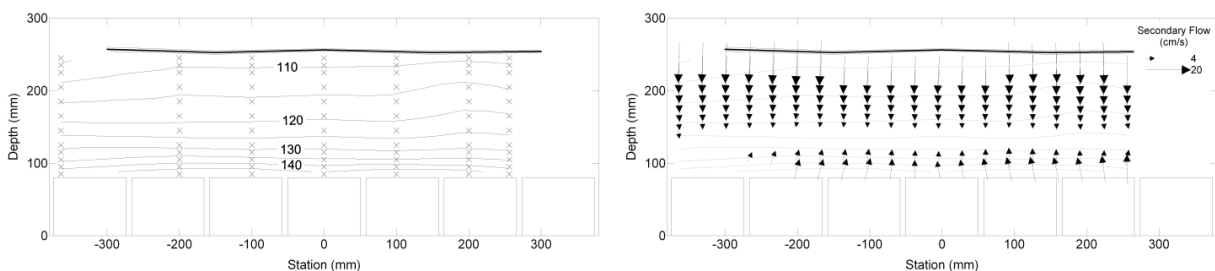


Figure 5.35 Typical cross sectional velocity distribution above step 1: variant I25_K8_L80, smooth bed, Q=178 l/s, Rapid Flow: streamwise velocities (left), secondary flow (right)

The streamwise velocity distribution above the first step is uniform in lateral direction with the highest velocities immediately above the step. This holds true for both the tumbling and the rapid

flow regime (Figure 5.35). The tumbling flow regime is dominated by a downstream pointing flow except for the region immediately above the step (Figure 5.36, right). On the other hand the rapid flow is characterized by an upstream pointing flow throughout the measured step cross section (Figure 5.37, right).

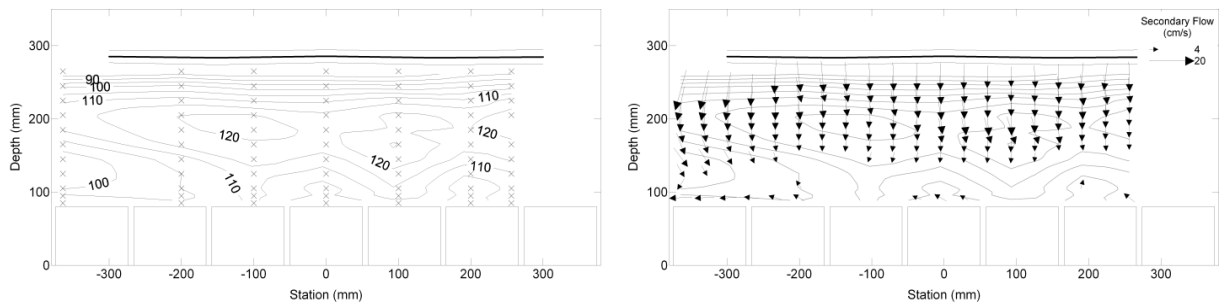


Figure 5.36 Typical cross sectional velocity distribution tumbling flow: variant I25_K8_L80, rough bed, step 5, Q=178 l/s: streamwise velocities (left), secondary flow (right)

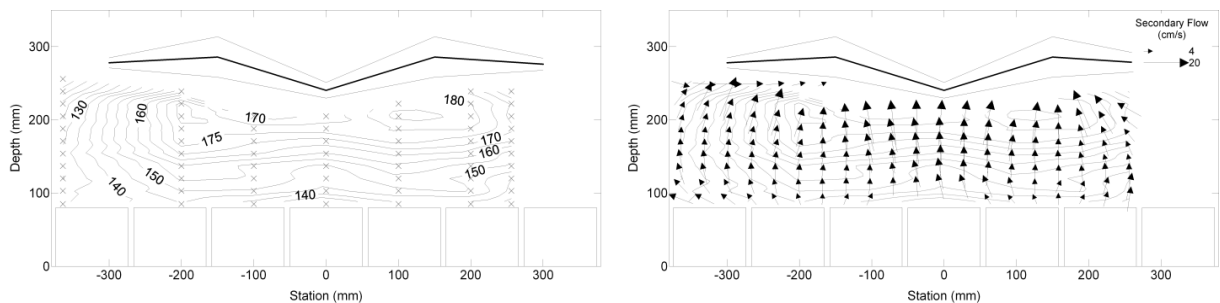


Figure 5.37 Typical cross sectional velocity distribution rapid flow: variant I25_K8_L93, rough bed, step 5, Q=240 l/s, rapid flow: streamwise velocities (left), secondary flow (right)

As the flow propagates downstream the streamwise velocities become inhomogeneous in lateral direction. Typically two or more velocity maxima develop which are often (but not always) symmetric with respect to the flume axis (Figure 5.36, left, Figure 5.37, left; see also Figure 5.43, Figure 5.47).

The turbulent kinetic energy per mass unit k (m^2/s^2), short TKE, is defined as the squared standard deviation of the velocity fluctuations of a velocity time series signal. The TKE plots are normalized by the squared maximum streamwise velocity u_{max}^2 (m^2/s^2). Two adjacent contour levels in the TKE plots (Figure 5.38) have a distance of 0.005. The “x”-symbols mark the measurement points used to generate the contour plot. The bold dashed line indicates the high velocity region. The bold and the fine solid lines on top of the contour plot indicate the mean water level and its standard deviations, respectively.

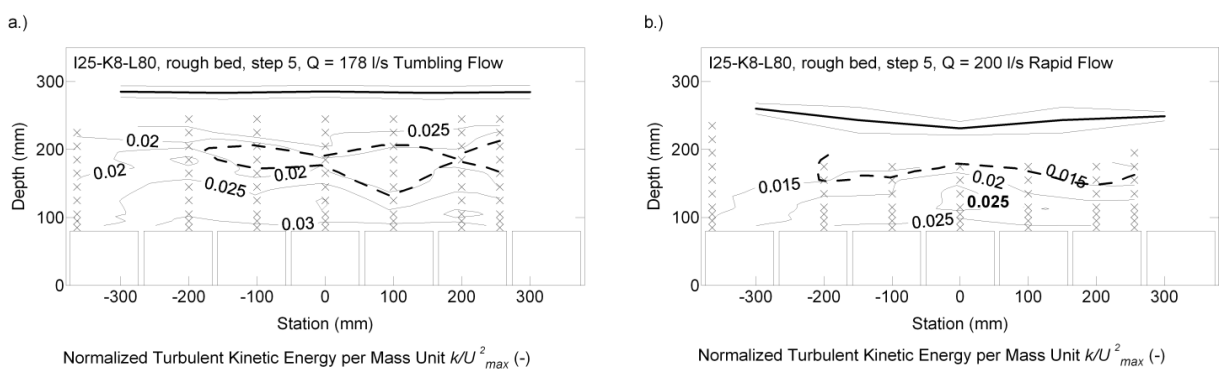


Figure 5.38 Typical TKE pattern with the smallest values in the high velocity region

The TKE distributions have the smallest TKE values in the vicinity of the high velocity regions while the turbulent kinetic energy is higher immediately below the water surface and close to the top of a step, i.e. the bottom of the cross section. As a very rough estimate the normalized TKE values for the steps 4 to 7 are 4 to 5 times higher than those for the first step. Figure 5.38 illustrates typical TKE distributions.

As a general result the normalized TKE values are smaller for the rapid flow regime than for the tumbling flow regime (cf. Figure 5.38 a.) and b.)). For a stable tumbling flow the normalized TKE values do not change for steps 4 to 7 while they increase in downstream direction for the unstable rapid flow regime. These measuring results are in agreement with the visual inspection that for the unstable rapid flow regime the flow becomes more turbulent (higher roll waves, increased air entrainment) as it propagates downstream.

5.4.5 Rough and Smooth Bed

In order to check whether the bed roughness plays a dominant role in large roughness flows a ramp configuration with gravel panels was contrasted with the appropriate ramp configuration with the smooth panels. As described in chapter *Panels* (pp. 127) the mean bed level of the gravel plates was assumed to be 15 mm above the plastic panel (Figure 5.7). For the gravel panels roughness elements of height 95 mm were used resulting in the effective step height $K = 80$ mm. For the smooth panels the roughness elements had a height of 75 mm which equals the effective step height $K = 75$ mm. The step spacing was $L = 800$ mm for both tested cases.

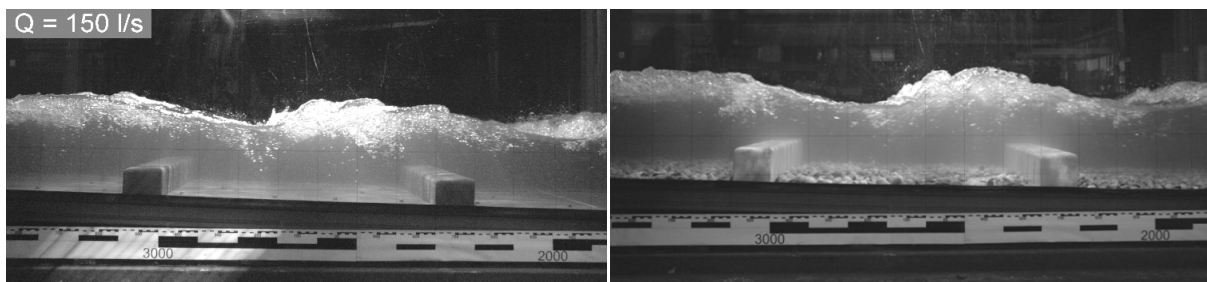


Figure 5.39 Varying bed roughness: variant I25_K8_L80, smooth bed (left) and rough bed (right)

The experiments prove that the bed roughness can be neglected for large roughness elements. As illustrated in Figure 5.40 and Figure 5.41 the mean water depths for smooth and rough bed cases coincide. The water level fluctuations for the smooth and the rough bed cases also show a similar behavior.

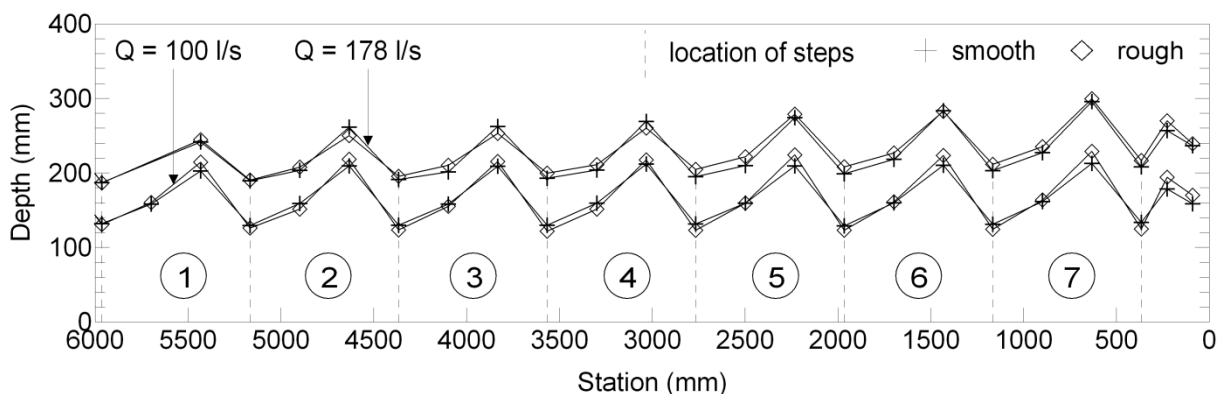


Figure 5.40 Comparison of mean water depths for smooth and rough bed: I25_K8_L80, tumbling flow

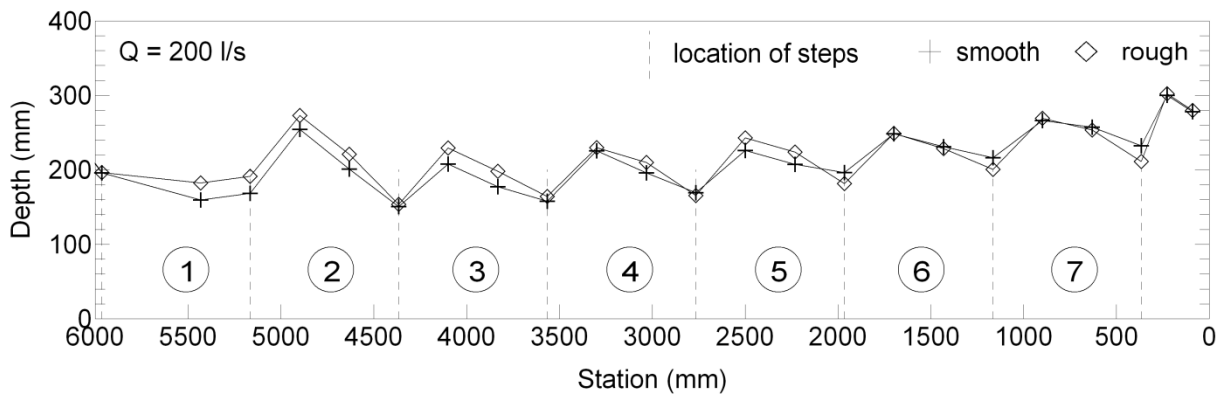


Figure 5.41 Comparison of mean water depths for smooth and rough bed: I25_K8_L80, rapid flow

As will be described in detail in chapter 5.4.8 the flow transitional discharge depends on the relative spacing L/K . Moreover a hysteresis effect concerning the flow transitional discharge can be observed: The discharge from tumbling flow to rapid flow occurs on higher discharges than the transition from rapid flow to tumbling flow. As for the smooth case the relative spacing $L/K = 10.6$ is higher than for the rough bed ($L/K = 10$) the flow transition occurs on a higher discharge for the smooth case.

Other than the bed levels the ADV-velocity measurements show differences between the two cases. While the streamwise velocity profiles above the first step agree well for all discharges for the smooth and the rough case (Figure 5.42) they differ considerably for the fifth step (Figure 5.43).

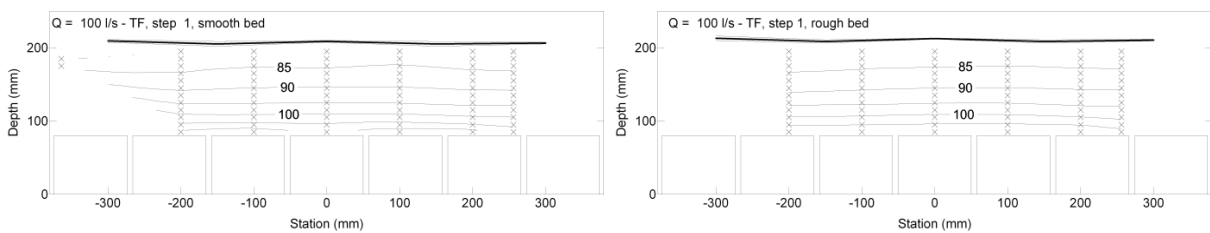


Figure 5.42 Comparison of streamwise velocities for smooth and rough bed: I25_K8_L80, step 1

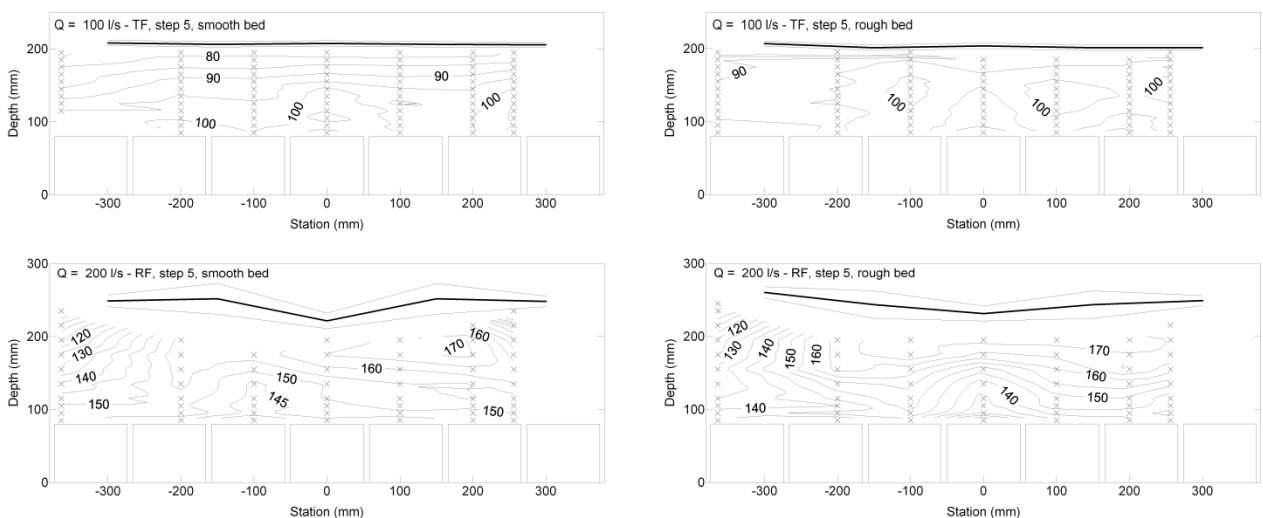


Figure 5.43 Comparison of streamwise velocities for smooth and rough Bed: I25_K8_L80, step 5

The velocity profiles for the rough bed are symmetric with respect to the flume axis. This is not the case for the smooth bed profiles.

A complete compilation of all ADV-measurements for these two cases can be found in Appendix A.6.

5.4.6 Laterally Inclined Steps vs Horizontal Steps

As described in detail in chapter *Roughness Elements* (pp.125) there exist two different step configurations with a mean effective height $K=80$ mm. One step consists of 7 roughness elements of equivalent effective height $K=80$ mm (Figure 5.7). The other step consists of 7 roughness elements with effective heights ranging from 65 to 85 mm (Figure 5.7). The latter step configuration serves to model the laterally inclined steps of the meandering ramp.

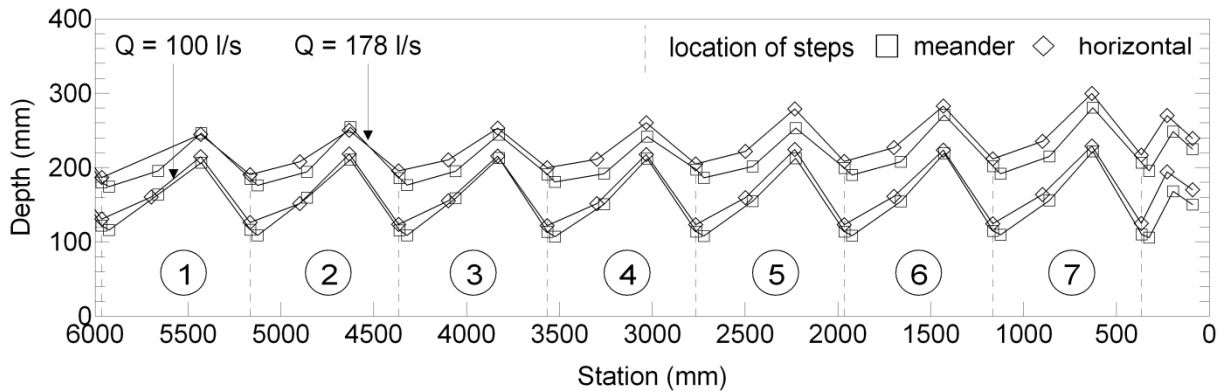


Figure 5.44 Comparison of mean water depths for horizontal and laterally inclined steps: I25_K8_L80, tumbling flow

As can be seen from Figure 5.44 the mean water depths for the two tested cases are similar for the low tumbling flow discharge ($Q=100$ l/s) with a slight tendency of the horizontal case to have higher water depths. This trend becomes more distinct as the discharge rises to $Q=178$ l/s and as the flow propagates downstream. For the rapid flow discharge $Q=200$ l/s (Figure 5.45) the water depths of the meandering case are clearly below those of the horizontal case.

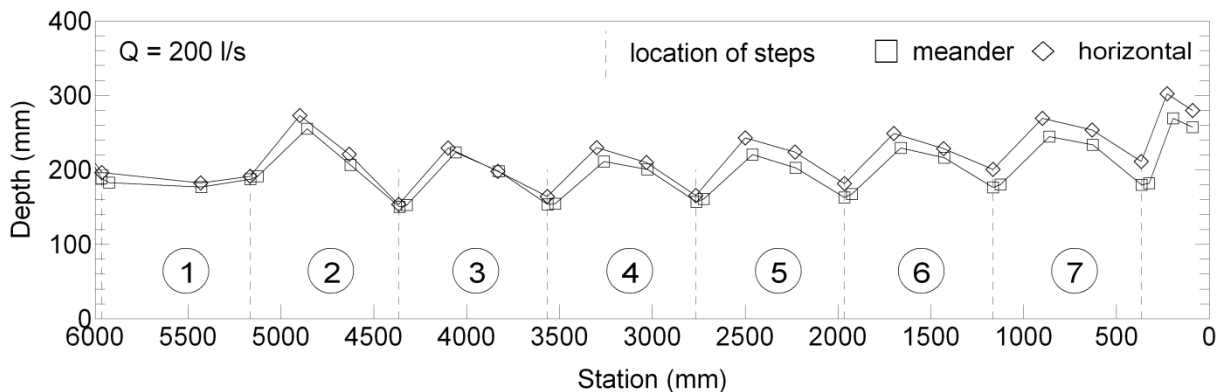


Figure 5.45 Comparison of mean water depths for horizontal and laterally Inclined Steps: I25_K8_L80, rapid flow

For all the measured discharges the streamwise velocities measured above the first (upper) step show a similar distribution for the two cases. Figure 5.46 illustrates this for the tumbling flow discharge $Q=100$ l/s (all other discharges see Appendix A.5).

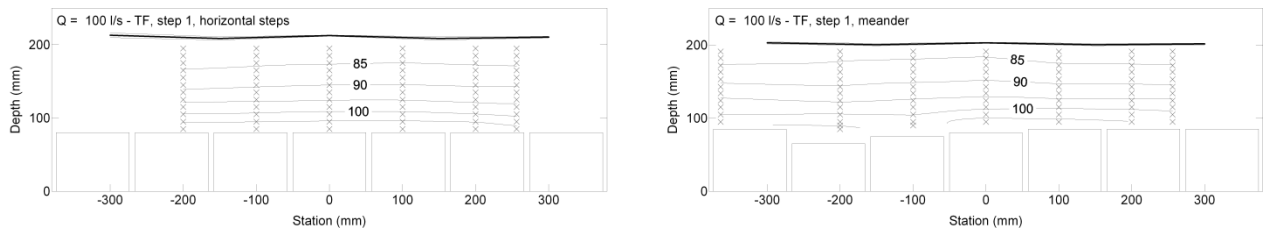


Figure 5.46 Comparison of streamwise velocities for horizontal and laterally inclined steps: I25_K8_L80, step 1

The streamwise velocity distributions above the fifth step differ for the two tested cases. While the horizontal steps typically have two (or more) velocity maxima per cross section the laterally inclined step of the meandering case seems to meld these maxima into a single one (Figure 5.47). To verify this assumption ADV-measurements were also performed for steps 4, 6 and 7 for the meandering case (see also Table 5.7). The results for step 4 & 6 support this assumption. Step 7 however yields two velocity maxima. This can be explained because of the vertical lamella at the downstream end of the flume which may have a flow straightening effect. A complete compilation of all ADV-measurements for these two cases can be found in Appendix A.6.

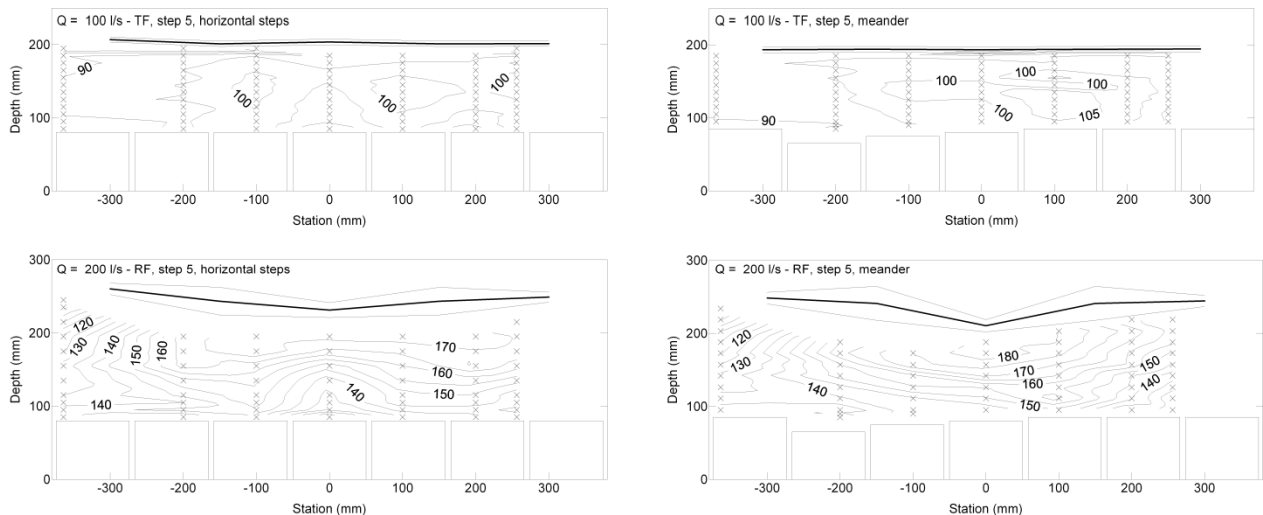


Figure 5.47 Comparison of streamwise velocities for horizontal and laterally inclined steps: I25_K8_L80, step 5

5.4.7 Step Spacing

For the mild slope the step spacing has an influence on the transitional discharge from tumbling flow to rapid flow. The larger the relative spacing the greater is the transitional discharge (chapter 5.4.8, pp. 158). For design purposes of step-pool ramps this finding suggests to use large relative spacings to keep the tumbling flow regime as long as possible. On the other hand the larger the step spacing the larger is the acceleration of the flow within the pools. As illustrated in Figure 5.48 b. for the largest tested step spacing $L = 933$ mm the minimum water depth in a pool equal the water depth of the flow without roughness elements. The same trend is valid for the spacing $L = 800$ mm. For the small spacings $L = 700$ mm (resp. 622 mm, see Figure 5.48 a.) the minimum water depth in a pool is well above the water depth without roughness elements. For the mild slope and for the rapid flow regimes these trends are similar.

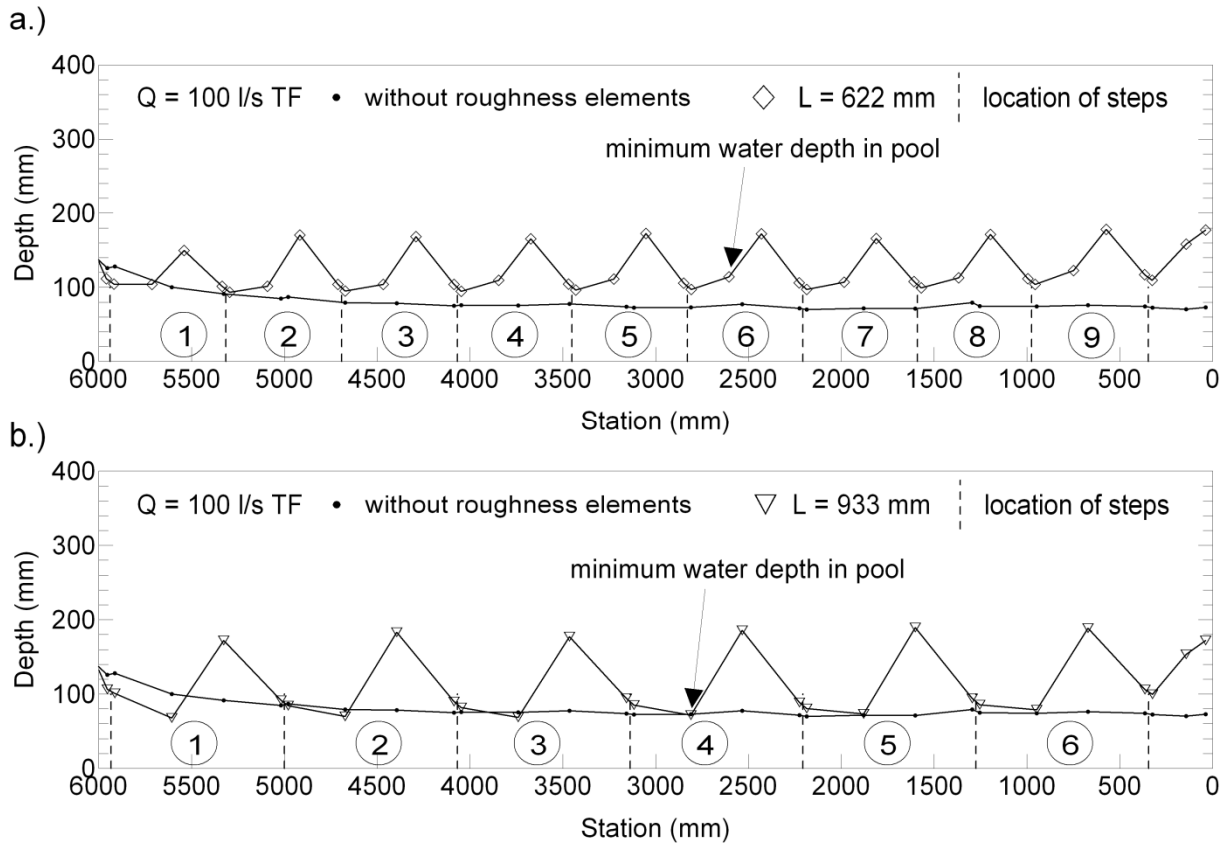


Figure 5.48 Pool water depths for variant I65-K8, rough bed: a.) $L = 622$ mm, b.) $L = 933$ mm, $Q = 100$ l/s, TF

For larger pool lengths the flow tends to attach to the pool bottom such that the main flow hits the downstream step instead of being swapped over the step. This way the unstable tumbling flow regime is prolonged. And illustrate the influence of the step spacing for the steep rough ramp with a roughness height $K = 80$ mm for the rapid flow discharge $Q = 170$ l/s. For the narrowest and the largest spacing two cross sections in the pools were measured with the ADV probe. For both cases the selected pools were located in the lowest part of the ramp (Figure 5.49).

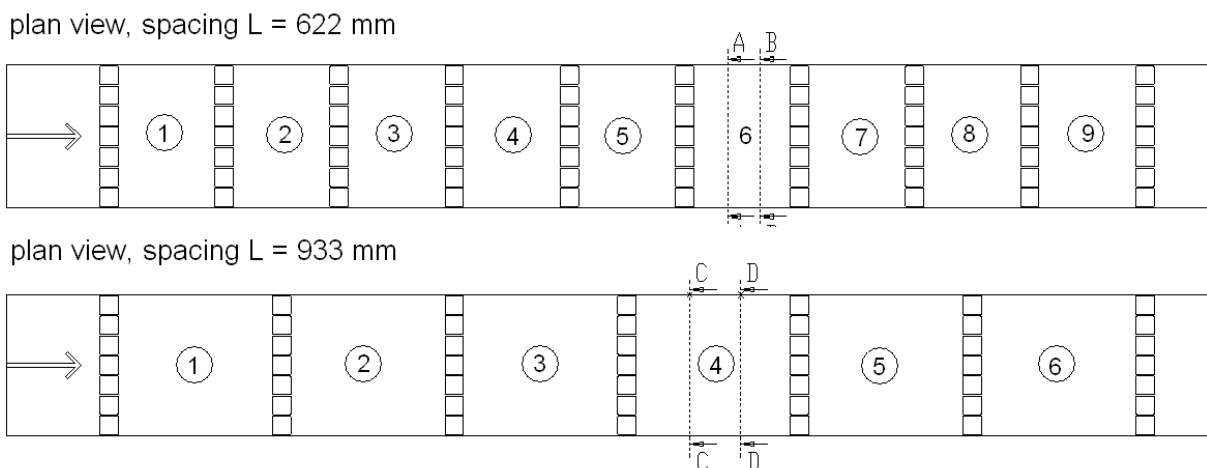


Figure 5.49 Location of pool cross sections A-A, B-B, C-C, D-D

For each streamwise velocity plot (Figure 5.50, Figure 5.51) the mean velocity is marked by a bold dashed line. Adjacent contour lines above this mean velocity have a distance of 5 cm/s. All contour lines below the mean velocity are labeled. For the narrow spacing $L = 622$ mm and both measured

cross sections the mean velocity is located approximately 50 mm above the pool bottom (Figure 5.50). The main flow is located above this mean velocity border. The same holds true for the cross section C-C of the wide spacing $L = 933$ mm (Figure 5.51, above). For the cross section D-D however the main flow attaches the pool bottom (Figure 5.51, below).

Like most step cross sections (cf. chapter 5.4.4) the pool cross sections display several flow maxima. This trend is more dominant for the wide spacing.

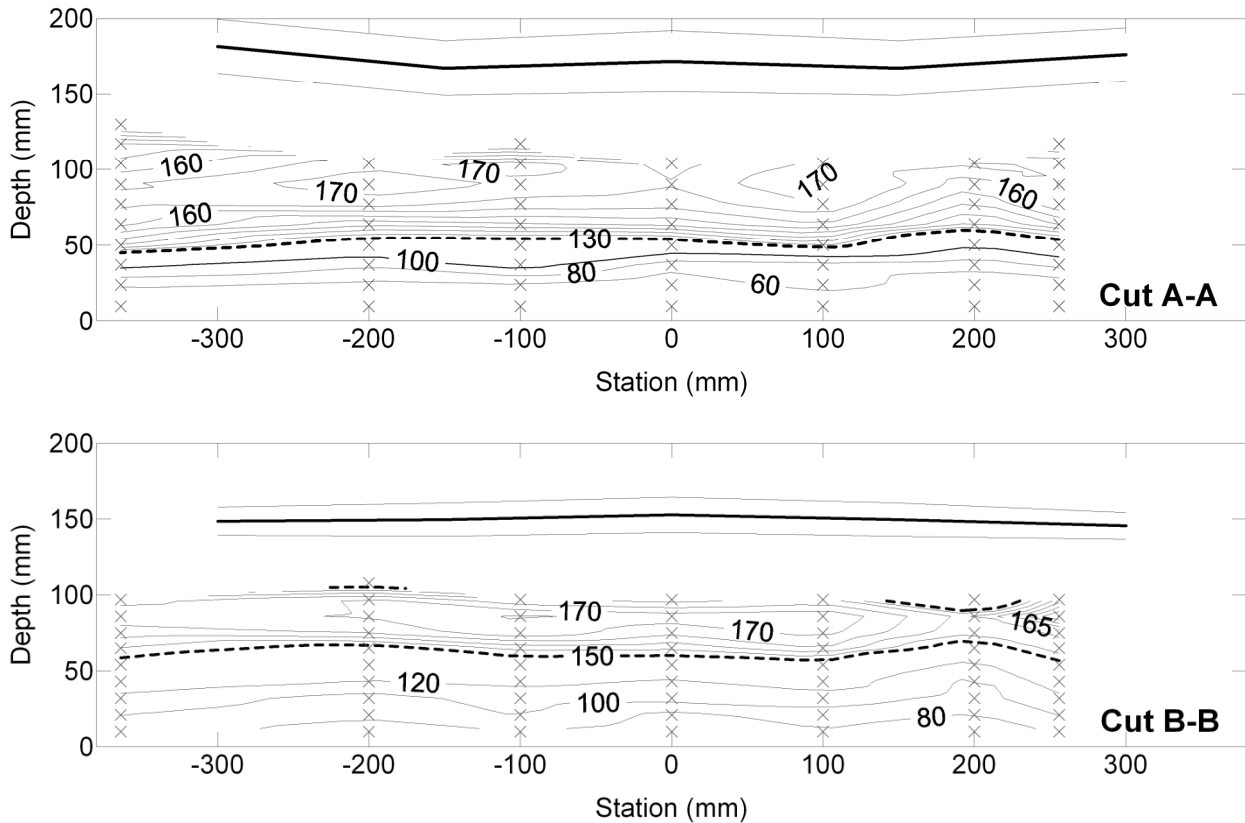


Figure 5.50 Velocity plots (cm/s) pool cross sections, narrow spacing: variant I65-K8-L62, rough bed, $Q = 170$ l/s, RF, cross sections A-A (above) and B-B (below) of step-pool unit 6

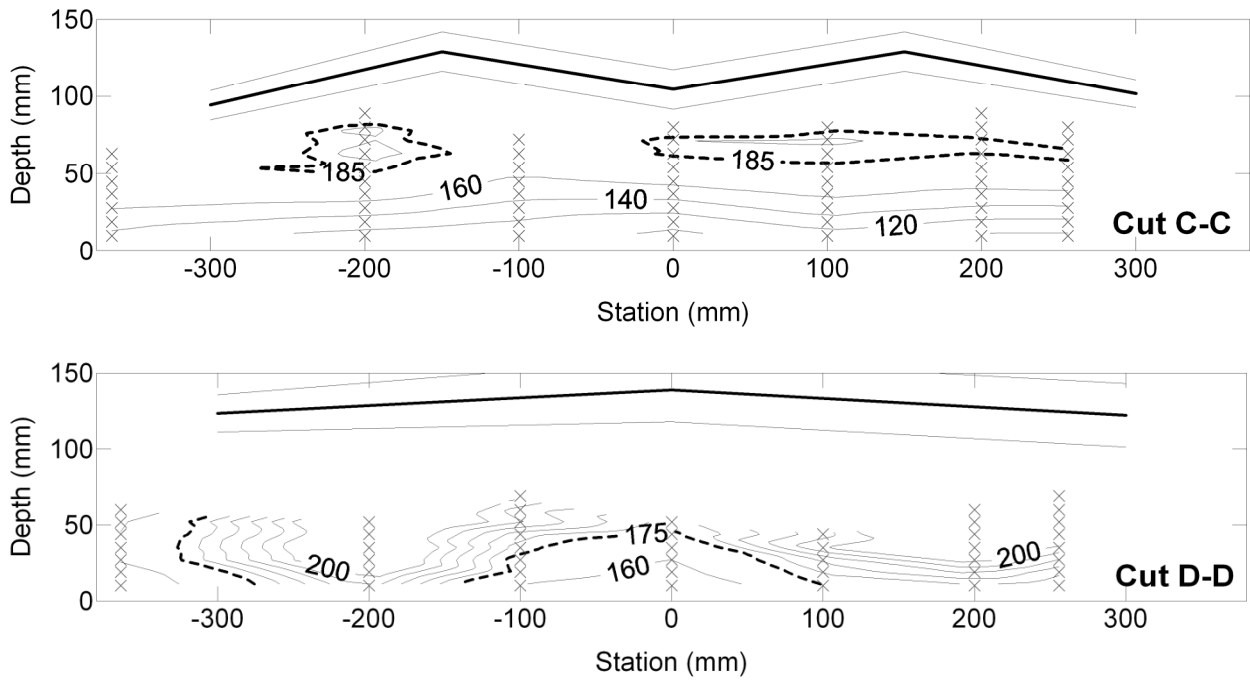


Figure 5.51 Velocity plots (cm/s) pool cross sections, wide spacing: variant I65-K8-L93, rough bed, $Q = 170$ l/s, RF, cross sections C-C (above) and D-D (below) of step-pool unit 4

Figure 5.52 illustrates the $u-w$ velocity vectors in $x-z$ plane, i.e. the streamwise and the vertical velocity components. Two vectors are plotted for each longitudinal station: a mean vector closest to the bottom and the mean vector of the measured region. For the mean bottom vector the average of the longest two vectors was chosen out of seven available bottom vectors. For the calculation of the mean vector the $U-W$ vectors are averaged in lateral direction for each vertical level. Then an average vector is calculated from the vertical mean vectors. In Figure 5.52 the mean bottom vector and the mean $U-W$ vector are plotted for the narrow and the wide spacing and both the tumbling flow and the rapid flow regime. The mean bottom vector has a higher vertical component than the mean vector. The vertical velocity component in the upper pool region is higher than the vertical component in the lower pool region. For the wide spacing and the rapid flow regime the magnitude of the $U-W$ vectors is considerably higher than for the narrow spacing.

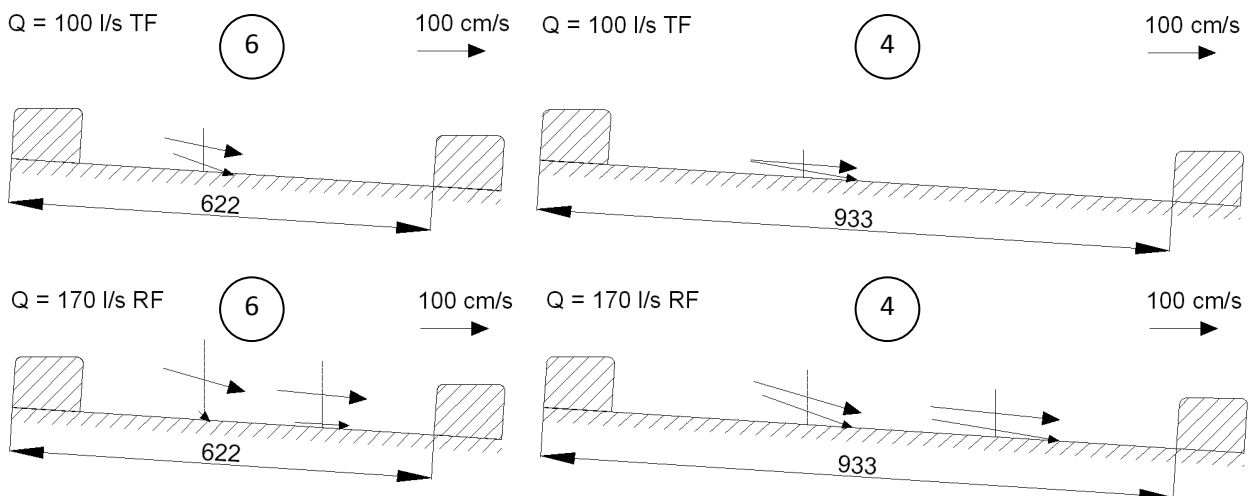


Figure 5.52 Velocity direction in $X-Z$ -plane: $l = 6.5\%$, $K = 80$ mm, rough bed; left: step-pool unit 6, narrow spacing; right: step-pool unit 4, wide spacing; tumbling flow (top); rapid flow (bottom)

5.4.8 Flow Transition from Tumbling to Rapid Flow

One major objective of the present flume study is to determine the flow transition from tumbling flow to rapid flow subject to the design parameter slope, step height and step spacing. In the experiments the flow transition could be determined clearly by visual inspection. For each ramp geometry the flow transitional discharge was determined three times to validate the result.

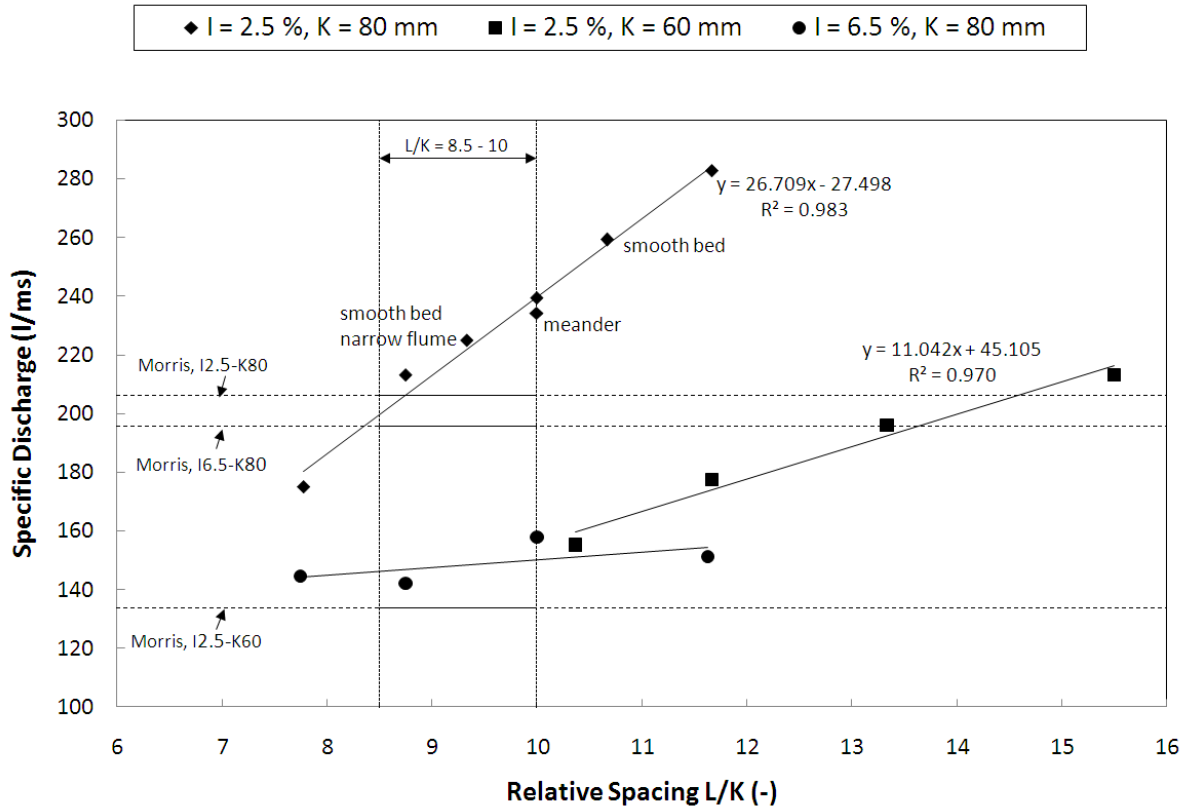


Figure 5.53 Flow Transition from Tumbling Flow to Rapid Flow

As described in detail in chapter 3.6.2, pp. 67 Morris (1969) provides a formula for the flow transition subject to the slope and the step height. The formula is independent of the relative spacing. To prevent undesired roll waves the recommended relative spacing should be in the range of $8.5 \div 10$.

In Figure 5.53 the flow transitional discharges of the present flume test are illustrated subject to the relative spacing and compared against Morris' flow transitional formula. In contrast to Morris' findings the experimental results show a clear linear dependence of flow transition and relative spacing for the mild slope $I = 2.5\%$. The slope of the linear function is steeper for step height $K = 80\text{ mm}$ than for $K = 60\text{ mm}$. This means that the flow transitional discharge cannot be described by the relative spacing alone. A criterion must also include the step height. For step height $K = 80\text{ mm}$ the linear function intersects Morris' constant criterion within the recommended relative spacing range. For step height $K = 60\text{ mm}$ all tested relative spacings are higher than recommended by Morris. The linear function extrapolated backwards intersects Morris' flow transitional discharge at $L/K = 8$ which is below Morris' recommendation. For the mild slope the flow transition occurs in a well-defined small range of discharges ($\pm 2.5\text{ l/sm}$).

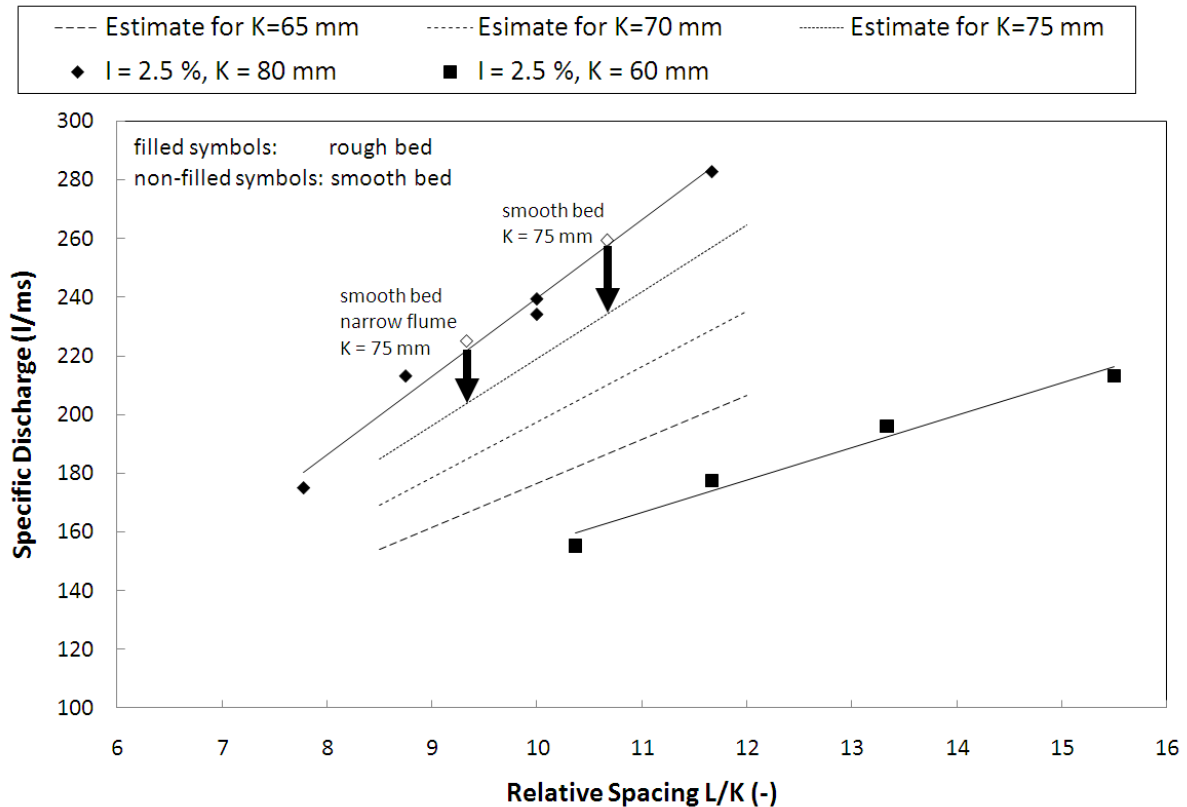


Figure 5.54 Flow Transition for Rough and Smooth Bed

For the mild slope it seems that the smooth bed variants fit perfectly into the rough bed variants. As pointed out in chapter 5.4.5, pp. 151 also the water depths match (Figure 5.40, Figure 5.41). One has to consider though, that the effective step height K of the smooth bed is 5 mm smaller than that of the rough bed variant, i.e. $K=75$ mm and $K=80$ mm for the smooth and the rough bed, respectively. In Figure 5.54, the function of the specific discharge subject to the relative spacing is estimated for the step heights $K=65$, 70 and 75 mm. According to these estimated lines the flow transition for the step height $K=75$ mm should occur on a lower discharge. This is an interesting result. One might have guessed that the flow transition for the rough bed occurs on higher discharges than for the smooth bed because of an increased energy dissipation due the higher near-bed turbulence. This near-bed turbulence must be responsible for the different behavior, but its effect on the flow transition is the opposite way round: The results suggest that the near-bed turbulence reduces the effective flow area, so the flow transition occurs on smaller discharges for the rough bed (cf. chapter 5.4.11, Figure 5.68).

For the steep slope the relative spacing does not seem to have a large effect on the flow transition. This is consistent with Morris' results. The flow transitional discharge however lies well below Morris' prediction. The flow transition for the steep slope occurs over a wide range of discharges (± 25 l/sm).

5.4.9 Flow Transition from Rapid to Tumbling Flow – Hysteresis

As described in chapter 5.4.3 the flow transitional discharge underlies a hysteresis effect, i.e. the transition from tumbling flow to rapid flow (TF2RF) occurs on higher discharges than the transition from rapid flow to tumbling flow (RF2TF).

Figure 5.55 illustrates the hysteresis effect by displaying both transitional discharges TF2RF and RF2TF.

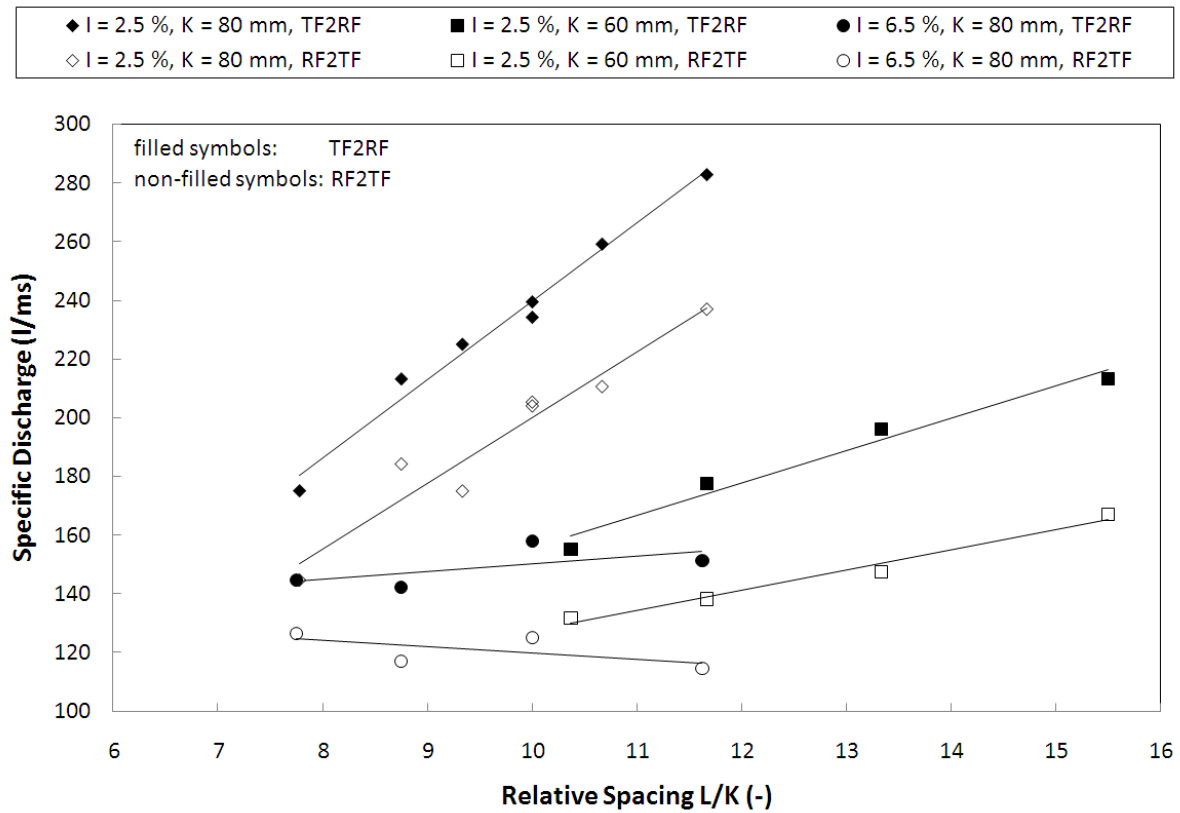


Figure 5.55 Flow Transition Underlies Hysteresis, Flow Transition TF2RF and RF2TF

Variant	bed, meander	L/K (-)	TF2RF		RF2TF	
			Q(l/s)	q(l/sm)	Q(l/s)	q(l/sm)
I25_K6_L62	rough	10.4	118	155	100	132
I25_K6_L70	rough	11.7	135	178	105	138
I25_K6_L80	rough	13.3	149	196	112	147
I25_K6_L93	rough	15.5	162	213	127	167
I25_K8_L62	rough	7.8	133	175	110	145
I25_K8_L70	rough	8.8	162	213	140	184
I25_K8_L80	rough	10.0	182	239	155	204
I25_K8_L80	smooth	10.7	197	259	160	211
I25_K8_L80	rough, meander	10.0	178	234	156	205
I25_K8_L93	rough	11.7	215	283	180	237
I65_K8_L62	rough	7.8	110	145	96	126
I65_K8_L70	rough	8.8	108	142	89	117
I65_K8_L80	rough	10.0	120	158	95	125
I65_K8_L93	rough	11.6	115	151	87	114

Table 5.11 Flow transitional discharges of all wide flume experiments in tabular form

5.4.10 Flow Transition and Slope – Narrow Flume Experiments

To get a picture of what happens for slopes between the mild and the steep slope ($I = 2.5\%$ and $I = 6.5\%$, respectively) additional experiments were performed in a narrow tilting flume of 12 m length, 0.2 m width and 0.5 m height.

The experiments in the narrow flume cover two objectives:

1. Up to which slope can the critical flow depth over the steps be preserved?
2. (How) does the flow transitional discharge change subject to the slope?

The flume can only be tilted up to 3.16%. Therefore a ramp with a slope of 2% and a length of 7 m was installed in lower part of the flume with the same plastic panels as for the wide flume. To prevent sudden changes in the flume bed an adversely sloped 0.5 m long section connects the flume bed with the upstream end of the ramp. The ramp inside the flume could not be built with a higher slope because of the flume height restriction. Roughness elements $K = 75$ mm were installed at a spacing $L = 700$ mm. For each step one roughness element was mounted in the flume axis. Two roughness parts of 40 mm width each were glued to the left and right side. Altogether 10 steps were installed. Starting from a slope $I = 2.5\%$ the slope was increased successively by 0.5%. Instead of 5% the maximum possible slope $I = 5.16\%$ was investigated. The experimental procedure for each tested slope was as follows:

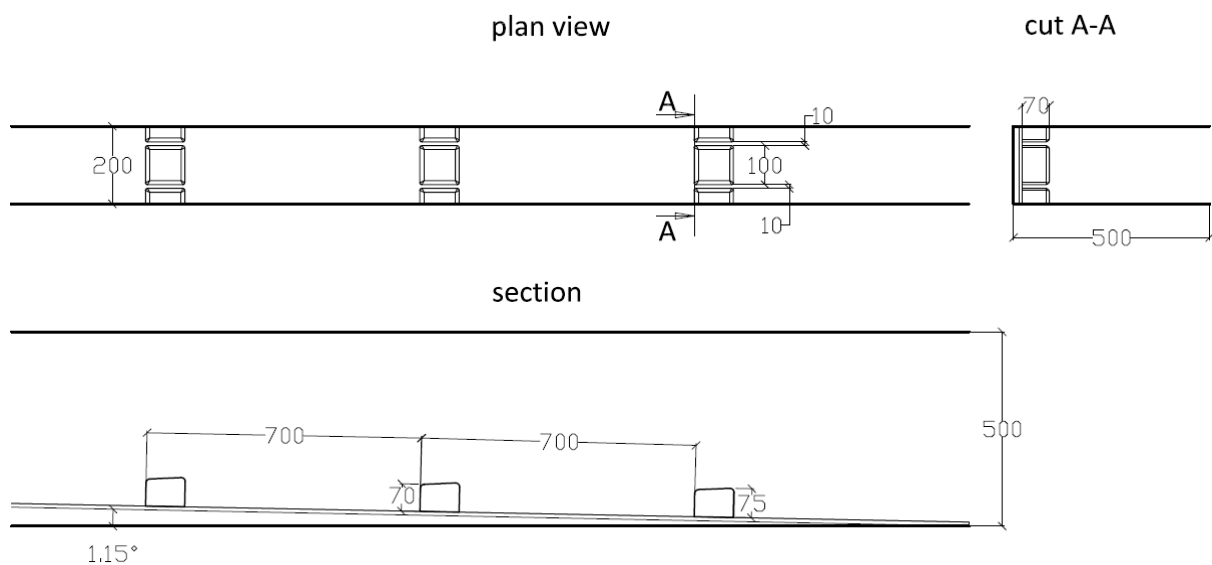


Figure 5.56 Cut-out of the lower part of the narrow flume (dimensions in mm)

1. Find the flow transitional discharges TF2RF and RF2TF
2. Select the discharge $q_1 = 0.132 \text{ m}^2/\text{sm}$ (this discharge corresponds to a total discharge of 100 l/s in the wide flume experiments)
3. Select a tumbling flow discharge q_2 as close to TF2RF as possible
4. For the discharges q_1 and q_2
 - a. Measure the water depth for step 5, 6 and 7 at the upstream face and the downstream face of the step with a point gauge
 - b. Take a picture of one step-pool sequence
5. For q_2
 - a. Find the location of the water surface trough
 - b. determine the water surface wave amplitude

$I(\%)$	$Q(l/s)$	$q(m^2/s)$	y_1/y_c	$y_c(cm)$	$y_1(cm)$	$y_2(cm)$
2.5	40.0	200.0	1.061	16.0	17.0	15.5
3.0	38.0	190.0	1.018	15.4	15.7	14.5
3.5	35.0	175.0	0.989	14.6	14.5	13.3
4.0	33.0	165.0	0.965	14.1	13.6	12.2
4.5	32.0	160.0	0.958	13.8	13.2	11.8
5.1	30.0	150.0	0.904	13.2	11.9	10.8
6.5 ⁺	100.0	0.132	0.845	12.1	10.2	9.8

⁺ Result from the wide flume experiments

Table 5.12 Narrow Flume Experiments: Normalized Control Depth y_1/y_c , critical depth y_c , control depth y_1 above upstream face, depth y_2 above downstream face

As can be seen from Table 5.12 the normalized control depth y_1/y_c decreases with rising slope and drops below 1 for $I > 3.0\%$. These results are consistent with the measured water depth in the wide flume for $I = 6.5\%$

Before the beginning of the narrow flume experiments there was the concern that due to the small flume width wall effects might be more dominant than for the wide flume experiments. Surprisingly enough the wall effects are negligible as can be seen from Figure 5.53. For the slope $I = 2.5\%$ the flow transition from tumbling to rapid flow in the narrow flume fits nicely into the results for the wide flume experiments.

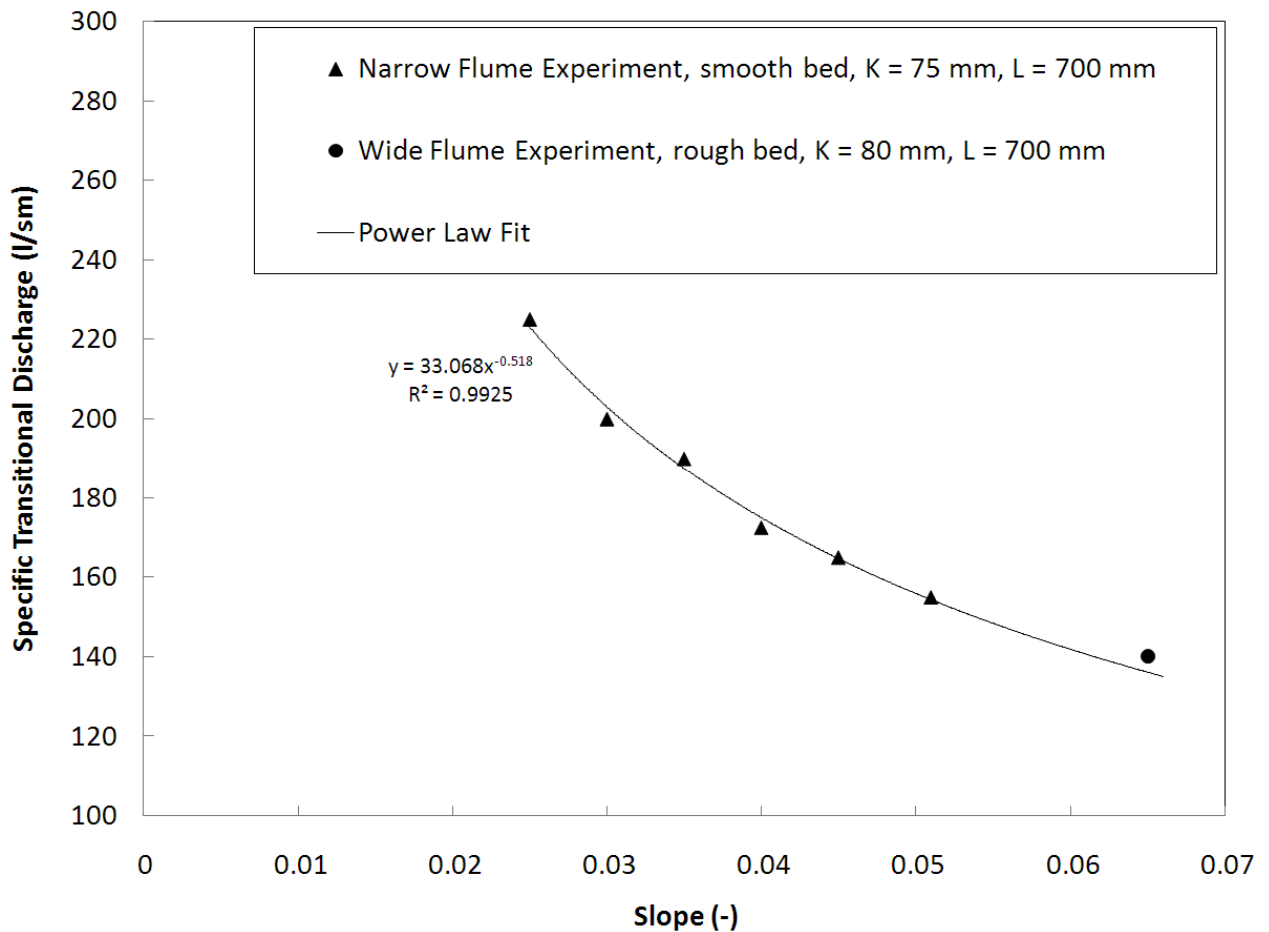


Figure 5.57 Flow Transition and Slope, Narrow Flume, $K = 75\text{ mm}$, $L = 700\text{ mm}$

Figure 5.57 illustrates that there exists a power law relationship between flow transitional discharge and slope for step height $K = 75$ mm, step spacing $L = 700$ mm and a smooth bed in the narrow flume. Also displayed in Figure 5.57 is the flow transitional discharge for step height $K = 80$ mm, spacing $L = 700$ mm, slope $I = 6.5$ % and a rough bed in the wide flume. Although the displayed power law fit was applied only for the narrow flume results the wide flume result integrates well into the calculated power law.

5.4.11 Flow Transition and Antidunes

As described in chapter *Formation of step-pool systems* (p. 43) there is an ongoing scientific discussion whether the formation of natural step-pool systems can be explained with the aid of the antidunes model. Although this thesis does not contribute to this discussion antidunes and large roughness elements have several things in common: Antidunes are characterized by a wavy bedform and a wavy water surface of a certain wave length. Despite the absence of a wavy bed form the constant step spacing of the large roughness elements induces a wavy surface which has a wave length equal to the step spacing as long as the tumbling flow regime is preserved (Figure 5.58). Moreover there is a strong resemblance between the flow patterns for 3D-antidunes and the rapid flow discharge of the present step-pool flume test. It seemed worth to take a closer look at these similarities.

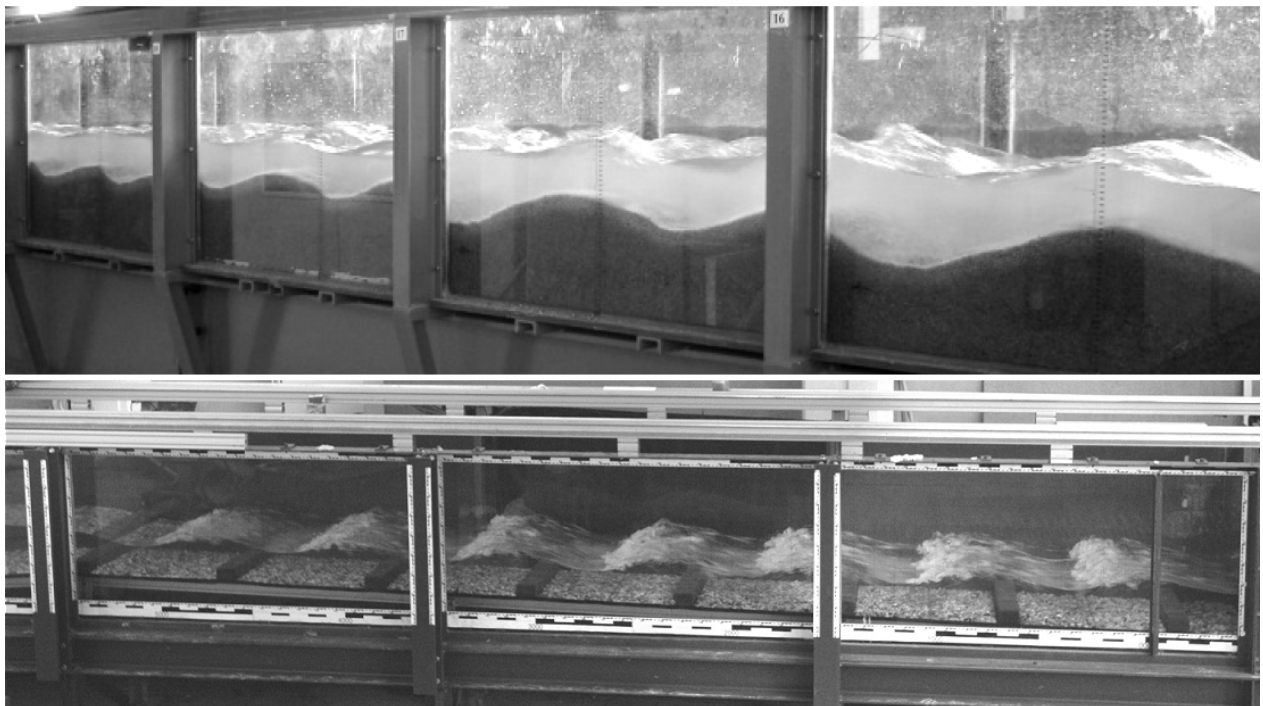


Figure 5.58 Flow Pattern 2D-antidunes (Núñez-González, Martín-Vide 2010) (top) – Tumbling Flow for variant: I25-K6-L80, rough bed, $Q = 145$ l/s (bottom), flow from left to right for both pictures



Figure 5.59 Flow Pattern 3D-Antidunes (Núñez-González, Martín-Vide 2010) (left), Rapid Flow for variant: I25-K8-L80, rough bed, flow from background to foreground for both pictures

Figure 5.59 (left) illustrates the flow pattern of 3D antidunes. A train of rooster tails in the flume axis is clearly visible. The right picture illustrates the flow over a step pool ramp of the present wide flume experiments. It has been flipped vertically for a better comparability with the antidunes picture. Slope, step height, step spacing and discharge are 2.5 %, 80 mm, 800 mm and 162 l/s, respectively. The rooster tails in the flume axis are not as spiky and pronounced as for the antidunes. Nonetheless the shape of the water surface is quite similar.

In his standard work on antidunes and stationary waves Kennedy (Kennedy 1961) provides a criterion to distinguish 2D from 3D antidunes which is derived from potential flow theory. At the transition from 2D to 3D antidunes the mean velocity v can be expressed in terms of the mean wave length L of the antidunes (equation 5-8). The corresponding critical Froude number for the transition from 2D to 3D antidunes subject to wave length L and the mean water depth \bar{y} is given by equation 5-9.

Wave Length – Velocity Relation

$$v = \sqrt{\frac{g \cdot L}{2 \cdot \pi}} \quad (\text{m/s}) \quad 5-8$$

Critical Froude number

$$\text{Fr}_c = \sqrt{\frac{L}{2 \cdot \pi \cdot \bar{y}}} \quad (-) \quad 5-9$$

In their experimental work on antidunes Núñez-González & Martín-Vide (2010) find a good agreement to the above equation.

The present flume results were evaluated to check the following assumption:

Equation 5-9 can be applied to determine the flow transition from tumbling flow to rapid flow where L corresponds to the step spacing.

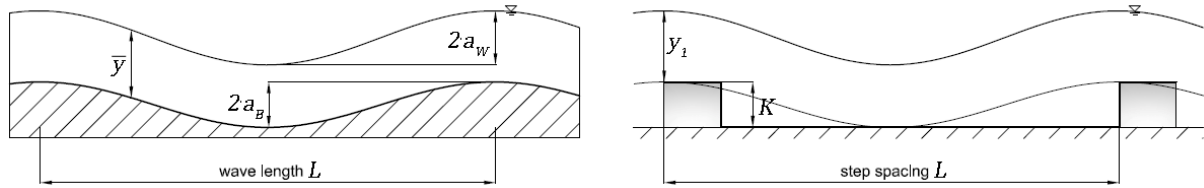


Figure 5.60 Defining parameter antidunes (left) and large roughness elements (right)

Indeed, the defining parameters for antidunes and large roughness elements are similar (Figure 5.60). The wave length of the antidunes L corresponds to the step spacing L of the large roughness elements. The doubled wave amplitude of the wavy bed $2 \cdot a_B$ corresponds to the step height K .

For each step-pool variant (given by L, K and L) and each tested discharge the mean water depth \bar{y} was calculated for each step-pool unit as follows:

$$\bar{y} = \frac{y_{step} \cdot L_{step} + y_{pool} \cdot (L - L_{step})}{L} \quad 5-10$$

y_{step} and y_{pool} are calculated according to Figure 3.1 where y_1 to y_4 are the water depths averaged over the four lateral water depth measurements.

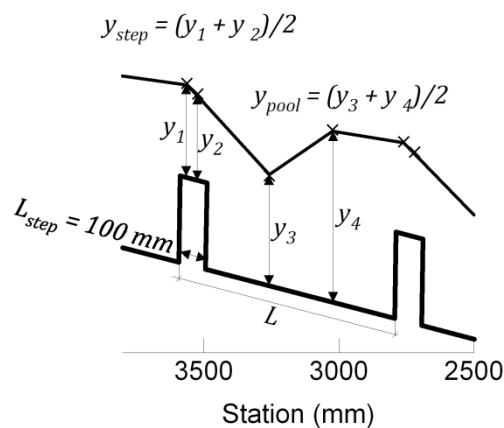


Figure 5.61 Calculation of Mean Water Depth for Each Step Pool Unit from Experimental Results

From Figure 5.62 it follows that equation 5-9 is appropriate to distinguish the tumbling flow regime from the rapid flow regime. A closer look at the results (Figure 5.63) reveals that there are some step-pool units in the tumbling flow regime that are classified as being in the rapid flow regime by equation 5-9 and vice versa.

All incorrectly assigned step-pool units concern discharges in the instable flow regime, i.e. discharges that may be manipulated manually to either of the two flow regimes. Three of the tumbling flow step-pool units that are assigned incorrectly to the rapid flow regime are the first step-pool units which typically have the lowest trough of the water surface and thus higher velocities. Almost all step-pool units of variant I65-K8-L62, rough bed, are close to the border line but nonetheless on the wrong side of it. All mismatched rapid flow step-pool units are located in the lower part of the ramp. Roll waves at a high amplitude are present which dissipate a lot of energy such that the energy level above these lower steps is similar to that of the tumbling flow regime.

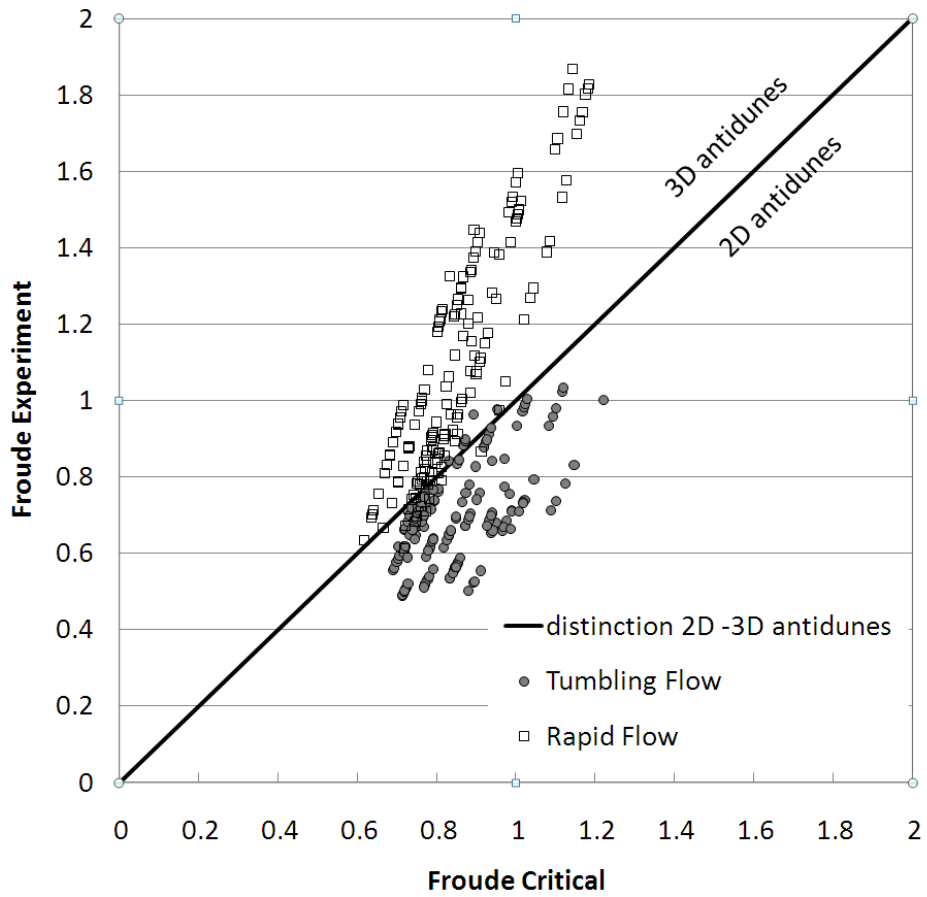


Figure 5.62 Tumbling flow and rapid flow regime for each step pool unit

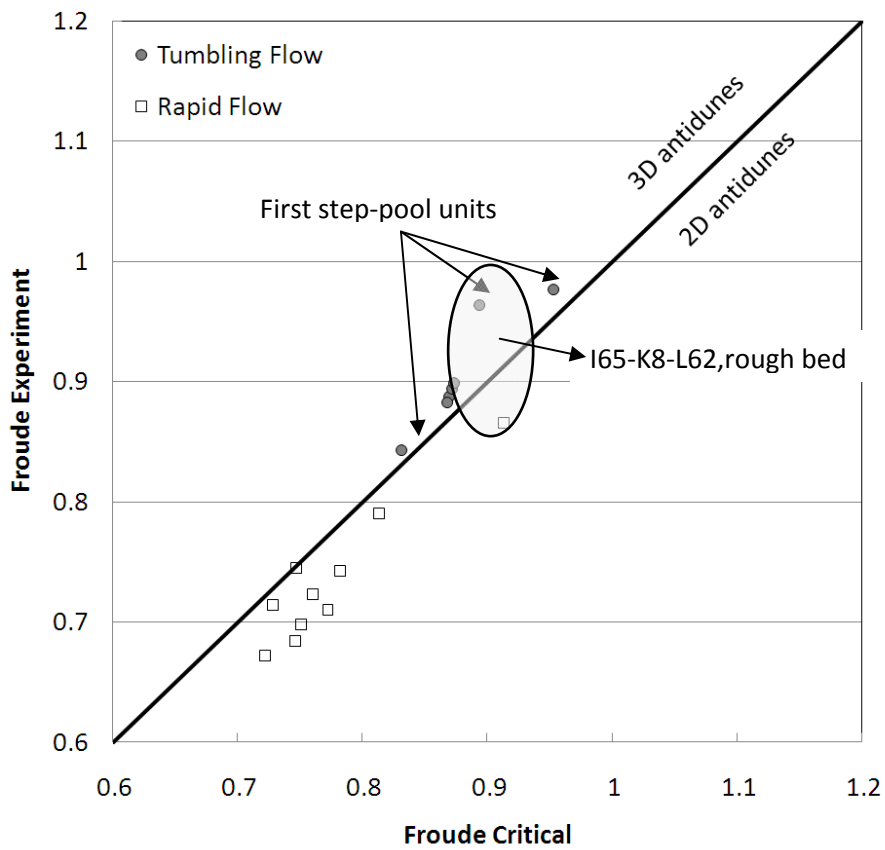


Figure 5.63 Detail of Figure 5.62, experimental flow regime incoherent with theoretical classification

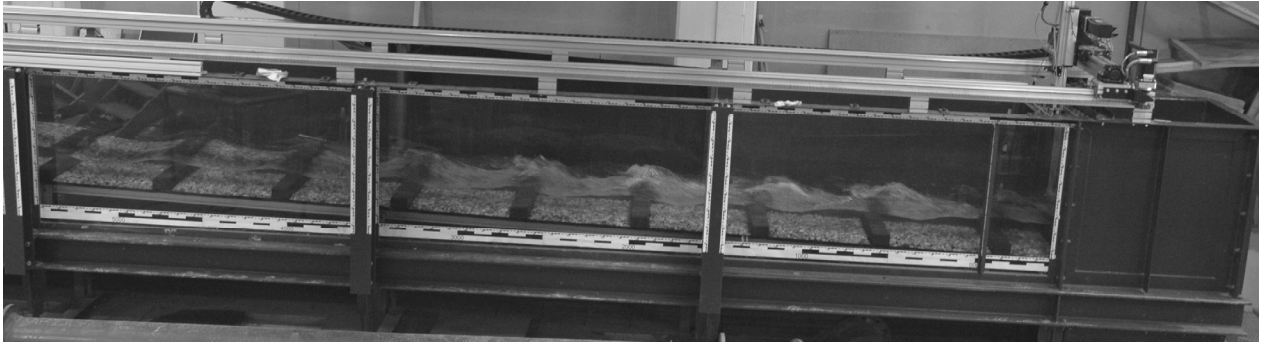


Figure 5.64 Experimental flow regime incoherent with theoretical classification: roll waves in the lower part of the ramp

The objective of the present flume test was to find a functional relationship of the flow transitional discharge q subject to I , K and L . The above considerations suggest that equation 5-9 is appropriate to distinguish the tumbling flow from the rapid flow regime. This is not yet the solution to the problem because it only shifts the question of finding the appropriate discharge to finding the mean water depth \bar{y} subject to I , K and L . Moreover, equation 5-9 neither contains I nor K .

Figure 5.65 illustrates how the step height K and the water surface wave amplitude a_w are related. While the wave length of the water surface equals the step spacing throughout all tumbling flow discharges the doubled wave amplitude approaches the step height as the discharge approaches the flow transitional discharge. The surface wave crest and trough move towards the step and the middle of the pool, respectively.

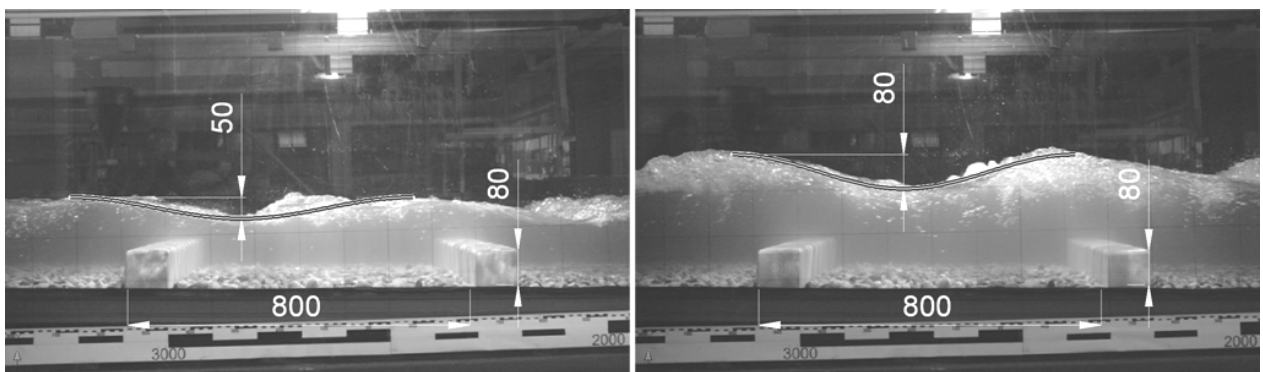


Figure 5.65 Surface wave amplitude and step height for variant I25-K8-L80, rough bed: $Q = 75$ l/s (left), $Q = 175$ l/s (right), flow transitional discharge: $Q = 182$ l/s

If this observation is generalized the mean water depth \bar{y} for the flow transition can be expressed as:

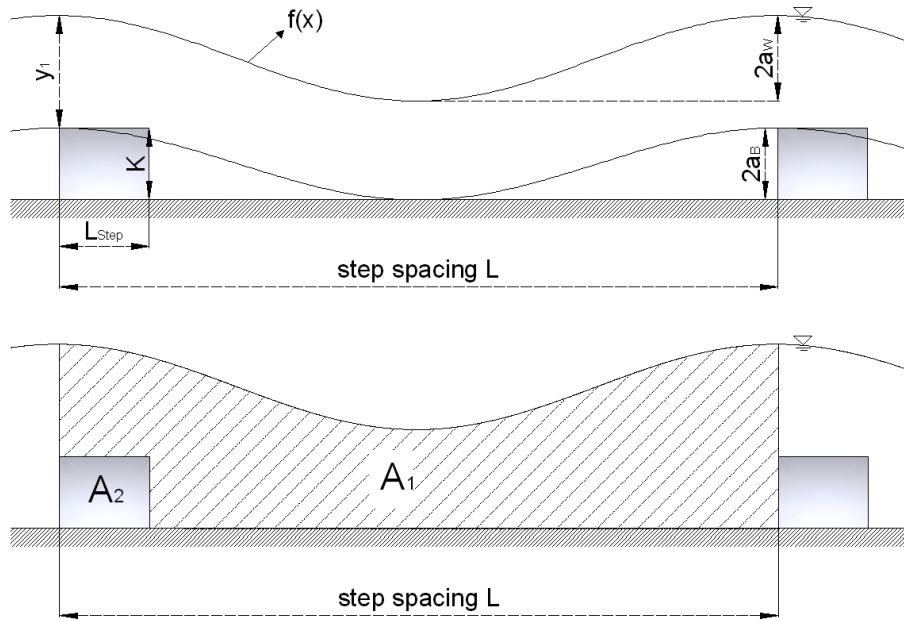


Figure 5.66 Flow Pattern and Mean Water Depth at Flow Transition

$$f(x) = K + y_1 - a_W + a_W \cdot \cos \frac{2\pi x}{L}$$

**Mean water
depth at flow
transition**

$$\begin{aligned} \bar{y} &= \frac{1}{L}(A_1 - A_2) = \frac{1}{L} \left(\int_0^L f(x) dx - L_{Step} \cdot K \right) & \text{5-11} \\ &= K + y_1 - a_W - L_{Step} \cdot K \cdot \frac{1}{L} = y_1 - a_W + K \cdot \frac{L - L_{Step}}{L} \end{aligned}$$

For the flow transitional discharge $a_B = a_W$. If y_1 is expressed as a multiple of the critical depth y_c , i.e. $y_1 = c \cdot y_c$, then the flow transitional discharge $q_{crit} = \bar{y} \cdot v$ for a rectangular channel with a geometry as in Figure 5.66 satisfies the following relationship (using equations 5-8, 5-11):

**flow
transitional
discharge**

$$q_{crit} = \left(c \cdot \sqrt[3]{\frac{q_{crit}^2}{g}} - a_W + K \cdot \frac{(L - L_{Step})}{L} \right) \cdot \sqrt{\frac{g \cdot L}{2 \cdot \pi}} \quad \text{5-12}$$

Equation 5-12 is a cubic function in implicit form. Unknown variables are the coefficient c and the water wave amplitude a_W . As a default value for a_W one can assume that for the flow transitional discharge the water wave amplitude equals the bed amplitude (cf. Figure 5.65), hence $a_W = a_B = K/2$. As described in chapter 5.4.2 the coefficient c depends on the slope, hence $c = c(I)$. The multiple c can be regarded as the dimensionless control depth y_1/y_c . The coefficients c of the narrow and the wide flume results are consistent. Figure 5.67 illustrates the c -values for all tested variants. For each variant water level measurements are available for two tumbling discharges. The discharge closest to the flow transitional discharge was selected to calculate y_1 and c . An empirical equation is derived from the results. Two outliers of c affect two variants with high relative spacings (Figure 5.67). To simplify matters a linear approach is used to calculate c subject to the slope although the results suggest that $c(I)$ satisfies a logarithmic function. The linear approximation is chosen such that it yields a lower limit of c , this way underestimating the transitional discharge rather than overestimating it.

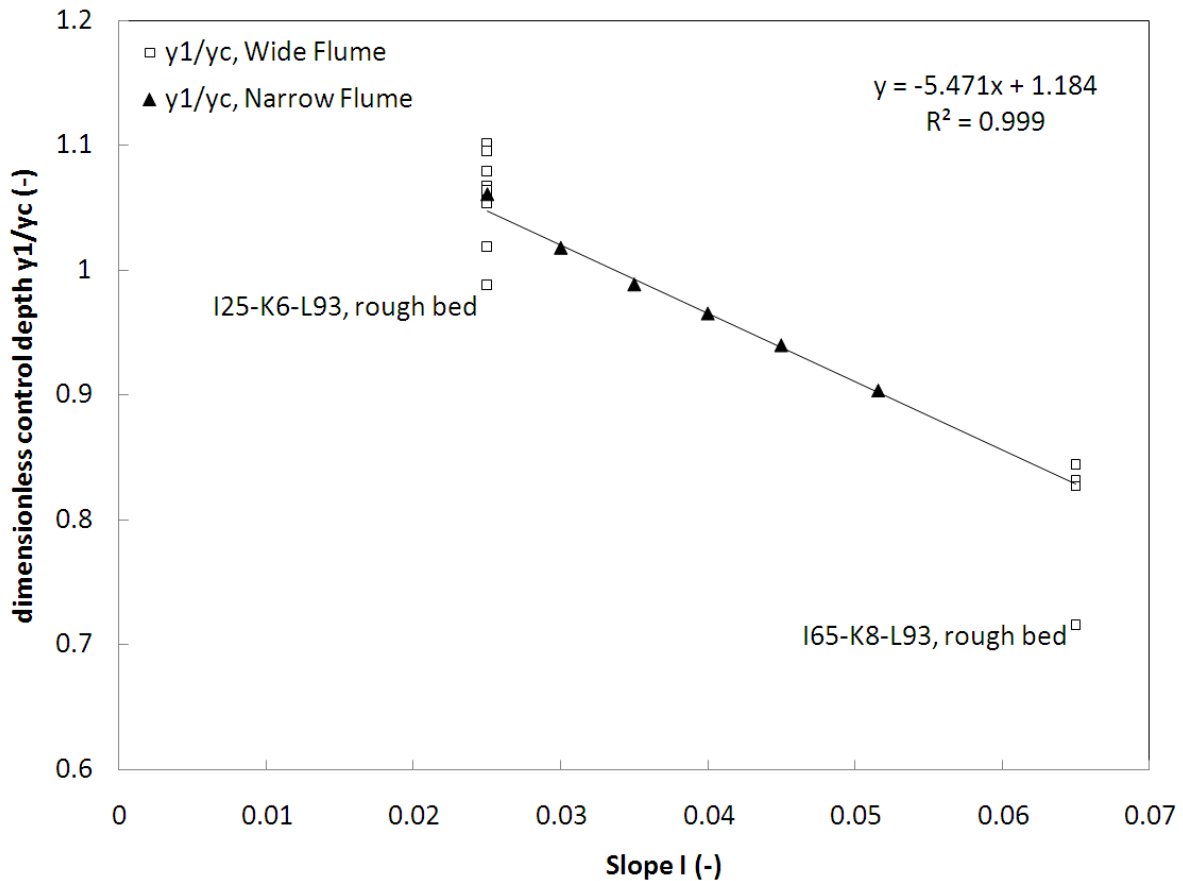


Figure 5.67 Linear Approximation for the Dimensionless Control Depth y_1

**Empirically derived
multiple c of y_c**

$$c(I) = 1.184 - 5.471 \cdot I \quad \mathbf{5-13}$$

Estimate for a_w

$$a_w = K/2 \quad \mathbf{5-14}$$

Figure 5.68 illustrates the experimental and the calculated transitional discharge for all tested variants. The flow transitional discharge is calculated from equation 5-12 using c and a_w as given by equations 5-13 and 5-14, respectively. Apart from the two variants where the c -values do not fit equation 5-13 there is a good agreement between calculated and the experimental discharge. In Figure 5.68 equation 5-12 (with c and a_w as given by equations 5-13 and 5-14) is also contrasted with experimental results from Morris' investigations (Morris 1968). In general Morris' focus was on steep slopes $> 30\%$ but there are some results available for the slope $I = 5\%$. The transitional discharge was determined for two relative spacings $L/K = 8.5$ and 10 for the step heights $K=0.5, 1, 1.25, 1.5$ and 2 inch, i.e. $K=12.7, 25.4, 31.8, 38.1$ and 50.8 mm, respectively. Other than in the present flume study the step length in Morris' investigation equals the step height, i.e. $L_{Step} = K$. Although Morris' geometry deviates from the present flume test and the step heights are significantly smaller than the minimum step height $K = 60$ mm of the present study, Morris' experimental results match the calculated discharge well.

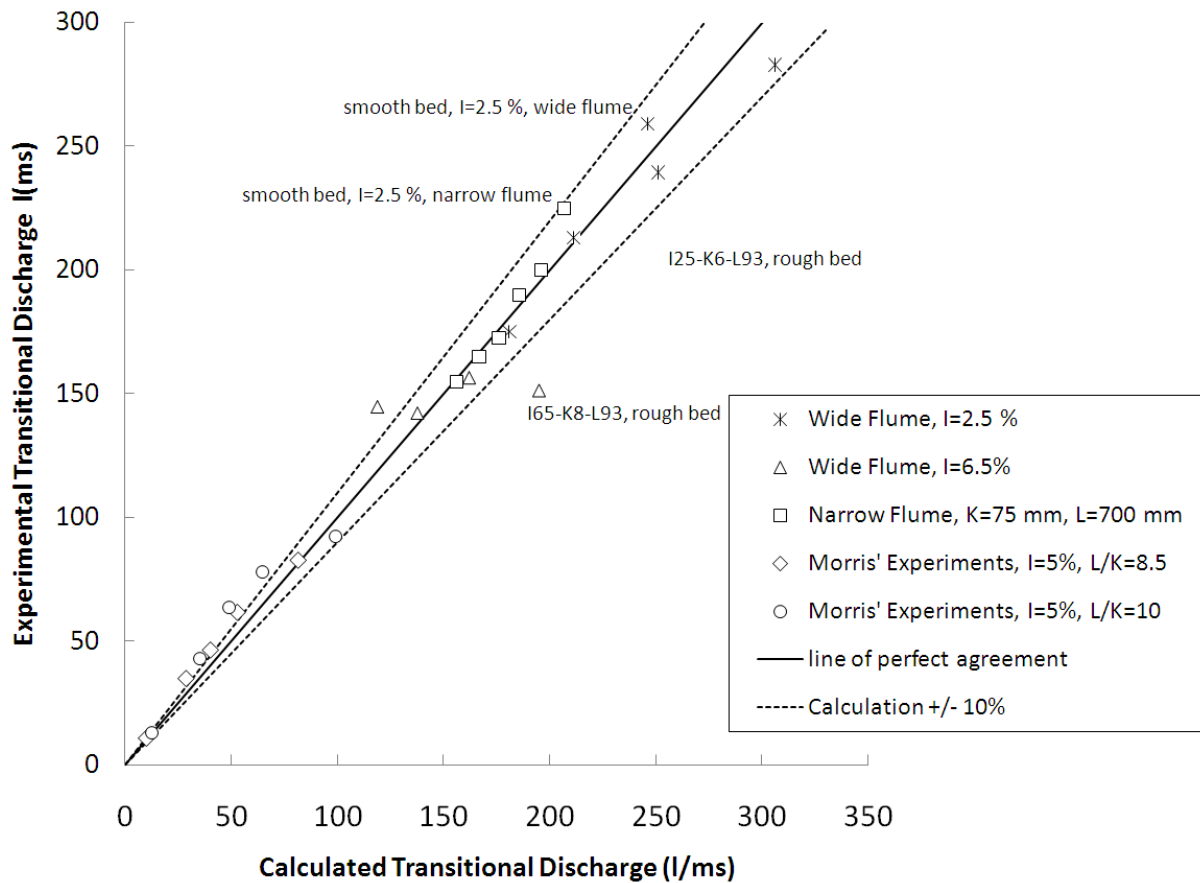


Figure 5.68 Calculated vs Experimental Transitional Discharge (Equation 5-12)

It should be noted the equation 5-12 tends to overestimate the flow transitional discharge for the mildly sloped rough bed variants although the calculated estimates for $c(I)$ and a_w are lower than the experimental counterparts. In other words, if the experimental values for $c(I)$ and a_w were inserted into equation 5-12 the calculated discharge would be even larger. On the other hand, for the smooth bed variants, equation tends 5-12 to underestimate the flow transitional discharge. One possible explanation could be that the rough bed causes so much near-bed turbulence that the effective flow area is reduced (cf. Figure 5.54).

5.4.12 Pressure Measurements

Experimental Setup

The pressure measurements were performed for a single ramp configuration: I65_K8_L62, rough bed. The roughness element containing the pressure transducers was located in the middle of the 7th step (Figure 5.69). Different locations of the 14 available pressure transducers on the roughness element were tested in preliminary experiments.

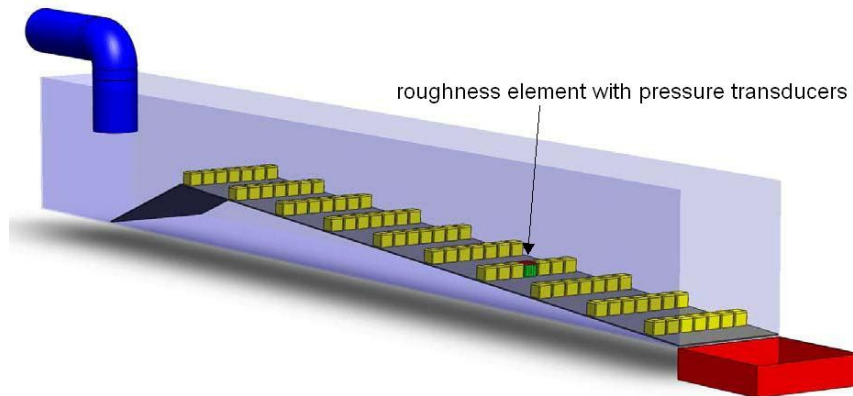


Figure 5.69 Location of the roughness element with the pressure transducers in the flume

For the main experiments the transducers were positioned as illustrated in Figure 5.70. Above the center of the roughness element (sensor number 13 Figure 5.70) an ultrasonic probe (Honeywell, 947-F4V-2D-1C0-300E) was placed to record the water level simultaneously with the pressure measurements. Before each test run the distance of the ultrasonic probe to the roughness element (without water) was determined to be able to calculate the water depth h_{step} .

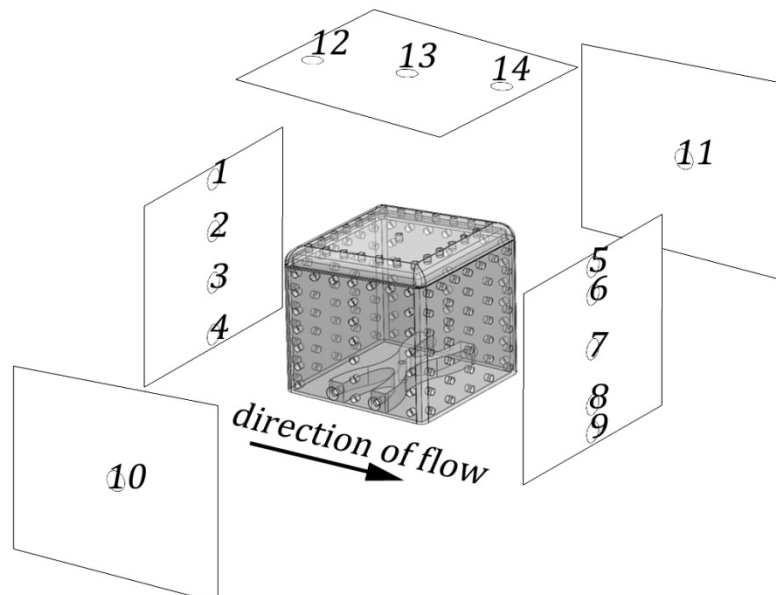


Figure 5.70 Location of the 14 pressure transducers on the roughness element

The ramp with the pressure roughness element was exposed to different flow regimes (Table 5.13, cf. Figure 5.33). The scale factor of the model is 10. The total model discharge Q_M (l/s) thus corresponds to a specific prototype discharge q_p (m^3/sm)

Specific prototype discharge

$$q_P = \frac{Q_M}{0.76 \cdot 1000} \cdot 10^{3/2}$$

5-15

where 0.76 m is the flume width.

	Flow Regime r	Q_M (l/s)	q_P (m ³ /sm)
1	Tumbling Flow	75	3.1
2	Instable Tumbling Flow ⁺	110	4.6
3	Instable Rapid Flow ⁺	110	4.6
4	Rapid Flow	150	6.2
5	Stable Rapid Flow	170	7.1

⁺ flow regime in the 6th pool, arbitrary flow regime in the other pools

Table 5.13 Tested flow regimes for pressure measurements

One measurement included the sampling of 14 pressure and 1 distance values (ultrasonic probe to water level) for 60 s at a sampling rate of 1000 Hz. These data including a time stamp was saved to an Ascii-file. The measurements were divided into several test series.

At the beginning of a test series a zero balance was performed, i.e. the ambient atmospheric pressure was set as reference pressure. The first measurement was performed at 0 l/s (no water in the flume). This way it was possible to determine the distance of the ultrasonic probe to the top of the roughness element containing the pressure transducers. Then the discharge was increased stepwise. At each discharge measurements were executed. For the discharge 110 l/s in the instable flow regime several measurements were performed. For the highest discharge 170 l/s two separate measurements were done. Then the discharge was decreased successively. Again, at 110 l/s several measurements were executed. Eventually a measurement at 0 l/s was performed to check whether the measured pressure matches the first 0 l/s-measurement at the beginning of the test series. This check was necessary as the transducers proved to be very sensitive to a medium change air-water.

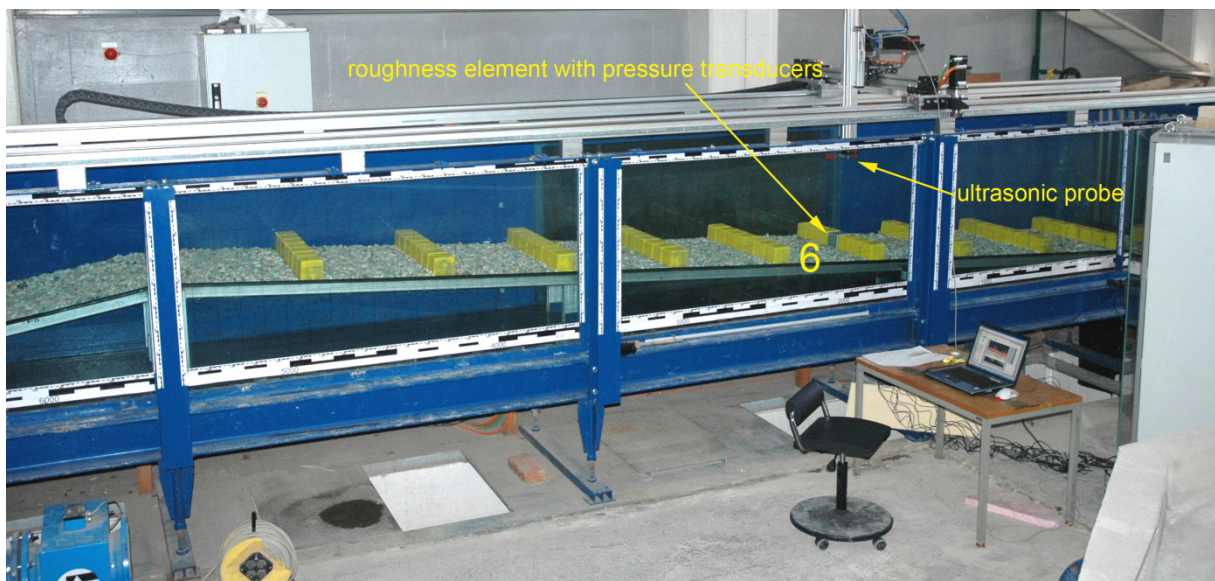


Figure 5.71 Pressure measurements: experimental setup, sixth pool labeled

Particular attention was paid to the discharge 110 l/s in the instable flow regime. If the discharge was adjusted from a lower discharge all the pools displayed a tumbling flow pattern. The flow regimes in each pool could be adjusted manually to either flow regime. Many different combinations of flow regimes in each pool could be adjusted. In the course of the evaluation of the measurement data it turned out that the flow regime in the sixth pool is crucial for the pressure distribution around the roughness element. The flow regime in all the other pools does not have an influence on the pressure distribution (Figure 5.71).

Test Program

Test series	75 l/s	110 l/s TF ⁺	110 l/s RF ⁺	150 l/s	170 l/s	Total
1	2	3	4	2	2	13
2	2	2	3	2	2	11
3	2	1	5	2	2	12
4	2	0	6	2	2	12
5	2	0	6	2	2	12
6	2	2	5	2	2	13
7	2	0	8	2	2	14
8	2	0	6	2	2	12
9	0	4	2	1	0	7
Total	16	12	45	17	16	106

⁺ flow regime in the 6th pool, arbitrary flow regime in the other pools

Table 5.14 Number of pressure measurements per test series and discharge (not listed: 0 l/s –measurements)

Altogether 109 measurements were performed in 9 different test series (Table 5.14).

General Results

As a general trend (for all measurements and all tested flow regimes) the pressure signals at the upstream face fluctuate much stronger than those of the downstream face (Figure 5.72, Figure 5.73). The pressure signals at the downstream face fluctuate only slightly. The sensors located at the side walls yield weak pressure fluctuations (Figure 5.75). The stronger the signal fluctuation at the upstream face the closer the sensor is to the water level (Figure 5.72). The sensor number 12 (top face, close to upstream face) and the sensor number 1 (uppermost sensor at upstream face) display the strongest fluctuations of all sensors (Figure 5.72, Figure 5.74). Sensor number 12 yields higher fluctuations than sensor number 13 which in turn fluctuates more than sensor number 14 (Figure 5.74).

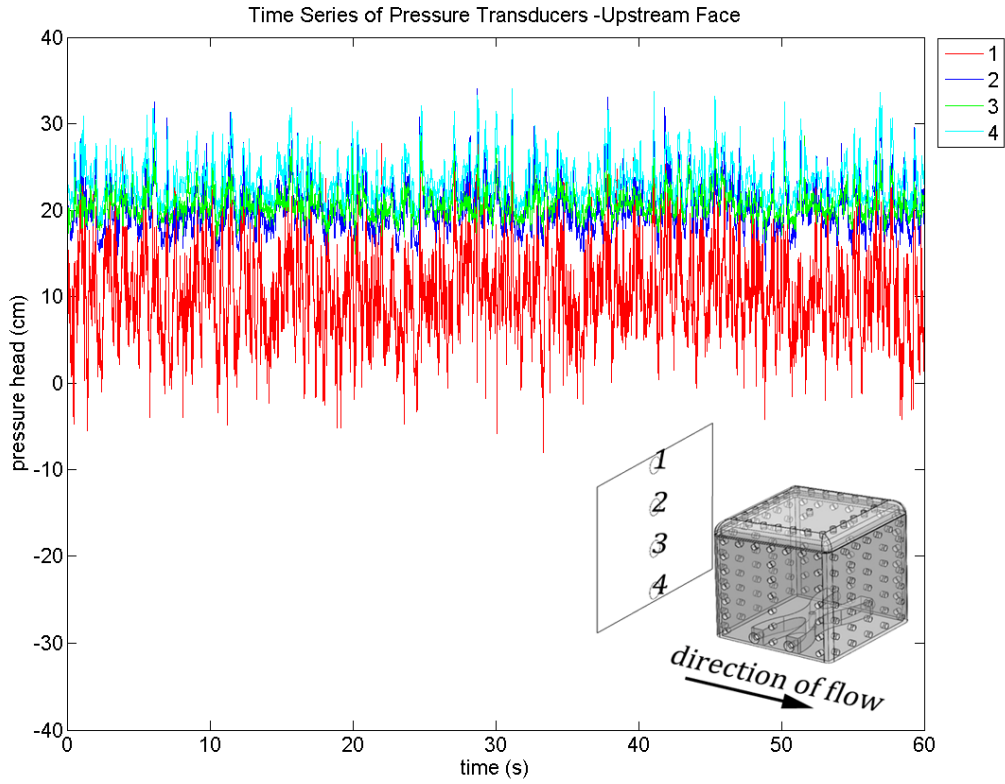


Figure 5.72 Characteristic pressure time series: upstream face

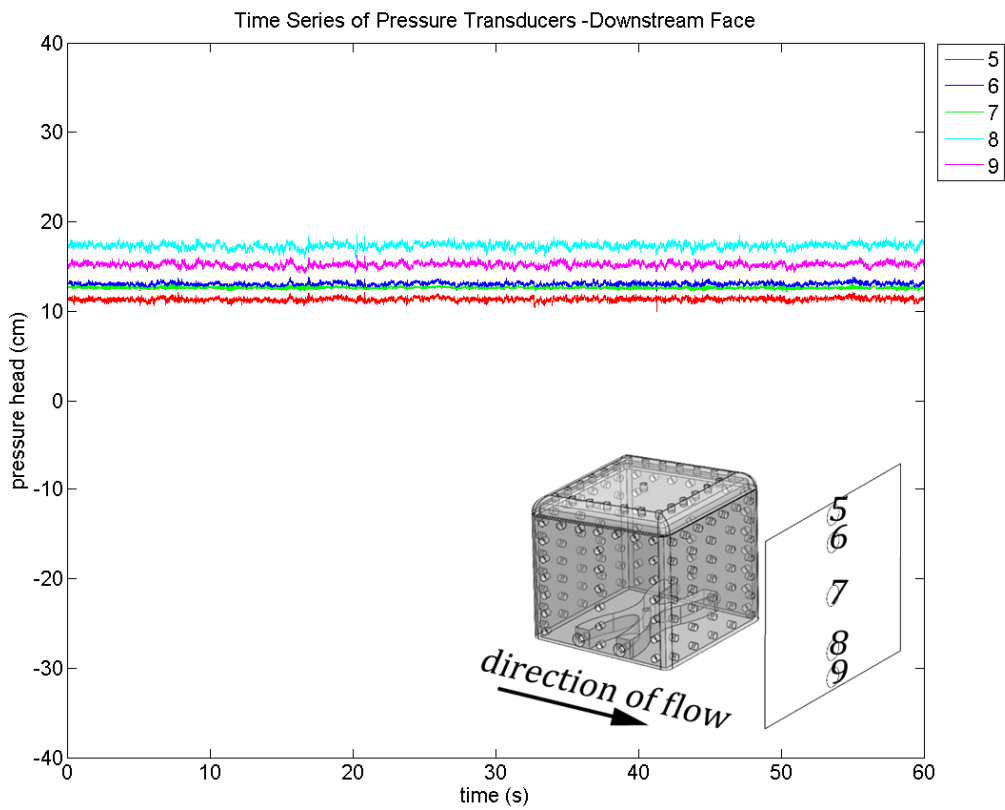


Figure 5.73 Characteristic pressure time series: downstream face

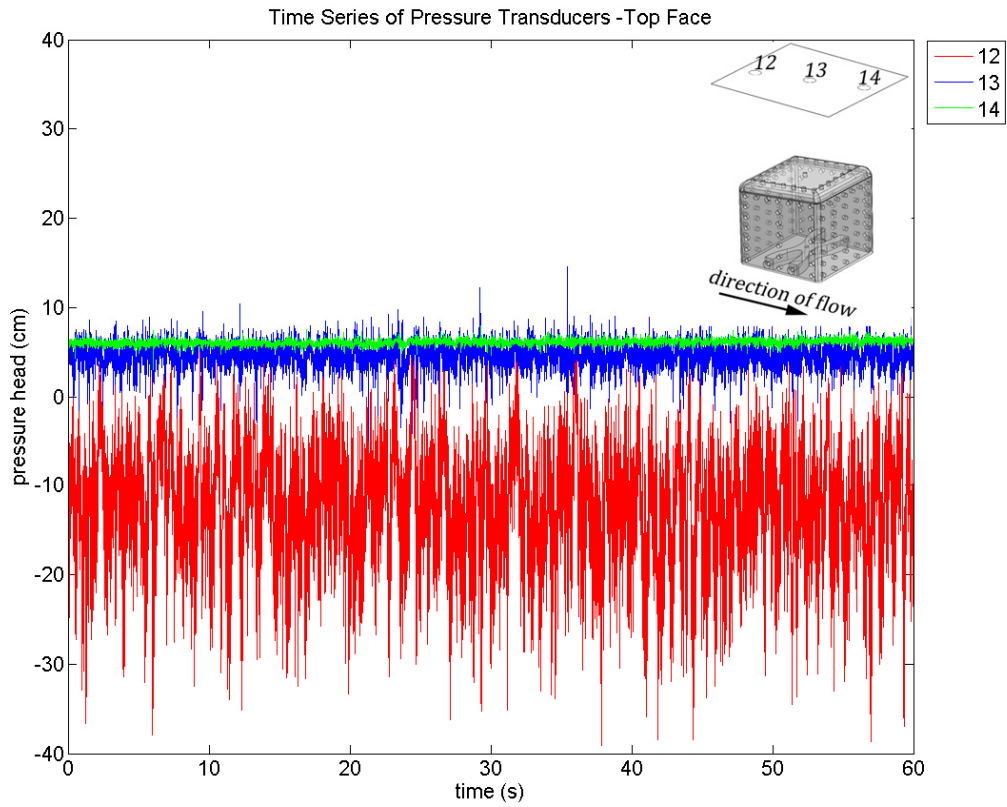


Figure 5.74 Characteristic pressure time series: top face

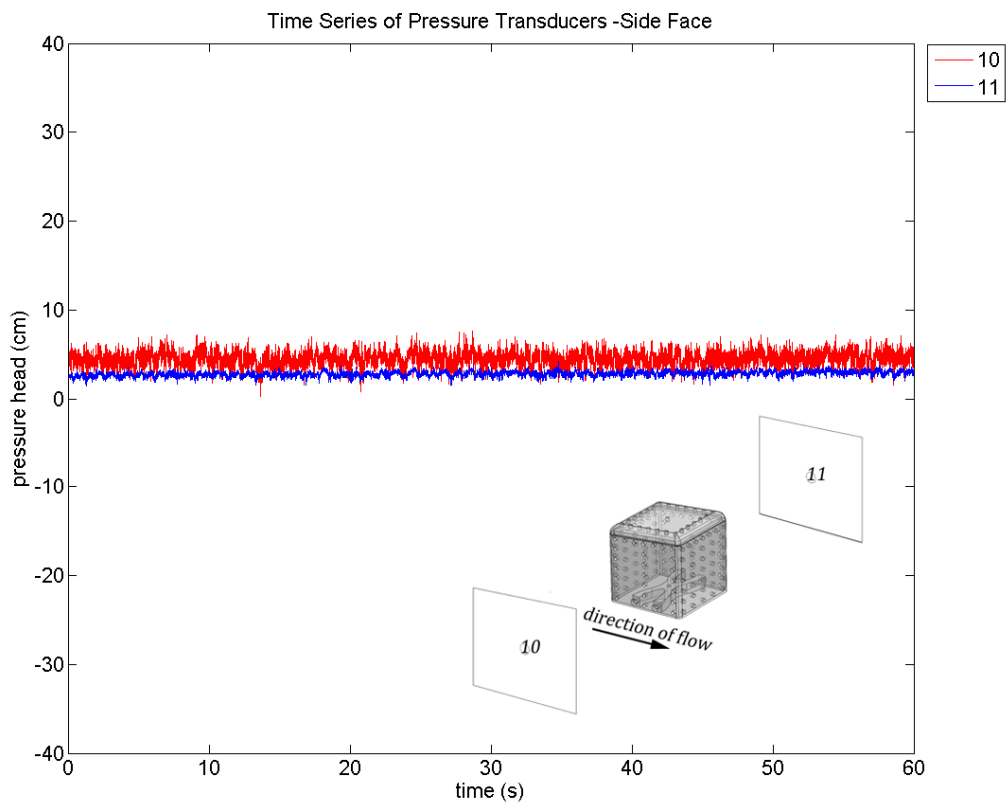


Figure 5.75 Characteristic pressure time series: side faces

The pressure time series for one transducer and one measurement is basically normally distributed. The fourier analysis of a pressure time series yields weak periodicities for low frequencies < 5 Hz (more details in Geiger, 2010).

For each pressure transducer i and each of the 5 tested flow regimes r an average pressure $\overline{p_{i,r}}$ and its standard deviation $\overline{\sigma_{i,r}}$ was calculated.

Mean total pressure head per transducer and flow regime

$$\overline{p_{i,r}} = \frac{1}{9 \cdot n_{i,r,j} \cdot 60000} \cdot \sum_{j=1}^9 \sum_{k=1}^{n_{j,r}} \sum_{l=1}^{60000} p_{i,r,j,k,l} \quad 5-16$$

Standard deviation of mean total pressure head

$$\overline{\sigma_{i,r}} = \max_{j=1..9, k=1..n_{j,r}} \sigma_{i,r,j,k} \quad 5-17$$

$p_{i,r,j,k,l}$ l^{th} pressure value of measurement k in test series j for flow regime r and transducer i
 $\sigma_{i,r,j,k}$ standard deviation of measurement k in test series j for flow regime r and transducer i
 $n_{j,r}$ number of measurements for test series j and flow regime r

The mean water depth y_{step} above transducer 13 was calculated analogously to equation 5-16. The hydrostatic pressure head of a transducer i is the sum of y_{step} and the vertical distance $h_{i,13}$ between transducer i and transducer 13:

Hydrostatic pressure head

$$p_h = y_{step} + h_{i,13} \quad 5-18$$

Figure 5.76 – Figure 5.80 illustrate the mean pressure distribution (equation 5-16) around the roughness element for the 5 tested flow regimes. The total pressure head (hydrostatic plus dynamic fraction) in mm is plotted perpendicular to the measuring plane. The positive directions point outwards. The bold bar plotted around the total pressure head indicates mean standard deviation according to equation. The bar around the hydrostatic head indicates the mean standard deviation of the water level measurement (equation 5-17). The assumed mean gravel bed level is also drawn in the plot. Two pressure transducers (one each at the upstream and downstream face) are located below this mean bed level.

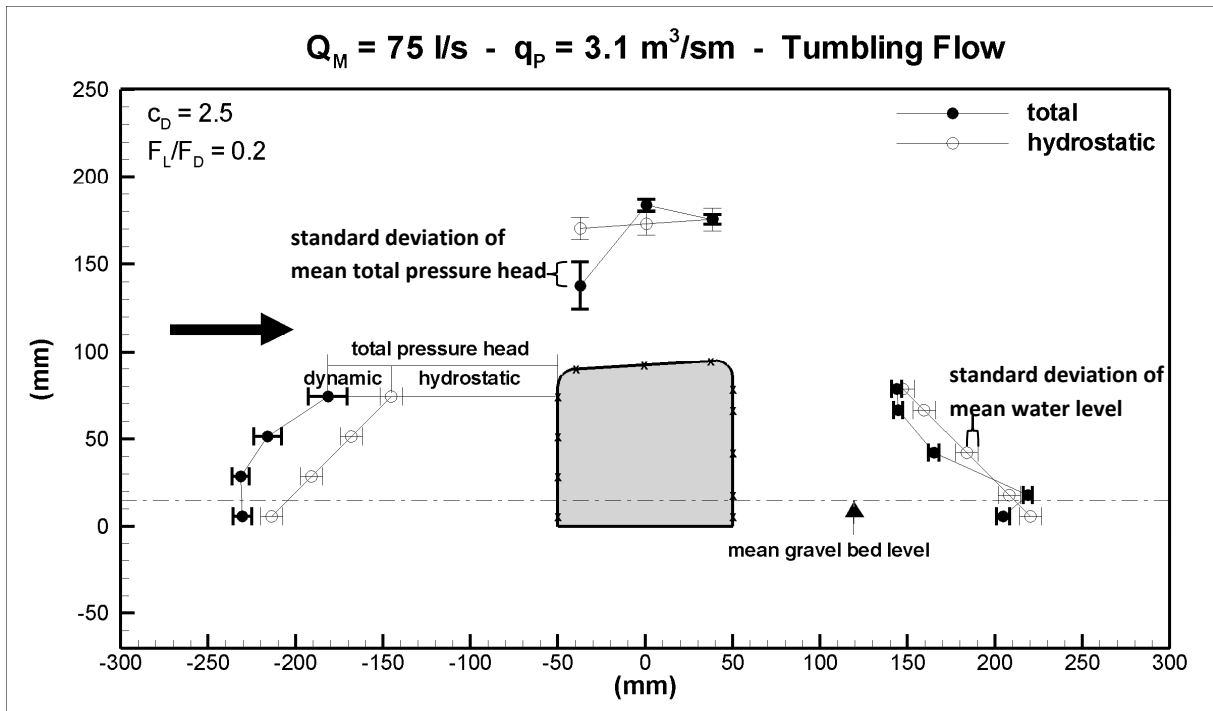


Figure 5.76 Mean total pressure head around roughness element, $q_p = 3.1 \text{ m}^3/\text{sm}$, Tumbling Flow

For the tumbling flow regime that is well below the flow transitional discharge (Figure 5.76) the dynamic pressure fraction is largest halfway of the effective roughness height at the upstream face. The pressure distribution at the downstream face is basically hydrostatic with a tendency to be below the hydrostatic pressure level, i.e. the flow generates a little suction effect. At the top face the total pressure lies well below the hydrostatic level close to the upstream face. This is a region where the flow separates into a downstream component and an accelerated flow over the top of the roughness element.

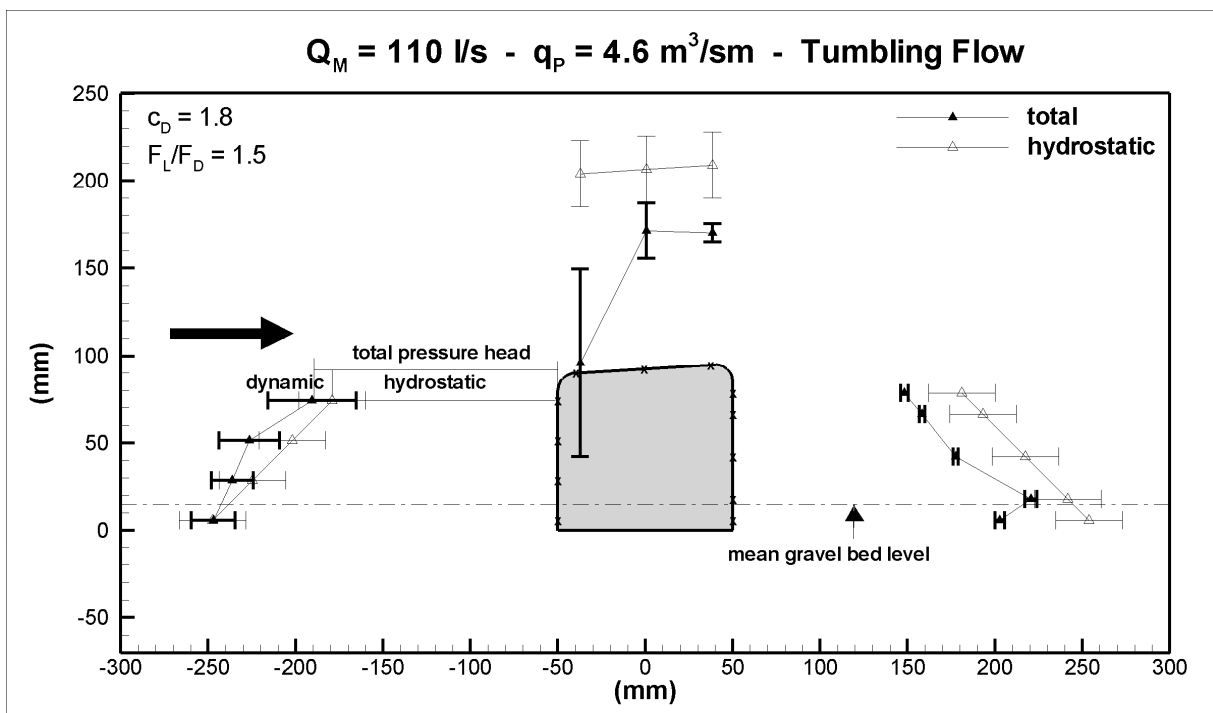


Figure 5.77 Mean total pressure head around roughness element, $q_p = 4.6 \text{ m}^3/\text{sm}$, Tumbling Flow

For the tumbling flow regime that is on the verge of the flow transition (Figure 5.77) the dynamic pressure fraction at the upstream face is smaller than that of the lower tumbling flow regime (Figure 5.76). The pressure distribution at the downstream face behaves basically hydrostatic but is quantitatively smaller. The suction effect generated by the flow is larger than for the lower tumbling flow regime (Figure 5.76). At the top face the trend as shown in Figure 5.76 is growing.

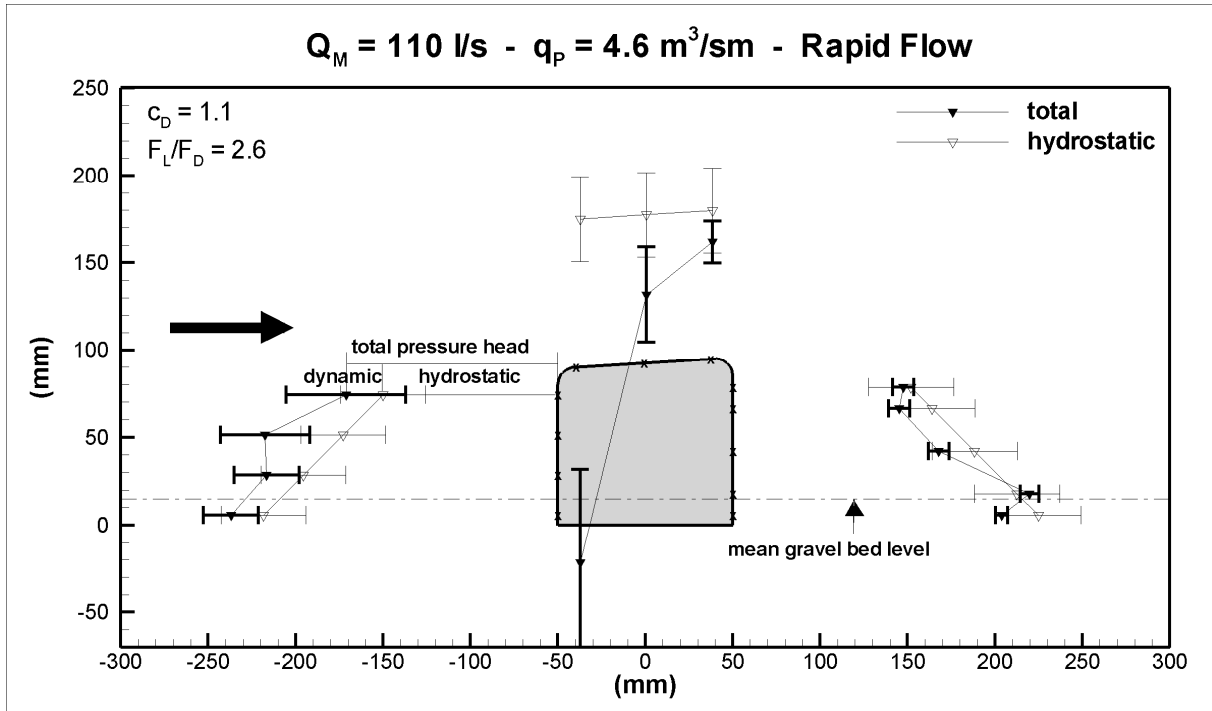


Figure 5.78 Mean total pressure head around roughness element, $q_p = 4.6 \text{ m}^3/\text{sm}$, Rapid Flow

For the rapid flow regime at the flow transitional discharge (Figure 5.78) the dynamic pressure fraction at the upstream face increases compared to that of the tumbling flow regime with the same discharge (Figure 5.77). The pressure distribution at the downstream face is basically hydrostatic with a tendency to be below the hydrostatic pressure level. At the top face the trend as shown in Figure 5.77 is fortified. The total pressure close to the upstream face drops below the atmospheric pressure.

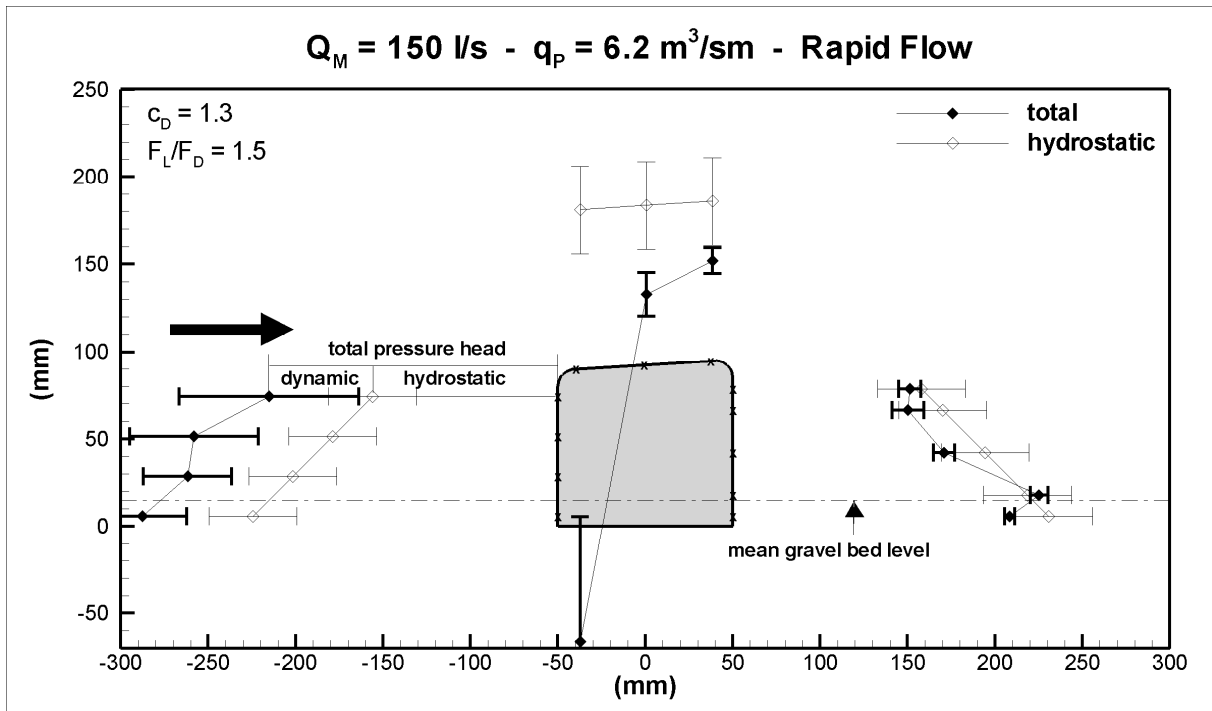


Figure 5.79 Mean total pressure head around roughness element, $q_p = 6.2 \text{ m}^3/\text{sm}$

For the rapid flow regime $q_p = 6.2 \text{ m}^3/\text{sm}$ (Figure 5.79) the dynamic pressure fraction at the upstream face increases significantly compared to that of the rapid flow regime at flow transition (Figure 5.78). The pressure distribution at the downstream face is basically hydrostatic. At the top face the trend as shown in Figure 5.78 is further intensified. The negative total pressure close to the upstream face is even larger than for the higher flow regime $q_p = 7.1 \text{ m}^3/\text{sm}$ (Figure 5.80).

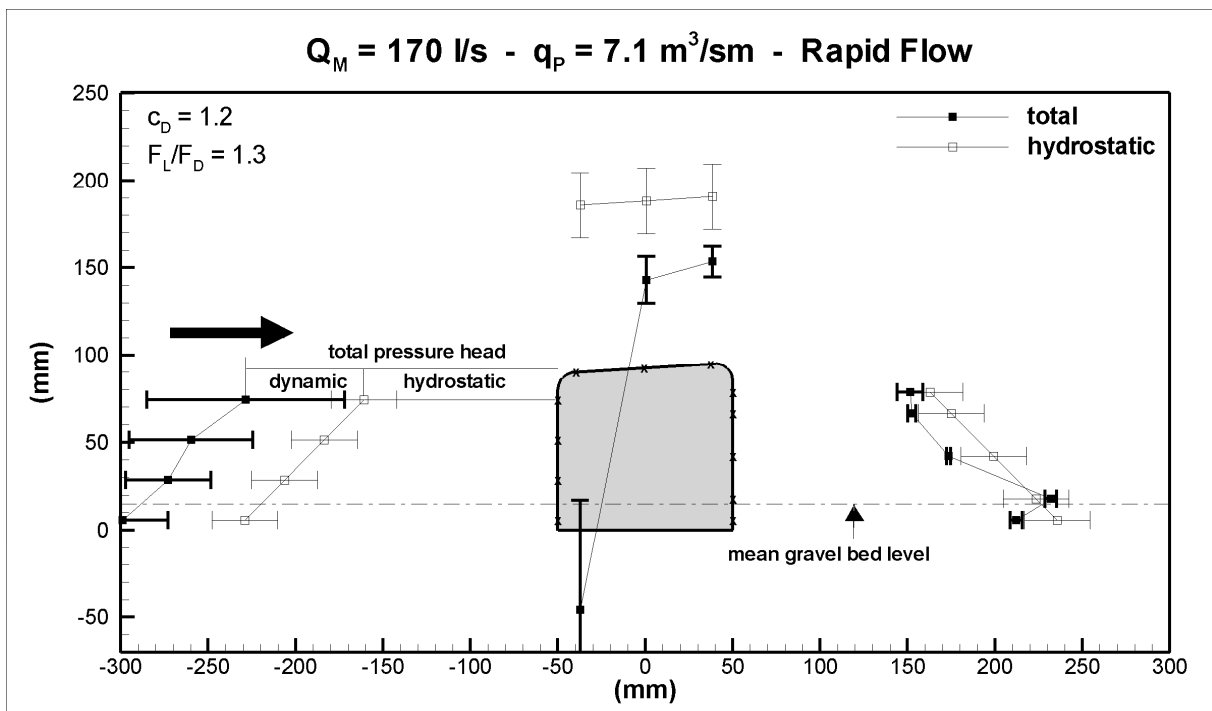


Figure 5.80 Mean total pressure distribution around roughness element, $q_p = 7.1 \text{ m}^3/\text{sm}$

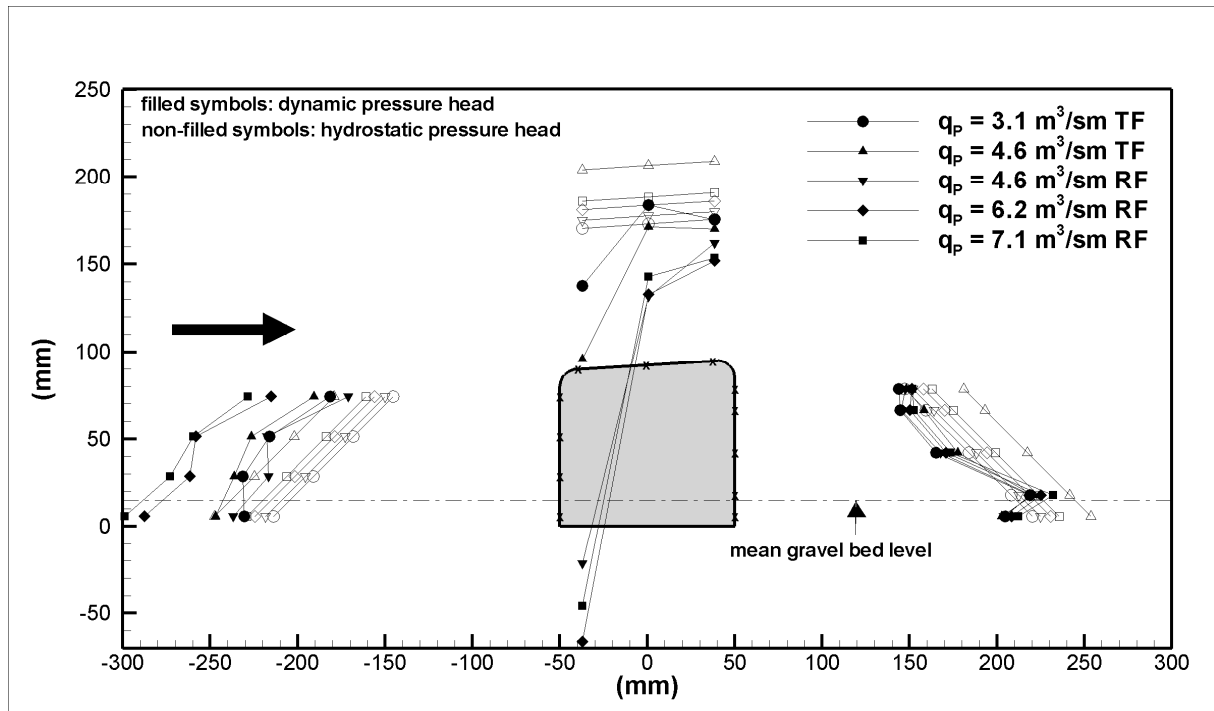


Figure 5.81 Mean total pressure head for all tested flow regimes

An interesting result is the fact that the pressure distribution at the downstream face is almost the same for all 5 tested flow regimes (Figure 5.81). This trend is also true but less distinct if only the dynamic pressure component is regarded (Figure 5.82). Moreover the qualitative distribution at the downstream face is alike for all flow regimes. The only location at the downstream face where the total pressure is larger than its hydrostatic fraction is immediately above the mean gravel bed level.

Except for the tumbling flow regime at the verge of the flow transition ($q_p = 4.6 \text{ m}^3/\text{sm}$) the pressure distribution at the downstream face is roughly hydrostatic with a tendency to be smaller than the hydrostatic fraction, i.e. the flow generates a suction effect. For the tumbling flow regime at the verge of the flow transition the pressure distribution lies well below the hydrostatic fraction. At the same time the dynamic fraction at the upstream face is smallest for this flow regime (Figure 5.82).

As can be seen from Figure 5.82 the dynamic pressure distributions at the upstream face are qualitatively the same for the two tumbling flow regimes and the three rapid flow regimes, respectively. The dynamic pressure fraction of the two tested regimes at the verge of the flow transition ($q_p = 4.6 \text{ m}^3/\text{sm}$) are smaller than for the lower tumbling flow discharge $q_p = 3.1 \text{ m}^3/\text{sm}$. A comparison of the dynamic pressure distributions of the two highest rapid flow regimes indicates that the dynamic load is almost the same. Moreover the negative pressure at the top face is even higher for the lower rapid flow discharge $q_p = 6.2 \text{ m}^3/\text{sm}$ (Figure 5.81). The latter statements support the hypothesis that once the flow is in the stable rapid flow regime the loading of the boulders does not increase further because the main flow goes over the tops of the roughness elements.

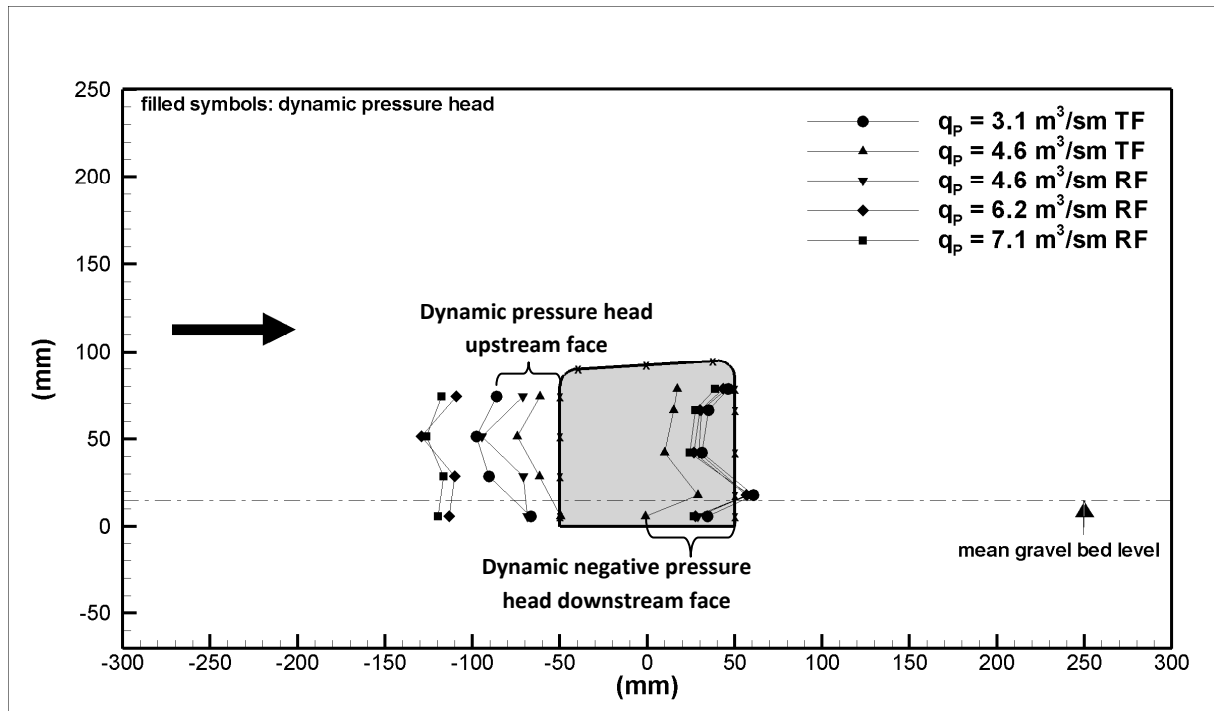


Figure 5.82 Mean dynamic pressure head for all tested flow regimes

Forces and Resistance Coefficients

From the pressure measurements it is possible to calculate the drag and the lift forces acting on the roughness element and its corresponding drag and lift coefficients.

Let c_D , c_L , v_a , A_D , A_L and V denote drag coefficient (-), lift coefficient (-), approach velocity (m/s), reference areas perpendicular to the acting forces (m^2) and volume (m^3) of the boulder, respectively. Then the forces (N) acting on the roughness element are defined as:

- Drag force: $F_D = c_D \cdot \frac{\rho}{2} \cdot v_a^2 \cdot A_D$
- Lift force: $F_L = c_L \cdot \frac{\rho}{2} \cdot v_a^2 \cdot A_L$
- Weight force: $F_W = \rho_S \cdot g \cdot V$
- Buoyancy: $F_B = \rho_W \cdot g \cdot V$
- Resistance: $F_R = (F_W \cdot \cos \alpha - F_B - F_L) \cdot \tan \varphi$

To simplify the reading the measured mean total pressure $\overline{p_{i,r}}$ for the transducer i and the flow regime r as defined in equation 5-16 is denoted p_i for the rest of this chapter and is given in Pascal (Pa).

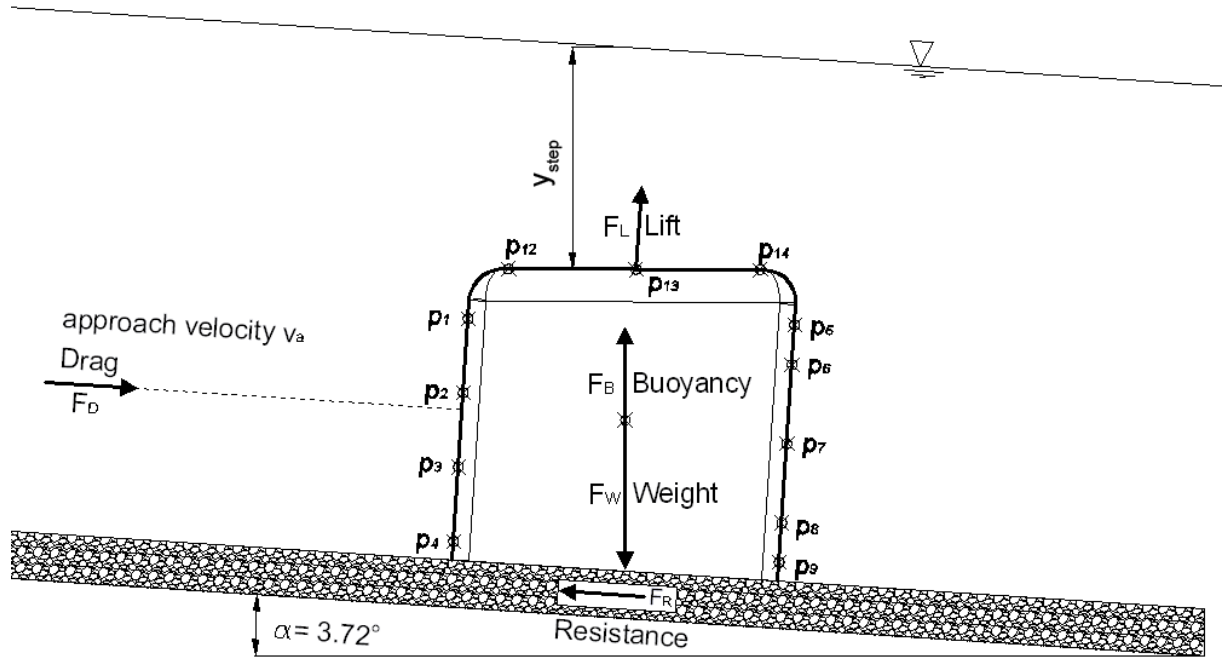


Figure 5.83 Forces acting on roughness elements, measured parameters $p_1 - p_{14}$, y_{step} , pressure transducers 11 and 12 located at the side faces are not displayed.

The pressure experiments yield the mean total pressure at 14 locations around the roughness element $p_1 \dots p_{14}$ and the mean water level above the step y_{step} for each tested flow regime. The reference areas A_D and A_L equal $K \cdot 0.1$ and $0.1 \cdot 0.1 \text{ m}^2$, respectively. $K = 0.095 \text{ m}$ denotes the height of the roughness element. The width of the roughness element equals 0.1 m . From the measured parameters the drag and the lift force are calculated for each flow regime as:

$$\text{Drag force (N)} \quad F_D = \left[\sum_{i=1}^4 w_i \cdot p_i / \sum_{i=1}^4 w_i - \sum_{i=5}^9 w_i \cdot p_i / \sum_{i=5}^9 w_i \right] \cdot A_D \quad 5-19$$

$$\text{Lift force (N)} \quad F_L = (p_{12} + p_{13} + p_{14} - \rho \cdot g \cdot y_{step}) \cdot A_L \quad 5-20$$

$$\text{Ratio lift to drag force (-)} \quad F_L / F_D \quad 5-21$$

w_i weight (reach) of i^{th} pressure transducer for the pressure integration (Figure 5.84)

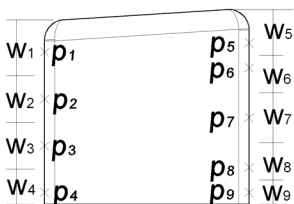


Figure 5.84 Weighted pressure integration

From the drag and the lift force as calculated from equations 5-19 and 5-20 the drag coefficient can be calculated by use of the approach velocity (equation 5-22) and the drag force ansatz where q_M denotes the specific model discharge in m^3/sm .

$$\text{mean approach velocity (m/s)} \quad v_a = q_M / (K + y_{step}) \quad 5-22$$

$$\text{drag coefficient (-)} \quad c_D = F_D \cdot \frac{2}{\rho \cdot v_a^2 \cdot A_D} \quad 5-23$$

Table 5.15 summarizes the calculated parameters for each of the 5 tested flow regimes. The grey shaded area marks the flow transitional regimes. As described before, for the flow transitional discharge $Q_M = 110 \text{ l/s}$ both flow regimes could be adjusted manually. The specified regime (tumbling or rapid) for the transitional discharge refers to the regime of the sixth pool. The flow regime in all other pools was irrelevant as it did not have an influence on the measured pressure distribution.

Except for the lowest tested tumbling flow regime all other tested regimes have a ratio F_L/F_D greater than 1, i.e. the lift force is larger than the drag force! The ratio is especially large, i.e. $F_L/F_D = 2.6$, for the flow transitional discharge in the rapid flow regime. Moreover, the amount and type of the load on the roughness element change severely on the flow transition: A switch from tumbling flow to rapid flow is characterized by a sudden increase of the lift force while the drag force diminishes at the same time. Except for the flow regime $Q_M = 110 \text{ l/s} - \text{RF}$ the drag coefficient diminishes with rising discharge. For the rapid flow regimes the ratio F_L/F_D decreases with rising discharge.

Flow Regime		TF	TF ⁺	RF ⁺⁺	RF	RF
Total model discharge (l/s)	Q_M	75	110		150	170
Specific prototype discharge (m^3/sm)	q_P	3.1	4.6	4.6	6.2	7.1
Lift force (N)	F_L	0.7	6.0	8.5	10.9	10.3
Drag force (N)	F_D	3.8	4.1	3.3	7.1	7.7
Ratio Lift and Drag Force (-)	F_L/F_D	0.2	1.5	2.6	1.5	1.3
Drag Coefficient (-)	c_D	2.5	1.8	1.1	1.3	1.2

+ flow transitional discharge, still tumbling flow in the sixth pool

++ flow transitional discharge, already rapid flow in the sixth pool

Table 5.15 Lift and drag force and its ratio, drag coefficient calculated from the pressure measurements for 5 tested flow regimes

As described in chapter 3.6.2 on roughness elements (pp. 67), Morris provides empirical formulas for the calculation of the drag coefficient c_D of roughness elements having a square cross sectional profile or a triangle top (Figure 5.85). In Table 5.16 the drag coefficients calculated from Morris' empirical formulas 3-101 and 3-102 are contrasted with the experimental results of the present study. Like in the experimental results the drag coefficients calculated from Morris' formulas decrease with rising discharge. Morris' calculated values for the squared roughness element lie well above the experimental values. The differences might be partly because of the sharp crested edges that offer more resistance than the rounded edges with a rising top edge. The main problem

presumably is the fact that Morris never tested roughness elements as high as $K = 95$ mm. The formula 3-101 is thus applied beyond the experimental range from which it was derived.

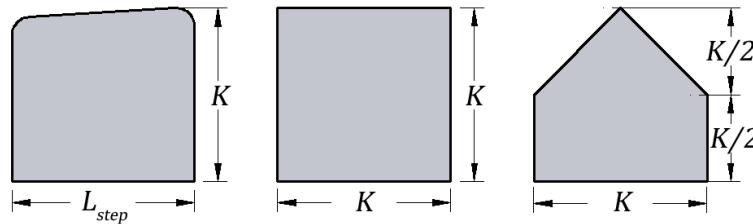


Figure 5.85 Shape of roughness elements: own experiment (left), Morris - square (middle), Morris - triangle top (right)

The results for the triangle top formula 3-102 match the experimentally derived drag coefficients of the present study much better although the formula yields larger drag coefficients. Again, a possible explanation is that the only roughness height that was tested to derive formula 3-102 was $K = 2$ in, which is only about half of the experimental roughness height of the present study.

Flow Regime		TF	TF ⁺	RF ⁺⁺	RF	RF
Total model discharge (l/s)	Q_M	75	110		150	170
Own experiments	c_D	2.5	1.8	1.1	1.3	1.2
Morris' formula 3-103 – square	c_D	8.7	6.1	6.1	4.7	4.2
Morris' formula 3-104 – triangle top	c_D	2.9	2.4	2.4	2.0	1.9
Morris' formula 3-104 – triangle top, $I = 2.5\%$	c_D	2.1	1.7	1.7	1.5	1.4

+ flow transitional discharge, still tumbling flow in the sixth pool

++ flow transitional discharge, already rapid flow in the sixth pool

Table 5.16 Comparison of drag coefficients calculated from own experimental result and according to Morris' formulas 3-101 and 3-102

To sum up, as a switch between the flow regimes may happen spontaneously the flow transition must be regarded as a critical loading case. The roughness elements in this flume test were screwed to the plastic panels and could not be washed away. For the prototype ramp where the roughness elements are boulders that are embedded into the river bed the large lift force severely affects the stability of the boulders.

5.4.13 Stability of a Step

The experimentally determined pairs of values ($c_D, F_L/F_D$) for the five different flow regimes are used in this chapter to calculate the required boulder mass of the step of a step-pool ramp. A “step” consists of a main boulder and two scour protection boulders up- and downstream of the main boulder. As there is no scour criterion for the pools at hand, stability considerations are provided for the scenario, that the boulders comprising a step are completely eroded.

For these stability considerations a step is approximated by a single substitute boulder of cuboidal shape with dimensions $l_{a,s} \times l_{b,s} \times l_{c,s}$ (longitudinal-horizontal x lateral x vertical direction). Let's assume that the pool between two steps is completely eroded such that the substitute boulder is entirely exposed to the flow. The forces acting on the boulder are: drag force, resistance of the bed, weight and lift force, respectively (Figure 5.86).

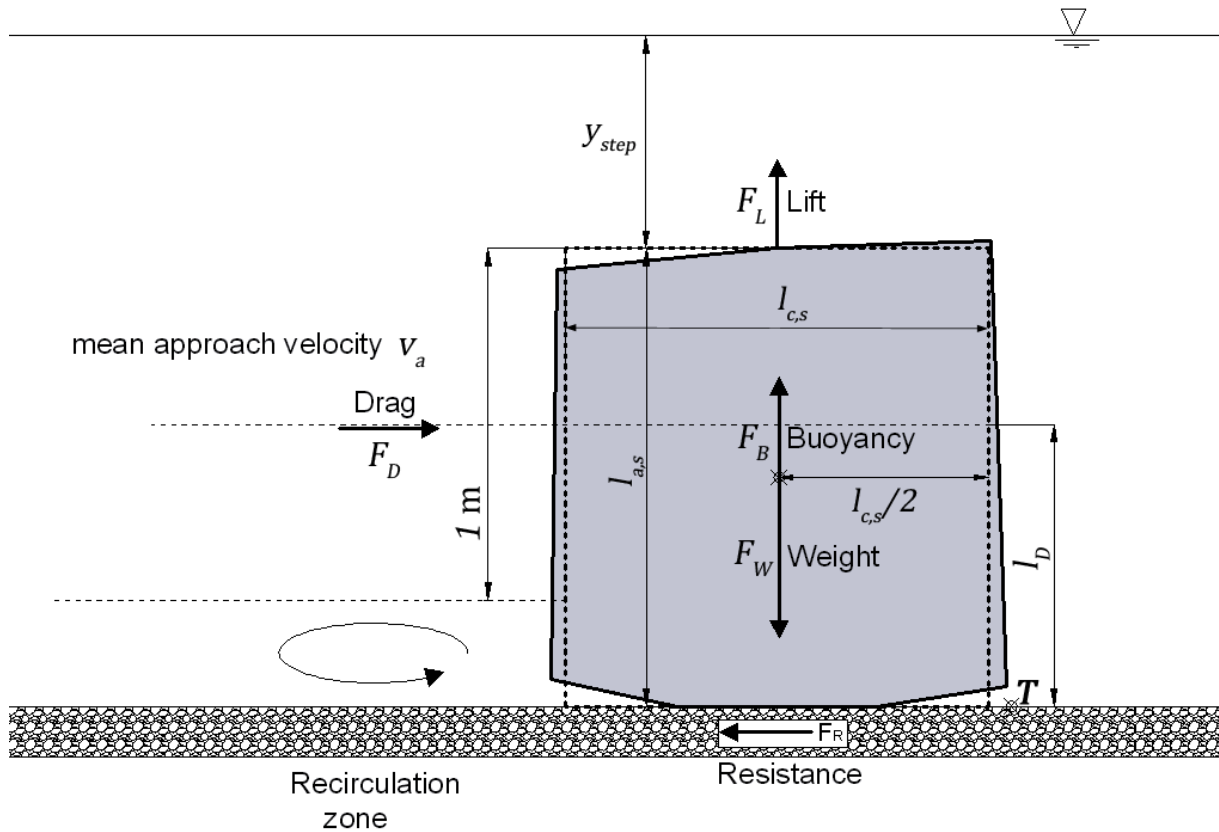


Figure 5.86 Forces acting on a single substitute boulder, longitudinal cut

Assumptions

- As the maximum slope of the ramp is 3 % it is tolerable to substitute $\cos \alpha \cong 1$.
- Angle of repose of the bed: $\varphi = 30^\circ$
- Density of the water: $\rho_W = 1000 \text{ kg/m}^3$
- Density of the boulders: $\rho_S = 2650 \text{ kg/m}^3$
- Volume of the boulder: $V = l_{a,s} \cdot l_{b,s} \cdot l_{c,s} \text{ m}^3$
- Drag coefficient: $c_D (-)$
- Lift coefficient: $c_L (-)$
- Reference area ($A_D \perp F_D$): $A_D = l_{a,s} \cdot l_{b,s} \text{ m}^2$
- Reference area ($A_L \perp F_L$): $A_L = l_{b,s} \cdot l_{c,s} \text{ m}^2$
- Mean approach velocity: $v_a \text{ (m/s)}$

Then the forces (N) acting on the step are defined as:

- Drag force: $F_D = \frac{1}{2} \cdot c_D \cdot \rho_W \cdot v_a^2 \cdot A_D$
- Lift force: $F_L = \frac{1}{2} \cdot c_L \cdot \rho_W \cdot v_a^2 \cdot A_L$
- Weight force: $F_W = \rho_S \cdot g \cdot V$
- Buoyancy: $F_B = \rho_W \cdot g \cdot V$
- Resistance: $F_R = (F_W - F_B - F_D) \cdot \tan \varphi$

Assumptions Based on Experimental Results of Chapter 5.4

- The flow separation zone is located 1 m below the top of the main boulder, as a consequence, the area affected by the flow is reduced: $A_D = \min(l_{a,s}, 1) \cdot l_{b,s}$
- The acting point of the drag force is 0.5 m below the top edge of the step, therefore $l_D = l_{a,s} - 0.5$ m (Figure 5.86)
- In the tumbling flow regime the Froude number for the flow above the step is: $Fr_{step} = 1$
- In the rapid flow regime the maximum Froude number for the flow above the step is: $Fr_{step} = 1.5$ (cf. Figure 5.34)

Given the mean approach velocity v_a and the Froude number above the step Fr_{step} one can calculate the water depth above a step as:

$$\text{Water depth above step} \quad y_{step} = v_a^2 \cdot \frac{Fr_{step}^2}{g} \quad 5-24$$

Theoretical Assumptions

For high discharges in the rapid flow regime and for deep pools the main flow does not hit the pool bottom any longer. Instead a vortex with a horizontal axis in lateral direction develops at the pool bottom (Figure 5.86). This vortex exerts a shear stress on the pool bottom which depends only indirectly on the discharge because it is separated from the main flow. As Volkart (1972) describes in his work on sills the pool bottom resists the flow for quite high discharges, but then fails all of a sudden.

The stability criteria below are derived under the assumption:

- The pool bottom doesn't erode below the bottom edges of the step boulders (Figure 5.86)

There is no criterion at hand to estimate the shear stress that the recirculating vortex exerts on the pool bottom. Neither can the depth of the scour hole in the pool be estimated. Therefore there is no way to validate the above assumption. To work around this problem, it is required that there is a bed load transport present before the flow transition from tumbling flow to rapid flow.

Stability Criteria

The question is how to determine the size of the boulder axes and the required mass of the substitute boulder in order to guarantee stability (Figure 5.86). A boulder may glide or overturn. To prevent it from gliding the resistance of the bed F_R must exceed the drag force F_D exerted by the flow (inequality 5-25). One must also take care of the moments acting on the boulder, i.e. the moment around the turning point T exerted by the vertical forces acting on the boulder must exceed the drag force F_D multiplied by the perpendicular distance l_D from the point T to the line of action of the F_D (inequality 5-26, Figure 5.86).

$$\text{Force} \quad F_D \leq F_R \quad 5-25$$

$$\text{Overturning Moment} \quad F_D \cdot l_D \leq (F_W \cdot \cos \alpha - F_B - F_L) \cdot l_{c,s}/2 \quad 5-26$$

As described in the previous chapter 5.4.12, the pressure distribution around a single roughness element was determined for 5 different discharges (2 tumbling flow and 3 rapid flow regimes). These measurements yield 5 different pairs of values $(c_D, F_L/F_D)$. Given the substitute boulder dimensions $l_{a,s}$, $l_{b,s}$ and $l_{c,s}$ and considering the assumptions of the previous subchapters the only unknown variable in inequalities 5-25 and 5-26 is the mean approach velocity v_a .

Let $v_{a,g}$ and $v_{a,t}$ denote the maximum possible approach velocity to prevent the boulder from gliding and overturning, respectively.

For each pair $(c_D, F_L/F_D)$ the maximum possible approach velocities $v_{a,g}$ and $v_{a,t}$ are calculated by assuming equality in 5-25 and 5-26, respectively.

$v_{a,g}$ cannot be calculated explicitly from 5-25. An appropriate algorithm has to be used to solve the implicit equation. $v_{a,t}$ can be calculated explicitly by transforming 5-26:

Maximum permissible approach velocity to prevent overturning

$$v_{a,t} = \sqrt{\frac{2 \cdot g \cdot (\rho_S - \rho_W) \cdot l_{a,s} \cdot l_{c,s}^2}{c_D \cdot \rho_W \cdot (2 \cdot l_D + F_L/F_D \cdot l_{c,s})}} \quad 5-27$$

The maximum permissible approach velocity and the maximum permissible discharge are calculated from the above velocities and from y_{step} (equation 5-24):

Maximum permissible approach velocity (m/s) $v_a = \min(v_{a,g}, v_{a,t})$ **5-28**

Maximum permissible discharge (m³/sm) $q = v_a \cdot (\min(l_a, 1) + y_{step})$ **5-29**

Table 5.18 illustrates the maximum permissible discharge calculated from inequalities 5-25 and 5-26 for each pair $(c_D, F_L/F_D)$ and the for boulder dimensions as listed in Table 5.17. It is remarkable that the lift force exceeds the drag force by a factor of 2.6 for a discharge that is on the verge to rapid flow. The maximum permissible discharge is smallest for these flow conditions (Table 5.18).

	$l_{a,s}$	$l_{b,s}$	$l_{c,s}$
axes of substitute boulder (m)	2.0	1.0	1.7

Table 5.17 Dimensions of the substitute boulder

Drag Coefficient (–)	c_D	2.5	1.8	1.1	1.3	1.2
Ratio Lift and Drag Force (–)	F_L/F_D	0.2	1.5	2.6	1.5	1.3
Permissible drag Force (kN)	F_D	28.7	17.3	12.7	16.9	17.9
Permissible approach velocity (m/s)	v_a	4.7	4.4	4.9	5.0	5.5
Permissible Discharge (m ³ /sm)	q_p	15.3	12.7	10.1	10.7	13.0

Table 5.18 Maximum permissible drag force, approach velocity and specific discharge for each pair $(c_D, F_L/F_D)$ to guarantee stability, grey shaded area: c_D and F_L/F_D values at flow transition

The mass of the substitute boulder equals $l_{a,s} \cdot l_{b,s} \cdot l_{c,s} \cdot \rho_S = 9.0$ t. Therefore the sum of the masses of the three boulders comprising the step must have at least the same mass as the substitute boulder.

**Required Mass
per unit width
of a step**

$$M = (l_a \cdot l_c + l_{a,sc} \cdot l_{c,sc}) \cdot \rho_S \geq 9.0 \text{ t/m} \quad \mathbf{5-30}$$

The dimensions of the main boulder and the two scour protection boulders listed in Table 5.19 fulfill the above mass requirement. They correspond to the recommended boulder dimensions of chapter 7.2.2 Step Dimensions & Build, pp. 198, Table 7.4. Again, the indices a, b and c refer to the streamwise horizontal, lateral and vertical axis, respectively.

	Main boulder			Scour protection boulders		
	l_a	l_b	l_c	$l_{a,sc}$	$l_{b,sc}$	$l_{c,sc}$
Boulder axes (m)	1.5	1.0	1.2	0.9	1.0	0.9

Table 5.19 Dimensions of main boulder and scour protection boulders (cf. Table 7.3)

Therefore, a ramp made of steps with boulders as in Table 5.19 (and Table 7.3) resists discharges up to $10 \text{ m}^3/\text{sm}$.

If the meandering ramp shall be constructed for a stream with a design discharge significantly less than $10 \text{ m}^3/\text{sm}$ Figure 5.87 is used to estimate the required boulder mass M . If the required boulder size is as small as 4 t/m , the step shall consist of a single boulder. For boulder masses between 4 and 7 tons per meter it is possible to omit the upstream scour protection in favor of higher masses of the other two boulders. In either case, the boulders should be embedded into the river bed such that a longitudinal cut of a step has a triangle shape.

Figure 5.87 also includes the required boulder masses if the meandering ramp has a slope of 6.5 %. The calculations are based on the following two assumptions:

- In the tumbling flow regime the water depth above a step y_{step} can be calculated from equation 5-13, i.e. $y_{step} = c(0.065) \cdot y_c = 0.83 \cdot y_c$, hence: $Fr_{step} = 1.32$
- In the rapid flow regime the maximum Froude number for the flow above the step is:
 $Fr_{step} = 2.3$ (cf. Figure 5.34)

Nonetheless, the recommended meandering ramp slope will be restricted to 3 % because of missing information on the scouring processes in the pools at slopes as high as 6.5 %. Further mobile bed experiments are required.

Figure 5.87 also includes the required boulder masses if the ramp is designed according to Korecky (2007), chapter 3.4.7. The boulder mass for the step alone is significantly smaller than for the meandering ramp. If the mass of the pool material is also taken into account the required boulder masses are in a similar range. The required pool mass for the ramp according to Korecky is calculated as follows: A step spacing of 6 m, a slope of $I = 3 \%$ and a tolerance parameter $\Omega = 0.006$ is assumed. The latter was chosen by Korecky to compare her results with an existing prototype step-pool ramp. According to Korecky the equivalent sphere diameter of the pool material should be a fifth of the equivalent sphere diameter for a boulder of a step. The required stone mass of a pool is calculated assuming three and four layers of the pool material, respectively.

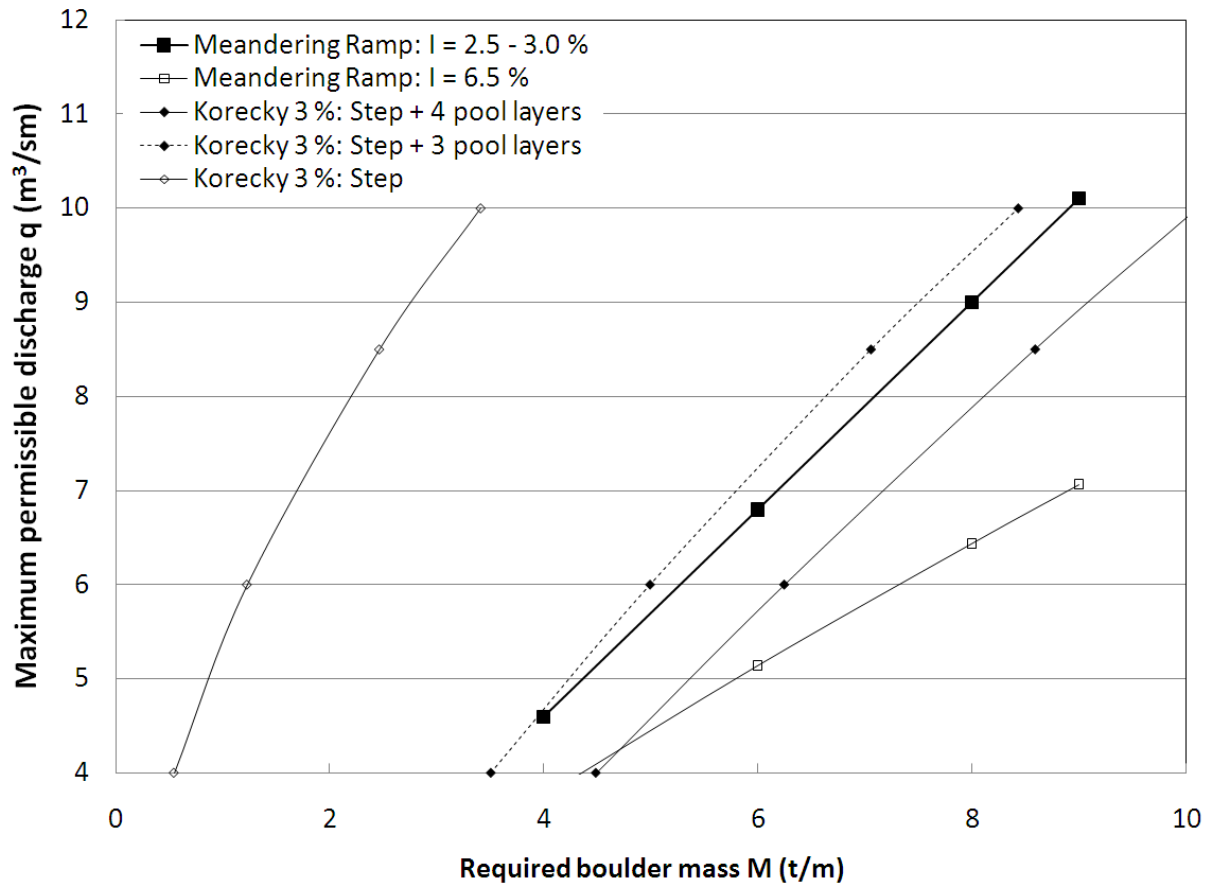


Figure 5.87 Required boulder mass for low specific discharges, meandering ramp and step-pool ramp with a slope $I = 3\%$ according to Korecky (2007),

The main advantage of the meandering ramp over the step-pool ramp after Korecky is that the former allows scouring of the pools. Apart from the positive ecological implications, deeper pools dissipate more energy and reduce the excess energy head that has to be dealt with in the tailwater section of the ramp.

The postulated c_D values are gathered from the experimental results. They overestimate the prototype c_D values for three reasons.

1. The steeper the slope the higher the drag force. The c_D values in the flume were determined for the slope $I = 6.5\%$.
2. The experimental c_D values were determined for a single cuboid boulder. The prototype step configuration additionally consists of smaller up- and downstream boulders which diminish c_D because of the triangle shape they build together with the main boulder.
3. The application of the Froude similitude rules out Reynolds similitude in the scaled model (length scale: 1: 10). The prototype Reynolds number is higher than in the model by factor of $10^{3/2}$. The Reynolds numbers in the model experiments range from $1 - 2 \cdot 10^5$ to $3 - 4 \cdot 10^5$ depending on whether the characteristic length scale D is chosen to be y_{step} or $y_{step} + K$. As the drag coefficient c_D typically decreases with rising Reynolds numbers the drag coefficient calculated from the scaled model rather overestimates the prototype drag coefficient.

With this respect the approximations are on the save side.

5.5 Conclusions

The experiments enlighten some of the complex flow patterns over large roughness elements. The tumbling flow regime is characterized by a wavy flow over the steps. From the top of a step the flow accelerates but is slowed down because of the next downstream step. Therefore a hydraulic jump occurs in the pools. The tumbling flow is a cyclic uniform flow, i.e. the flow pattern in each step pool unit is the same. For slopes $I \leq 3\%$ critical flow conditions can be preserved over the step crest, provided that the relative spacing $L/K < 10$. For steeper slopes the water depth over the step crest drops below the critical depth. Typically, in the tumbling flow regime, the water surface is out-of phase with the bed. As the discharge approaches the flow transitional discharge the water surface becomes in-phase with the bed. The flow transitional discharge from tumbling flow to rapid flow was found to depend on K , L/K and the slope I . The step height K and the slope I alone are not sufficient to determine the transitional discharge which also depends linearly on the relative spacing L/K . Although the flow transitional discharge increases with the relative spacing L/K a maximum value $L/K < 10$ is recommended. Larger relative spacings lead to undesired side effects such as:

- too much acceleration in the pools
- higher roll waves in the instable and the 3-dimensional rapid flow regime, respectively
- the flow reattaches the pool bottom resulting in higher bed shear stresses
- supercritical flow over the steps

The flow transition occurs within a well-defined small range of discharges (± 2.5 l/sm) for mild slopes up to 3 % while it happens over a large range of discharges for higher slopes (± 25 l/sm). After the flow transition roll waves appear upstream of a step as the flow propagates downstream. From an energy dissipating point of view this is not too bad but the roll waves increase in height as they travel downstream that might result in a freeboard problem. What's more the roll waves might lead to stability problems of the step.

A hysteresis effect for the transitional discharge can be observed, i.e. the flow transition from tumbling flow to rapid flow TF2RF occurs on higher discharges than the transition from rapid flow to tumbling flow RF2TF. Within these two discharges the flow is very unstable and can be manipulated manually to either of the two flow regimes.

Referring to the four objectives of the experiments as stated in chapter 5.1.1, p. 121:

5.5.1 Objective 1 – find formula for transitional discharge

The objective was to find a functional relationship for the transitional discharge from tumbling flow to rapid flow q_{crit} subject to the step height K , the ramp slope I and the step spacing L :

$$q_{crit} = f(K, L, I)$$

A semi-empirical criterion as given by equations 5-12, 5-13 and 5-14 predicts the flow transitional discharge with an accuracy of $\pm 10\%$ for $L/K < 10$. This criterion is derived from theoretical considerations (linearized potential flow theory) and empirically based relations (equations 5-13 and 5-14).

5.5.2 Objective 2 – Morris' formula appropriate?

Morris' criterion for the transitional discharge (see equation 3-100) is inappropriate for the present experiments. The following reasons explain the discrepancy:

- Morris' focus was on steeper slopes for which the step spacing doesn't seem to have an effect on the flow transition. Also in the present experiments the influence of the step spacing becomes less dominant for the steep spacing $I = 6.5\%$
- Morris' criterion doesn't predict his own experimental data well for slopes $I < 10\%$, i.e. it overestimates the flow transitional discharge. This, again, can be explained by that fact that his focus was on steeper slopes

5.5.3 Objective 3 – Laterally inclined steps dissipate more energy?

The fixed bed configuration of the present study does not support the assumption that laterally inclined steps dissipate more energy than horizontal steps. The lateral inclination of the steps is visible in the secondary velocity plots of the steps, however. As the mobile bed experiments of the meandering ramp for the Große Tulln River (chapter 5.4.12, pp. 71) have shown, the lateral inclination of the steps is reflected in the scour patterns. The scours that are also inclined in lateral direction hence reinforce the secondary flow. Two opposite explanations seem plausible:

- in the presence of a strong lateral velocity component the energy distribution is enhanced because of an additional lateral momentum exchange
- the secondary flow causes the flow to become more stable and less turbulent, so less energy is dissipated

5.5.4 Objective 4 – determine Pressure Distribution Around Roughness Element

The pressure distribution around a roughness element placed in middle of the seventh step of variant I65_K8_L622 was determined for 5 different flow regimes. At the downstream face of the element the flow generates a little suction effect, i.e. the measured total pressure is lower than the hydrostatic pressure. The hydrostatic pressure was determined from the measured water depth. The drag coefficient of the roughness element diminishes with rising discharge except for the rapid flow regime close to the flow transitional discharge. For the flow transitional discharge and for higher discharges the lift force dominates the drag force. For the flow transitional discharge in the rapid flow regime the ratio between lift and drag force is 2.6. The flow transition from tumbling flow to rapid flow thus is a crucial loading case for the stability of a step-pool ramp.

6 Field Survey of the Prototype Ramp in the “Stübmingsbach” Stream

The following results have been published and presented. The Stübmingsbach stream (Styria, Austria) is located in the trout region with typical fish species such as the rainbow and the brook trout. According to an information board close to the ramp, the stream has a mean slope of 2.5 % and a mean flow of 330 l/s. The mean annual precipitation is 1240 mm. There is no gauging station in the Stübmingsbach stream.

In 2004 two vertical drops near Turnau that were heavily log-jammed should be replaced by a ramp. Therefore the first so-called “meandering ramp” was constructed by the district authority “Baubezirksleitung Bruck and der Mur” (BBL Bruck). The meandering ramp (GPS: N 47°34'41”, E 15°23'57”, 859 m a.s.l.) consists of 8 step-pool units and a ground sill at the downstream end of the ramp (Figure 6.2). The following morphological parameters refer to a field survey in December 2009: The area downstream of the ramp covers a length of 6 m and has a slope of 3.9 %. The ramp is 31 m long (1st to 8th step) and 2.1 m high, i.e. it has a slope of 6.8 %. The vertical distance between two adjacent steps is 24 – 39 cm, the horizontal distance amounts to 3.3 – 5.45 m. The steps consist of boulders with a diameter of approximately 1.5 m, which are embedded into the natural river bed such that the upstream top edge of a boulder is level with the bed. Downstream of the step boulders, smaller boulders (diameter $D \sim 0.8$ m) reinforce the steps. The pools are not armored but consist of the natural river sediments. Since the construction of the ramp some flood events have occurred. The maximum flood event so far was estimated to have a return period of 20 years, but for lack of a gauging station this specification is vague. The University of Technology Graz and the district authority BBL Bruck have performed two field surveys so far (December 2007, December 2009). In December 2009 the grain sizes in the pools could be documented and classified due to a very low discharge.



Figure 6.1 Melt Water Discharge on March, 25th 2010, 18:27, CET (left), Sediment Sorting in Step-Pool Unit 4 of the Meandering Ramp (right)

The results of the monitorings are summarized as follows:

- Scours have developed downstream of each step; the lateral inclination of the steps is reflected in scour depths, that also differ in lateral direction. The scour depths averaged over the stream width are between 37 and 73 cm. At selective locations the scour depths amount up to 91 cm. The scours are only located in the upper third of a step-pool sequence. Below, the pool bed constantly rises until the next downstream step (Figure 6.2, bottom).

- For traditional block ramps the scour development downstream of the ramp toe is a major concern. Below the meandering ramp in the Stübmingbach stream no scours have developed (Figure 6.2, bottom).
- Up- and downstream of the ramp the sediment fractions are well mixed. In the pools of the ramp however, the sediments are sorted. Figure 6.3 (bottom) illustrates the grain size fractions as determined by visual inspection. In Figure 6.1 (right) the sorted sediments of the fourth step pool unit are well visible.
- Although the ramp serves mainly a bed stability purpose, it also exhibits substantial depth and flow varieties which are good ecological indicators.

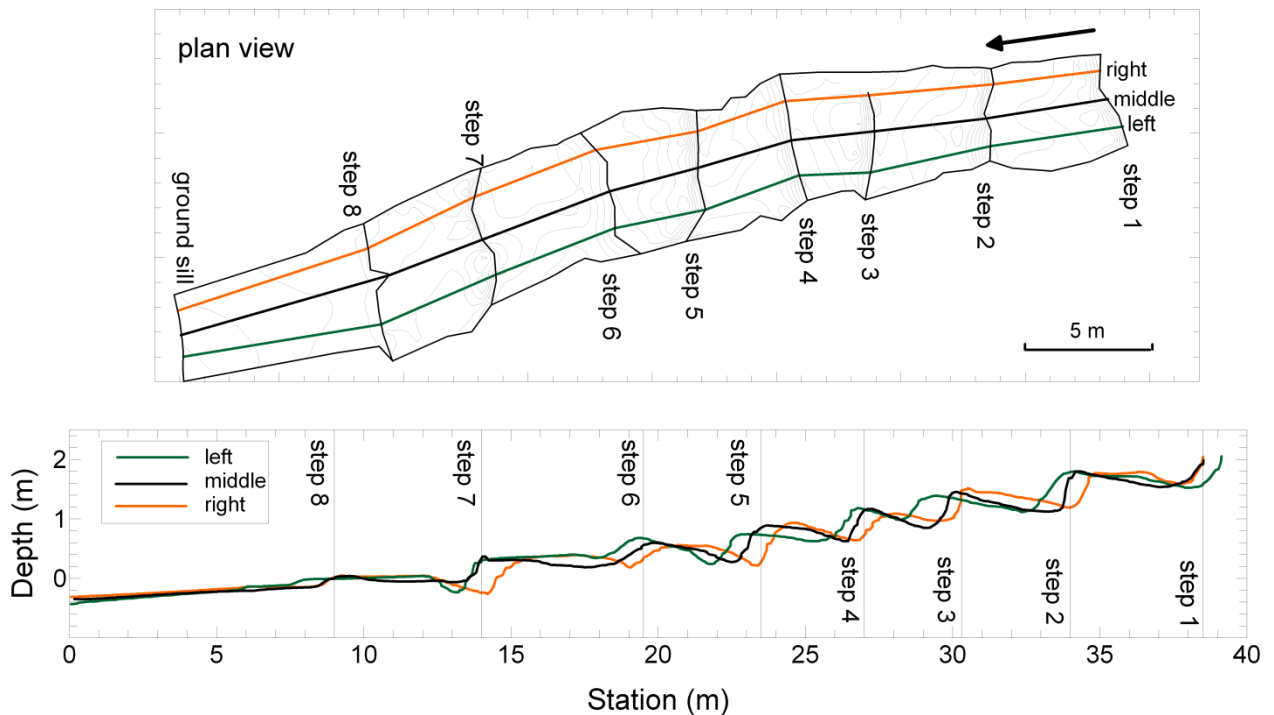


Figure 6.2 Meandering ramp Stübmingbach, field survey results, December 2009: Plan view of the ramp (top), longitudinal cuts (bottom, vertical exaggeration: 2)

In his investigations on sills (see chapter 3.4.3, pp.46), Volkart also reports sediment sorting processes. According to his experimental results the sediments immediately downstream of the sill consist of the fine grain sizes while the sediments in the vicinity of the maximum scour depth consist of the coarse parts of the grain size distribution (Volkart 1972).

According to Volkart’s scour classification the Stübmingbach ramp has scour patterns as illustrated in Figure 3.36 a.). The occurrence of upstream scours (cf. Figure 3.36 d.)) is reported by Volkart (1972), Whittaker (1987) and Sindelar & Knoblauch (2010) (cf. chapter 4.8.3, pp.92). This scour type occurs if - on rising discharge - the wavy water surface becomes in-phase with the bed and the hydraulic jump is located immediately of the upstream of the lower pool step, hence the name „upstream scour“. Whittaker surmises that upstream scours do not occur in natural step-pool systems because of armoring processes (Whittaker 1987, cf. chapter 3.4.4). This might be true for steep mountain streams where the sediment sizes and the slope of the stream are at a dynamic equilibrium. A man-made ramp, however, is typically steeper than the river section where it is built. If the pools consist of the natural river sediment – as this is the case for the meandering ramp of the Stübmingbach

do not show upstream scours until now may therefore indicate that a critical discharge producing such scours has not yet occurred, rather than it implies that armoring processes have prevented its development.

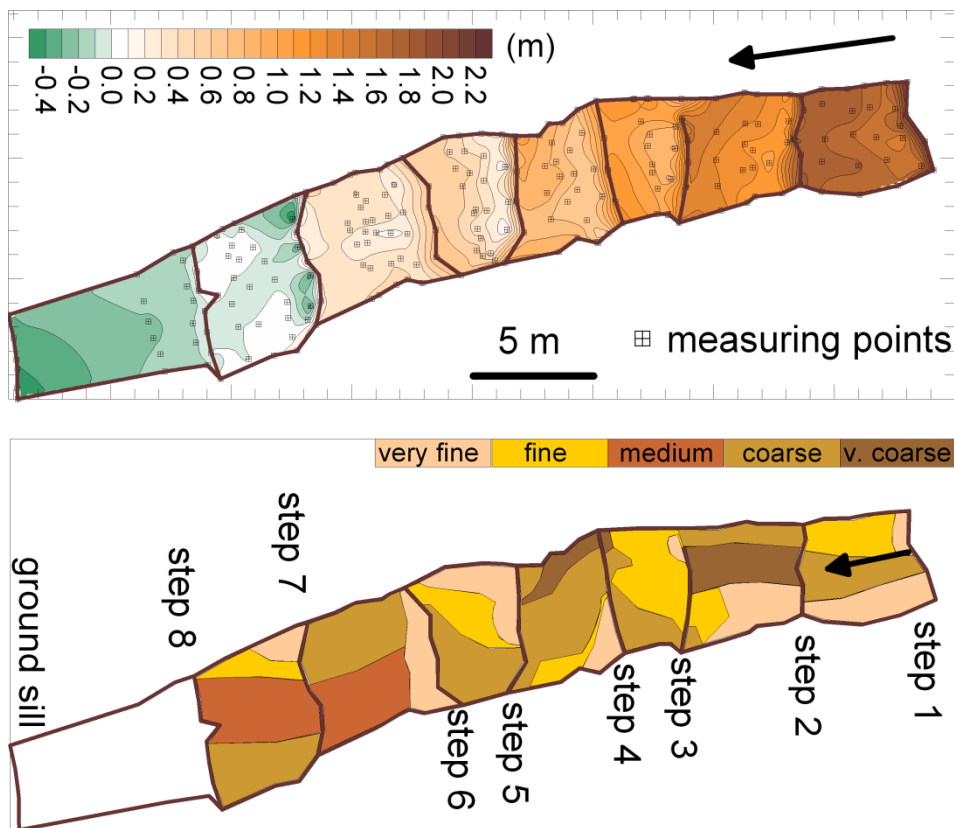


Figure 6.3 Meandering ramp Stübmingbach, field survey results, December 2009, plan view: Measuring points (top) and sediment sorting classification (bottom)

To investigate this question further, a solar-powered measuring station was installed at the Stübmingbach ramp in March 2010. At 10-min intervals a picture is taken of the ramp and the temperature is measured. Flood events that can be documented this way shall shed light on the interaction of water surface and scour development. Since the installation of the measuring station there was just one increased discharge due to melt water. Figure 6.1 (left) illustrates this event. The meandering flow pattern is well visible. No major flood event has occurred until now (December 2010).

7 Design Guidelines for Meandering Ramps

This chapter includes practical design guidelines which are gathered from the previous chapters.

Outline of this chapter:

- Chapter 7.1 serves as a feasibility check whether a location is appropriate for the installation of a meandering ramp
- Chapter 7.2 comprises the dimensioning of the ramp
- Chapter 7.3 provides background information on and explanations of the derivation of the design rules

Chapters 7.2 and 7.3 are separated for the sake of a clear and coherent presentation of the design rules in chapter 7.2.

7.1 Morphological and Hydrological Preconditions

The field of application of the meandering ramp are small gravel-bed rivers with moderate discharges. The river width should not exceed 10 m to limit the maximum protrusion of the laterally inclined steps from the river bed.

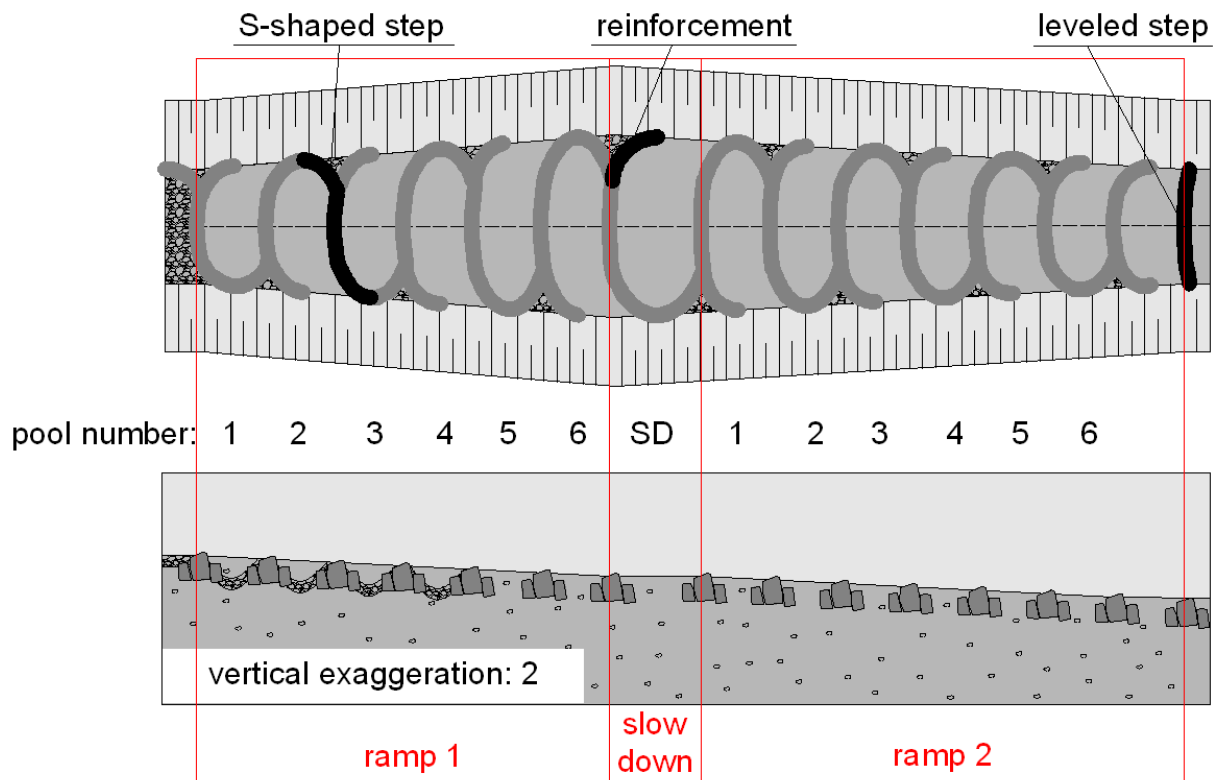


Figure 7.1 Meandering ramp scheme, plan view (top), longitudinal cut in river axis (bottom), cross section see Figure 7.2

The presence of a bed load from upstream is thus required to diminish the development of upstream scours. The dimensioning of the ramp (see chapter 7.2) is such that the flow transition from tumbling flow to rapid flow will take place for discharges $q = 3.5 - 6 \text{ m}^3/\text{sm}$. Hence:

- Determine the discharge $q_{crit, sed}$ (m^3/sm) for the incipient motion of the sediments in the headwater section

- Use an appropriate sediment transport formula (e.g. Meyer-Peter Müller)
- Verify that $q_{crit, sed} < 3.5 \text{ m}^3/\text{sm}$
- Take care of potential bed-load traps (e.g. debris basins or hydro power plants and their flushing strategies) upstream of the ramp that might reduce the natural sediment discharge q_b (kg/ms). As a rule of thumb verify it is required that the natural sediment transport rate is not reduced by more than 50%. (In the physical model test “Große Tulln”, chapter 4, pp.71, only 25 % of the calculated sediment transport rate was added.)

Another precondition is that the flow in the head and tailwater sections of the ramp are subcritical for all discharges up to the design discharge q_{design} (Figure 7.4).

Table 7.1 sums up the morphological and hydrological preconditions.

	Optimal	Permissible range
Design discharge q_{design} (m^3/sm)		≤ 10
River Width W (m)		$W \leq 10$
Characteristic diameter of natural river sediment $d_{90,b}$ (mm)	≥ 140 , see ¹	further research required
Characteristic diameter $d_{m,b}$ (mm)	≥ 60 , see ¹	further research required
Pool armor layer diameter d_a (mm)	500 ¹	Terzaghi' filter criterion 2-5 must be fulfilled
Critical discharge for the incipient motion of sediment transport $q_{crit, sed}$ (m^3/sm)		< 3.5

¹ obtained from a physical model test for the design of a meandering for the “Große Tulln” river in Neulengbach, Austria

Table 7.1 Morphological and Hydrological Preconditions

7.2 Dimensioning of the Ramp

Table 7.2 lists the main design parameters which are illustrated in Figure 7.6 and Figure 7.2.

	Optimal	Permissible range
Slope I (%)	2.5	$\leq 3\%$
Step spacing L (m)	6	$5 \leq L \leq 7$
Vertical distance between two steps in river axis Δh (m) $\alpha = \tan^{-1}(I/100)$	0.15	$\Delta h = \frac{I}{100} \cdot L \cdot \cos \alpha$
Lateral Step Inclination I_{lat} (%)	3	
Protrusion of the step in river axis p_{axis} (m)	$0.5 \cdot W \cdot I_{lat}$	
Maximum protrusion of step from the bed (m)	$W \cdot I_{lat}$	

Table 7.2 Ramp geometry

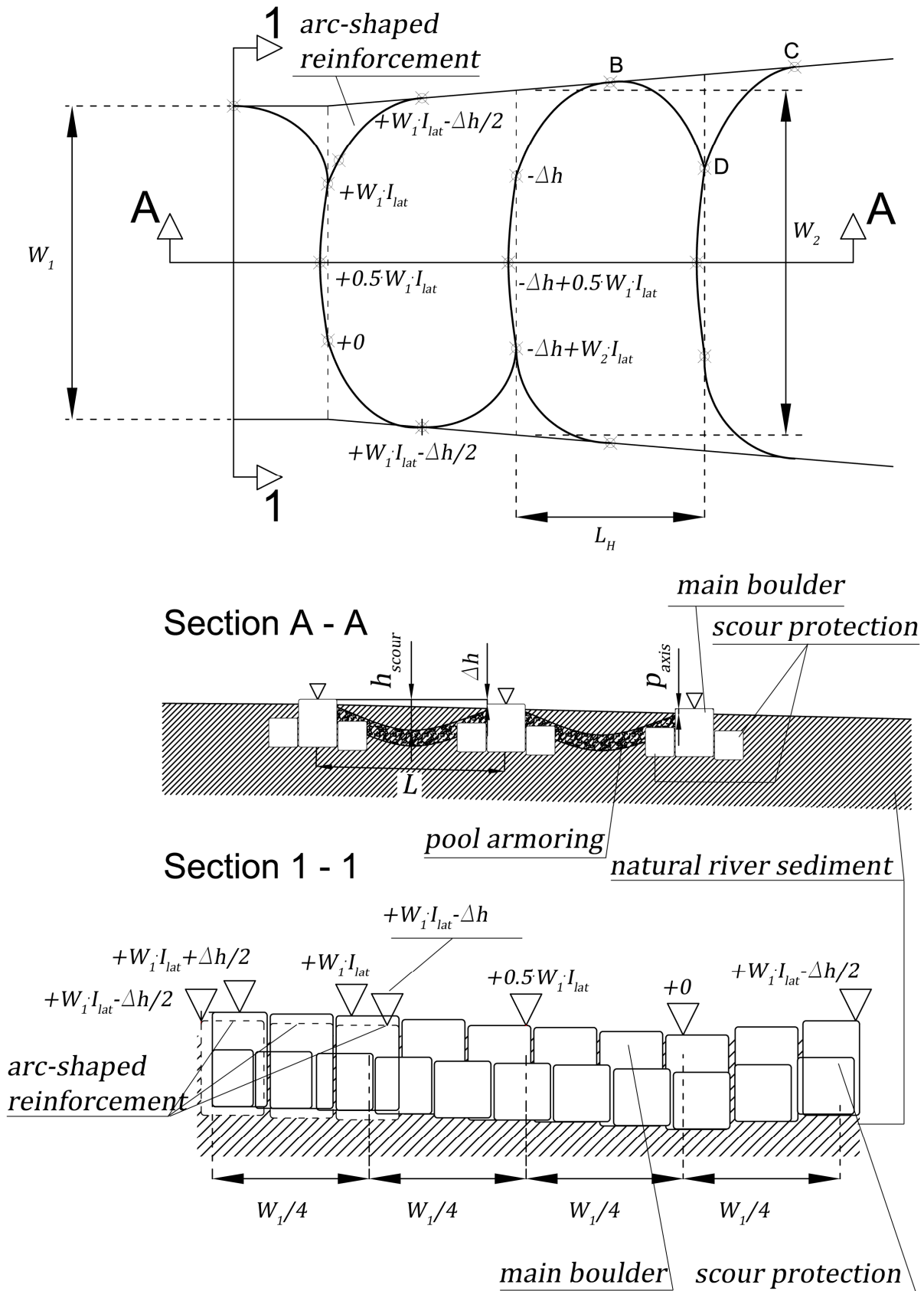


Figure 7.2 Ramp geometry: plan view and sections – relative elevation of the steps

7.2.1 Step Shape

- The steps are S-shaped in plan view (Figure 7.1)
- The higher end of a step – located alternately at the left and right bank, respectively – is reinforced by an arc-shaped row of boulders (Figure 7.1, Figure 7.2)
- A step consists of a main boulder and two smaller boulders up- and downstream of the main boulder for scour protection (Figure 7.2, section A-A)
- A scour protection of the arc-shaped reinforcement can be omitted (cf. Figure 4.52)
- The boulders of the steps are block-shaped

The boulders are defined by three axes lengths:

Axes	Main Boulder	Boulders up- and downstream
Vertical axis (m)	l_a	$l_{a,sc}$
Horizontal axis in lateral direction (m)	l_b	$l_{b,sc}$
Horizontal axis in flow direction (m)	l_c	$l_{c,sc}$

Table 7.3 Axes of the block-shaped boulders of a step: denotations

7.2.2 Step Dimensions & Build

The boulder dimensions listed in Table 7.4 guarantee the stability of the ramp for discharges up to $10 \text{ m}^3/\text{sm}$ if the density of the boulders is $\rho_s = 2,65 \text{ t/m}^3$ (5.4.13, pp.184).

Step – required mass per unit width (t/m)	$(l_a \cdot l_c + l_{a,sc} \cdot l_{c,sc}) \cdot \rho_s \geq 9$	
Step Build – Main Boulder	Optimal	Permissible range
Vertical axis l_a (m)	1.5	$l_a \geq 1.5$
Horizontal axis in flow direction l_c (m)	1.2	$l_c \geq 1.2$
Step Build – Scour Protection		
Vertical axis $l_{a,sc}$ (m)	0.9	Main boulder and scour protection must fulfill weight condition above
Horizontal axis in flow direction $l_{c,sc}$ (m)	0.9	
Armor layer (chapter 7.2.4)		
Armor layer diameter d_a (m)	0.5 ¹	Terzaghi's filter criterion 2-5 must be fulfilled

¹ obtained from a physical model test for the design of a meandering for the "Große Tulln" river in Neulengbach, Austria

Table 7.4 Boulder Dimensions to ensure stability for a maximum design discharge of $10 \text{ m}^3/\text{sm}$

If the meandering ramp shall be constructed for a stream with a design discharge significantly less than $10 \text{ m}^3/\text{sm}$ Figure 7.3 is used to estimate the required boulder mass M . If the required boulder size is as small as 4 t/m , the step shall consist of a single boulder. For boulder masses between 4 and 7 tons per meter it is possible to omit the upstream scour protection in favor of higher masses of the other two boulders. In either case, the boulders should be embedded into the river bed such that a longitudinal cut of a step has a triangle shape.

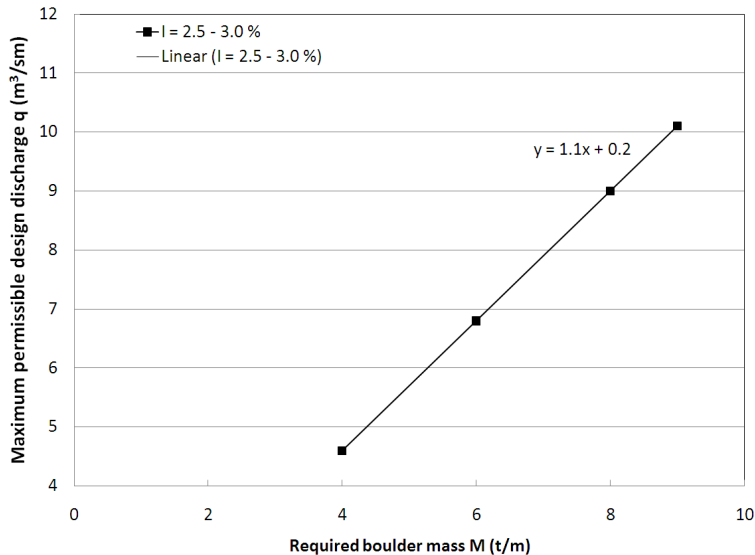


Figure 7.3 Required boulder mass M (t/m) to ensure stability

7.2.3 Channel Widening – Slow-Down Pool

- Arrange a slow-down pool after about 6 pools
 - $L \approx 8$ m, $\Delta h = 0$ m
- Along the ramp allow for a continuous widening and re-narrowing of the channel width, s. t.
 - the largest channel width W_{max} is located in the slow-down pool
 - below the slow-down pool the channel narrows continuously until it reaches its original channel width W at the toe of the ramp
 - $W_{max} \approx 1.5 \cdot W$
 - If possible keep the original bank slope throughout the ramp area, i.e. the bank top line widens (and re-narrows) the same way as the channel

The slow-down serves a hydraulic and an ecological purpose (chapter 4.10, p. 119).

7.2.4 Additional Armoring

- Armor the first 4 pools of the ramp with a layer of sediments with a diameter d_a (Table 7.1), the layer is trough-shaped with the lowest point halfway between two steps, the maximum depth of the trough is 0.9 m measured from the top of the upper step. For small step spacings (~ 5 m) the maximum scour depth should be 0.75 m (Figure 7.6).
- The resulting triangle (bank – step – reinforcement, defined by points BCD in Figure 7.2) is filled up with sediments of diameter d_a .

As a result of the physical model test of the meandering ramp (chapter 4), the diameter of the pool armor layer d_a should be 500 mm. One has to verify though, that Terzaghi's filter criterion 2-5 is fulfilled (cf. chapter *Pool Armoring*, pp.111).

7.2.5 Leveled Step

A leveled step in the tailwater section completes the ramp structure. The spacing between the last step at the ramp toe and the leveled step equals the step spacing L . The leveled step is U-shaped in plan view and is level with the bed in the river axis. The step integrates into the banks $L/2$ meters further downstream. There the step protrudes from the bed by $W \cdot I_{lat}$ meters.

7.2.6 Head- and Tailwater Protection Required?

Headwater

Assuming subcritical conditions upstream of the ramp for all discharges, critical flow conditions will occur at the ramp crest. The resulting drop-down curve may endanger the headwater section. Thus, for the design discharge:

- determine uniform flow depth y_{HW} (from roughness and slope assumptions)
- determine the critical flow depth y_c
- Determine the length $L_{dropdown}$ by comparing the energy head at the ramp crest and at a cross section where uniform flow conditions are present
- Compare the energy gradient I_f of the dropdown section with the bed slope I_b

If $I_f \gg I_b$ armor the dropdown area accordingly.

It is recommended to armor at least $L_{dropdown} = 10$ m of the head water section with sediments of diameter d_a to prevent backward erosion.

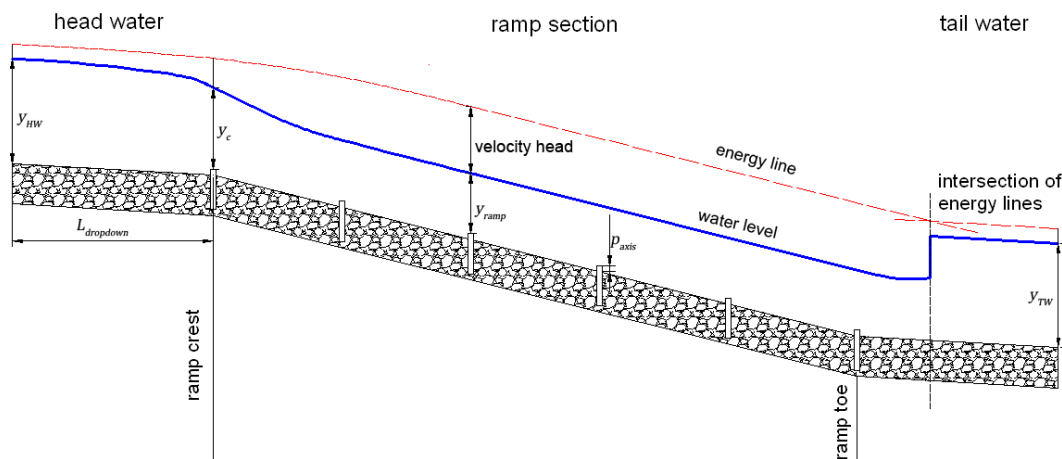


Figure 7.4 Comparison of energy levels for head and tailwater of the ramp

Tailwater

For traditional block ramps it is common to demand a Froude minimum at the ramp toe to ensure that a hydraulic jump with a surface roller develops. The German standard DIN 19661-2, for instance, requires a Froude minimum of $Fr \geq 1.7$ (cf. chapter 3.5.1). For step-pool ramps the flow is typically in the tumbling flow regime, i.e. the Froude number at the toe of the ramp equals 1. Therefore the above criterion cannot be applied for step-pool ramps. Instead the following procedure is recommended:

- Select the following discharges:
 - $q = 3.5 \text{ m}^3/\text{sm}$: lower boundary of expected flow transition, $Fr_{\text{step}} = 1.0$
 - $q = 6 \text{ m}^3/\text{sm}$: upper boundary of expected flow transition, $Fr_{\text{step}} = 1.0$
 - $q = q_{\text{design}} \text{ m}^3/\text{sm}$: design discharge, $Fr_{\text{step}} = 1.5$

Fr_{step} estimate: see Figure 5.34

- For the selected discharges determine the tailwater depth y_{TW} from slope and roughness assumptions

- For the selected discharges determine: $y_{step} = \sqrt[3]{q^2 \cdot Fr_{step}^2 / g}$ and $v_{step} = q / y_{step}$
- For each discharge determine the location of the hydraulic jump by comparing the energy levels
- If the hydraulic jump is located in the tailwater section (like in Figure 7.4) use additional armoring of the bed in the tailwater section

7.2.7 Bank Stability

- To protect the banks reinforce the bank toe with a boulder having the same dimensions as the main boulder along the ramp (Table 7.4)
- Integrate the boulders of the steps into the bank toe protection
- keep the height of the bank protection of the river
- above the bank protection plant trees that are native in the area if the trees do not affect the flood control negatively

7.3 Comments and Explanations

The flow transition from tumbling flow to rapid flow marks a critical situation for the stability of the ramp. Some researchers (Whittaker 1987, Volkart 1972, Sindelar, Knoblauch 2010) report that deep scour holes immediately upstream of a step may develop at this flow condition.

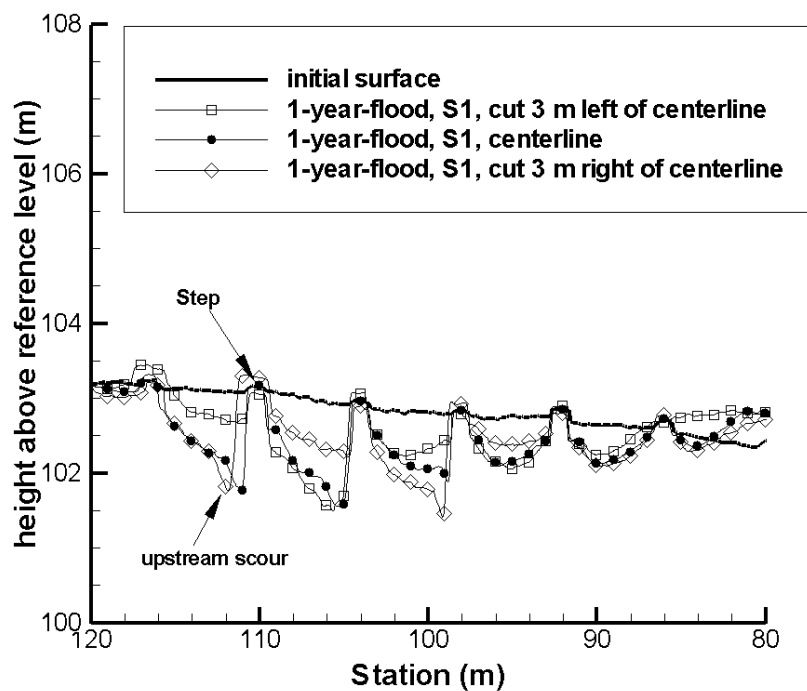


Figure 7.5 Upstream Scour in the Physical Model of a Meandering for the “Große Tulln” River, longitudinal cut, steps without up- and downstream scour protection, rounded gravel, (Sindelar & Knoblauch 2010)

During the mean and low flow discharges which will typically affect more than 300 days a year, a scour will develop immediately downstream of the step because the step acts as a small weir and the flow will pass the step at critical conditions and impinge the pool bottom (Figure 6.2). On very high discharges the location of the hydraulic jump will move further downstream until it finally hits the next downstream step (Figure 3.35). These conditions mark the flow transition from tumbling flow to rapid flow. Upstream scours may develop (Figure 7.5).

Although the stability considerations for the ramp can be applied for slopes up to 6.5 % (chapter 5.4.13) the recommended ramp slope is restricted to 3 %. This is because there are no mobile bed experiments at hand for higher slopes and therefore there is no information available on the scouring processes for steeper slopes.

The flume experiments of chapter 5 support Morris' recommendations (equation 3-98) for the relative spacing L/K which should be in the range of $8.5 \div 10$. Figure 7.6 illustrates that the maximum scour depth of a pool h_{scour} can be transformed into an equivalent step height K by demanding equality of the area covered by the scour hole (dashed area) and the grey shaded area with a plane bed. Postulating a maximum scour depth of 0.75 – 0.9 m (chapter 7.2.4) and a scour hole of parabolic shape the relative spacing L/K is within or close to Morris' recommended range for step spacings $L = 5 \div 7$ m (Table 7.5).

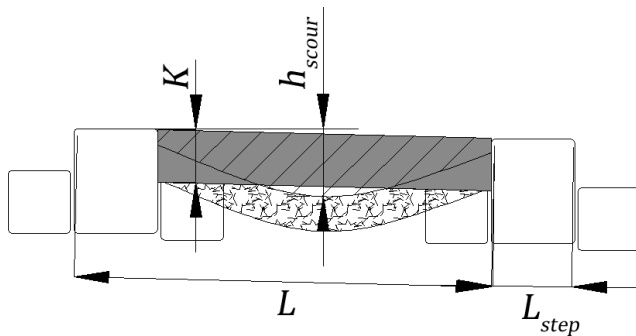


Figure 7.6 Maximum scour depth - equivalent step height K

L (m)	h_{scour} (m)	K (m)	L/K	q_{crit} for $I = 2.5 \%$	q_{crit} for $I = 3.0 \%$
5	0.75	0.59	8.5	3.5	3.3
6	0.9	0.70	8.5	4.8	4.5
7	0.9	0.69	10.1	6.0	5.6

Table 7.5 Relative Spacing L/K for $L_{step} = 1.5$ m and for different step spacings, corresponding flow transitional discharge according to equation 5-12

8 Conclusions and Prospects

This thesis provides design rules for a meandering ramp (chapter 7) which are supported by a synthesis of a literature review (chapter 3), a physical model test for a specific meandering ramp for the “Große Tulln” river (chapter 4), a basic flume test on different flow regimes along step-pool ramps (chapter 5) and field measurements at an existing prototype step-pool ramp (chapter 6).

The meandering ramp is a special kind of step-pool ramp. The steps of the meandering ramp are alternately inclined to the left and right bank, thus inducing a meandering flow on low and mean flow discharges. Additional pool armoring can be avoided in general. This allows natural processes of scouring and deposition in the pools. The lateral inclination of the steps is also reflected in the pool scours which tend to have the maximum depth alternately on the left and right side of the river axis. Thus, the meandering ramp displays substantial flow and depth variations which in turn are responsible for sediment sorting processes that can be observed in the pools. All these properties are commonly regarded as indicators of good ecological quality.

On the other hand the meandering ramp also provides hydraulic advantages. The typical flow regime along a meandering ramp is the so-called tumbling flow. This flow regime is characterized by an alternate succession of subcritical and supercritical flow through critical flow over each step. Small hydraulic jumps within the pools are responsible for a very good energy dissipation along the ramp. As long as the flow regime is tumbling, critical depth will occur at the step located at the toe of the ramp. This is the lowest theoretically possible energy level. As a consequence, the scour protection in the tailwater section of the ramp can be reduced. In contrast, the remaining excess energy at the ramp toe is higher for the traditional block ramp, which often requires expensive riprap protection of the tailwater section.

As can be concluded from investigations on artificial roughness elements (chapter 3.6 and chapter 5) the energy dissipation along step-pool ramps is the better the deeper the pools are. On the rising limb of a flood wave the pools of the meandering ramp get eroded, therefore the tumbling flow regime is prolonged. On the falling limb of a flood wave the transported sediments settle, filling up the pools again.

Taking advantage of the tumbling flow regime also has a downside: On very high discharges there is a flow transition from tumbling flow to the so-called rapid flow regime. In the rapid flow regime the flow skims over the tops of the steps at supercritical conditions. The energy dissipation decreases at this flow condition. The crucial point is the flow transitional process itself. As could be observed in the mobile bed experiments for the specific meandering ramp (chapter 4) at the flow transition, scours immediately upstream of a step may develop which endanger the stability of the step. These scour patterns can be reduced by ensuring that the longitudinal cut of a step has a triangular shape. This can either be achieved by a main boulder that is reinforced by two smaller boulders up- and downstream of the main boulder, or by embedding a single boulder such that its top face is adversely sloped.

Pressure measurements (chapter 5.4.12) around a single boulder of a step have shown that the flow transitional discharge marks **the** crucial loading case for the stability of a step. At these flow conditions the lift force acting on the boulder of the step dominates the drag force exerted by the flow by a multiplicative factor up to 2.6. At this discharge the danger of a step boulder to be washed

away is severe. Therefore it is important to know at which discharge the transition from tumbling flow to rapid flow takes place.

This was investigated in the basic flume test described in chapter 5. It was possible to relate the flow transitional discharge to the design parameters step height K , step spacing L and ramp slope I . It turned out that a criterion to distinguish 2D antidunes from 3D antidunes is also applicable to determine the flow transition from tumbling flow to rapid flow. A semi-empirical criterion based on linearized potential flow theory (as adopted from the transition from 2D to 3D antidunes) is provided to determine the flow transitional discharge (equations 5-12, 5-13 5-14).

The design rules provided in chapter 7 are such that the flow transitional discharge will happen for discharges ranging from $3.5 - 6 \text{ m}^3/\text{sm}$. The presence of a bed load transport for the flow transitional discharge helps to protect the boulders of the step because a part of the kinetic energy of the flow is used to transport the sediments. It is therefore required that the natural bed load rate of the river is not limited by bed-load traps or hydro power plants upstream of the ramp for discharges close to or higher than the flow transitional discharge. Moreover the rivers sediments must be a least of the same size as for the tested ramp.

The flow transitional discharge is a more critical loading case for the stability of a step-pool ramp than higher discharges in the stable rapid flow regime. To my knowledge, this transitional discharge has not yet been investigated by researchers who deal with step-pool ramps.

Further research is required to estimate the maximum scour depth h_{scour} of the pools subject to the parameters discharge, grain size distribution of the pool sediments and ramp slope in the presence or absence of a sediment rate from upstream.

- $h_{scour} = \mathbf{f}(q, I, L, d_{90}, d_m, \text{TF/RF, clear water/live bed})$

In the rapid flow regime a recirculating vortex (with a horizontal axis in lateral direction) occurs at the bottom of the pools. This vortex exerts a shear stress on the pool bottom which depends only indirectly on the discharge as the main flow skims of the tops of the steps. How can this shear stress be estimated and what is the critical shear stress for the incipient motion of the pool sediments?

As the physical model test for the specific meandering ramp (chapter 4) was performed with fixed banks it seems necessary to investigate the bank stability in further physical model tests. From theoretical considerations it follows that the u-shaped steps (in plan view) of the meandering ramp cause the flow to be directed towards the river centerline for high relative submergences of the ramp. This way the banks are protected.

The meandering ramp is a so-called “instream” river training structure. Instream river training identifies the flow as the source of river bank damages. Rather than reinforcing the banks, small installations in the river channel are designed to direct the destructive flow away from the banks. The appropriate use of secondary flow is a key function of these structures. Jacob Odgaard has made major contributions to this topic. A summary of his research is provided in Odgaard (2009). Other examples of instream river training structures such as micro groins are described in Sindelar & Mende (2008) and Mende & Sindelar (2010).

Although this topic is gaining significance, I personally believe that the concept of spiral flow is paid too little attention in hydraulic engineering so far.

9 Acknowledgements

The physical model test for the Große Tulln river has been funded by the Austrian Federal Ministry of Agriculture, Forestry, Environment and Water Management and the Office of Niederösterreich. We like to thank Otmar Grober for sharing his invaluable experimental knowledge of river engineering. We also thank Dr. Michael Hengl, head of the Institut für Wasserbau und hydrometrische Prüfung of the Bundesamt für Wasserwirtschaft, Vienna, for his pertinent and helpful comments. Ing. Michael Knoll was the responsible technician in the laboratory.

The basic flume test has been funded by the Austrian Federal Ministry of Agriculture, Forestry, Environment and Water Management, Department VII/6. Ing. Christian Kraker (measuring engineer, † March 2010) set up the automated positioning system, Ing. Wolfgang Rois (measuring engineer) selected and prepared the measuring devices. Dietmar Schönauer (locksmith) installed the ramp configurations. Dipl.-Ing. Thomas Gomerski carried out the sometimes tiresome experimental preparation and most of the experiments for the flat ramp configuration. He also wrote his diploma thesis about this flume test. Shkelzen Kryeziu (graduate assistant) performed most of the experiments for the steep ramp. Herbert Geiger (master student) accomplished the pressure measurements with great care and a profound technical knowledge.

References

- ABERLE, J., 2000. Untersuchung der Rauheitsstruktur zur Bestimmung des Fließwiderstandes in Gebirgsbächen unter Klarwassereinfluss. *Mitteilungen des Instituts für Wasserwirtschaft und Kulturtechnik, Universität Karlsruhe*, 207.
- ABERLE, J., DITTRICH, A. and NESTMANN, F., 1999. Estimation of gravel-bed river flow resistance - Discussion. *Journal of Hydraulic Engineering-Asce*, 125(12), pp. 1315-1317.
- ABRAHAMSON, A.D., LI, G. and ATKINSON, J.F., 1995. Step-Pool Streams - Adjustment to Maximum Flow Resistance. *Water Resources Research*, 31(10), pp. 2593-2602.
- AFZALIMEHR, H. and ANCTIL, F., 1998. Estimation of gravel-bed river flow resistance. *Journal of Hydraulic Engineering-Asce*, 124(10), pp. 1054-1058.
- BARKDOLL, B.D., ETTEMA, R. and ODGAARD, A.J., 1999. Sediment control at lateral diversions: Limits and enhancements to vane use. *Journal of Hydraulic Engineering-Asce*, 125(8), pp. 862-870.
- BATHURST, J.C., 1978. Flow Resistance of Large-Scale Roughness. *Journal of the Hydraulics Division-Asce*, 104(12), pp. 1587-1603.
- BATHURST, J.C., LI, R.M. and SIMONS, D.B., 1981. Resistance Equation for Large-Scale Roughness. *Journal of the Hydraulics Division-Asce*, 107(12), pp. 1593-1613.
- BILLI, P., D'AGOSTINO, V., LENZI, M.A. and MARCHI, L., 1998. Bedload, Slope and Channel Processes in a High-Altitude Alpine Torrent. In: P.C. KLINGELMANN, R.L. BESCHTA, P.D. KOMAR and J.B. BRADLEY, eds, *Gravel-Bed Rivers in the Environment*. Highlands Ranch, CO: Water Resources Publications, pp. 15-38.
- BLAISDELL, F.,W and DONNELLY, C.,A., 1955. The box inlet drop spillway and its outlet. *Journal of the Hydraulics Division*, 81(841), pp. 1-2.
- BLAISDELL, F.,W and DONNELLY, C.,A., 1954. The box inlet drop spillway and its outlet. *Journal of the Hydraulics Division*, 80(534), pp. 1-41.
- BLEINES, W., 1951. Hydraulisch wirksame Absturzbauwerke. *Die Wasserwirtschaft*, 42(1), pp. 11-16.
- CHARTRAND, S.M. and WHITING, P.J., 2000. Alluvial Architecture in Headwater Streams With Special Emphasis on Step-Pool Topography. *Earth Surface Processes and Landforms*, 25, pp. 583-600.
- CHIN, A., 2002. The periodic nature of step-pool mountain streams. *American Journal of Science*, 302(2), pp. 144-167.
- CHIN, A., 1999. The morphologic structure of step-pools in mountain streams. *Geomorphology*, 27(3-4), pp. 191-204.
- CHIN, A. and WOHL, E., 2005. Toward a theory for step pools in stream channels. *Progress in Physical Geography*, 29(3), pp. 275-296.

- COMITI, F., ANDREOLI, A. and LENZI, M.A., 2005. Morphological effects of local scouring in step-pool streams. *Earth Surface Processes and Landforms*, 30(12), pp. 1567-1581.
- DIN 19661-2 - *Sohlenbauwerke*. 2000. German standard.
- DONNELLY, C.,A. and BLAISDELL, F.,W, 1966. Straight drop spillway stilling basin - Closure. *Journal of the Hydraulics Division*, 92(HY4), pp. 140-145.
- DONNELLY, C.,A. and BLAISDELL, F.,W, 1965. Straight drop spillway stilling basin. *Journal of the Hydraulics Division*, 91(HY3), pp. 101-131.
- DROBIR, H. and SIMMLER, H., 1970. *Modellversuch Gefällstufe der Feistritz in Ratten*. Graz: Institut für Konstruktiven Wasserbau der Technischen Hochschule Graz.
- FANNIN, J., 2008. Karl Terzaghi: From theory to practice in geotechnical filter design. *Journal of Geotechnical and Geoenvironmental Engineering*, 134(3), pp. 267-276.
- FENTON, J.D. and ABBOTT, J.E., 1977. Initial Movement of Gravels on a Stream Bed. *Proceeding Royal Society, London*, , pp. 523-537.
- FEUERHAKE, F., 1957. Sohlenabstürze - Absturzbauwerke. *Wasser und Boden*, 9(10), pp. 400-408.
- FRANKE, P.-., 1970. *Abfluß über Wehre und Überfälle (Abriß der Hydraulik Band 4)*. Wiesbaden und Berlin: Bauverlag.
- GARBRECHT, G., 1957. Seitenkolke an Wehren, Abstürzen und Grundswellen. *Die Wasserwirtschaft*, 47(9), pp. 230-235.
- GEBLER, R., 2009. Bau von Sohlengleiten. *DWA-Naturnahe Sohlengleiten*, January, pp. 109-123.
- GEBLER, R., 2007. Hydraulische und konstruktive Anforderungen an Blockrampen zur Herstellung der biologischen Durchgängigkeit. *Mitteilungen der Versuchsanstalt für Wasserbau, Hydrologie, Glaziologie, ETH Zürich*, 201, pp. 37-48.
- GEBLER, R., 1991. *Sohlrampen und Fischaufstiege*. 1 edn. Walzbachtal: Eigenverlag.
- GEIGER, H., 2010. *Druckmessung, Grundlagenversuch an einer Riegelrampe (Masterprojekt)*, Institut für Wasserbau und Wasserwirtschaft, TU Graz.
- GOMERSKI, T., 2010. *Energieumwandlung an Riegelrampen (Diplomarbeit)*, Institut für Wasserbau und Wasserwirtschaft, TU Graz.
- GORING, D.G. and NIKORA, V.I., 2002. Despiking acoustic Doppler velocimeter data. *Journal of Hydraulic Engineering-Asce*, 128(1), pp. 117-126.
- GUNZELMANN, F., 1966. "Blocksteinrampen" und "Blocksteinsohlabstürze". *Wasser und Boden*, 18(1), pp. 7-9.
- HACKL, R., 2008. *Glasgerinne-Grundlagenversuch über die Funktionsweise von Bühnen*, Institut für Wasserbau und Wasserwirtschaft, TU Graz.
- HAGER W,H. 1993. Absturzbauwerke. *Schweizer Ingenieur u. Architekt*, Sonderdruck aus Heft 4:50-6.

- HARTUNG, F., 1973. Stützwirkungskraftwerke. *Die Wasserwirtschaft*, 11-12.
- HARTUNG, F. and SCHEUERLEIN, H., 1970. Design of Overflow Rockfill dams, *10th International Congress on Large Dams (ICOLD)*, Montreal 1970, pp. 587.
- HASSINGER, R., 1991. Beitrag zur Hydraulik und Bemessung von Blocksteinrampen in flexibler Bauweise. *Institut für Wasserbau der Universität Stuttgart*, 74.
- HENGL, M., AUFLEGER, M., NIEDERMAYR, A. and SPANNRING, M., 2008. Sanierung Untere Salzach - Aufgelöste Sohlrampe als Mehrzweckbauwerk. *Mitteilungen der Versuchsanstalt für Wasserbau, Hydrologie, Glaziologie, ETH Zürich*, 208, pp. 751-761.
- HENGL, M., KORGER, H. and KROUZECKY, N., 2007. *Step-Pool Ramps For Epipotamal Rivers - Example Saalach*, , XXXII IAHR-Congress, Venice, 1-6 July 2007 2007, pp. 481-488.
- HENGL, M. and STEPHAN, U., 2007. Aufgelöste Blockrampen zur Stabilisierung von Fließgewässersohlen unter Berücksichtigung der Fischdurchgängigkeit. *Mitteilungen der Versuchsanstalt für Wasserbau, Hydrologie, Glaziologie, ETH Zürich*, 201, pp. 83-93.
- HESKE, F. and SHEPARD, W.M.F., 1937. Die neuen Triftanlagen in den Mürzforsten in der Nordsteiermark. *Zeitschrift für Weltforstwirtschaft - Review of World's Forestry*, Band V(Heft 2, November), pp. 1-103.
- HÖSS, R., 1968. Sohlabsatz mit eingeeignetem Überfallquerschnitt und dreidimensional erweitertem Tosbecken. *Wasser und Boden*, 20(1), pp. 15-18.
- JUDD, H.E. and PETERSON, D.F., 1969. Hydraulics of large bed element channels. *Utah Water Research Laboratory, Logan*, Report PRWG17-6.
- KENNEDY, J.F., 1961. *Stationary Waves and Antidunes in Alluvial Channels*. KH-R-2. California Institute of Technology.
- KEUTNER, C., 1937a. Die Ausbildung der Gefällbrechpunkte geregelter kleinerer Wasserläufe. *Bautechnik*, 15(40/41), pp. 518-533.
- KEUTNER, C., 1937b. Die Regelung kleiner Wasserläufe durch Errichtung von Gefällestufen. *Bautechnik*, 15(13/14), pp. 173-188.
- KNAUSS, J., 1979. Flachgeneigte Abstürze, glatte und rauhe Sohlrampen. *Mitteilung der Versuchsanstalt für Wasserbau der Technischen Universität München*, 41.
- KNAUSS, J., 1976. Gestaltung und Auswirkung von Sohlstufen, *Fortbildungslehrgang "Gewässerausbau"*, March 1976 1976, DVWK, pp. 1-41.
- KNIGHT, D.W. and MACDONALD, J.A., 1979. Hydraulic Resistance of Artificial Strip Roughness. *Journal of the Hydraulics Division-Asce*, 105(6), pp. 675-690.
- KOBUS H, editor. *Wasserbauliches Versuchswesen*. 2., revidierte Auflage ed. Hamburg und Berlin: Paul Parey; 1984.

- KORECKY N. Flach geneigte Riegelrampen, Bauwerksbemessung sowie konstruktive Ausführung des Ufer- und Nachbettschutzes. Schriftenreihe Bundesamt für Wasserwirtschaft, Österreich. 2007;28.
- LANE, S.N., CHANDLER, J.H. and PORFIRI, K., 2001. Monitoring River Channel and Flume Surfaces with Digital Photogrammetry. *J.Hydr.Engrg.*, 127(10), pp. 871-877.
- Leistungsbeschreibung für den Flussbau. Wien: BMLFUW / Sektion VII/5; 2003. Report No.: V02.
- MAXWELL, A.R., PAPANICOLAOU, A.N., HOTCHKISS, R.H., BARBER, M.E. and SCHAFFER, J., 2001. Step-pool morphology in high-gradient countersunk culverts. *Hydrology, Hydraulics, and Water Quality; Roadside Safety Features - Highway and Facility Design*, (1743), pp. 49-56.
- MENDE, M. and GASSMANN, E., 2009. Pendelrampen – Funktionsweise und Erfahrungen. *Ingenieurbiologie*, Heft 3, pp. 29-36.
- MENDE, M. and SINDELAR, C., 2010. Instream River Training: Lenkbuhnen und Pendelrampen, P. RUTSCHMANN, ed. In: *Wasserbau in Bewegung - Von der Statik zur Dynamik*, July 1-3 2010 2010, Institut für Wasserbau, TU München, pp. 36-44.
- MEYER-PETER, E. and MÜLLER, R., 1948. Formulas For Bed-Load Transport, 1948.
- MONTES, J.S. and CHANSON, H., 1998. Characteristics of undular hydraulic jumps: Experiments and analysis. *Journal of Hydraulic Engineering-Asce*, 124(2), pp. 192-205.
- MORRIS, H.M., 1969. Design of Roughness Elements for Energy Dissipation in Highway Drainage Chutes. *Highway Research Record*, 261, pp. 25-37.
- MORRIS, H.M., 1968. Hydraulics of Energy Dissipation in Steep, Rough Channels. *Virginia Polytechnic Institute, Research Division*, Bulletin 19.
- MORRIS, B.,T. and JOHNSON, D.,C., 1943. Hydraulic design of drop structures. *Transactions American Society of Civil Engineers*, 108, pp. 887-940.
- MORRIS, H.M., 1955. Flow in Rough Conduits. *Transactions American Society of Civil Engineers*, 120, pp. 373-410.
- NICKOLOTSKY, A. and PAVLOWSKY, R.T., 2007. Morphology of step-pools in a wilderness headwater stream: The importance of standardizing geomorphic measurements. *Geomorphology*, 83(3-4), pp. 294-306.
- NIEL, A., 1960. Über die Vernichtung kinetischer Energie durch niedere Gefällstufen. *Österr. Wasserwirtschaft*, 12(4/5),.
- NÚÑEZ-GONZÁLEZ, F. and MARTÍN-VIDE, J.P., 2010. Downstream-migrating antidunes in sand, gravel and sand-gravel mixtures, A. DITTRICH, K. KOLL, J. ABERLE and P. GEISENHAINER, eds. In: *Riverflow 2010*, Sept 8-10 2010 2010, Bundesanstalt für Wasserbau, pp. 393-400.
- ODGAARD, A.J., 2009. *River Training and Sediment Management with Submerged Vanes*. Reston, Va: ASCE.

- ODGAARD, A.J., 2005. Submerged Vanes - an Inexpensive Sediment Management Strategy. *Proceedings of the 2nd International Yellow River Forum on Keeping Healthy Life of the River, Vol IV*, , pp. 31-35.
- ODGAARD, A.J. and WANG, Y., 1991a. Sediment Management with Submerged Vanes .1. Theory. *Journal of Hydraulic Engineering-Asce*, 117(3), pp. 267-283.
- ODGAARD, A.J. and WANG, Y., 1991b. Sediment Management with Submerged Vanes .2. Applications. *Journal of Hydraulic Engineering-Asce*, 117(3), pp. 284-302.
- PAGLIARA, S., 2007. Influence of sediment gradation on scour downstream of block ramps. *Journal of Hydraulic Engineering-Asce*, 133, pp. 1241-1248.
- PAGLIARA, S. and CHIAVACCINI, P., 2006a. Energy dissipation on block ramps. *Journal of Hydraulic Engineering-Asce*, 132(1), pp. 41-48.
- PAGLIARA, S. and CHIAVACCINI, P., 2006b. Energy dissipation on reinforced block ramps. *Journal of Irrigation and Drainage Engineering-Asce*, 132(3), pp. 293-297.
- PAGLIARA, S., DAS, R. and PALERMO, M., 2008. Energy dissipation on submerged block ramps. *Journal of Irrigation and Drainage Engineering-Asce*, 134(4), pp. 527-532.
- PAGLIARA, S. and PALERMO, M., 2008a. Scour control and surface sediment distribution downstream of block ramps. *Journal of Hydraulic Research*, 46(3), pp. 334-343.
- PAGLIARA, S. and PALERMO, M., 2008b. Scour control downstream of block ramps. *Journal of Hydraulic Engineering-Asce*, 134(9), pp. 1376-1382.
- PAGLIARA, S., PALERMO, M. and CARNACINA, I., 2009. Scour and hydraulic jump downstream of block ramps in expanding stilling basins. *Journal of Hydraulic Research*, 47(4), pp. 503-511.
- PETERKA, A.,J., 1964. *Hydraulic Design of Stilling Basins and Energy Dissipators*. No. 25 edn. Bureau of Reclamation, U.S. Department of the Interior.
- PETERSON, D.F. and MOHANTY, P.K., 1960. Flume Studies of Flow in Steep, Rough Channels. *Journal of the Hydraulics Division*, 86(HY9), pp. 55-76.
- PLATZER, G., 2000. Dimensionierung muldenförmiger Blocksteinrampen. *Schriftenreihe Bundesamt für Wasserwirtschaft, Österreich*, 9.
- PLATZER, G., 1983. Die Hydraulik der breiten Blocksteinrampe. *Schriftenreihe Bundesamt für Wasserwirtschaft, Österreich*, Sonderheft.
- RAND, W., 1965. Straight drop spillway stilling basin- Discussion. *Journal of the Hydraulics Division*, 92(HY1), pp. 102-107.
- RAND, W., 1956a. Flow Geometry at straight drop spillways. *Journal of the Hydraulics Division*, 82(HY1), pp. 57-62.
- RAND, W., 1956b. Flow Geometry at straight drop spillways. *Journal of the Hydraulics Division*, 82(HY3), pp. 7-9.

- RAND, W., 1955. Flow Geometry at straight drop spillways. *Journal of the Hydraulics Division*, 81(HY5), pp. 1-13.
- RAUDKIVI, A.J. and ETTEMA, R., 1982. Stability of Armour Layers in Rivers. *Journal of the Hydraulics Division*, 108(HY9),.
- RENNIE, C.D. and MILLAR, R.G., 1999. Estimation of gravel-bed river flow resistance - Discussion. *Journal of Hydraulic Engineering-Asce*, 125(12), pp. 1317-1319.
- ROSIER, B., BOILLAT, J.-. and SCHLEISS, A.J., 2004. Mapping of bed morphology for lateral overflow using digital photogrammetry Proceedings, , 14 to 17 November 2004 2004.
- ROSPORT, M., 1998. Fließwiderstand und Sohlstabilität steiler Fließgewässer unter Berücksichtigung gebirgsbachtypischer Sohlstrukturen. *Mitteilungen des Instituts für Wasserwirtschaft und Kulturtechnik, Universität Karlsruhe*, 196.
- SCHÄLCHLI, U., 1991. Morphologie und Strömungsverhältnisse in Gebirgsbächen: ein Verfahren zur Festlegung von Restwasserabflüssen. *Mitteilungen der Versuchsanstalt für Wasserbau, Hydrologie, Glaziologie, ETH Zürich*, 113.
- SCHAUBERGER, J., 2006. Viktor Schauburger, Das Wesen des Wassers. Baden und München: AT Verlag.
- SCHAUBERGER, V., 1930. Temperatur und Wasserbewegung - Grundlagen der Flußregulierung bei Berücksichtigung der Temperaturverhältnisse. *Die Wasserwirtschaft*, (24),.
- SCHAUBERGER, W., 1975. Die räumliche Krümmung von Gefällsstufen und Sturzbettenschwellen. *Wasser und Boden*, 27(10), pp. 265-268.
- SCHAUBERGER, W., 1973. Die räumliche Krümmung von Gefällsstufen und Sturzbettenschwellen. *Österr. Wasserwirtschaft*, 25(5/6), pp. 120-124.
- SCHAUBERGER, W., 1957. Naturgemäßer Wasserbau an geschiebeführenden Flüssen. *Wasser und Boden*, 9(11), pp. 434-437.
- SCHEUERLEIN, H., 1968. Der Rauherinneabfluß. *Mitteilung der Versuchsanstalt für Wasserbau der Technischen Universität München*, 14.
- SINDELAR, C. and KNOBLAUCH, H., 2010. Design of a Meandering Ramp located at the River "Große Tulln", A. DITTRICH, K. KOLL, J. ABERLE and P. GEISENHAINER, eds. In: *Riverflow 2010*, Sept 8-10 2010 2010, Bundesanstalt für Wasserbau, pp. 1239-1246.
- SINDELAR, C. and KNOBLAUCH, H., 2008. Modellversuch zur Aktivierung des Sedimenttransports unterhalb von Flusskraftwerken, H.-. MINOR, ed. In: *Neue Anforderungen an den Wasserbau*, Sept 11-12 2008 2008, VAW, ETH Zürich, pp. 859-868.
- SINDELAR, C., KNOBLAUCH, H., BADURA, H. and GROBER, O., 2007. Monitoring of a Bent Training Structure at the River Mur, E.A. COWEN and D. HILL, eds. In: *Hydraulic Measurements and Experimental Methods, Book of Extended Abstracts*, Sept 10-11 2007 2007, ASCE/IAHR, pp. 118-123.

- SINDELAR, C. and MENDE, M., 2009. Lenkbuhnen zur Strukturierung und Stabilisierung von Fließgewässern. *Wasserwirtschaft*, Heft 1-2, pp. 70-75.
- SINGER, G., BESEMER, K., SCHMITT-KOPPLIN, P., HODL, I. and BATTIN, T.J., 2010. Physical Heterogeneity Increases Biofilm Resource Use and Its Molecular Diversity in Stream Mesocosms. *Plos One*, 5(3).
- THOMPSON, P.,L. and KILGORE, R.,T., 2006. *Hydraulic Engineering Circular of National Highway Institute*, Third Edition(14),.
- VALLE, B.L. and PASTERNAK, G.B., 2006. Submerged and unsubmerged natural hydraulic jumps in a bedrock step-pool mountain channel. *Geomorphology*, 82(1-2), pp. 146-159.
- VOGEL, S., 2003. Ansätze zur Bemessung rauer Rampen in aufgelöster Bauweise. *Mitteilungen des Instituts für Wasserwesen, Universität der Bundeswehr München*, 88.
- VOLKART, P., 1972. Die Stabilisierung von Flussläufen mittels einer Folge von Querswellen. *Mitteilungen der Versuchsanstalt für Wasserbau, Hydrologie, Glaziologie, ETH Zürich*, 6.
- WANG, Y.L. and ODGAARD, A.J., 1993. Flow-Control with Vorticity. *Journal of Hydraulic Research*, 31(4), pp. 549-562.
- WANG, Y.L., ODGAARD, A.J., MELVILLE, B.W. and JAIN, S.C., 1996. Sediment control at water intakes. *Journal of Hydraulic Engineering-Asce*, 122(6), pp. 353-356.
- WEICHERT, R.B., BEZZOLA, G.R. and MINOR, H., 2008. Bed morphology and generation of step-pool channels. *Earth Surface Processes and Landforms*, 33(11), pp. 1678-1692.
- WFD, 2000. *Water Framework Directive 2000/60/EC of the European Parliament and The Council Of The European Union*. Official Journal of the European Communities: L327.
- WHITTAKER, J.G., 1987. Sediment Transport in Step-pool Streams. In: C.R. THORNE, J.C. BATHURST and R.D. HEY, eds, *Sediment Transport in Gravel-Bed Rivers*. New York: John Wiley & Sons, pp. 545-579.
- WHITTAKER, J.G. and JÄGGI, M., 1986. Blockswellen. *Mitteilungen der Versuchsanstalt für Wasserbau, Hydrologie, Glaziologie, ETH Zürich*, 91.
- WHITTAKER, J.G. and JÄGGI, M., 1982. Origin of step-pool systems in mountain streams. *Journal of the Hydraulics Division*, 108(HY6), pp. 758-773.
- WOHL, E.E. and THOMPSON, D.M., 2000. Velocity characteristics along a small step-pool channel. *Earth Surface Processes and Landforms*, 25(4), pp. 353-367.
- WOOLDRIDGE, C.L. and HICKIN, E.J., 2002. Step-pool and cascade morphology, Mosquito Creek, British Columbia: a test of four analytical techniques. *Canadian Journal of Earth Sciences*, 39(4), pp. 493-503.
- ZIMMERMANN, A. and CHURCH, M., 2001. Channel morphology, gradient profiles and bed stresses during flood in a step-pool channel. *Geomorphology*, 40(3-4), pp. 311-327.